ÉTUDE DE MATÉRIAUX HYBRIDES À BASE DE NANOPARTICULES À CONVERSION ASCENDENTE ET POLYMÈRES: DE NANOVECTEURS À FILMS MINCES

par

Jun Xiang

Thèse présentée au Département de chimie en vue

de l'obtention du grade de docteur ès sciences (Ph.D.)

FACULTÉ DES SCIENCES

UNIVERSITÉ DE SHERBROOKE

Sherbrooke, Québec, Canada, Juin 2018

STUDY OF UPCONVERSION NANOPARTICLE/POLYMER HYBRID MATERIALS: FROM NANOVECTORS TO THIN FILMS

by

Jun Xiang

A Thesis

Presented to the Département of Chimie

in Partial Fulfillment of the Requirements for the Degree of

Doctor of Philosophy (Ph.D.)

FACULTÉ DES SCIENCES

UNIVERSITÉ DE SHERBROOKE

Sherbrooke, Québec, Canada, Juin 2018

Le 30 Juin 2018

le jury a accepté la thèse de Monsieur Jun Xiang
dans sa version finale.

Membres du jury

Professeur Yue Zhao
Directeur de recherche
Département de chimie

Professeur Fiorenzo Vetrone
Évaluateur externe
INRS-EMT
Université du Québec

Professeur Pierre D. Harvey
Évaluateur interne
Département de chimie

Professeur Serge Lacelle
Évaluateur interne
Département de chimie

Professeur Gessie Brisard
Président-rapporteur
Département de chimie

SOMMAIRE

La recherche réalisée dans cette thèse porte sur le design, la synthèse et l'investigation de trois nouveaux types de matériaux hybrides à base des polymères et des nanoparticules à conversion ascendante (NPCA). Ces matériaux sont sensibles à la lumière proche infrarouge (PIR) en raison de la NPCA qui absorbe la lumière ayant une longueur d'onde de 980 nm et émette la lumière dans le visible et l'ultraviolet (UV). Pour deux systèmes étudiés, leur application potentielle comme nanovecteur de médicament dont la libération est déclenchée par un rayonnement PIR est démontrée. Quant à l'étude de l'autre système sous forme de film mince, elle permet de démontrer que la méthode d'assemblage couche-par-couche est efficace pour organiser les NPCA dans un film conjointement avec des nanoparticules d'or (NPAu). Les résultats obtenus valident les nouvelles stratégies ou méthodologies proposées, lesquelles sont générales et offrent de nouvelles perspectives dans le développement et l'exploitation pour applications des matériaux hybrides de NPCA/polymère.

Dans le premier projet (chapitre 1), l'auto-assemblage d'un copolymère dibloc amphiphile sur la surface de NPCA est réalisée pour donner naissance à micelle dont le noyau contient une seule NPCA. À l'aide de polymérisation radicalaire par transfert d'atome initiée en surface de NPCA, le copolymère dibloc couvre la NPCA, avec poly(4,5-diméthoxy-2-nitrobenzyl méthacrylate) (PNB) comme bloc interne et hydrophobe et poly(méthoxy polyéthylène glycol monométhacrylate) (POEG) comme bloc extérieur et hydrophile. Sous une exposition au laser de 980 nm, la lumière UV émise par la NPCA est absorbée par PNB, ce qui entraîne le clivage des groupes *o*-nitrobenzyle et la formation de groupes acide carboxylique. L'hydrophilie accrue du copolymère résultant de la réaction photochimique déclenchée par la lumière PIR perturbe le nanovecteur et ainsi conduit à la libération de la doxorubicine (DOX).

Dans le second projet (chapitre 2), les NPCA sont complexées avec un polyélectrolyte UV-labile par interaction électrostatique entre charges de signes opposés, ce qui permet le

couvrement de chaque NPCA par une couche polymère. Un médicament modèle chargé, la fluorescéine (FLU), est encapsulé dans la couche de polyélectrolyte via un processus de co-assemblage. De même, sous l'irradiation laser de 980 nm, la lumière UV émise par la NPCA est absorbée par des groupes latéraux photolytiques du polyélectrolyte, ce qui entraîne le clivage des groupes *o*-nitrobenzyle et la formation de groupes acide carboxylique. Par conséquent, une partie des charges positives portées par le polyélectrolyte est convertie en espèces chargées négativement, et cette inversion perturbe l'équilibre entre les composants chargés et conduit à la libération de molécules de FLU.

Dans le dernier projet (chapitre 3), la méthode couche-par-couche est utilisée pour assembler les NPCA dans un film mince de manière contrôlée, en ajustant notamment l'ordre de dépôt de quatre bicouches NPCA/polyélectrolyte et quatre bicouches NPAu/polyélectrolyte. Les spectres d'absorption et les spectres d'émission à conversion ascendante de ces films minces hybrides plasmoniques et sensibles au PIR révèlent que l'organisation spatiale déterminée par les séquences de dépôt influence l'interaction entre ces deux types de nanoparticules et ainsi leurs propriétés optiques.

Mots-clés: nanoparticules à conversion ascendante, polymères UV-sensibles, nanovecteurs, matériaux hybrides, auto-assemblage de polymères, assemblage couche-par-couche

ABSTRACT

The research carried out in this thesis involves the design, synthesis, and investigation of three new types of hybrid materials based on polymers and upconversion nanoparticles (UCNP). These materials are sensitive to near-infrared light (NIR) because UCNP can absorb light with a wavelength of 980 nm then emit light in the visible and ultraviolet (UV) light region. For the first two systems studied, their potential application as a drug nanovector whose release is triggered by NIR radiation is demonstrated. As for the other system in the form of a thin film, it demonstrates that the layer-by-layer assembly is an effective method for organizing UCNP in a film together with gold nanoparticles (AuNP). The obtained results validate the proposed new strategies or methodologies, which are general and offer new perspectives in the development and exploration of UCNP/polymer hybrid materials applications.

In the first project (Chapter 1), the self-assembly of an amphiphilic diblock copolymer on the surface of UCNP is carried out to form a micelle with single UCNP encapsulation inside. Using surface-initiated atom transfer radical polymerization, UCNP is covered by the diblock copolymer with poly(4,5-dimethoxy-2-nitrobenzyl methacrylate) (PNB) as the inner and hydrophobic block and poly(methoxy polyethylene glycol monomethacrylate) (POEG) as the outer and hydrophilic block. Under 980 nm laser exposure, the UV light emitted by the UCNP is absorbed by PNB, resulting in the cleavage of *o*-nitrobenzyl groups and formation of carboxylic acid groups. The increased hydrophilicity of the copolymer resulting from the photochemical reaction triggered by the NIR light disturbs the nanovector and thus leads to the release of doxorubicin (DOX).

In the second project (Chapter 2), UCNP are complexed with a UV-labile polyelectrolyte by electrostatic interaction between charges of opposite sign, which allows the covering of each UCNP by a polymer layer. A charged model drug, fluorescein (FLU), is encapsulated in the polyelectrolyte layer via a co-assembly process. Also, under the 980 nm laser irradiation, the UV light emitted by the UCNP is absorbed by photolytic side groups of the

polyelectrolyte, resulting in cleavage of *o*-nitrobenzyl groups and formation of carboxylic acid groups. As a result, a portion of the positive charges carried by the polyelectrolyte is converted to negative charges, and this inversion disrupts the balance between the charged components and leads to the release of FLU molecules.

In the last project (Chapter 3), the layer-by-layer method is used to assemble UCNP into a thin film in a controlled manner, in particular by adjusting the deposition order of four UCNP/polyelectrolyte bilayers and four AuNP/polyelectrolyte bilayers. The extinction spectra and the upconversion emission spectra of these plasmonic and NIR-sensitive hybrid thin films reveal that the spatial organization determined by the deposition sequences influences the interaction between these two types of nanoparticles and thus their optical properties.

Keywords: upconversion nanoparticles, UV-responsive polymers, nanovectors, hybrid materials, polymer self-assembly, layer-by-layer assembly

ACKNOWLEDGEMENT

First and foremost, I would like to express my most sincere gratitude to my supervisor Prof. Yue Zhao for his guidance, patience, encouragement, and support during the whole period of my Ph.D. studies at Université de Sherbrooke. I appreciate him to give me the valuable opportunity to do research that I am really interested in, and always support me and believe in me whenever I meet problems. I really learned a lot from Prof. Zhao over the past years. I believe his wide academic experience and rigorous scientific attitude will be my lifetime wealth. Also, I thank him for giving me the financial support which allows me to finish my Ph.D. program.

I would like to thank two members of my doctoral committee, who are also in the jury of my thesis, Prof. Gessie Brisard and Prof. Serge Lacelle, as well as all the professors and staff working in the Department of Chemistry, Université de Sherbrooke for their kind help. I would like to thank Prof. Fiorenzo Vetrone (Université du Québec) and Prof. Pierre D. Harvey for serving in the jury of my thesis. I also would like to thank Mr. Paul-Ludovic Karsenti for his help in taking the upconversion luminescence spectra.

I acknowledge the following people, my colleagues and dearest friends, who made my four years' stay in Sherbrooke full of joys and memories: Mrs. Xia Tong, Prof. Dongchen He, Dr. Li Wang, Dr. Feng Shi, Dr. Qiang Yan, Dr. Olivier Boissière, Dr. Hu Zhang, Dr. Bing Yu, Dr. Weizheng Fan, Dr. Guo Li, Dr. Hongji Zhang, Dr. Shangyi Fu, Dr. Shengwei Guo, Dr. Xin Zhao, Dr. Rong Yang, Dr. Juan Xuan, Dr. Dehui Han, Dr. Xili Lu, Dr. Hui Xiao, Dr. Xiancong Lu, Dr. Xiaorong Wang, Dr. Di Gao, Dr. Lei Hu, Dr. Aurélie Lespes, Dr. Hojjat Seyedjamali, Mr. Damien Habault, Mr. Feijie Ge, Mr. Farhad Farnia, Mr. Liangliang Dong, Mrs. Amélie Augé, Mr. Ricardo Da Silva Lemos, Mrs. Laura Mourot, Mr. Zhichao Jiang, Mrs. Yaoyu Xiao, and Mr. Lu Yin.

I would like to give my thanks and respect to the Ministère de l'Éducation, du Loisir et du Sport du Québec and Chinese Scholarship Council (CSC) for awarding me a scholarship to support my living and study in Canada.

I also would like to thank all the members of the Service d'éducation du Consulat Général de la République Populaire de Chine à Montréal, especially Ms. Suli Yan, for all their kind helps.

I express my sincere thanks to my family for their exceptional care and encouragement during my study in Canada, especially my parents, my parents-in-law, my wife Yutong Xie, my little son Vincent Xiang and my younger brother Xingxing Xiang. Without your encouragement and accompany, none of this would have been possible.

Finally, I would like to acknowledge the following organizations for their financial support: Natural Sciences and Engineering Research Council of Canada (NSERC), Le Fonds de recherche du Québec: Nature et technologies (FQRNT), Centre for Self-Assembled Chemical Structures (CSACS) and La Fondation de Université de Sherbrooke.c

TABLE OF CONTENT

LIST OF FIGURES

INTRODUCTION

CHAPTER 2

LIST OF TABLES

INTRODUCTION

In the past decade, researches on rare-earth (RE) doped upconversion nanoparticles (UCNP) for constructing novel functional materials have witnessed an explosive growth (1-3). Particularly, these inorganic nanoparticles (NPs) have promising applications in the fields of biomedicine (4-6), energy conversion (7-9), and security patterns (10-12). As one kind of advanced material, UCNP provide innovative solutions or ideas for some major problems in numerous areas. For instance, in the bioimaging field, UCNP can be utilized in multiplexing and multimodal imaging for deep bio-tissues owing to their excitation wavelength located in the biological transparency window, high stability, low cytotoxicity and non-photobleaching properties (13, 14). Another example is that integration of UCNP into organolead halide perovskite solar cells can enhance the power conversion efficiency by extending the spectral absorption in the near-infrared (NIR) light region (15). These are attributed to the distinctive non-linear optical property of UCNP, which has the capability of converting multiple low-energy photons (NIR light) into high-energy photons (ultraviolet (UV) or visible light). Hence, these fascinating nanocrystals can act as antennas to bridge NIR and UV/visible light, making NIR light-initiated photoreactions and expansion of the spectral absorption range possible. In section **1.1**, a brief introduction to UCNP is presented.

Integration of UCNP with organic polymer materials for applications in, for instance, drug delivery, anti-counterfeiting materials and solar cells, have attracted much research interest around the world (16-21). The reasons for their combination are multiple, such as endowing UCNP with water dispersity, improving compatibility with polymer matrix, loading guest molecules and offering stimuli-responsive properties (pH, temperature, light, and so on). In the first two works of this thesis, we designed two nanovectors capable of NIR light-triggered payload release, which involves the surface modification of UCNP with polymer materials. Thus, the surface coating strategies to endow UCNP with water dispersity by hydrophilic polymers are summarized in section **1.2**. In section **1.3**, an

overview of recent progress in the development of nanovectors based on UCNP/polymers for the application of NIR light-triggered cargo release is presented.

In the preparation of UCNP/polymers hybrid materials, knowledge on how to organize these two types of materials for potential uses is crucial. Fundamentally, it is desirable to find a generalized and straightforward approach to organize UCNP in the polymer matrix. To this end, the third work accomplished in this thesis is about using the layer-by-layer (LbL) assembly technique to organize UCNP and gold nanoparticles (AuNPs, also extensively explored with polymers) through polyelectrolytes. Therefore, a brief introduction to the preparation of UCNP/polyelectrolytes thin films by LbL assembly is presented in section **1.4**. The introduction will be ended with a statement of the objective of the thesis work.

I.1 A Brief Introduction to UCNP

RE doped UCNP (<100 nm) are inorganic nanocrystals with trivalent lanthanide ions as dopants. Their outstanding property is the conversion of low-energy photons (NIR light) into high-energy photons (visible or UV light) through sequential absorption of multiple photons, which is attributed to the ladder-like electronic transition levels of RE metallic ions and long luminescence lifetime (up to millisecond). Although lanthanide-doped UC bulk materials have been known for several decades, the first investigation on UCNP (5-20 nm) with good photoluminescence property was reported in 2000 (22). The reason is that the surface quenching effect caused by the high surface-to-volume ratio of NPs leads to the reduction of emission centers (23). After an extended period of research, it is now known that the type of host matrix, the concentration of dopant and the phase construction should be carefully adjusted to obtain UCNP with high quantum yield (QY) of upconversion luminescence (UCL). It should be mentioned that the most frequently used host matrix is $NaREF_4$, which has relatively low phonon energy, adequate thermal and environmental stability, and excellent optical transparency over a broad wavelength range (24).

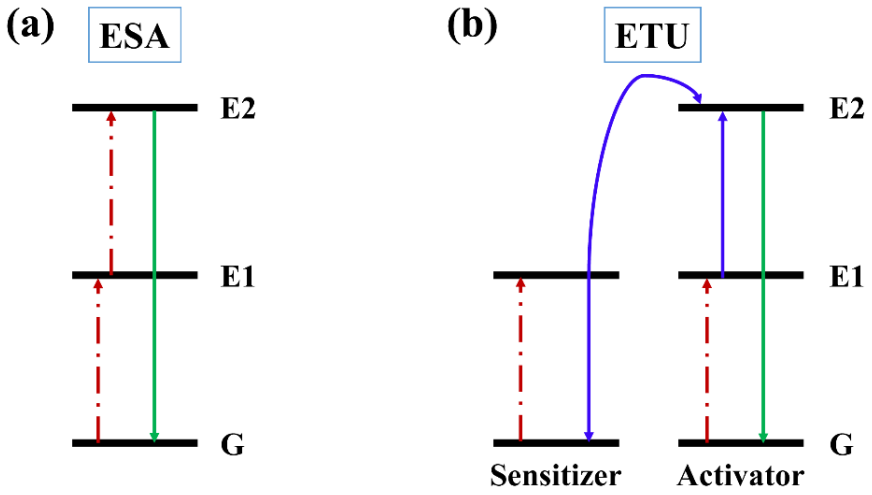

Figure 1. (a) Excitation-state absorption (ESA). (b) Energy transfer upconversion (ETU).

Three primary mechanisms explain the UC process of UCNP: excitation-state absorption (ESA), energy transfer upconversion (ETU) and photon avalanche (PA). Noteworthy, PA is not often observed in UCNP because the observation of this phenomenon needs exceptionally high pumping intensity (25). Also, PA mechanism is restricted within a few typical ions, like Pr^{3+}, limiting their further exploration. Consequently, most UC processes involve ESA and ETU. In ESA, only one RE ion participates in the UC process. When one electron stays in a metastable excited state as shown in Figure 1a, it can be further populated to a higher excitation state after absorbing another photon of the incident light. The UCL emissions can be detected when the pumped electrons at higher energy levels return to their ground states. However, this process has a relatively low efficiency due to the low absorption cross-sections of lanthanide trivalent ions. By contrast, ETU process involves two different lanthanide ions (sensitizer and activator). The sensitizer is responsible for harvesting the light energy, and the activator takes charge of emitting high-energy photons. Figure 1b shows a typical ETU process. At the beginning, electrons of the sensitizer and activator are both populated in their metastable intermediate excitation states. Then the energy is transferred from the sensitizer to the adjacent activator through a non-radiative process, which allows the activator to populate to a higher energy state. UC emissions take place when the activator drops to the ground state in a radiative manner. By

carefully modulating the concentration of these two ions, UC emissions from the as-synthesized UCNP can be readily observed by a NIR light laser excitation at a low power density through the ETU process.

As mentioned above, sensitizer and activator are often co-doped into the same host matrix to obtain high quality of UCNP. So far, the Yb^{3+}/Tm^{3+} (sensitizer/activator) dual ions-doped β-$NaREY_4$ have been extensively investigated (26, 27). In Figure 2a, the population process together with the UCL mechanism between Yb^{3+} and Tm^{3+} are depicted. The UCL takes place when the populated electrons go back to the ground state by a radiative manner. We can see the emission bands from the UPL spectrum in Figure 2b. UCNP have narrow emissions in the 250-550 nm region, with UV light at 291, 341 and 361 nm, blue light at 451 and 475 under excitation with a continuous-wave (CW) 980 nm diode laser. These emission bands can be attributed to the electron transitions from $^1I_6 \rightarrow {}^3H_6$ (294 nm), $^1I_6 \rightarrow {}^3F_4$ (345 nm), $^1D_2 \rightarrow {}^3H_6$ (368 nm), $^1D_2 \rightarrow {}^3F_4$ (450 nm) and $^1G_4 \rightarrow {}^3H_6$ (475 nm).

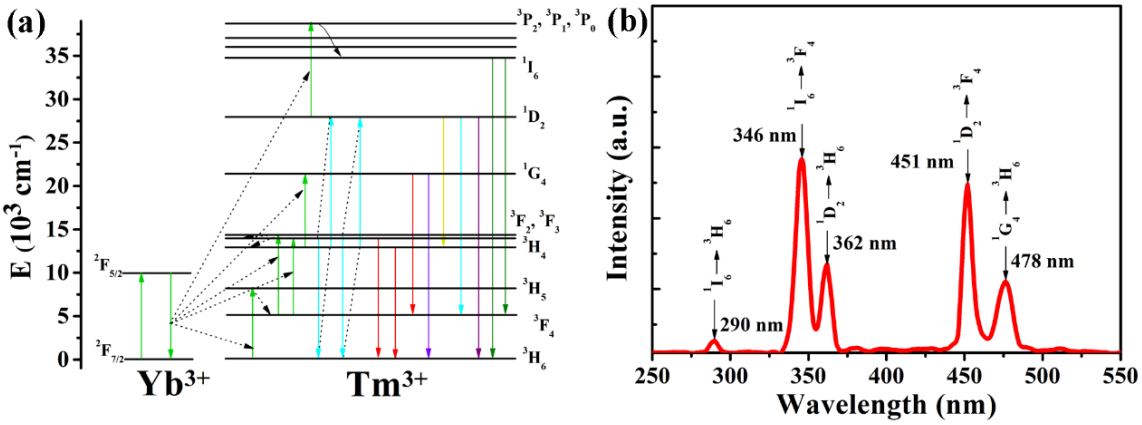

Figure 2. (a) A schematic diagram of upconversion processes in a Yb^{3+}-Tm^{3+} codoped system upon excitation with a 980 nm laser. Yb^{3+} and Tm^{3+} serve as the sensitizer and activator, respectively. (b) UCL spectrum of $NaYF_4$:20%Yb,0.5%Tm nanocrystals. The term symbol $^{2S+1}L_J$ used to label the f states is according to the Russel-Saunders notation and refers to the total spin quantum number (*S*), the total orbital quantum number (*L*) and the total angular momentum quantum number (*J*), respectively.

Due to the rapid growth of nanotechnology, a variety of methodologies have realized the preparation of UCNP with excellent photoluminescence property at low power density excitation in the past decade. Primarily, the solution-based synthetic routes (hydro-/solvothermal synthesis, thermolysis method, emulsion method, etc.) are powerful for the convenient and reproducible synthesis of high-quality UCNP (28). For example, their sizes can be precisely tuned below 10 nm without sacrificing their brightness or stability through the thermolysis method (29). These technologies significantly promote the exploration of the usage of UCNP in functional materials over the last few years. As shown in Figure 3, smart materials based on UCNP have large potential applications in diverse fields, such as bioimaging, anti-counterfeiting, displaying and so on (2). Owing to the large anti-stokes shift, narrow emission bands, non-photobleaching and chemical stability of UCNP, these chemical and optical properties make them act as excellent candidates for the biomedical uses, such as bioimaging, drug delivery, and photodynamic therapy (PDT). It is expected that UCNP will be transferred from the academic stage into real-world applications shortly.

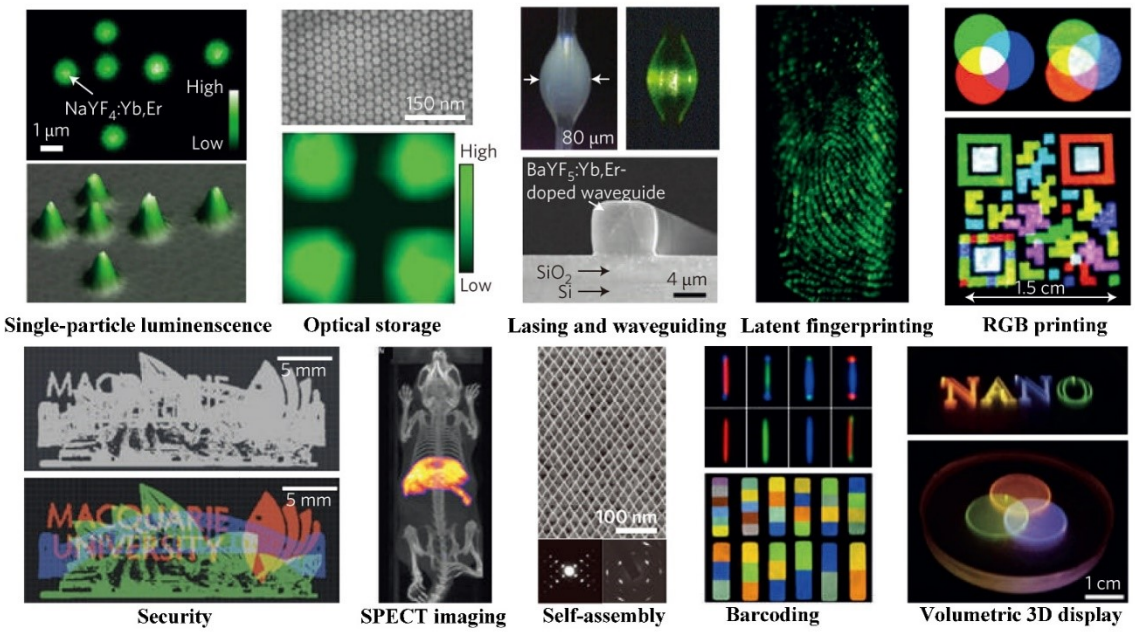

Figure 3. Applications of RE doped UCNP. Adapted with permission from [2].

I.2 From Hydrophobic to Hydrophilic: Coating of UCNP with Polymer Materials

In general, UCNP are synthesized by a thermolysis approach, which produces UCNP with high crystallinity, high UCL efficiency and low polydispersity. Unfortunately, the as-synthesized UCNP can only be dispersed in non-polar organic solvents (e.g., cyclohexane) due to their surface hydrophobic ligands, like oleic acid (OA) and oleylamine (OM). These organic ligands significantly restrict UCNP applications. So, it is necessary to modify their surface for preparing novel functional materials. For instance, decoration of UCNP can improve their dispersity and compatibility in composites (20, 30), which is favorable for fabricating materials with high transparency (31). Moreover, particularly in the biomaterials fields, adjusting the surface of UCNP from hydrophobic to hydrophilic is required because of the aqueous environment in biological tissues. Besides the modified UCNP should also be biocompatible, biodegradable and multi-functional (protein conjunction, drug loading and release) in some cases to meet various needs. Undoubtedly, surface coating of UCNP is the first step to explore their further usage. Several comprehensive reviews related to this topic have been published in the past few years (32-34).

So far, various kinds of materials, including inorganic (e.g., silica) and organic materials (small organic molecules or polymers), have been successfully coated onto the surface of UCNP. Among them, polymers have received considerable attention due to their light-weight, low-cost, flexibility and easy process (35-37). Especially in the biomedical fields, some specific polymers, like polyethylene glycol (PEG)-coated NPs can attenuate nonspecific uptake by cells and reduce plasma protein adsorption, thereby resulting in increased circulation half-life in the bloodstream (1, 38-41). Therefore, the combination of polymers and UCNP shows considerable prospects for potential applications. A variety of strategies have been put forward for regulating UCNP surface from hydrophobic to hydrophilic by using polymer materials. They can be broadly divided into two categories. One is the direct synthesis of hydrophilic polymer-capped UCNP and the other is post-functionalization of UCNP with hydrophilic polymers.

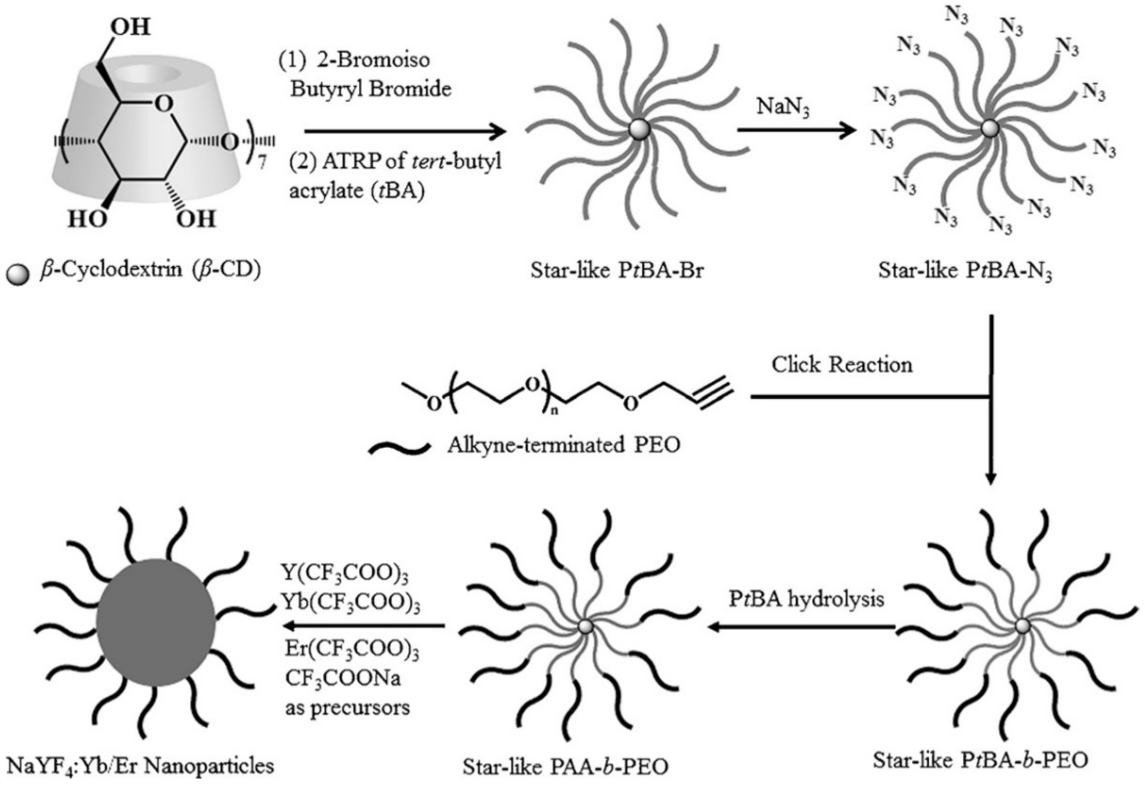

Figure 4. Synthesis of water-soluble UCNP via an unconventional method. Reproduced with permission from [15].

I.2.1 Synthesis of Hydrophilic Polymer-capped UCNP

To combine UCNP with a hydrophilic polymer, the frequently used method is hydro- or solvothermal approach. Specifically, polar solvents (like H_2O or diethylene glycol) are employed to produce UCNP at elevated temperature (typically < 250 ^oC) under high pressure for which an autoclave is often utilized. Before reaction, the polymer is added as an additive to form coordination with precursors. During the formation of nanocrystals, it acts as a macromolecular surfactant to coat and stabilize NPs, and simultaneously modulate

the growth kinetics. The polymers can be polyethylenimine (PEI) (42), polyacrylic acid (PAA) (43), polyvinylpyrrolidone (PVP) (44), PEG (45) and so on.

Lin and co-workers reported an unconventional method in 2016 (15). As shown in Figure 4, they prepared a star-like polymer micelle with PAA as inner blocks and PEG as outer blocks. Due to the strong coordination interactions between the RE metallic ions and carboxyl groups, the precursors preferentially enriched in the inside PAA blocks. During the reaction, the outer PEG chains prevented the agglomeration while the PAA chains were buried in the nanocrystals. After purification, the as-synthesized UCNP with a high degree of monodispersity and highly pure phase can be used without further modification.

I.2.2 Post-modification of UCNP with Hydrophilic Polymers

For the methods belonging to this category, hydrophobic ligands-capped UCNP with high UC luminesce efficiency are first synthesized via thermolysis method and then post-modified with polymer materials. Like the hydrothermal method, thermolysis method is also a solution-based process. In comparison with the synthesis process of the hydrothermal method, its significant advantage is that the synthesis of UCNP can be carried out under normal pressure at elevated temperature (generally > 250 ^{o}C) without the requirement of expensive instruments. Also, the reaction is readily monitored during the reaction, which makes it accessible. Once hydrophobic ligands-capped UCNP are obtained, their surfaces are further modified by various kinds of approaches. Here, a brief survey on the main strategies related to polymers are presented, including ligand exchange, layer-by-layer (LbL) assembly, ligand attraction (amphiphilic polymer encapsulation), silica shell assisted coating and mussel-inspired polydopamine (PDA) coating.

For the ligand exchange method (Figure 5a), the underlying principle is the strong coordination interactions between RE metallic ions on the surface and organic groups (such as —C=O, —NH_2 and —SH) in polymers. Hence, polymers with these specific functional groups can be utilized to replace the initially capped ligand, like poly(allylamine) (46), polyethylenimine (PEI) (47), PAA (10, 48-50) and multidentate thiolate-grafting

polymer (51). To enhance the exchange efficiency, polydentate or excess monodentate polymer ligands should be added. In a typical example, Van Veggel and co-workers successfully transferred oleate-stabilized UCNP from toluene to water by ligand exchange (52). First, UCNP were dispersed into a dimethylformamide/dichloromethane (1:1, v/v) solution of PVP. After refluxing at 100 ºC for six hours, OA was successfully replaced by PVP (10,000 Da). Notably, Murray et al. reported a generalized and simple method to replace OA by nitrosonium tetrafluoroborate ($NOBF_4$) (53). After addition of this salt, the resulting UCNP dispersions in DMF are stable for several years without any aggregation or precipitation. Owing to the weak coordination interaction between RE ions and BF_4^-, the surface of UCNP can be further coated with polymer materials, like polypyrrole (PPy) (54) and phosphate-PEG (55). Furthermore, Qian and co-workers prepared hydrophilic polymer brushes grafted UCNP by surface-initiated atom transfer radical polymerization (SI-ATRP) (56). To replace OA with 2-bromo-2-methylpropionic acid (BMPA), excess BMPA was added to a chloroform solution containing UCNP. The experiment was carried out in a relatively mild condition (40 ºC, 2 h). After the replacement of ligand, the anchored BMPA was utilized to initiate *in situ* growth of hydrophilic polymer brushes. The thickness of brushes can be easily tuned from 4 to 11.8 nm by adjusting reaction time. Due to the various choices of monomers, this grafting-from method enriches the family of polymers on the surface of UCNP. It should be mentioned that the drawback of ligand exchange is that the surrounding water may dramatically quench the UCL intensity of UCNP (57, 58).

LbL assembly is a generalized and facile approach utilizing electrostatic interactions to modify substrates. It involves sequential adsorption of oppositely charged polyelectrolytes onto a substrate. (Figure 5b) (48, 50, 59-61). Li et al. designed a fluorescence resonant energy transfer (FRET) system based on UCNP via LBL assembly (62). The as-synthesized ethylenediaminetetraacetic acid (EDTA)-capped UCNP carries negative surface charges at pH 8.5 in an aqueous solution. Then the sequential adsorption of polycations, poly(allylamine hydrochloride) (PAH) and polyanions, poly(styrene sulfonate) (PSS) was performed in aqueous solutions at the same pH. Zeta potential measurements tracked the

surface charge alternations in this process. Finally, biotin was conjugated to UCNP/PAH/PAA/PAH through the cross-linking reaction between carboxylic groups of biotin and primary amine groups on the polyelectrolyte functionalized phosphors. This system was successfully applied to detecting trace amounts of avidin (from 0.5 to 370 nM). The primary advantage for coating surface via LBL assembly is that it permits preparation of coated objects at any size and shape. Moreover, the coated surface is extraordinarily uniform and the thickness of polyelectrolyte layer can be precisely controlled (63, 64).

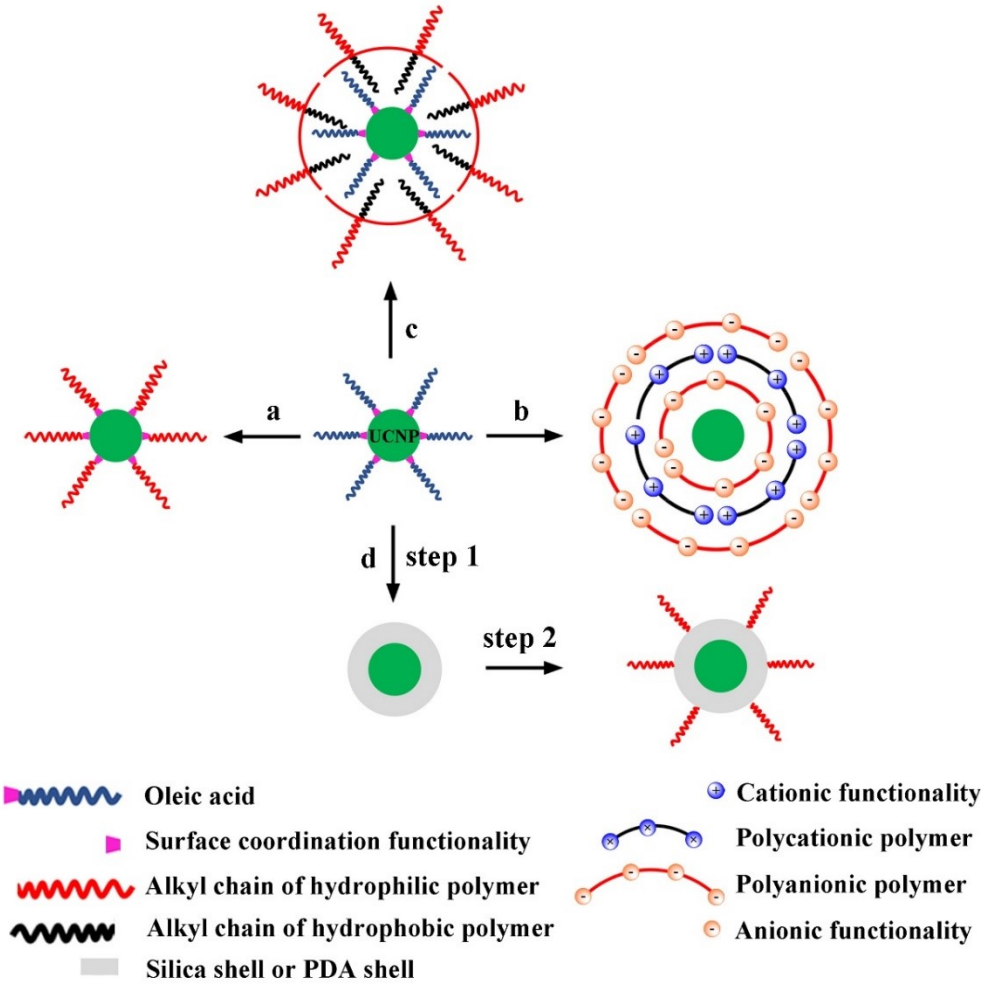

Figure 5. Schematic illustration of the routes for post-modification of oleic acid-coated UCNP with hydrophilic polymers: (a) ligand exchange, (b) LbL assembly, (c) ligand attraction and (d) silica-shell or mussel inspired PDA coating (two-step method).

Ligand attraction is a simple method conferring water-solubility without removing hydrophobic ligands of UCNP (65-72). UCNP can be encapsulated into the hydrophobic domain of polymer micelles through van der Waals forces between water repelling ligands and polymer chains, while the hydrophilic corona ensures water-solubility (Figure 5c). In 2015, Jiang et al. designed and synthesized a NIR light-triggered payloads release platform based on UCNP/photoresponsive polymer composites (73). A novel amphiphilic random copolymer was synthesized with photoremovable moieties as side groups. This polymer was capable of co-assembling with hydrophobic UCNP to obtain core-shell structured micelles. Upon irradiation with 980 nm light, the photocleavage reaction in the hydrophobic domain induced the dissociation of micelles (photocleavage of the N—O bond in side groups resulted in the generation of sulfonic acid groups), resulting in the release of dye molecules (Nile Red). The significant advantage of ligand attraction is the availability of exceptionally stable UCNP and the preservation of photoluminescence property of UCNP (still in the hydrophobic environment) (74). However, one of the most significant shortcomings is the uncontrolled encapsulation of two or more UCNP into one single micelle, resulting in heterogeneity and high UCNP content.

Silica-shell assisted polymer coating represents an important method for decorating UCNP with polymer materials. In a two-step method (Figure 5d), it requires a coating of an amorphous silica layer first onto UCNP followed by a further polymer coating. As is known, surface silanization is also a versatile and facile way to modify NPs (such as Fe_3O_4, QDs and AuNPs) with low cytotoxicity, excellent chemical stability, biocompatibility, and water-solubility (75-78). By modulating the hydrolysis and condensation of silane couple agents (like TEOS and APTES), the thickness of silica can be controlled ranging from a few nanometers to tens of nanometers either by the Stöber process or reverse microemulsion method (79-83). Moreover, the primary advantage of surface silanization is that it offers numerous functional groups (—SH, —NH_2, —$CH{=}CH_2$, etc.) for further modification (drug loading or growth of polymers). Hence, the introduction of polymers can be accomplished either by grafting from or grafting onto approaches (84-86). Lin et al. designed and synthesized a temperature/pH dual-sensitive nanoplatform for drug release

based on UCNP and polymer (86). A uniform mesoporous silica layer ($mSiO_2$) was coated on the surface of UCNP via a microemulsion system. After removal of template surfactant (CTAB), double bonds were introduced into the cavities and surface of UCNP@$mSiO_2$. Then poly[(*N*-isopropylacrylamide)-*co*-(methacrylic acid)] was synthesized by a photo-induced polymerization. By regulating the extension/collapse state of polymer brushes through temperature or pH, the release of antitumor drug doxorubicin exhibited an "on-off" release pattern. It should be noted that the silica shell has excellent optical transparency, thus resulting in very low or undetectable the influence of silica coating on the UCL intensity (87-89).

Mussel-inspired PDA coating is a recently developed coating technique (90). It is reported that PDA can modify most substrates attributed to the auto-oxidation of dopamine at a weak alkaline pH by the dissolved oxygen. Since then, PDA has been widely used in different areas, such as flame retardant nanocoating (91), nanocatalysts (92) and Li-ion batteries (93, 94). Besides PDA exhibits high biocompatibility and water-solubility, which significantly expands its uses in biomaterials areas (95-97). Like silica coating, PDA offers a flexible platform for further modifications owing to the reaction between catechol or quinone moieties of PDA and nucleophiles (such as thiols and amines) (Figure 5d) (98). Recently, Liu et al. designed and prepared nanoplatforms based on PDA coated UCNP for *in vivo* multimodality imaging and chemo-photothermal synergistic therapy (99). Various thickness of PDA (3, 5 and 8 nm) was coated onto the surface of UCNP by a microemulsion system. Then amino-terminated PEG was grafted onto UCNP@PDA by a Schiff base reaction or Michael-type addition. This exceptionally photostable (808 nm, >100 min under 1.3 W/cm^2) PEGylated UCNP@PDA exhibited excellent photothermal conversion capability (200 s from 30 ºC to 50 ºC when doped lanthanide Gd content reached 100 ppm) in aqueous solution. After loading DOX, this new nanoplatform shows the tremendous synergistic interaction between photothermal therapy and the enhanced chemotherapy when combined with 808 nm irradiation. Noteworthy, in comparison with silica coating, thick PDA layer (dark-brown color) may substantially affect the upconversion emissions (particularly in the UV region) due to the strong absorption of PDA

layer (100, 101). Therefore, the thickness of PDA should be carefully controlled in the synthesis. Moreover, anti-oxidation agents may be added as well (101).

Though diverse types of methods are available as listed above, a judicious choice of approach is the key to the success of future applications. When we select a modification strategy, simplicity, controllability and accessibility should be considered. In addition, assisted platforms (silica or PDA) and appropriate use of environment (e.g., aqueous solution) are also relevant (57, 102). In all, whatever the method used, a vital prerequisite for surface coating is the preservation of high upconversion emissions, which is beneficial for their future applications.

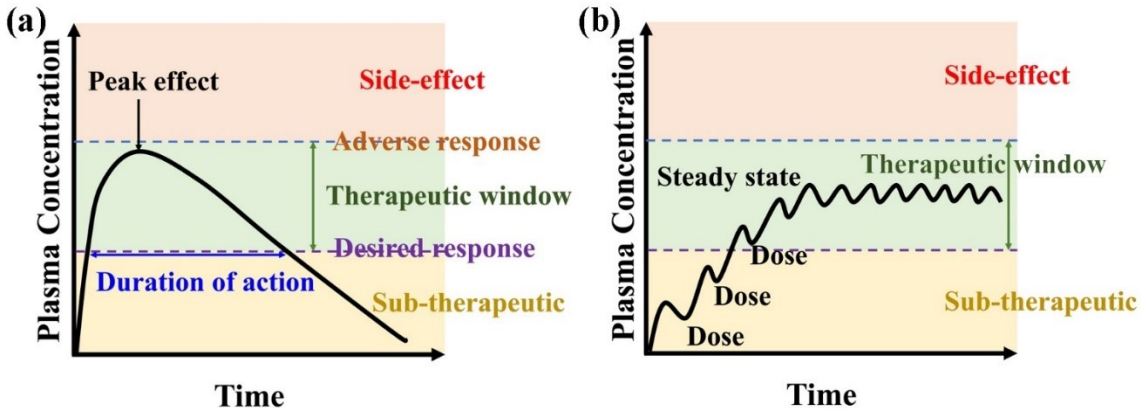

Figure 6. (a) The pharmacokinetic profile of conventional drug formulation. Adapted from [103]. (b) Serval doses are needed to maintain the concentration in the therapeutic window for a longer duration. Adapted from [104].

I.3 Nanovectors based on UCNP/Polymers for NIR Light-Triggered Drug Release

In traditional chemotherapy, anticancer drugs diffuse nonspecifically during biodistribution. To produce a therapeutic response with these drugs, their concentrations in plasma should remain in a proper range defined as the therapeutic window. As shown in Figure 6a, the concertation of drug molecules should be over the minimum effective level (desired-response) to cause therapeutic effect and below the toxic concentration (adverse response) which will put patients in risks (103). Because the anticancer drugs cannot

distinguish the healthy cells and the cancer cells, the level of concentration should always keep a balance between killing cancer cells and sparing the healthy cells. In addition, the patients should retake the medicines to maintain the therapeutic level due to the fast decay of drug concentration as time goes on (Figure 6b) (104), leading to reduced compliance in patients.

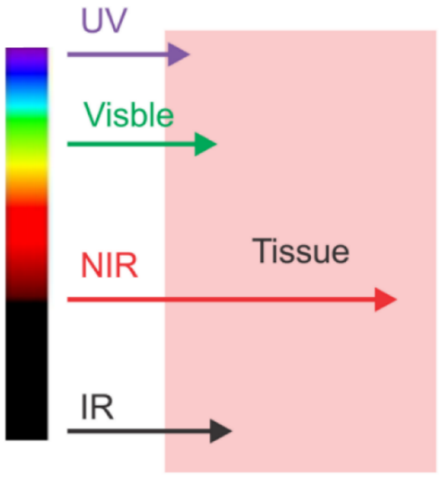

Figure 7. Tissue penetration depth of light with different wavelengths. UV light can only penetrate hundreds micrometer. By contrast, NIR light can deeply penetrate into tissues (several centimeters). Reproduced from [118] with permission.

In contrast to the nonspecifically targeted drug delivery in traditional chemotherapy, nanovectors (<500 nm) have the ability to transfer payloads to the targeted site. They can selectively accumulate in tumor lesions through the enhanced permeability and retention (EPR) effect or conjugation with targeting ligands, resulting in improved pharmacokinetic and pharmacodynamics (105). Development of stimuli-responsive nanovectors allows us to release cargoes in a controllable manner under external stimulation (pH, temperature, light, enzyme, etc.). Though pH- and thermo-sensitive nanovectors are well known, it is difficult for them to become a universal stimulating source because the microenvironment varies from individual to individual (106-109). Furthermore, it is hard to modulate the concentration of chemicals to be within a therapeutic/toxicity range owing to the fixed release profiles at the specific environment. In comparison, light is a preferred stimulus

because it offers spatiotemporal convenience to release species in a non-contact way with remote and instant control, which reduces the possibility of implant complications caused by using a scalpel (110-113). Moreover, the combination of different wavelength of light allows us to achieve multiple complex therapies. Last but not the least, parameters like irradiance, beam diameter, and duration of exposure, are easily adjusted to tune the drug release profiles.

For endowing nanovectors with light-sensitivity, the combination of organic photosensitive chromophores and organic materials is a simple and frequently utilized approach. The reason for using organic materials is that their drug loading capacity tends to be high. Under light irradiation, the photoresponsive moieties in the nanovectors change structure or chemical composition. Noteworthy, the wavelength of the excitation light for biomedical applications is crucial. The photodamage and penetration depth in live organisms should be considered. In the conventional design, UV and visible light are frequently applied but indeed they have poor penetration depth in live bio-tissues and UV light may cause cancer issues particularly for those with chronic diseases (114-117). The tissue penetration by the light of different frequencies is shown in Figure 7 (118). Empirically, the longer the wavelength is, the better the penetration capability and the less the photodamage are. Taking NIR light as an example, it can penetrate deeply in live organisms because its wavelength lies in the “biological transparency window”, which makes it exhibit less absorption and scattering by water and hemoglobin, leading to deep penetration capability and minimal phototoxicity (119). However, the majority of photoresponsive moieties do not absorb NIR light directly. Traditionally, this issue can be resolved by simultaneous two-photon absorption (TSA) of chromophores (120, 121). This non-linear optical process allows us to excite a molecule from the ground state to high electronic state with the absorption of two photons (identical or different frequency). However, this process requires exceptionally high excitation power density (range from 10^6 to 10^9 W/cm^2) due to small TSA cross-sections. Moreover, this ultrahigh power density very often kills cells (boiling). Another promising solution is using UCNP as transducers to convert NIR light into UV light or visible light for initiating photoreactions. The primary advantage is that their

excitation power density (<10^3 W/cm^2) is many orders of magnitude lower than that of TSA. This distinct property allows inexpensive diode lasers to induce photoreactions.

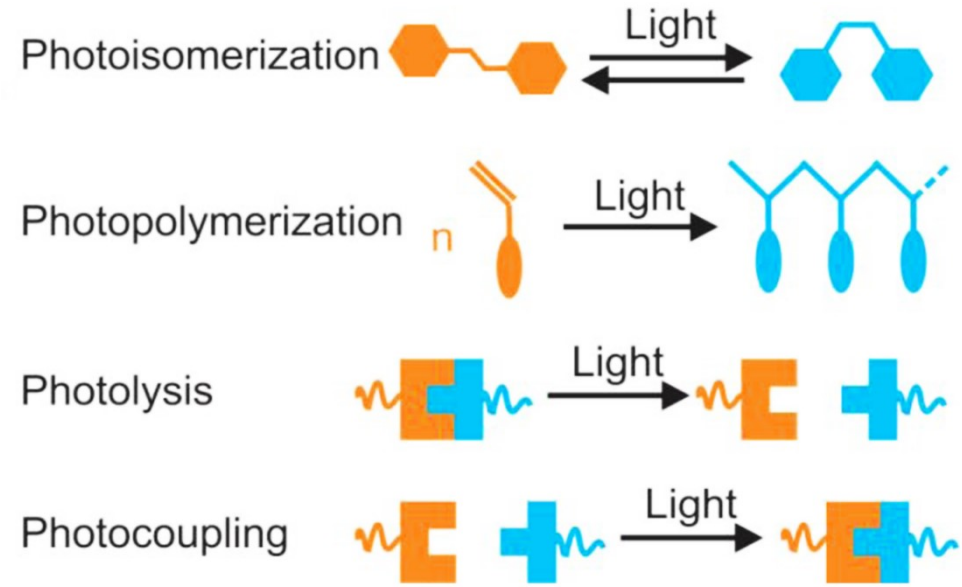

Figure 8. Four types of UCNP-assisted photoreactions. Reproduced with permission from [118].

Up to now, UCNP have been applied to initiate photoreactions, such as photoisomerization, photopolymerization, photolysis and photocoupling (Figure 8) (118, 122-126). Among them, UCNP-assisted photolysis reactions have been widely employed for numerous applications, like the patterning of biomaterials (127), cell adhesion (126) and siRNA release (128). In these systems, *o*-nitrobenzyl (ONB) alcohol derivatives are the most frequently used organic photolytic chromophores (80, 115, 129, 130). Because these ONB derivatives, as photolabile groups, have been well-studied and readily available (131, 132). The cleavage mechanism is based on the photo-induced isomerization of ONB into *o*-nitrosobenzaldehyde (Figure 9) (132). Their absorption band of ONB groups (280-360 nm) overlaps with the upconverted UV emissions from Tm^{3+}-doped UCNP. In a system comprised of Tm^{3+}-UCNP and ONB photolytic chromophores, the cleavage reaction can be triggered by the NIR light.

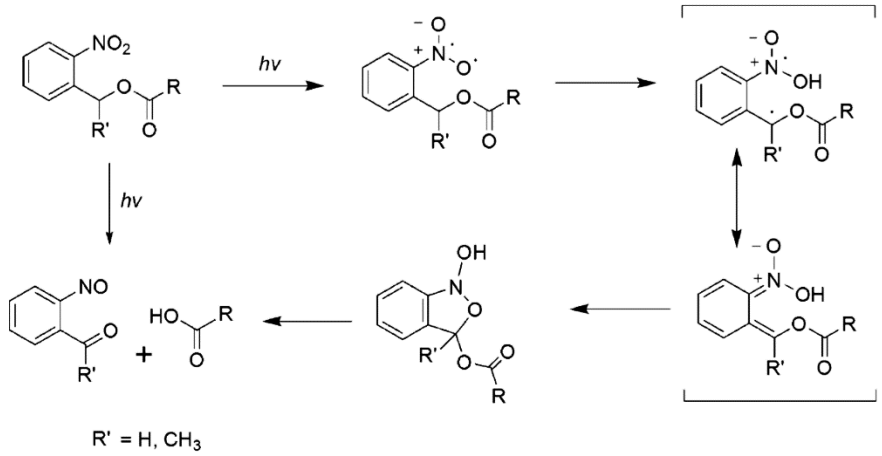

Figure 9. Photoisomerization mechanism of *o*-nitrobenzyl alcohol derivatives into an *o*-nitrosobenzaldehyde, releasing a carboxylic acid. Adapted with permission from [132].

Constructing NIR light-sensitive nanovectors with UCNP and polymer materials for drug delivery has generated intense interest in the past seven years. These elaborately designed generally include three parts: UCNP, polymers and payloads. As a core component, Tm^{3+}-doped UCNP are commonly used with the capability of emitting UV and visible lights upon NIR light irradiation (980 nm). In general, the UV upconversion photons are used to initiate photoreactions and the visible upconversion emissions are employed for fluorescence imaging. As for polymer materials, they can be hydrophilic ones, amphiphilic random or diblock copolymers, or nanogels prepared by various polymerization techniques. In most cases, they possess light-sensitivity by incorporating organic photosensitive units. So far, numerous types of payloads (drug molecules, siRNA, large biomolecules, etc.) have been encapsulated into the structures of nanovectors with UCNP and polymers. After assembling these three parts, the release of cargos is always caused by UCNP-assisted photoreactions of photocaged drug molecules or photoresponsive polymers.

Regarding the ways for incorporating cargos, these nanovectors are broadly classified into two categories. One is that guest molecule is conjugated to nanovectors through covalent bonding. The other is that payloads are entrapped into nanovectors through non-covalent interactions. In the following sections, a brief survey of them is presented.

I.3.1 Covalent Conjugation of Payloads with UCNP/Polymer Nanovectors

In this category, guest molecules are linked into the structure of nanovectors (UCNP/polymer) through chemical modifications. The significant advantage is that the amount of drug in these nanovectors can be precisely tuned. Noteworthy, drug molecules must keep their therapeutic effect during chemical modifications. Upon exposure to NIR light, UC photons are utilized to induce cleavage of anchor points, resulting in the release of active drugs. Two typical examples are given in this section regarding the position of payloads in the structure of nanovectors.

Payloads can be covalently bonded to UCNP (133-135). Rubio-Retama et al. designed a nanovector based on PEGylation of SiO_2-coated UCNP (Figure 10) and the investigation of their toxicity was carried out at the cellular level (135). The hydrophilic polymer chains, PEG_{5000}, were grafted onto the SiO_2-coated UCNP. Then a potent cytotoxic drug, doxorubicin (DOX), was covalently attached to the surface with a photolabile group of an *o*-nitrobenzyl alcohol molecule. In the absence of the NIR light stimulus, these NPs exhibited little cytotoxicity to Hela cells. By contrast, upon NIR light irradiation, the active drug molecules cleaved from these NPs dramatically reduced the cells viability.

Payloads can also be integrated into the structure of polymers (13, 136, 137). As shown in Figure 11, Liu and co-workers designed and synthesized a multifunctional nanovector (combination of chemotherapy and PDT) based on conjugated polyelectrolyte encapsulated UCNP (137). First, the chemotherapeutic drug, DOX, was covalently linked to a conjugated polyelectrolyte (acting as a surface coating agent and photosensitizer) through a UV-cleavable ONB linker. Then this polyelectrolyte and OA-capped UCNP were assembled through ligand attraction. The UV and visible upconversion emissions emitted by UCNP were utilized to control DOX release and initiate the polymer photosensitizer to generate reactive oxygen species (ROS), respectively. In comparison with the control group, their results showed that the combination therapy upon 980 nm irradiation could exhibit enhanced inhibition of cell growth.

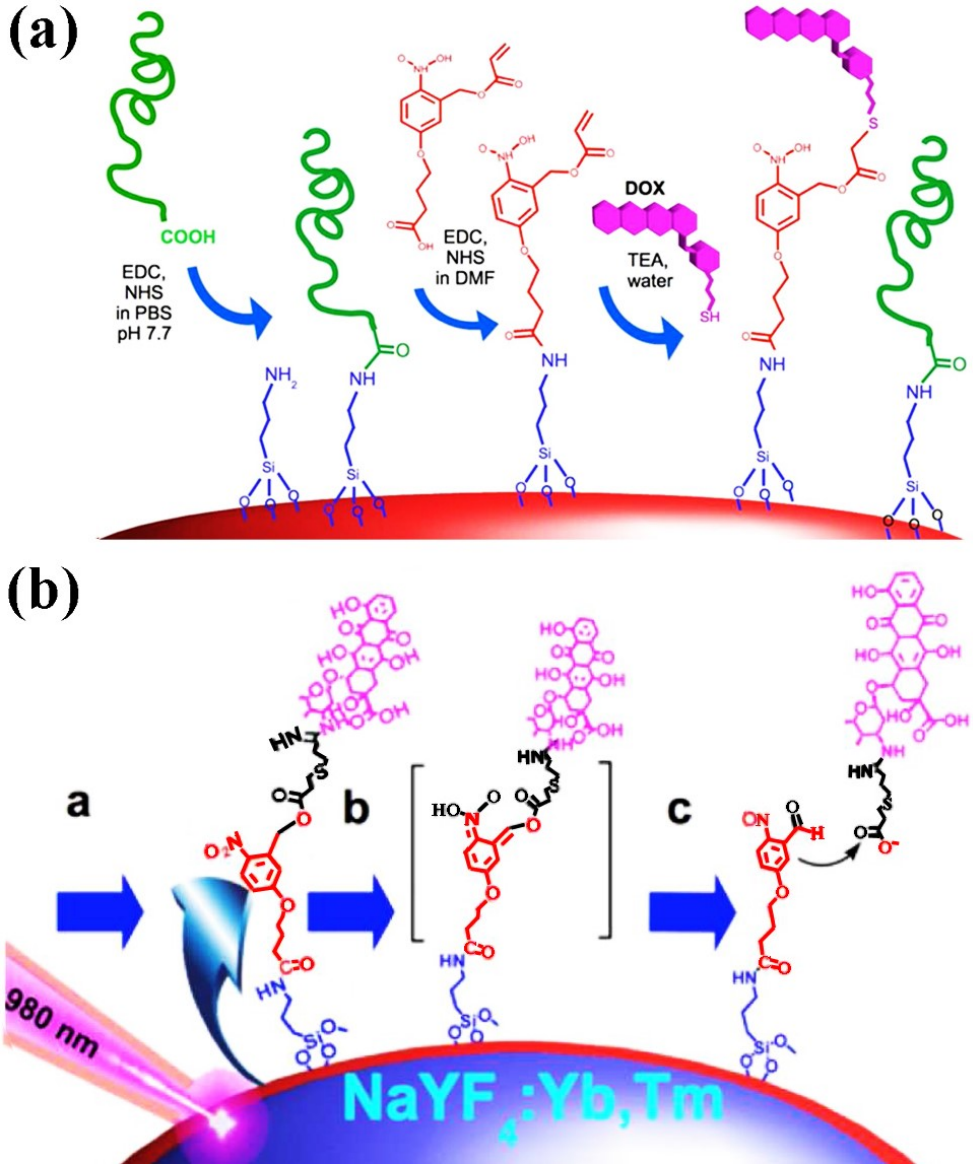

Figure 10. (a) Surface modifications of SiO_2-coated UCNP for incorporating hydrophilic polymer chains with drug molecules. (b) The initiation of the release of drug molecules under 980 nm light irradiation. Reproduced from [135] with permission.

Despite the appealing features, the weakness of utilizing covalent bonds to connect drug molecules is that it involves complicated chemical modifications and multistep procedures. In addition, the chemical modifications must not affect the therapeutic effect of drugs.

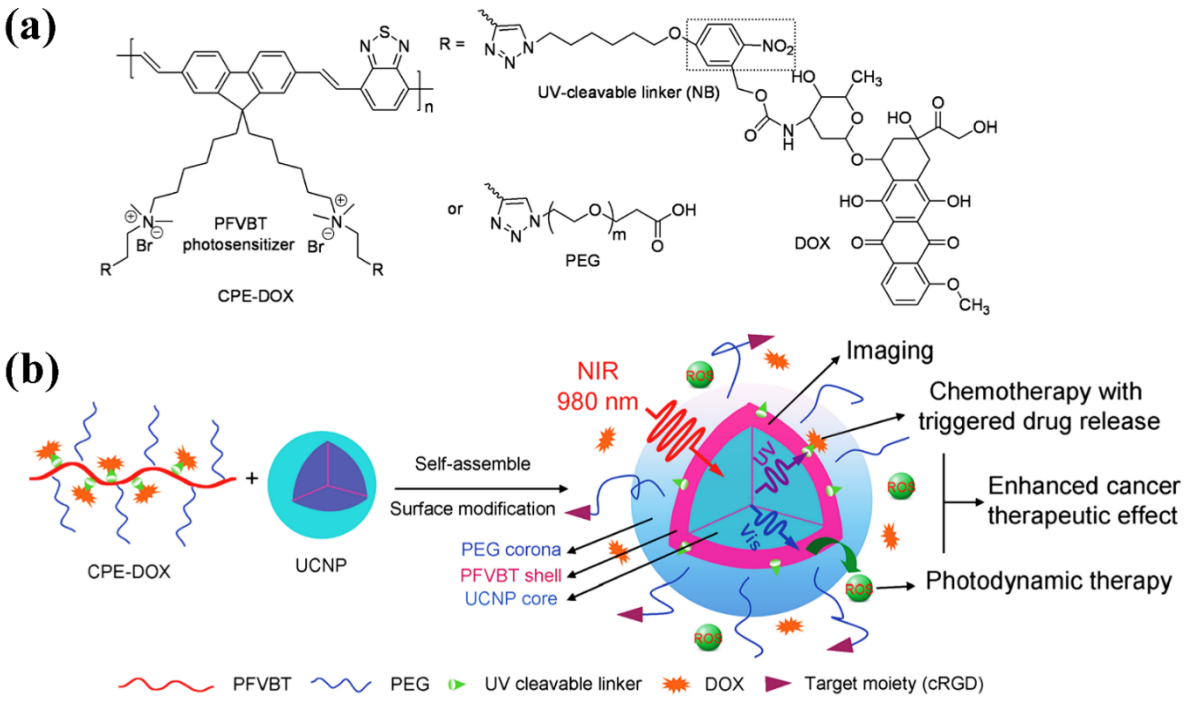

Figure 11. (a) Chemical structure of the designed conjugated polyelectrolyte. (b) Schematic illustration of 980 nm light regulated initiation of the photosensitizer to generate ROS for PDT and DOX release for chemotherapy. Reproduced from Ref. [137] with permission from The Royal Society of Chemistry.

I.3.2 Non-covalent Conjugation of Payloads with UCNP/Polymers Nanovectors

In contrast to the former type of nanovectors, the introduction of payloads using non-covalent bonds avoids the time-consuming and costly chemical synthesis. In some cases, the preparation of nanovectors can be accomplished in one step when the surface coating of hydrophobic UCNP is not required. Also, a series of photoresponsive polymers can be synthesized to endow NIR light-responsivity with nanovectors. As depicted in Figure 12, upon the absorption of UC luminescence, the release of payloads can be initiated by the photoreactions of photoresponsive polymers, such as the shift of hydrophobic-to-hydrophilic balance, cleavage of junctions and main chain degradation. To

simplify the classification of nanovectors in this category, we divide them into two parts according to whether hydrophobic UCNP are decorated or not.

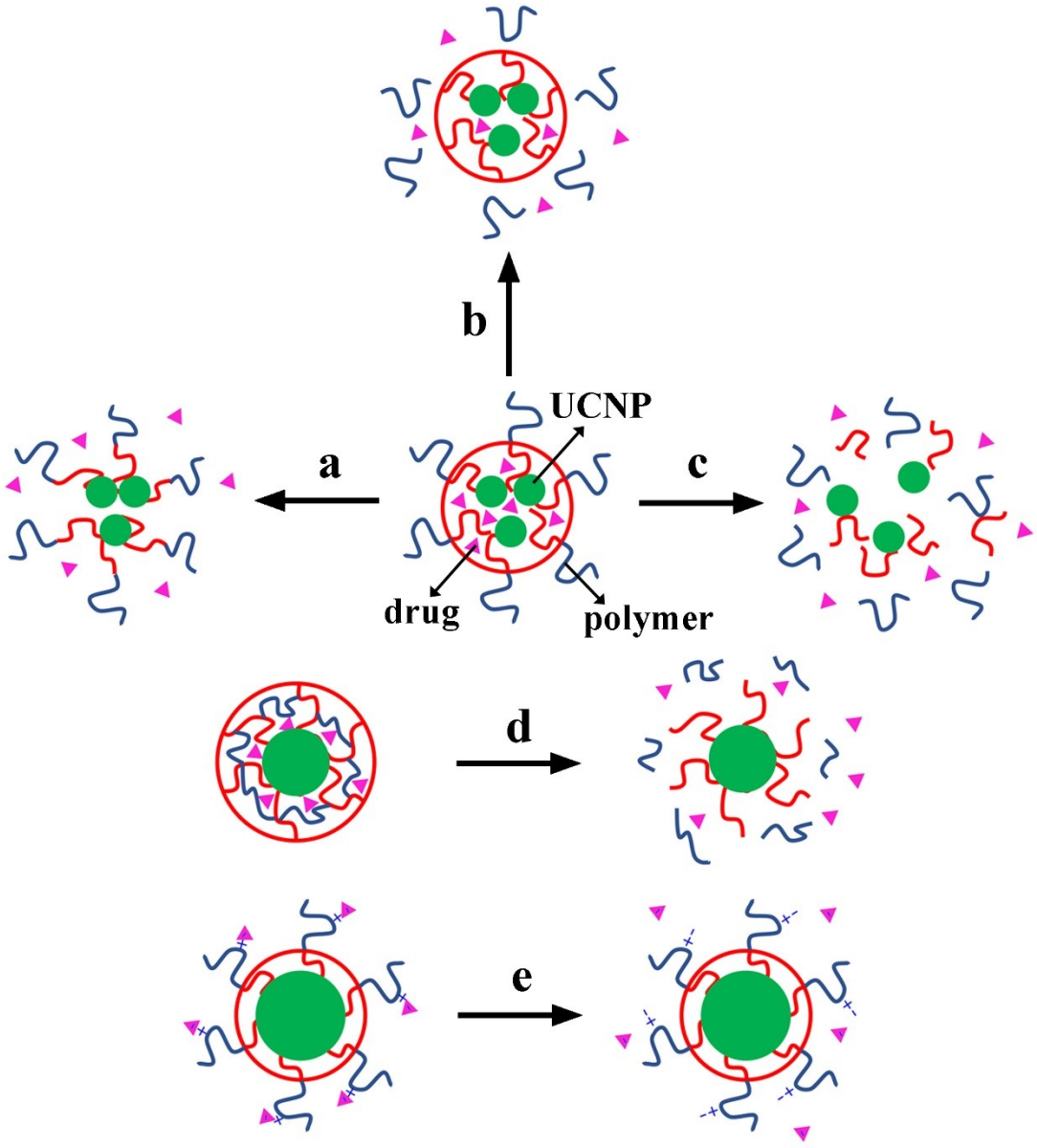

Figure 12. Schematic illustration of drug release mechanisms from nanovectors based on UCNP-assisted photoreactions of photoresponsive polymers: (a) shift of hydrophobic-hydrophilic balance, (b) cleavage of junctions, (c) main chain degradation, (d) gel-sol transition and (e) variation of surface charge.

I.3.2.1 Integration of hydrophobic UCNP with photoresponsive polymers for nanovectors

In this category, the as-synthesized hydrophobic UCNP are not required for surface functionalization. Hence, ligand attraction is commonly used to assemble the NIR light-responsive nanovectors. As a typical example, our group designed a UV-sensitive polymer micelle system containing UCNP and demonstrated that the release of nile red (NR) could be initiated by a CW 980 nm diode laser (Figure 13) (138) . The as-synthesized diblock polymer was utilized to encapsulate NR together with UCNP into the core of micelles by ligand attraction in one step. Specifically, a tetrahydrofuran (THF) solution of UCNP, polymer and NR was dropwise added into water. Owing to van der Waals forces among ligands of UCNP, NR molecules and hydrophobic blocks of polymer, OA-capped UCNP and NR tended to be entrapped in the core of polymer micelles. When the resulting micellar solution was exposed to 980 nm light, the UV upconversion emissions caused a hydrophobic-to-hydrophilic shift of the photoresponsive polymer, resulting in the dissociation of micelles and thus release of cargos. Using this concept, amphiphilic random copolymer (139), amphiphilic diblock polymer (140, 141) and polypeptide copolymer (129, 142) have been employed. Moreover, their release mechanisms are either a photo-induced shift of hydrophobic-to-hydrophilic balance or photocleavage of block junctions.

Notably, the release of payloads can also be caused by depolymerization of the photoresponsive polymer triggered by UV upconversion luminescence. In 2013, Almutairi's group presented the first example related to this mechanism by loading UCNP into the sophisticated design of polymeric nanoparticles (Figure 14) (143). The hydrophobic UCNP and a hydrophobic model drug (coumarin 153) were encapsulated into a light-sensitive polymer (biomaterial) capsules using a single-step electrospray process. Under 980 nm excitation with low power, UV photons emitted by UCNP induced the degradation of polymer nanoparticles leading to the release of coumarin 153.

Recently, the release of siRNA from a UCNP/polyelectrolyte nanovector was realized by modulating surface charges by UV upconversion emissions as shown in Figure 15 (144). Combining the siRNA release with PDT, Fan and co-workers developed a nanoplatform based on a charge-variable conjugated polyelectrolyte (CPE) and UCNP. First, CPE was utilized to encapsulate hydrophobic UCNP by the ligand attraction method. Then siRNA was attached to the nanoplatform by the electrostatic interactions. Under 980 nm irradiation, the siRNA was released from this nanosystem owing to the conversion of positively photoremovable side-chains in CPE into zwitterionic groups.

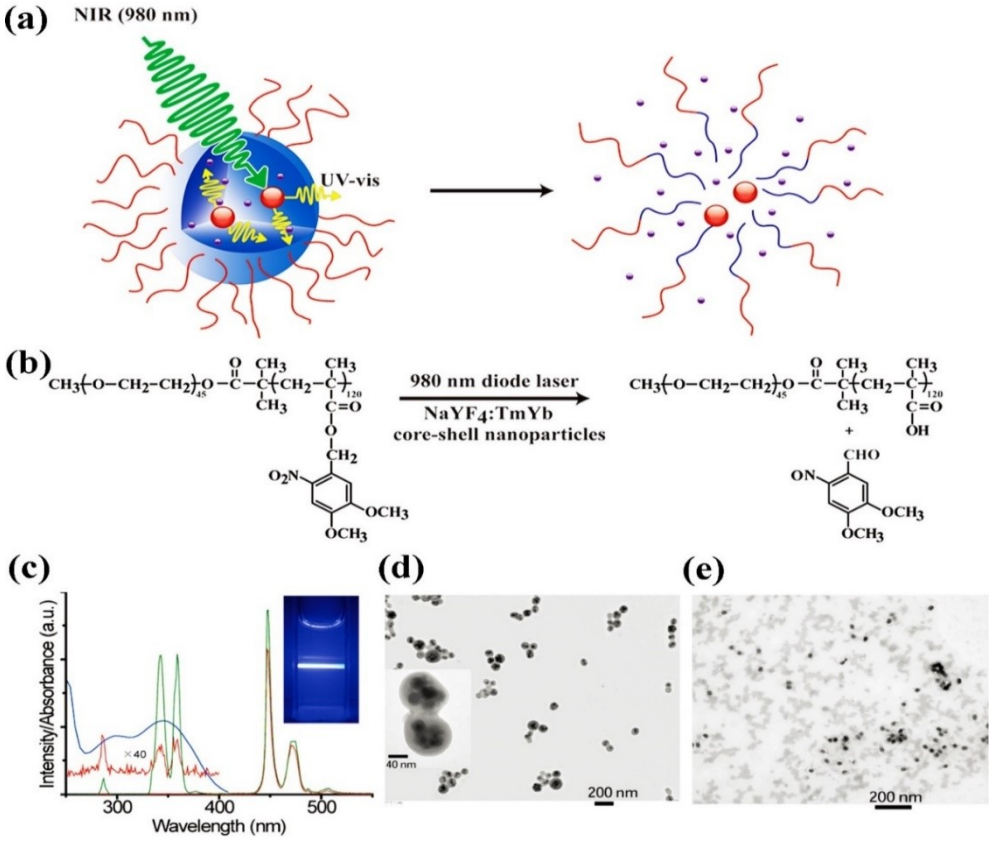

Figure 13. (a) Schematic illustration of using 980 nm light to trigger dissociation of polymer micelles. (b) Photolysis reaction of the polymer. (c) UV-vis spectra of resulted micelles and UCL spectra of UCNP and micelles. TEM images of micelles before (d) and after (e) NIR light excitation. Reprinted with permission from [138]. Copyright (2018) American Chemical Society.

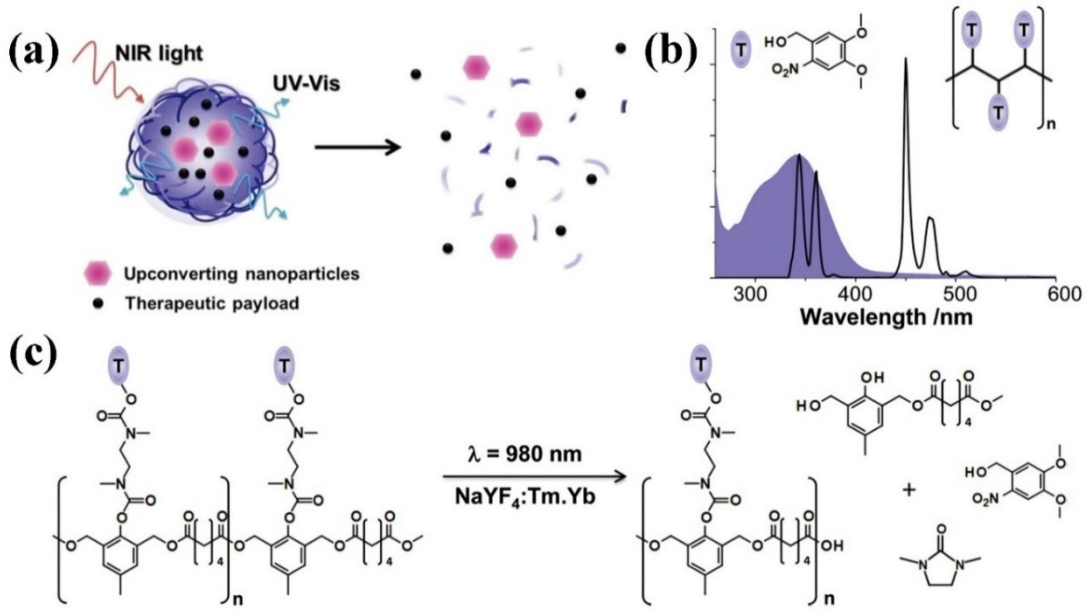

Figure 14. (a) The degradation of light-sensitive nanoparticles after absorbing UC luminescence and simultaneously initiating the release of guest molecules. (b) UV-vis spectra of light-sensitive nanoparticles and UCL spectra of neat UCNP. (c) Photodegradation mechanism of photoresponsive polymers. Reproduced with permission from [143].

I.3.2.2 Integration of surface-modified UCNP with photoresponsive polymers for nanovectors

During the preparation process of these nanovectors, the steps for modifying UCNP should be performed. So far, diverse types of materials, like mesoporous silica layers and polymer materials, have been utilized to decorate UCNP.

Cerruti and co-workers designed and synthesized a nanoplatform (Figure 16) for NIR imaging and on-demand drug delivery based on photocleavable hydrogel coated UCNP (145). A SiO_2 layer (~10 nm) with epoxide-terminated groups was coated onto UCNP by a reverse emulsion method. Then chitosan (CH), a biomaterial, was grafted onto UCNP@SiO_2 through the reaction of the epoxy groups and the amine groups in CH. The remained amine groups further reacted with the succinimidyl groups in the photocleavable

cross-links. Taking advantage of the interaction between flexible CH chains and FITC-BSA, these large biomolecules were entrapped inside before completing the cross-linking reactions to form a hydrogel. By design, the upconversion emissions from UCNP were used to cleave the cross-linked hydrocarbon chains, simultaneously liberating entrapped FITC-BSA.

In 2015, Lu and co-workers designed and synthesized a NIR light-triggered drug release system (DDS) based on polymer/mesoporous silica coated UCNP (Figure 17) (146) . The photoresponsive amphiphilic copolymer was synthesized by free radical copolymerization. To modify UCNP, a mesoporous silica was coated (UCNP@MSN) and utilized to encapsulate the anticancer drug (DOX) into its cavities. To facilitate their integration by ligand attraction, UCNP@MSN was further functionalized with long alkyl chains. When irradiated by 980 nm, the release of drug molecules was initiated because of the isomerization reaction in polymer's side groups, which turned the hydrophobic spiropyran into the hydrophilic merocyanine.

As depicted in Figure 18, Gong et al. designed and synthesized UCNP-based polymer micelles for multiple purposes (chemotherapy, PDT and imaging) (147). By ligand exchange, the surface ligand of OA-capped UCNP was replaced by 2-aminoethyl dihydrogen phosphate to give amine-terminated UCNP (UCNP-NH_2). Then the photosensitizer, Rose Bengal (RB), was introduced by the esterification reaction between UCNP-NH_2 and RB hexanoic acid. Afterward, the light-sensitive amphiphilic diblock copolymer was grafted onto the nanoplatform through an azide-alkyne cycloaddition reaction. The upconversion emissions from UCNP were utilized for three purposes. First, the UV lights could initiate hydrophobic-to-hydrophilic transition of the micelle core, resulting in the release of the hydrophobic drug AB3 (a histone deacetylase). Second, the 540 nm visible light was used for the generation of $^1O_2$ for PDT. Third, the light of 650 nm in wavelength was devoted to fluorescence imaging.

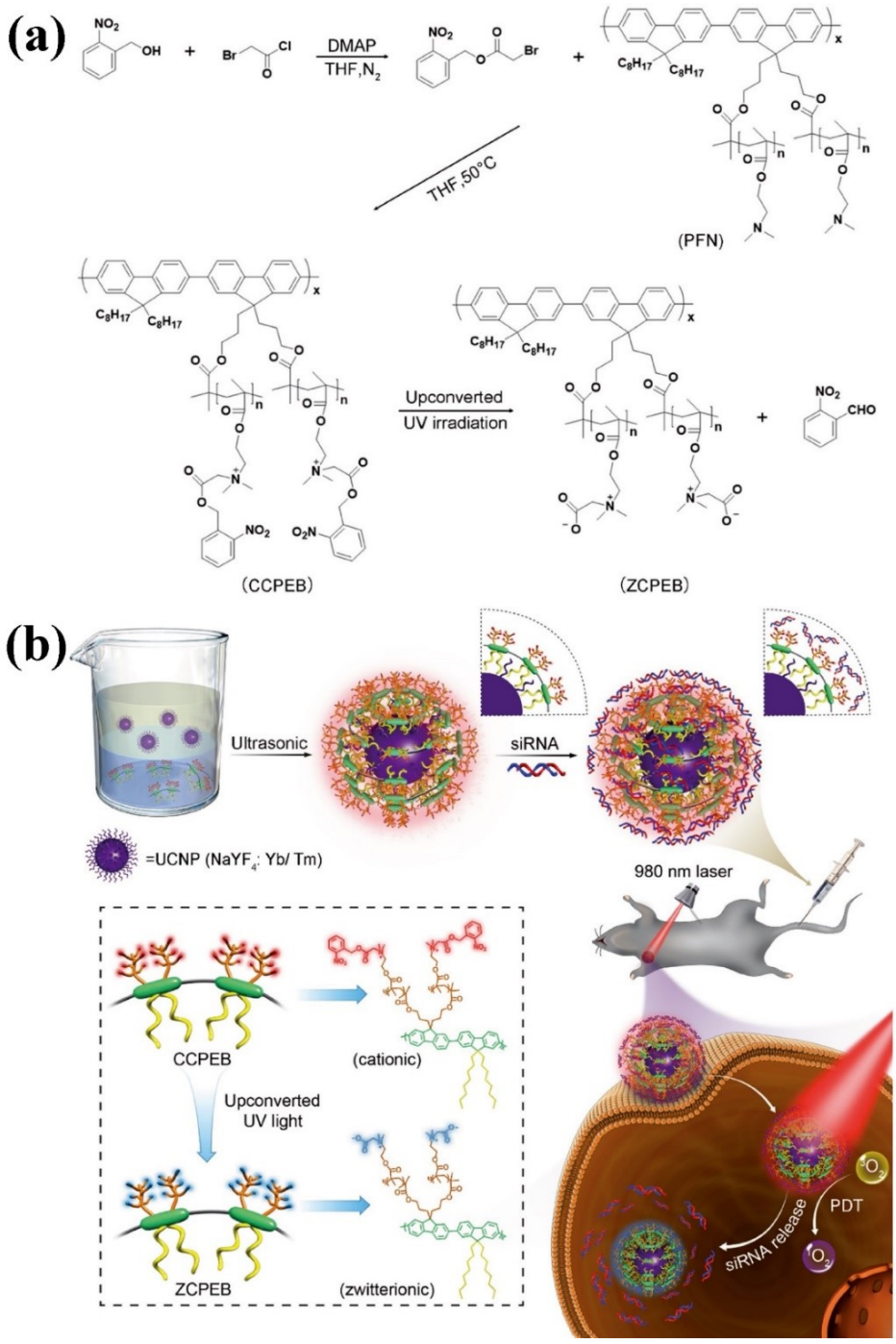

Figure 15. (a) Synthesis route of designed polyelectrolyte and its photolytic process. (b) Schematic illumination of the nanotherapeutic system for combing PDT with siRNA therapy. Reproduced with permission from [144].

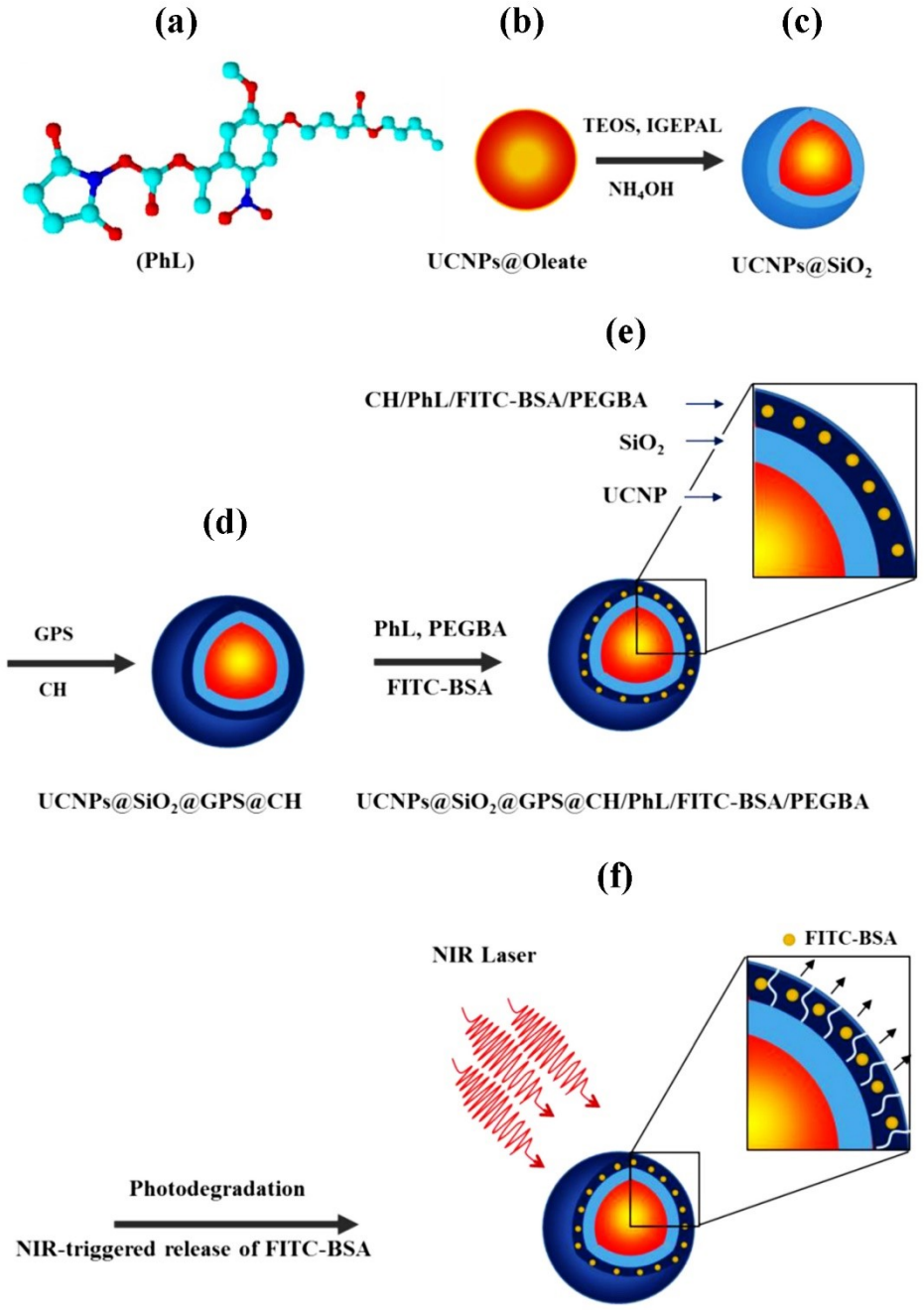

Figure 16. (a) Chemical structure of the photocleavable cross-linker (PhL). (b) Oleate-capped UCNP. (c) UCNP@SiO_2. (d) (3-glycidyloxypropyl) trimethoxysilane and chitosan (CH) modified UCNP. (e) Encapsulating FITC-BSA inside the CH shell and formation of hydrogel-coated UCNP. (f) NIR light-triggered photodegradation of hydrogel and thus drug release. Reproduced with permission from [145].

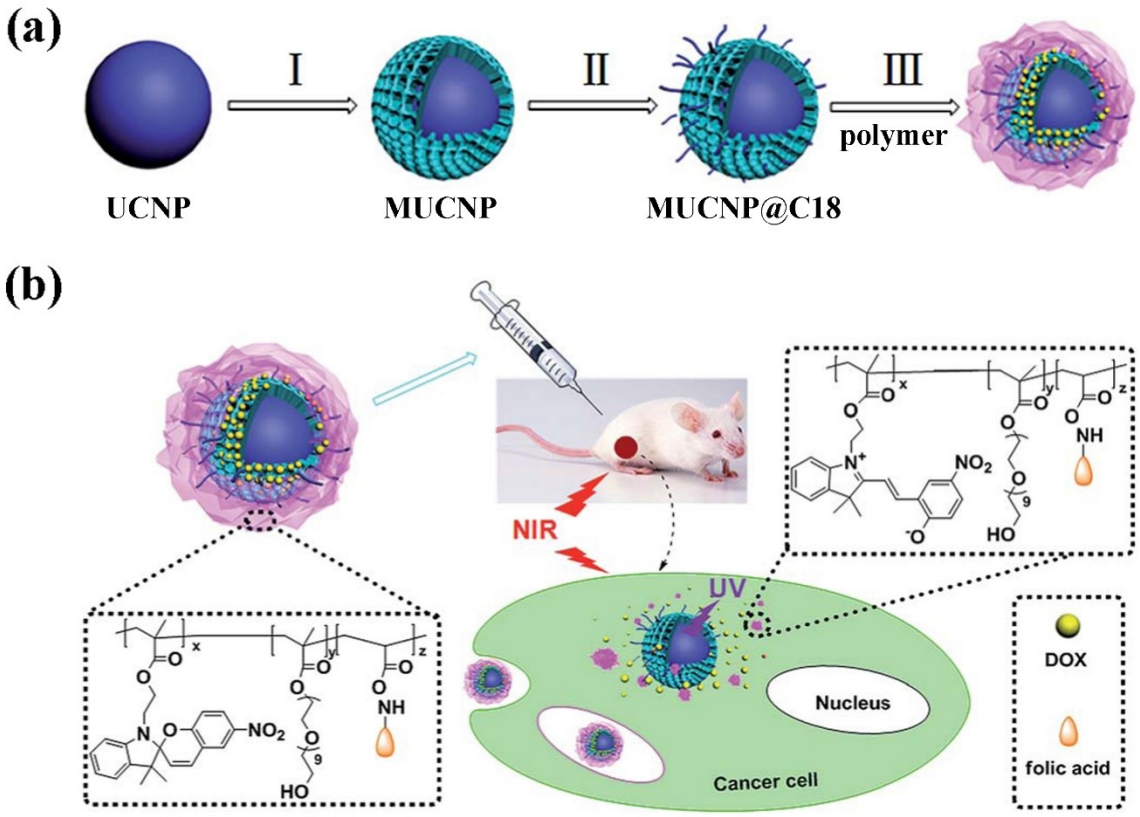

Figure 17. (a) Synthetic route: (I) TEOS and CTAB for coating mesoporous silica layer, (II) the introduction of long alkyl chains, (III) DOX loading and self-assembly. (b) Schematic illustration of multifunctional nanocomposites and NIR light-initiated drug release. Reproduced from Ref. [146] with permission from The Royal Society of Chemistry.

I.4 Preparation of Thin Films with UCNP by LbL Assembly

In addition to the aforementioned UCNP/polymer combinations in the form of nanoparticles, the fabrication of UCL thin-films also has great interest due to their broad applications including multilayer optical storage disks (148), photoluminescence screens for optically written displays (149), and photovoltaic cells (150). Increasingly, UCL films are fabricated by directly using UCNP with high upconversion luminescent property, which avoids heat treatment in the postdeposition step and makes the luminescence properties more predictable (151). Hence, it is desired to find a generalized and robust approach to

building them. Among the methods for preparation of films, LbL assembly has many merits, such as the possibility of all-aqueous processing, easily controlled thickness and the acquisition of stratified films (152-157). As motioned in section **1.2.2**, the LbL assembly has been utilized to coat UCNP (particulate substrates) with multilayer polyelectrolytes. Through the electrostatic interactions, it will be easy to prepare multilayers (planar substrate) with UC nanocrystals. So far, in fact, only a few works have been published regarding the utilization of LbL assembly for fabricating these hybrid membranes (158, 159).

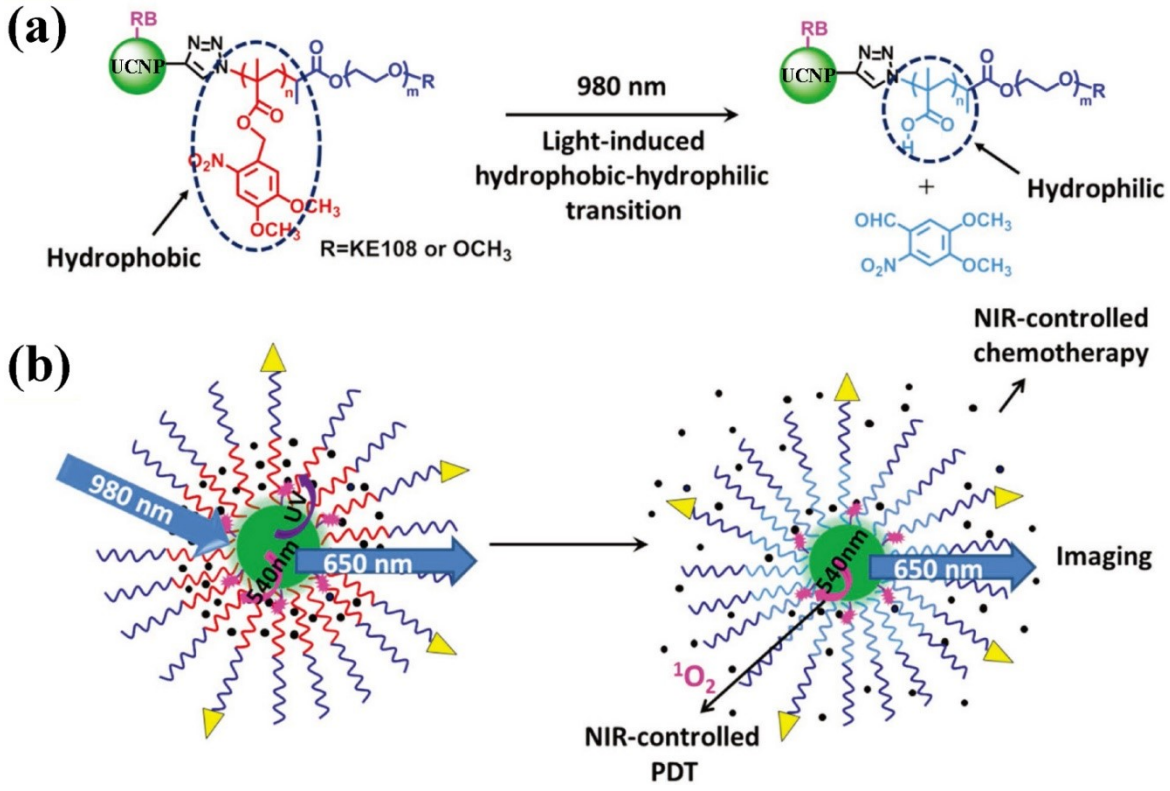

Figure 18. (a) Schematic illustration of the NIR light-triggered hydrophobic-to-hydrophilic transition of polymer chains. (b) An illustration of NIR-controlled combination chemotherapy, PDT and imaging. Reproduced with permission from [147].

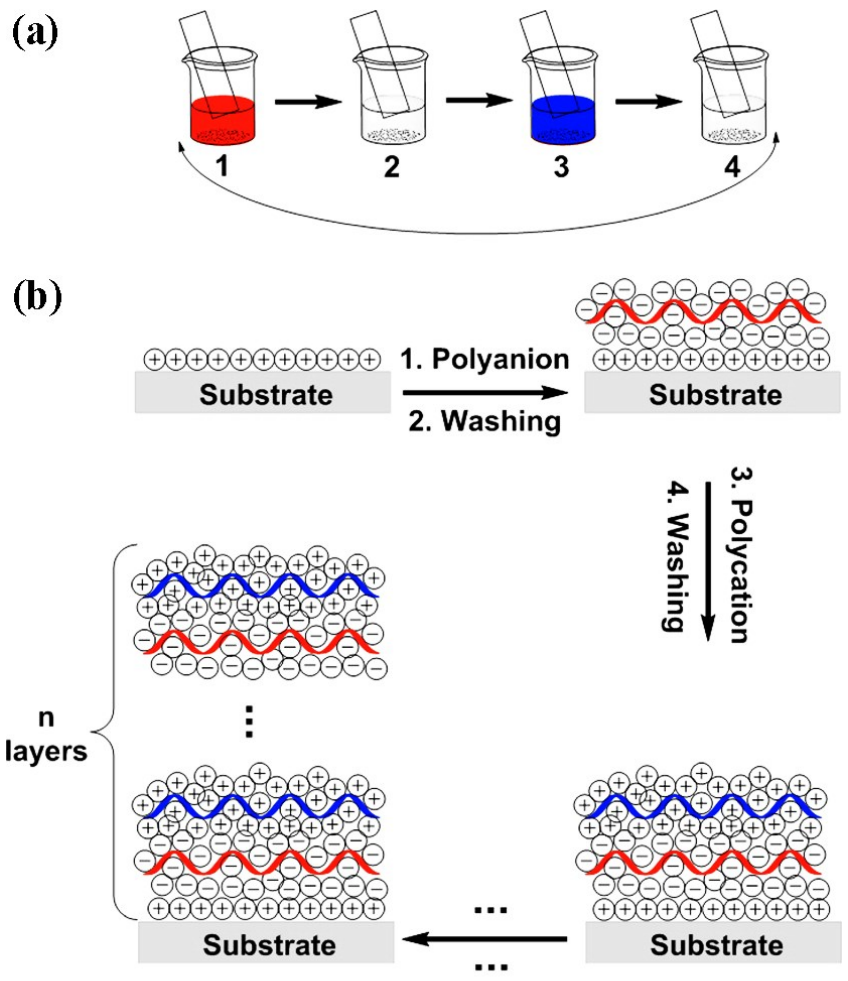

Figure 19. (a) Schematic illustration of immersive LbL assembly on a planar substrate. (b) The charge characteristics of the films after deposition step. Reproduced with permission from Ref [160].

The LbL assembly can be performed in different ways, like dip coating or immersive assembly, spin assembly and spray assembly (152). Among them, immersive assembly, one of the conventional LbL assembly methods, receives broad interest because of ease of handling and no requirement of the complex instrument. In a typical experiment, only beakers, aqueous solutions of oppositely charged polyelectrolytes and substrates are needed. As depicted in Figure 19, a planar substrate (like glass or quartz) is coated with multilayer

films by alternating deposition of oppositely charged polyelectrolytes with washing steps between them (160). As an example, first, poly(styrene sulfonate) (PSS) bearing negative charges and poly(allylamine hydrochloride) (PAH) carrying positive charges are dissolved into aqueous solutions, respectively. Then in a coating cycle (step 1 to 4), a substrate with positive charges is firstly immersed in the solution of PSS to deposit one polyanion layer onto the surface by electrostatic interaction. After the removal of excessive PSS with a washing step (step 2), this substrate is put into the PAH solution to coat a layer of polycation (step 3). Lastly, one cycle is ended with a rinse step (step 4). This cycle makes the positively charged substrate lie the outmost layer. When the coating cycle is repeated, a substrate with multilayer polyelectrolytes films will be prepared.

I.5 Objectives of the Thesis

The primary objective of this thesis is to propose and investigate novel approaches for the preparation of UCNP/polymer hybrid materials and expand their applications. To this end, we try to adopt a bottom-up strategy and utilize block copolymer self-assembly and electrostatic interactions to design NIR light-responsive nanovectors with UV-labile polymers and UCNP. In addition, we would like to study new ways to prepare thin films with spatially organized UNCP in polymer matrices. Hence, following an introductory chapter, our research works are presented in three chapters in the thesis.

In the first study, we put forward a bottom-up strategy to prepare a type of nanovectors for NIR light-responsive drug release through in situ growth of a UV-sensitive diblock copolymer. The aim of this project is to obtain polymer-coated UCNP nanovectors uniform in size (with low polydispersity) and exhibiting NIR light-controlled drug release. During the preparation process, UCNP is first coated with a thin silica layer to maintain their intense upconversion luminescence in aqueous solution. Then the polymer and UCNP are linked through covalent bonding, which is beneficial for their stability even at high dilution. With this study, we also try to answer three fundamental questions: (1) whether or not UV photons emitted by single UCNP loaded in the micelle-like core are enough to regulate

drug release, (2) whether or not the coated block copolymer self-assembly affects the photoluminescence property of UCNP, and (3) whether or not the photolysis reaction of polymers breaks the integrity of the nanovector system. Owing to the biocompatibility of the selected polyether and near monodispersity of the resulting nanovector, the demonstrated design of UCNP/polymer nanovector deserves further exploration for biomedical applications.

In the second study, we present a facile and robust approach to fabricating a NIR light-controllable payload release nanovector by combing UCNP with a UV-labile polyelectrolyte through electrostatic interactions. The strategy described is different from that in the first one, but it allows us to build NIR-sensitive nanovectors with high uniformity and flexibility as well. By design, the UCNP surface is charged with opposite sign to the UV-cleavable polyelectrolyte, so that they can self-assemble through electrostatic interactions. For the encapsulation of charged drug molecules, our hypothesis is that they can be loaded in the co-assembly process of UCNP and polyelectrolyte. In this project, one of the significant challengings is to obtain well-controlled architecture of nanovector, which requires the preparation of surface-modified UCNP with high uniformity before polyelectrolyte added. Moreover, the amount of polyelectrolyte added also is another crucial parameter which may affect the stability, drug loading capacity, and drug release behavior of the resulted nanovector. We hope to modulate the electrostatic equilibrium of the resulting nanovector by NIR light-triggered photochemical reaction, leading to the release of guest molecules. Our designed UCNP/polyelectrolyte nanovector also deserves further exploration for biomedical uses due to the biocompatibility, non-toxicity of the used building blocks (UCNP, mesoporous silica, and hydrophilic polyether chains).

In the third study, we try to combine the LbL assembly with UCNP to fabricate UCNP/polymer hybrid thin films. We believe that these NIR-responsive thin films can be exploited for NIR light-triggered drug delivery using thin films as patches in our future works. The preparation of these thin films is completed at room temperature by dipping planar substrate into aqueous solutions of polyelectrolytes. Through this way, the thickness

of multilayer UCNP membrane should be easily tuned by the deposition times, which may endow the obtained films with better predictability in their photoluminescence property. Moreover, we hope to achieve the spatial organization of UCNP and plasmonic gold nanoparticles in polymer thin films by controlling their deposition sequences. The optical property of the resulted thin films will also be investigated.

I conclude my thesis with a general discussion and provide a few ideas that are worthy of pursuing as future works.

CHAPTER 1 NEAR-INFRARED LIGHT-TRIGGERED DRUG RELEASE FROM UV-RESPONSIVE DIBLOCK COPOLYMER-COATED UPCONVERSION NANOPARTICLES WITH HIGH MONODISPERSITY

1.1 About the Project

Synthesizing ultraviolet (UV)-sensitive polymers which undergo either charge conversion or isomerization or band cleavage after absorbing high energy photons emitted by upconversion nanoparticles (UCNP) has been widely used to build near-infrared (NIR)-sensitive nanovectors. The methods for preparing these novel nanovectors can be divided into two categories according to whether the surface of UCNP is modified or not during the preparation process. For those without surface-modified UCNP, nanovectors can be prepared by amphiphilic polymer assembly in one step. Despite its simplicity, the obtained nanovector often encapsulates two or more hydrophobic UCNP in the single micellar core, resulting in heterogeneity and a low utilization ratio of UCNP. As for others, like the surface coating of UCNP or the introduction of photocaged drug molecules into the polymer structure, they involve multi-step chemical modifications, which makes the preparation process complicated and demanding. To address the scarcity of the methodologies for preparation of polymer-functionalized UCNP with well-controlled architecture (one UCNP encapsulated in single micelle), in this chapter, we present a study that adopts a bottom-up strategy to build nearly monodisperse nanovectors based on in situ growth of UV-sensitive polymers on the surface of UCNP through covalent bonding. By design, upon 980 nm light excitation, the UV upconversion emissions of UCNP can be absorbed by the UV-sensitive blocks, which induces the photocleavage reaction and, consequently, shifts the hydrophobic-hydrophilic balance of this blocks towards destabilization of UCNP surface micelles and simultaneously release of anti-tumor drug molecules.

1.2 Contributions

This work was published in *Journal of Materials Chemistry B*, **2018**, 6, 3531 by Jun Xiang, Xia Tong, Feng Shi, Qiang Yan, Bing Yu and Yue Zhao. This research work was conducted in the Université de Sherbrooke under the supervision of Prof. Zhao. I designed and performed all the experiments described in this study. I collected all the experimental data and analyzed them with my collaborators. Moreover, I drew all the figures in this work and got some useful suggestions from my collaborators. Xia Tong helped me with some characterizations and gave me a lot of useful suggestions. Feng Shi assisted me with the synthesis of upconversion nanoparticles. Qiang Yan gave me a lot of useful suggestions and assisted me with the data and figures processing. Bing Yu helped me synthesize the silica -coated upconversion nanoparticles. I have written the full manuscript and submitted it to Prof. Zhao for final revision.

1.3 Paper Published in Journal of Materials Chemistry B 2018, 6, 3531.

Near-infrared light-triggered drug release from UV-responsive diblock copolymer-coated upconversion nanoparticles with high monodispersity

Jun Xiang,[a] Xia Tong,[a] Feng Shi,[b] Qiang Yan,[c] Bing Yu[a] and Yue Zhao*,[a]

[a]Département de Chimie, Université de Sherbrooke, Sherbrooke, Québec, J1K 2R1, Canada. E-mail: yue.zhao@usherbrooke.ca

[b]School of Materials Science and Engineering, Shaanxi Normal University, Xi'an 710119, China.

[c]State Key Laboratory of Molecular Engineering of Polymers, Fudan University, No. 220, Handan Rd. Shanghai 200433, China.

1.3.1 Abstract

The preparation of a new near-infrared (NIR) light-responsive nanocarrier for controlled drug release is demonstrated. Upconversion nanoparticles (UCNPs) were coated with an amphiphilic diblock copolymer through surface-initiated atom transfer radical polymerization, of which the inner block is hydrophobic, ultraviolet (UV)-sensitive poly(4,5-dimethoxy-2-nitrobenzyl methacrylate) (PNB) and the outer block is hydrophilic poly(methoxy polyethylene glycol monomethacrylate) (POEG). The resulting polymer/UCNP nanocarrier is thermally stable in water over a wide temperature range (5-70 ^{o}C) and is uniform in size (120 nm hydrodynamic diameter, polydispersity index < 0.1). The diblock copolymer self-assembly on the surface of each UCNP occurs in aqueous solution, which allows encapsulation of antitumor drugs like doxorubicin (DOX) by the hydrophobic "micelle-like" core of PNB surrounding the NIR-sensitive UCNP. Under 980 nm laser exposure, UV light emitted by the single UCNP is absorbed by the PNB inner layer, which results in cleavage of *o*-nitrobenzyl groups and formation of carboxylic acid groups. The increasing hydrophilicity of the diblock copolymer resulting from the NIR light-triggered photochemical reaction can thus disrupt the nanocarrier and leads to release of DOX molecules. This diblock copolymer self-assembly-based approach to constructing NIR light-responsive nanocarriers of well-defined structures is general and offers possibilities for photocontrolled drug delivery.c

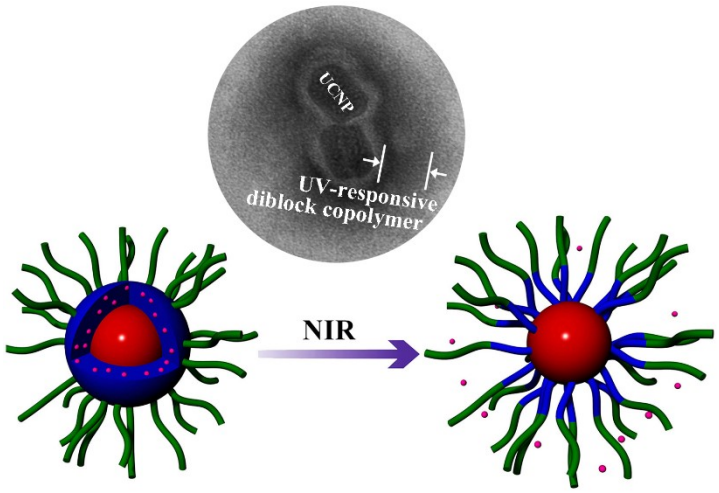

1.3.2 Introduction

Photoresponsive polymers have been extensively used to construct nanocarriers for light-controlled drug delivery applications over the past decade or so.[1-3] Most photoresponsive polymers require absorption of ultraviolet (UV) light for disruption of their nanocarriers. However, UV light has poor penetration depth through tissues and may damage healthy cells.[4, 5] In comparison with UV light, near-infrared (NIR) light has minimal phototoxicity and can penetrate deeply in live organisms because of its longer wavelengths in the "biological transparency window" resulting in less absorption and scattering by water and hemoglobin.[6-8] Unfortunately, the majority of photoresponsive polymers cannot absorb NIR light to activate a specific photochemical reaction. Upconversion nanoparticles (UCNPs) are inorganic nanocrystals and can absorb NIR light to emit higher-energy UV and visible light.[9-11] Moreover, they have narrow emission peaks, low toxicity and excellent photostability, making them attractive for biomedical applications.[12-15] In recent years, combining UCNPs and UV-sensitive polymers in hybrid nanocarriers has become a widely applied strategy to circumvent the direct UV excitation obstacle.[16-23] The basic principle is to use NIR light to excite UCNPs, and the UV light emitted by UCNPs from inside the nanocarrier is then absorbed by the UV-sensitive polymer to carry out the photochemical reaction leading to the nanocarrier's disruption and concurrent payload release.

Up to now, diverse methodologies have been put forward to organize UCNPs and UV-sensitive polymers in constructing nanocarriers for NIR light-triggered drug delivery. Of them, encapsulation of UCNPs in amphiphilic polymer assemblies is the most utilized approach.[16, 24-29] By employing this method, hydrophobic UCNPs and non-water soluble drugs tend to be entrapped in the hydrophobic core of polymer micelles, while the hydrophilic polymer corona stabilizes the whole nanocarrier in aqueous solution. Despite its simplicity and efficiency, the method often lacks control of UCNP and polymer coassembly in that two or more UCNPs can be loaded in one single micelle, resulting in heterogeneity and a high UCNP content. Recently, a method based on ligand exchange was

proposed to assemble UV-sensitive polymer around each UCNP.[30] However, the ligand exchange approach may suffer from some shortcomings including limited thickness of polymer layer due to the use of low molecular weight polymer and usually low polymer density because of the steric hindrance effect among polymer chains,[31] and also, as a result of low grafting density, quenching of upconversion luminescence (UCL) intensity by surrounding water molecules.[32] Moreover, the combination of UCNPs and UV-sensitive polymers through a silica layer was also investigated. Cerruti et al. reported a NIR light-triggered drug-delivery nanocarrier built up by coating UCNP with silica that, in turn is coated with a UV-cleavable nanogel.[20] Despite those interesting progresses, it is still challenging and is of fundamental interest to develop novel methodologies for preparation of UCNP-loaded polymer assemblies of well-controlled architecture and investigate the NIR light-triggered release of payloads.

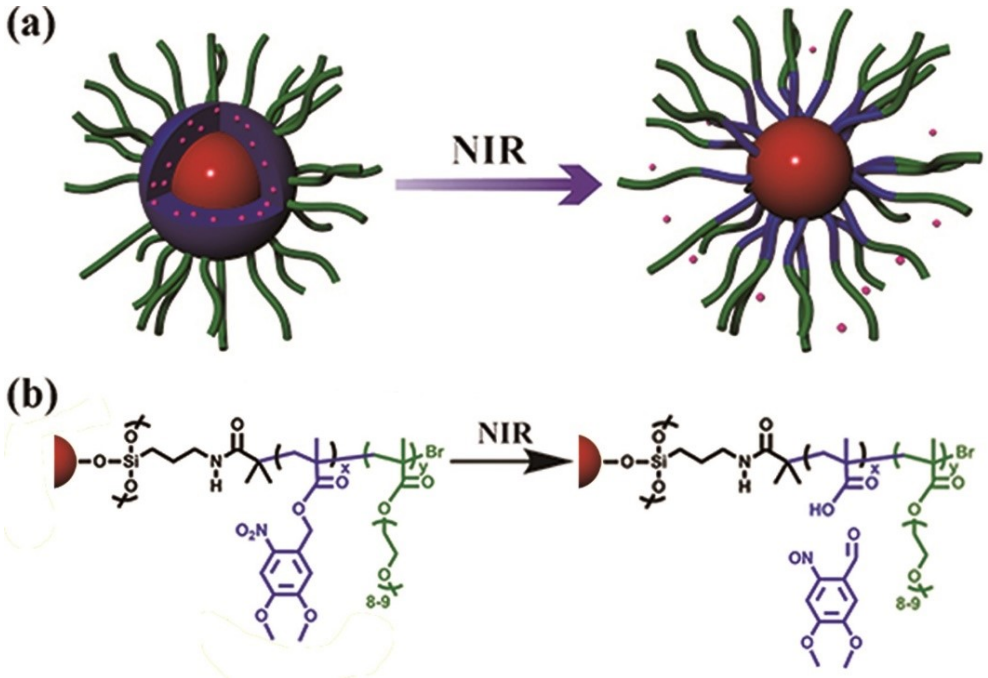

Figure 1. (a) Schematic illustration of UCNP coated with self-assembled micelle of an amphiphilic diblock copolymer and use of NIR light excitation of UCNP to induce the micelle disruption and the release of encapsulated drug molecules. (b) Chemical structure of the diblock copolymer and NIR light-triggered photocleavage of nitrobenzyl groups.

Herein we demonstrate an approach to preparing block copolymer micelles confining one single UCNP inside the core with high monodispersity. Figure 1a is a schematic illustration of the nanocarrier design. An amphiphilic diblock copolymer is grown from UCNP with a hydrophobic, UV-sensitive polymer as the inner block and a hydrophilic polymer as the outer block. Micellization of the diblock copolymer on UCNP is expected in aqueous solution, resulting in UCNP surrounded by collapsed hydrophobic polymer chains. Upon NIR light excitation, the hydrophobic polymer absorbs the UV light emitted by the UCNP to undergo a photochemical reaction that transforms the hydrophobic block onto hydrophilic block and thus the dissolution of the diblock copolymer with concurrent payload release. Figure 1b shows the chemical structure of the amphiphilic diblock copolymer and the NIR light-triggered photochemical reaction. More specifically, the synthetic route to our designed nanocarrier has four steps (Fig. S1). The first step is the silica coating of UCNP with amine groups by the co-condensation of silane coupling agents, giving UCNP-NH_2. ATRP initiators, -Br, are then immobilized by the acylation reaction between UCNP-NH_2 and α-bromoisobutyryl bromide. The last two steps are for the growth of an amphiphilic diblock copolymer through ATRP polymerization, the hydrophobic UV-sensitive poly(4,5-dimethoxy-2-nitrobenzyl methacrylate) (PNB) first, followed by the hydrophilic poly(methoxy polyethylene glycol monomethacrylate) (POEG). Upon 980 nm light excitation, the UV upconversion emissions of UCNP can be absorbed by the PNB blocks, inducing the photocleavage of *o*-nitrobenzyl (ONB) groups; the resulting carboxylic acid groups on the polymer will increasingly shift PNB toward hydrophilic and thus disrupt the micelle on UCNP. As will be shown below, uniform-sized nanocarrier can be obtained, and NIR light-triggered micelle disruption and release of an antitumor drug, tested using encapsulated doxorubicin (DOX), is achievable with a single UCNP in the micelle core.

1.3.3 Experimental

Materials

All chemicals were of analytical grade and used without further purification except where noted. Chemical reagents were purchased from Sigma-Aldrich. 4,5-Dimethoxy-2-nitrobenzyl methacrylate (NB) and UCNP ($NaYF_4$:Yb/Tm@$NaYF_4$) were synthesized and characterized by following the procedures reported previously.[16, 33]

Synthesis of Aminated UCNP (UCNP-NH_2)

A silica layer with amine groups was coated on the surface of UCNP by co-condensation of silane coupling agents in one pot. Typically, a chloroform ($CHCl_3$) solution of UCNP (100 mg) was added to an aqueous solution (80 mL) of cetyltrimethylammonium bromide (CTAB, 200 mg). The resulting turbid microemulsion was stirred at 60 °C to remove $CHCl_3$. Then this solution was heated to 70 °C, and the pH was adjusted to 8-9 using 0.1 N sodium hydroxide (NaOH) solution. Afterwards, a solution composed of 150 μL tetraethyl orthosilicate (TEOS) and 350 μL anhydrous ethanol (EtOH) was added dropwise to the above solution. After 0.5 h reaction, the mixture of (3-aminopropyl) triethoxysilane (APTES, 250 μL) and EtOH (450 μL) was added. The whole solution was kept at 70 °C for 4 h and stirred overnight at room temperature. Finally, the product of UCNP-NH_2 was isolated by centrifugation with EtOH and redispersed in acetone. This washing procedure was repeated for four times to remove the unreacted species, and the sample recovery was carried out by lyophilization. The resulting white powder UCNP-NH_2 was used without further purification.

Synthesis of Initiator-coated UCNP (UCNP-Br)

The powder of UCNP-NH_2 (100 mg) and triethylamine (TEA, 0.16 mL) were first added to anhydrous toluene (10 mL). Next, this solution was cooled in an ice-water bath. Then 170 μL α-bromoisobutyryl bromide was slowly added to the solution. After keeping it in the ice bath for 2 h, the reaction mixture was heated to room temperature and stirred continuously

overnight. Afterwards, the UCNP-Br was washed several times with first abundant acetone/water solution (v/v, 1/1) and then acetone. Finally, it was precipitated by centrifugation until supernatants became clear, and collected by lyophilization.

ATRP of NB on UCNP for UCNP@PNB

UCNP-Br (125 mg), NB monomer (655 mg), tris[2-(dimethylamino)ethyl]amine (Me_6TREN, 37 μL) and DMF (2 mL) were first placed in a one-neck flask of 5 mL. Next, 20 mg Cu(I)Br was added into the solution under argon gas protection. The mixture was then degassed three times using the freeze-pump-thaw procedure and sealed under vacuum. After keeping stirring at room temperature for 10 min, the whole setup was placed in a pre-heated oil bath (90 °C) for 12 h. Afterwards, the reaction was stopped with liquid nitrogen. Finally, the solution was precipitated into methanol once and centrifuged with DMF for several times. The light brown UCNP@PNB was collected through lyophilization.

ATRP of OEG on UCNP@PNB for UCNP@PNB-*b*-POEG

In this step, UCNP@PNB was used to initiate polymerization of OEG (M_n 500 g/mol) to grow the second block of hydrophilic POEG. The OEG monomer was purified by passing through a column filled with basic alumina to remove inhibitor. DMF (2.5 mL), UCNP@PNB (200 mg), OEG (2.5 mL) and PMDETA (105 μL) were charged into a one-neck round-bottom flask. Cu(I)Br (28.6 mg) was then added under argon gas protection. The whole solution was degassed three times using the freeze-pump-thaw procedure and sealed under vacuum. The reaction was carried out at 90 °C for 1.5 h. UCNP@PNB-*b*-POEG was collected by centrifugation (20,000 RPM × 15 min) with DMF for three times, dialyzed against deionized (DI) water for three days (3,500 MWCO dialysis tubing from Spectra/Por) at room temperature and then recovered by lyophilization.

Cleavage of Grafted Diblock Copolymer Chains

Hydrofluoric acid (HF, 48 wt%, 0.3 mL) was added to a plastic bottle containing a tetrahydrofuran (THF, 5 mL) solution of UCNP@PNB-*b*-POEG (20 mg) under constant stirring. (**Caution**: HF is extraordinarily corrosive, and all operations with aqueous HF should be conducted in a fume hood with suitable personal protective equipment). After keeping at room temperature for 4 h, this solution was neutralized with $NaHCO_3$. To completely remove impurities, the supernatant after centrifugation was dialyzed against DI water (frequently refreshed) for 24 h. The cleaved polymer was collected through freeze-drying.

Preparation of DOX-UCNP@PNB-*b*-POEG

To load a drug in the diblock copolymer layer on UCNP, doxorubicin hydrochloride (DOX·HCl, 4 mg) was dissolved in 2.5 mL of DMF and treated with 4 μL TEA for 4 h. Subsequently, 20 mg UCNP@PNB-*b*-POEG was added to this solution, which was then stirred overnight using a magnetic stirring bar in the dark. The resulting solution was dialyzed against Tris buffer solution (pH 7.4) to remove free drug molecules for 3 days. The obtained solution was concentrated by centrifugation and the sample was kept in a refrigerator and used within one month.

Photolysis of UCNP@PNB-*b*-POEG under 980 nm Excitation

The aqueous solution of UCNP@PNB-*b*-POEG nanocarrier (5 mg/mL, 0.5 mL) was placed in a dialysis cup (MWCO 3,500). By inserting it on top of a quartz cuvette filled with aqueous solution, molecules photocleaved from UCNP@PNB-*b*-POEG can diffuse through a membrane into the bottom solution in the cuvette. During the irradiation experiment, the whole setup was irradiated by a continuous-wave (CW) 980 nm NIR laser from the top for a number of consecutive cycles of 5 min irradiation followed by 5 min irradiation-off in order to avoid overheating of the solution. Then absorption spectra of the bottom solution were recorded.

NIR Light-triggered Release of Drug Molecules

To initiate the release of DOX loaded in UCNP@PNB-*b*-POEG, the aqueous solution of DOX-UCNP@PNB-*b*-POEG (3 mg/mL, 0.4 mL) was placed in the dialysis cup and subjected to 980 nm NIR light irradiation under the same conditions as described above. Likewise, DOX molecules released from the nanocarrier into the solution in the dialysis cup can diffuse into the bottom solution in the cuvette, and the absorption spectra of the bottom solution were recorded every 10 min during the experiment.

Characterizations

The morphologies of surface coated UCNP were examined using a Hitachi H-7500 transmission electron microscope (TEM) at an acceleration voltage of 80 kV. TEM specimens were prepared by dropping dilute sample solution (~10 μL) onto carbon-coated copper grids while allowing the solvent to evaporate completely and then stained with phosphotungstic acid (PTA). Infrared spectra were recorded on a Bomen FTIR spectrometer (ABB MB104PH) using the diffuse reflection mode. Thermogravimetric analysis (TGA) was performed in an argon atmosphere at a heating rate of 10 °C/min from room temperature to 700 °C. Size exclusion chromatography (SEC) measurements were performed on a Waters system equipped with a photodiode array detector (PDA 996) and a refractive index detector (RI 410). THF was used as the eluent at an elution rate of 1 mL/min, while polystyrene standards were used for calibration. Dynamic light scattering (DLS) was carried out on a Malvern Zetasizer Nano ZS ZEN3600 system with a helium-neon laser (wavelength, $\lambda = 633$ nm) in a quartz cuvette. To investigate the effect of temperature on the size of nanoparticles, samples were kept for 15 min at each temperature before the measurement. All measurements were carried out at a scattering angle of 173°. The photolysis of *o*-nitrobenzyl groups, as well as the release of drug molecules, were monitored by recording UV-vis spectra on a Varian 50 Bio UV–vis spectrophotometer. Upconversion luminescence (UCL) spectra of as-synthesized nanoparticles in solution in a quartz cuvette with 10 mm path length were recorded with a double-monochromator Fluorolog 2 instrument from Spex. A power-adjustable 980 nm laser diode (MDL-H-980nm-4W, Changchun New Industries Optoelectronics Tech. Co., Ltd.) was

employed as the upconversion pump source for the UCL measurement as well as the NIR irradiation experiments. The cleavage of *o*-nitrobenzyl groups from PNB-*b*-POEG grafted UCNP with or without loaded DOX upon UV light irradiation was conducted utilizing an OmniCure@Series 1000 UV lamp with 365 nm filter (approximately 1 mW/cm^2). In this experiment, the emission spectra of DOX (λ_{ex} = 480 nm) from UCNP@PNB-*b*-POEG was recorded immediately on a Varian Cary Eclipse fluorescence spectrophotometer after each irradiation period. For the control test, the solution free of UV irradiation was kept in the dark and the emission spectra were taken at the same time points.

1.3.4 Results and Discussion

1.3.4.1 Characterization of UCNP@PNB-*b*-POEG

The $NaYF_4$:18%Yb/0.5%Tm@$NaYF_4$ (UCNP) was synthesized using a thermal decomposition method according to our previously reported work.[33] As shown in Fig. 2a, these uniform nanocrystals have a rod-like shape with an average dimension of 34.7 (*L*) × 22.1 (*W*) nm. Then a silica layer with amine groups was coated onto the surface of UCNP (UCNP-NH_2) by the co-condensation of TEOS and APTES through a one-pot method. It should be mentioned that the residual surfactant (CTAB) was retained for the next steps of modification. Afterwards, ATRP initiators were anchored on their surface to obtain UCNP-Br through the acylation reaction between UCNP-NH_2 and α-bromoisobutyryl bromide. To determine whether the silica layer was coated on UCNP to form a core-shell structure and the diblock copolymer was grown from the silica layer surface after ATRP, TEM measurements were carried out. The core-shell structure of UCNP-NH_2 was first revealed by the TEM observation (Fig. S2). The TEM specimens of UCNP-Br were stained with PTA for comparing the difference before and after grafting diblock copolymer under the same conditions. As shown in Fig. 2b, the centered UCNP are surrounded by a light-gray ring as the outmost layer (SiO_2-Br) with an average thickness of 6 nm. Thus, the average size of UCNP-Br is 47 × 34 nm before further functionalization. Afterwards, UV-sensitive PNB and hydrophilic POEG polymers were grown by surface-initiated ATRP,

successively. Negative staining TEM images in Fig. 2c and Fig. 2d show that the outmost layers are different from that in Fig. 2b and the core-shell-shell structured nanoparticles are observed. Moreover, the length of the polymer layer increased from ~30 nm for PNB to ~42 nm for PNB-*b*-POEG. Therefore, the average size of UCNP@PNB-*b*-POEG is estimated to be 120 nm (dry state) assuming it is spherical. More TEM images are given in Supporting Information (Fig.S3-5).

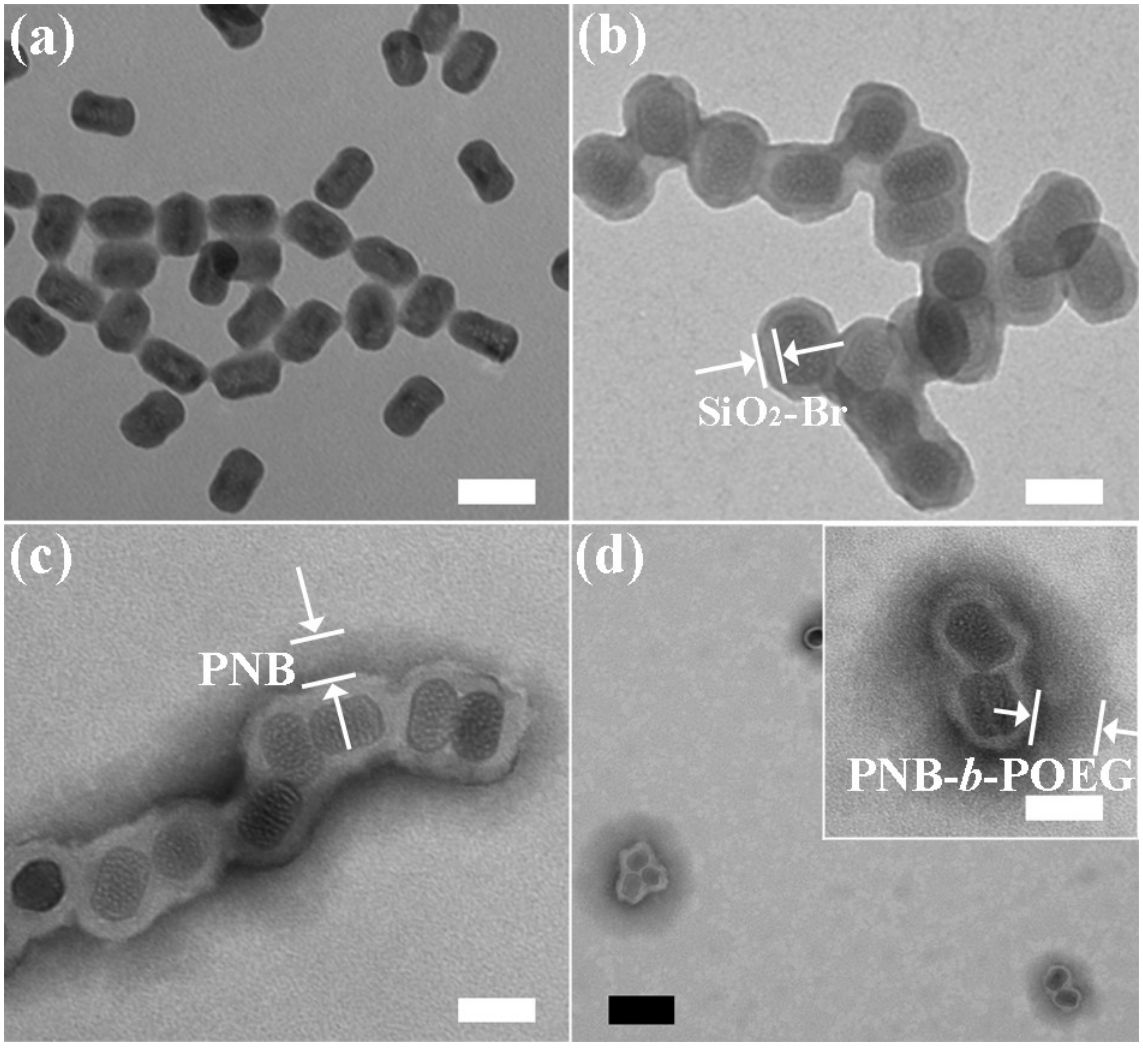

Figure 2. TEM images for UCNP (a), UCNP-Br (b), photoresponsive polymer-grafted UCNP (UCNP@PNB) (c), and diblock copolymer grafted UCNP (UCNP@PNB-*b*-POEG) (d). Scale bar is 40 (white) or 100 nm (black).

To calculate the grafting density of polymer chains and initiation efficient, thermogravimetric analysis was performed. As shown in Fig. S6, three main regions of weight loss were found (i) loss of moisture (T<80 ºC), (ii) decomposition of residual CTAB (80-150 ºC),[34] and (iii) organic species (APTES/initiators/polymers) plus co-condensation of silica matrix (T>250 ºC). For simplicity, we assume that no dehydration of silica takes place in 250-450 ºC and initiation efficiency of PNB-Br is 100%. In addition, the molecular weight of PNB-*b*-POEG (M_n 10.9 × 10^3 g/mol, PDI 1.48) was obtained from the SEC (Fig. S7) by etching silica layer with HF. Based on the above information, the estimated initiator and polymer grafting densities (Supporting Information) are approximately 4.4 and 0.26 chains/nm^2, respectively. Notably, the initiator grafting density of UCNP-Br (4.4 chains/nm^2 or 0.34 mmol/g) is a relatively high value.[35] Furthermore, the initiation efficiency is around 6%. This relatively low value is likely to be caused by the large bulky groups of the monomers.

FTIR spectroscopy also confirmed the successive steps of UCNP surface coating (Fig. 3). With the organic ligand of oleic acid (OA) on nanoparticle surface, the IR spectrum of UCNP shows the characteristic bands at 2926 (–CH_3 stretching), 2853 (–CH_2– stretching), 1447 (C–H bending) and 1556 cm^{-1} (COO– asymmetric stretching) of OA molecules (Fig. 3a).[36] In comparison with the FTIR spectrum of UCNP, new characteristic bands at 1034 (Si–O stretching), 1551 (N–H bending) and 1636 cm^{-1} (N-H shear bending) appear in the spectrum of UCNP-NH_2 (Fig. 3b).[34, 37] It is worthy of noting that there is a little CTAB left in UCNP-NH_2 as revealed by the C–H stretching band at 3000-2800 cm^{-1}.[38] For UCNP-Br, new absorption bands appear at 1535 (C–N in NH–O=C stretching), 1703 (C=O stretching) and 3319 cm^{-1} (stretching vibration of secondary amide N–H), which confirms the immobilization of initiator groups (Fig. 3c). After growth of the first polymer block of PNB, the spectrum of UCNP@PNB displays the presence of nitro groups by 1333 (symmetric vibration) and 1524 cm^{-1} (asymmetric vibration) (Fig. 3d).[16] In addition, the characteristic band at 1732 cm^{-1} assigned to the ester carbonyl stretch of the methacrylate[38, 39] also proves the formation of PNB. After the second ATRP for POEG, the characteristic peaks of UCNP@PNB-*b*-POEG at 2876 (C–H stretching), 1728 (ester carbonyl stretching) and 1100

cm^{-1} (C–O–C stretching) are enhanced due to overlapping of the absorptions of the two polymers, indicating that the second POEG block had grown from the UCNP@PNB surface (Fig. 3e).

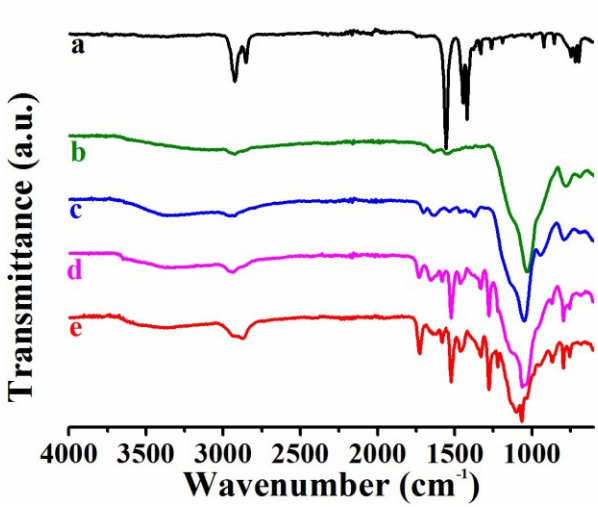

Figure 3. FTIR spectra of (a) UCNP, (b) UCNP-NH_2, (c) UCNP-Br, (d) UCNP@PNB, and (e) UCNP@PNB-*b*-POEG.

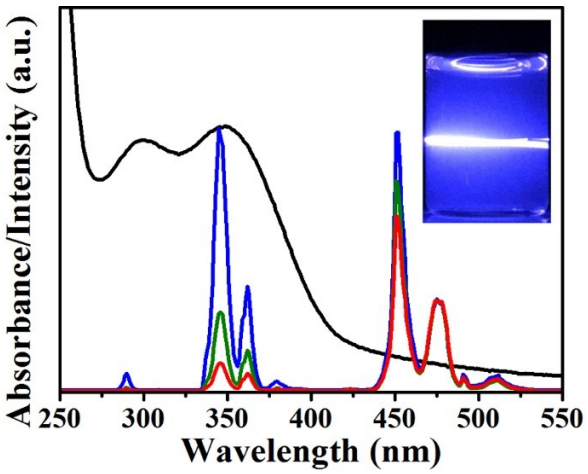

Figure 4. Absorption spectrum of UCNP@PNB-*b*-POEG aqueous solution (black), and upconversion emission spectra under 980 nm excitation for neat UCNP in hexane (blue), UCNP@PNB in DMF (green), and UCNP@PNB-*b*-POEG in H_2O (red). Inset is a photograph of an aqueous solution of UCNP@PNB-*b*-POEG.

To reveal whether or not the grafted diblock copolymer can absorb the emitted UV light of UCNP, extinction and upconversion luminescence (UCL) spectra are shown in Fig. 4. The inset of Fig. 4 is a picture of an aqueous solution of UCNP@PNB-*b*-POEG upon 980 nm excitation. The emitted visible light from UCNP is readily observed where the laser beam passes through the solution (the scattering of the main emission at 450 nm gives the apparent blue color of the solution). Also shown are the UCL spectra of neat UCNP, UCNP@PNB and UCNP@PNB-*b*-POEG, together with the absorption spectrum of UCNP@PNB-*b*-POEG. The intensity of UV light emitted by UCNP with respect to visible light (475 nm) emission is significantly reduced for UCNP functionalized with UV-sensitive PNB. Since the SiO_2-Br layer has no influence on the upconversion emissions (Fig. S8), the decreased UV light emission is mainly attributed to the absorption of PNB layer. As confirmed by the UV-vis absorption spectra, *o*-nitrobenzyl groups in the grafted polymers show a strong absorption at ~350 nm, which overlaps with the emission of UCNP in the UV region.

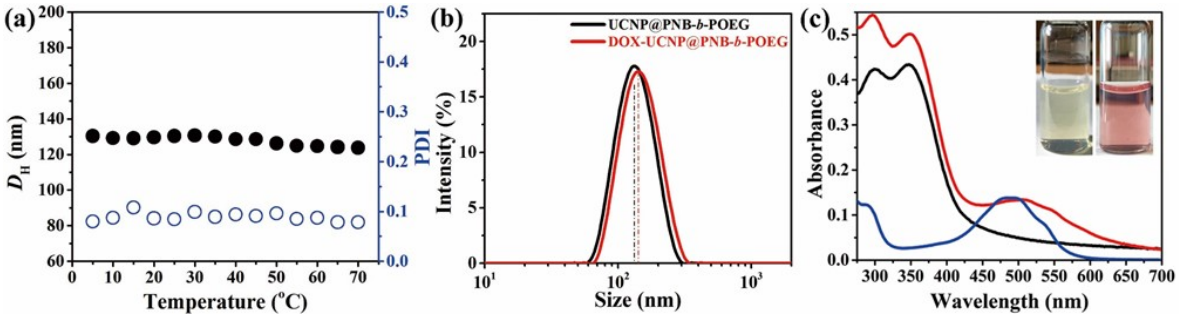

Figure 5. (a) Effect of temperature on the hydrodynamic diameter (D_H, solid cycle) and polydispersity index (PDI, hollow cycle) of UCNP@PNB-*b*-POEG in H_2O (1 mg/mL). (b) The DLS results of UCNP@PNB-*b*-POEG (black) and DOX-UCNP@PNB-*b*-POEG (red) in H_2O at 25 °C. (c) Absorption spectra of DOX (blue), UCNP@PNB-*b*-POEG (black, 0.1 mg/mL), and DOX-UCNP@PNB-*b*-POEG (red, 0.1 mg/mL). Inset photos are the aqueous solutions of nanoparticles before (left) and after (right) DOX encapsulation.

As mentioned above, it is of interest to prepare nanocarriers with high monodispersity. In the present case, it is difficult to assess from TEM images of UCNP@PNB-*b*-POEG that

show apparent formation of aggregates. Therefore, DLS measurements were carried out to measure polydispersity of the designed nanocarrier. Fig. 5a shows the mean hydrodynamic diameter (D_H) and polydispersity index (PDI) for UCNP@PNB-*b*-POEG in water over a wide temperature range, indicating an almost constant size of 130 nm and a PDI around 0.07. This extremely low PDI (<0.1) confirms the near monodispersity of UCNP@PNB-*b*-POEG. Thus, the aggregates in TEM images (Fig. 2) are caused by the evaporation process during the preparation of the sample. By combing the DLS and TEM results, it is safe to say that each single UCNP is covered by the amphiphilic diblock copolymer and that the dispersion in water is thermally stable.

To investigate the NIR light-triggered drug release, the loading of an antitumor drug, doxorubicin (DOX), by UCNP@PNB-*b*-POEG was first examined. DLS measurements in Fig. 5b indicate that the average D_H of DOX-loaded NP is slightly larger than that without DOX encapsulation, from 130 to 140 nm. The inset pictures (Fig. 5c) show aqueous solutions of UCNP@PNB-*b*-POEG before and after DOX encapsulation. While the transparent solution of unloaded nanoparticles has a light-yellow color, the solution of DOX-UCNP@PNB-*b*-POEG becomes light-pink colored. The UV-vis spectra of DOX and the two solutions of nanoparticles are also shown. At first, the DOX molecules possess a strong absorption band in the 475-500 nm region, while DOX free UCNP@PNB-*b*-POEG has no absorption in the same region. By contrast, the nanoparticle solution after DOX encapsulation shows the absorption of DOX and the absorption band displays a slight (about 5 nm) red-shift, which may be attributed to the π-π stacking interaction among drug molecules or between DOX and benzyl rings in PNB blocks within the micellar core.[40] These results show clearly that the drug molecules are loaded in the diblock copolymer (likely in the hydrophobic PBN inner layer) surrounding the single-UCNP core. The pink color of DOX-UCNP@PNB-*b*-POEG solution is caused by absorption of loaded DOX.

1.3.4.2 Light-induced Disruption of UCNP@PNB-*b*-POEG

The photochemical reactions of ONB-containing polymers activated by UV light (365 nm) are well known.[39, 41, 42] In the present study, we also first applied UV light to induce the photocleavage reaction. As shown in Fig. 6, under UV light exposure of low intensity, the absorption band at 355 nm decreases continuously over irradiation time, indicating the removal of *o*-nitrobenzyl groups from UCNP@PNB-*b*-POEG. In addition, an isosbestic point appears at 380 nm when the 355 nm continuously decreases, implying the existence of two distinct absorbing species in equilibrium with each other at a given UV irradiation time. Apparently, the peak at 355 nm decreases by about 17% after 90 min of low-intensity UV exposure.

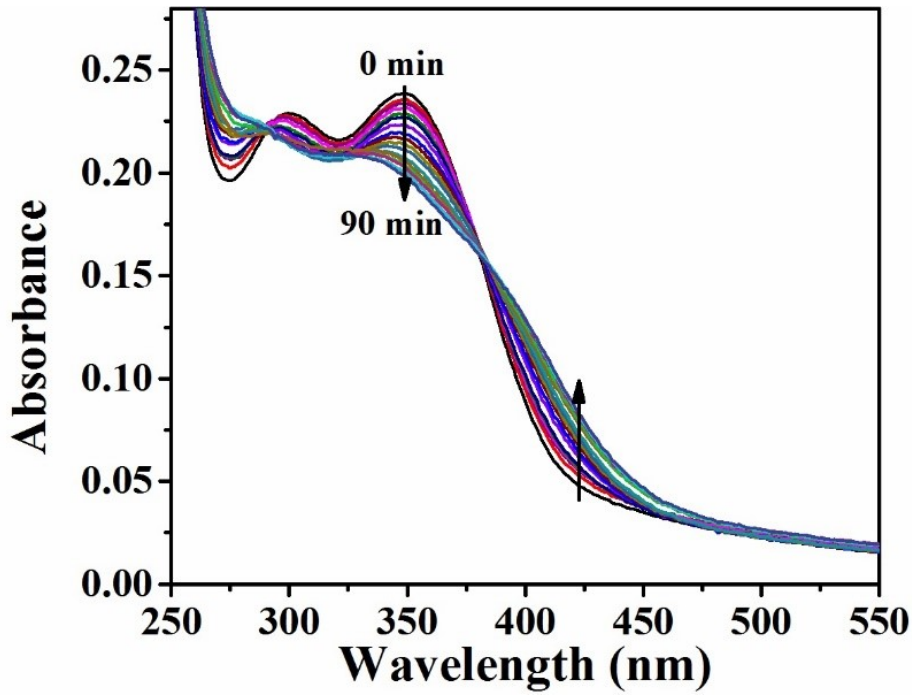

Figure 6. Absorption spectra of UCNP@PNB-*b*-POEG (0.05 mg/mL, 1 mL) recorded after various times of 365 nm UV irradiation (1 mW/cm^2) showing photocleavage reaction of PNB in H_2O.

We further went on to investigate the photocleavage of ONB groups initiated by a continuous-wave 980 nm diode laser. Owing to the small beam diameter (3 × 3 mm) of the NIR light laser, it is hard to collect the UV-vis spectra using a large volume of the

nanocarrier solution like that in the UV irradiation experiment. While using a small volume, the overheating problem caused by 980 nm light is difficult to avoid. Therefore, a setup was utilized to monitor the photocleavage reaction. As shown in Fig. 7a, a dialysis cup containing an aqueous solution of UCNP@PNB-*b*-POEG (0.5 mL) was immersed into water in a quartz cuvette. Once the photoreaction occurs, the cleaved molecules of low molecular weight can diffuse into the underneath solution through a dialysis membrane (MWCO 3,500) for equilibrium. By tracking the UV-vis spectra of the solution in the cuvette, cleaved chromophores can be observed. Since the methacrylic acid groups formed after cleavage of ONB from of UCNP@PNB-*b*-POEG are pH sensitive, which may affect the stability of the nanocarriers,[41] tris(hydroxymethyl)aminomethane (Tris) buffer solution (pH 7.4, 10 mM) was utilized to maintain the pH constant during the NIR irradiation experiment of UCNP@PNB-*b*-POEG (see Experimental for details). The solution in dialysis cup was irradiated by a NIR laser from the top for a number of consecutive cycles of 5 min NIR irradiation-on followed by 5 min irradiation-off to avoid overheating of the solution. The absorption spectra of the solution in the cuvette were recorded every 1 h during the irradiation test. In Fig. 7b, the collected UV-vis spectra during the reaction are presented. When the sample was kept in the dark, the absorption in the 300-550 nm region was absent for over 15 h, indicating that there were no cleaved molecules in the solution. By contrast, the absorption band in the 300-425 nm region was observed after 1 h of 980 nm irradiation and increased in intensity with increasing the irradiation time, indicating the presence of photocleaved nitroso compound in solution. To better reveal the effect of NIR light irradiation on the cleavage reaction, Fig. 7c plots the absorbance at 375 nm (in Fig. 7b) as a function of time. Upon switching on the 980 nm laser, the slopes of the curve in the 0-2, 3.5-5.5 and 18.5-20.5 h regions are larger than those in 2-3.5, 5.5-7 and 20.5-22 h regions during which the laser is off. These results confirm that the UV light emitted by UCNP upon NIR irradiation can be absorbed by PNB blocks in UCNP@PNB-*b*-POEG to initiate the photocleavage of ONB groups and thus disrupt the nanocarrier.

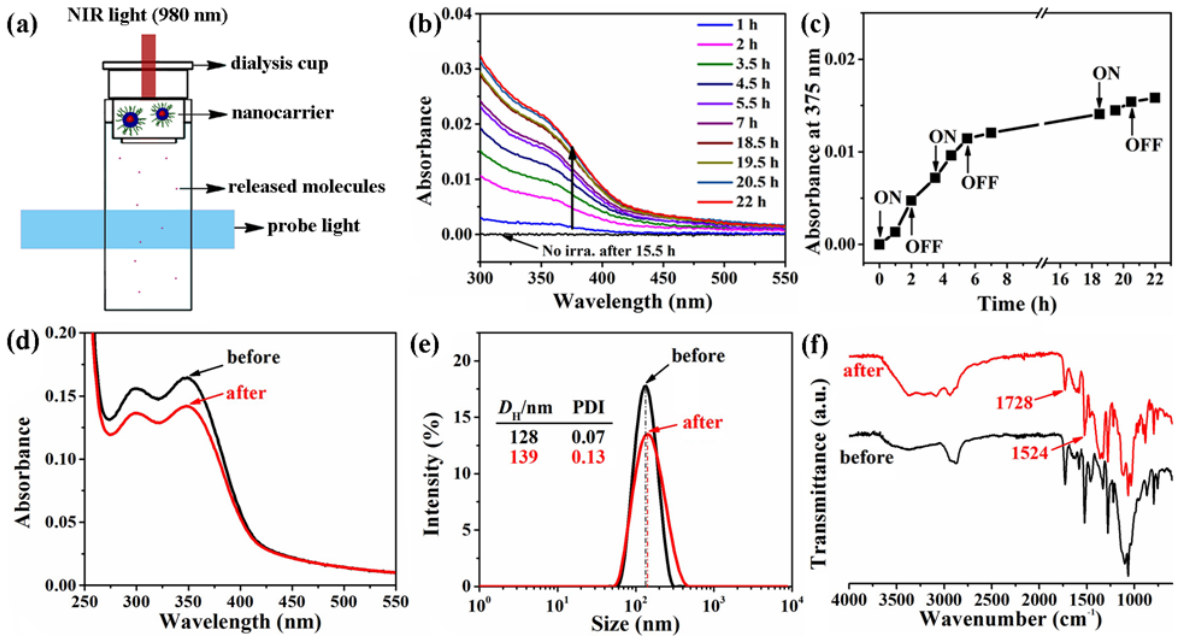

Figure 7. (a) Schematic of the setup used to detect species diffusing from the nanocarrier solution through a dialysis membrane into aqueous solution filled in the cuvette induced by 980 nm laser irradiation (diffusing molecules are either photocleaved nitrosobenzaldehyde or released drug molecules). (b) Absorption spectral change over time for nitrosobenzaldehyde molecules cleaved by NIR light exposure of UCNP@PNB-*b*-POEG (4 W). (c) Plot of absorbance at 375 nm in (b) *vs.* time. The times at which the NIR laser is turned on or turned off are indicated. (d) UV-vis spectra, (e) DLS hydrodynamic diameter (D_H) measurement, and (f) FTIR spectra of UCNP@PNB-*b*-POEG before (black) and after (red) NIR light irradiation.

After the exposure to the NIR light, the rest of the solution in the dialysis cup was taken out for further analysis. This solution was first dialysed against two litres of deionized water (pH ~7.0 and frequent change) for eight hours to remove any residual photocleaved molecules. Its UV-vis spectrum was then recorded and compared to the initial spectrum before the NIR light irradiation experiment on the UCNP@PNB-*b*-POEG solution. As can be noticed from Fig. 7d, the occurrence of photocleavage of ONB groups under 980 nm laser irradiation is indicated by the decreased absorption of ONB remained in the

nanocarrier, with the absorbance at 350 nm decreased by about 16%. Fig. 7e shows the hydrodynamic diameter (D_H) of the nanoparticles before and after the 980 nm laser exposure. It swells from 128 (PDI 0.07) to 139 nm (PDI 0.126), indicating the NIR light induced disruption of the nanocarrier due to shifting hydrophobic-hydrophilic balance in PNB chains. Indeed, as ONB groups are cleaved upon irradiation, carboxylic acid groups are formed (ionized at pH 7), which makes the diblock copolymer chains more hydrophilic and adopt a more extended chain conformation, resulting in increase in hydrodynamic diameter (Fig.7e). Moreover, the FTIR spectra in Fig. 7f for UCNP@PNB-*b*-POEG before and after 980 nm irradiation also show the effect of the photocleavage reaction. There is a broad characteristic band in the 2750-3300 cm^{-1} region, which is attributed to O–H stretching of the carboxylic acid groups. This is also consistent with the decrease in band intensity at 1524, 1728 and 2980 cm^{-1}, implying diminishing carbonyl and nitro groups in UCNP@PNB-*b*-POEG after 980 nm irradiation. All these results indicate the occurrence of photolysis reaction under 980 nm excitation, resulting in the conversion of carbonyl groups into carboxylic acid groups.

1.3.4.3 Photoinduced Drug Release from UCNP@PNB-*b*-POEG

After confirming the disruption of the UCNP@PNB-*b*-POEG by 980 nm laser, the antitumor drug DOX was loaded in the nanocarrier and NIR light-triggered drug release was investigated with DOX-UCNP@PNB-*b*-POEG in the same Tris buffer to keep pH constant during the process. The choice of DOX was made considering its excellent stability in Tris buffer solution[43] and its wide use for *in vitro* and *in vivo* studies.[44-46] Likewise, DOX release upon direct low-intensity UV light exposure of the DOX-UCNP@PNB-*b*-POEG solution was first assessed. In Figs. 8a and 8b, the UV-vis and fluorescence spectra of the DOX-UCNP@PNB-*b*-POEG solution were monitored during the UV light irradiation. Under 365 nm irradiation, the absorbance at 350 nm gradually decreases to about 80%, indicating the occurrence of photocleavage reactions. However, the absorption band of DOX (475-500 nm) remains essentially unchanged in the meantime, which indicates the photostability of DOX under UV irradiation. As for the

fluorescence spectra, there is a weak emission band in the 550-600 nm region before irradiation, indicating that the fluorescence of DOX is quenched after encapsulating into the nanocarrier. By contrast, after 2 h of UV the fluorescence intensity increases by 30%. To better observe the change during the whole period of the experiment, Fig. 8c shows the plot of emission intensity at 585 nm *vs.* UV exposure time. The intensity gradually increases with increasing the irradiation time, while it remains constant in the control test where no UV was applied to the nanocarrier solution. These results confirm that UV light induced disruption of DOX-UCNP@PNB-*b*-POEG can lead to changing micro-environment of DOX molecules. In the beginning, the fluorescence intensity of DOX is significantly quenched by the hydrophobic region of micelles, which is consistent with a previous report.[47] Upon 365 nm irradiation, the hydrophobic region turns increasingly into hydrophilic due to the photocleavage reaction, which gives rise to the dissolution of DOX into the aqueous solution and thus enhances the emission intensity.

To further prove the release of DOX from DOX-UCNP@PNB-*b*-POEG under low-intensity UV irradiation, the setup with a dialysis cup immersed in water in a cuvette (Fig. 7a) was utilized. Fluorescence emission of DOX was indeed observed in the solution underneath the dialysis cup containing the DOX-UCNP@PNB-*b*-POEG solution subjected to UV irradiation, indicating release of DOX molecules from the nanocarrier and diffusion through the membrane into the solution. The release amount of DOX was monitored by recording the fluorescence emission intensity at 585 nm of the bottom solution; the results are shown in Fig. 8d. Over the 16 h period prior to UV irradiation, only a little DOX was detected. However, when the solution was exposed to 365 nm UV of 1 mW/cm^2 for 15 min, the release amount showed a threefold increase in the following 16 h.

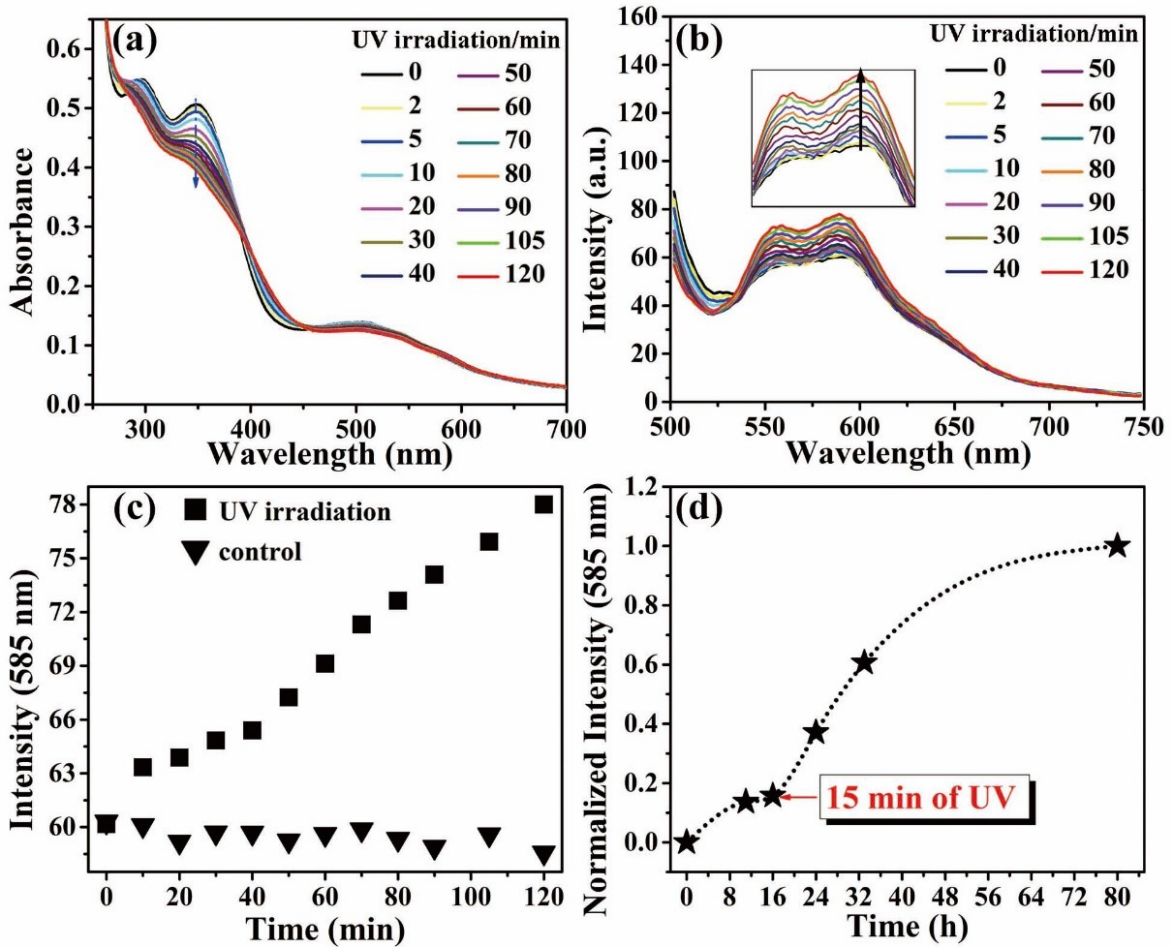

Figure 8. Spectral changes of DOX-UCNP@PNB-*b*-POEG (0.1 mg/mL, 2.5 mL) under UV light (365 nm, 1 mW/cm^2) irradiation: (a) absorption spectra, (b) emission spectra (λ_{ex} = 480 nm), and (c) change in fluorescence intensity (at 585 nm) *vs.* irradiation time. (d) Using the setup in Fig. 7a, change in the normalized fluorescence intensity of DOX (at 585 nm) in the aqueous solution underneath the dialysis cup containing DOX-UCNP@PNB-*b*-POEG solution (0.1 mg/mL, 0.5 mL) *vs.* time, only 15 min of UV light irradiation being applied after 16 h as indicated. In all experiments, the solution is still without stirring.

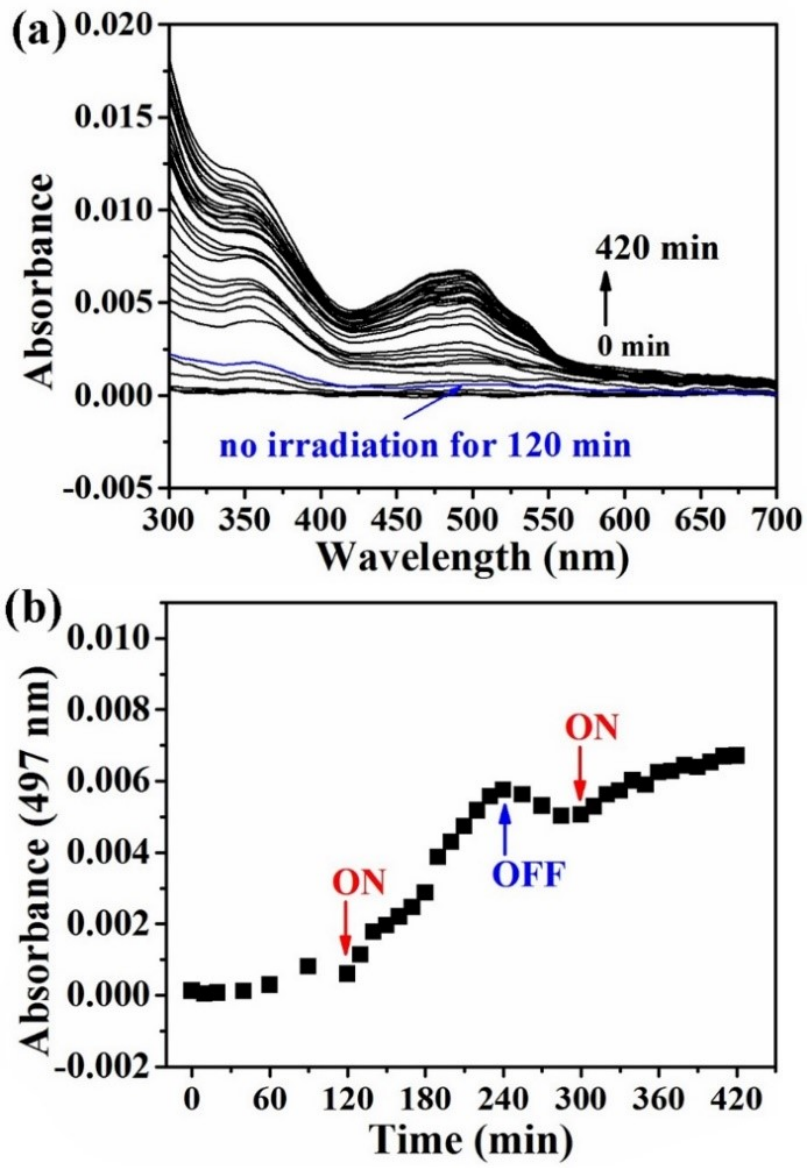

Figure 9. (a) Absorption spectral change over time for the aqueous solution separated from DOX-UCNP@PNB-*b*-POEG solution (3 mg/mL, 0.4 mL) through a dialysis membrane (see the setup in Fig. 7a) before and after 980 nm laser exposure (4 W). (b) Change in the absorbance at 497 nm over time with data from (a), the times at which the NIR laser being turned on or off are indicated.

Finally, the release of DOX molecules triggered by NIR light irradiation was investigated using the same setup. The DOX-UCNP@PNB-*b*-POEG solution in dialysis cup was

exposed to the 980 nm laser from the top. The absorption spectra of the bottom solution were taken every 10 min, i.e., after each cycle of 5 min irradiation on followed by 5 min irradiation off. The UV-vis spectra collected in the process are presented in Fig. 9a. Without NIR light illumination, after 2 h of immersion of the dialysis cup with water in the cuvette, the bottom solution basically has no absorption in the 300-700 nm region, indicating little DOX diffusion from the top solution of DOX-UCNP@PNB-*b*-POEG across the membrane, and thus the DOX encapsulation stability. However, after NIR irradiation of the top solution, absorption bands of DOX in the 450-550 nm region are detected, indicating release of DOX molecules from DOX-UCNP@PNB-*b*-POEG as a result of NIR induced photocleavage of ONB groups on the PNB blocks. Shown in Fig. 9b is the plot of absorbance at 497 nm as a function of time, the change in the amount of DOX molecules in the bottom solution is better revealed. Before 980 nm laser irradiation, the absorbance increases slightly up to 120 min. After switching on the 980 nm laser, the absorbance increases significantly in the 120-240 min period, indicating NIR light-induced disruption of DOX-UCNP@PNB-*b*-POEG and the concomitant drug release. Then, after switching off the 980 nm laser during the period of 240-300 min, no further increase in absorbance is observed; instead, there appears to be a slight decrease, implying some kind of equilibrium of DOX molecules across the solution. Upon switching on the NIR light again in the 300-420 min period, the absorbance starts to increase again, indicating resumed nanocarrier disruption and drug release. However, the increase is smaller than in the first NIR light on period. This is understandable, because under continuous exposure to 980 nm laser, the nanocarrier disruption and DOX release should eventually reach a stationary state with no further change observed. All these results confirm that the release of DOX molecules from UCNP@PNB-*b*-POEG can be activated by NIR light.

1.3.5 Conclusions

In this work, a bottom-up strategy has been put forward to prepare a NIR light-responsive nanocarrier with a high degree of monodispersity (PDI<0.1) based on combining UCNP with photoresponsive polymer. We showed that coating a thin silica layer (~6 nm) on the

surface of UCNP facilitates the incorporation of ATRP initiators through covalent bonding, which allows the use of surface-initiated controlled radical polymerization to grow an amphiphilic diblock copolymer comprising PNB (UV-sensitive hydrophobic polymer) and POEG (hydrophilic polymer). The rationally designed UCNP@PNB-*b*-POEG was investigated as a new NIR light-responsive nanocarrier for controlled drug delivery. In aqueous solution, each UCNP is covered by a hydrophobic PNB inner layer and a water-soluble POEG corona ensuring the stable dispersion of the nanoparticles. The nanocarrier, in a sense, is like a self-assembled diblock copolymer micelle whose hydrophobic core contains one single UCNP. Our study found that despite the single UCNP at the center of each diblock copolymer assembly, upon 980 nm NIR light irradiation, UCNP-emitted UV light is absorbed by the UV-labile PNB, resulting in photocleavage of *o*-nitrobenzyl groups and, consequently, making the PNB block increasingly hydrophilic due to the formation of carboxylic acid. This photoreaction under NIR light excitation was found to shift the hydrophobic-hydrophilic balance of the diblock copolymer assembly on UCNP surface, which gives rise to disruption of the nanocarrier and concomitant release of encapsulated DOX molecules. In all, we have demonstrated, for the first time to our knowledge, an approach to preparing NIR light-triggered drug release nanocarrier by using UCNP-assisted photolysis reaction in diblock copolymer self-assembly surrounding UCNP. This general method offers new possibilities for further development and exploitation for applications of UCNP/polymer hybrid materials of controlled structures.

Acknowledgements

Y. Z. acknowledges the financial support from the Natural Sciences and Engineering Research Council of Canada (NSERC) and le Fonds de recherche du Québec: Nature et technologies (FRQNT). J. X. and B. Y. thank FRQNT and China Scholarship Council (CSC) for awarding them scholarships. F. S. thanks the National Key Research and Development Program of China (2017YFC0107400 and 2017YFC0107401). Q. Y. acknowledges the National Natural Science Foundation of China (21674022 and 51703034). Y. Z. is a member of the FRQNT-funded Centre Québécois sur les matériaux fonctionnels (CQMF).

Notes and references

1 P. Xiao, J. Zhang, J. Zhao and M. H. Stenzel, *Prog. Polym. Sci.*, 2017, **74**, 1-33.

2 N. Fomina, J. Sankaranarayanan and A. Almutairi, *Adv. Drug Deliver. Rev.*, 2012, **64**, 1005-1020.

3 Y. Zhao, *Macromolecules.*, 2012, **45**, 3647-3657.

4 M. M. Valejo Coelho, T. R. Matos and M. Apetato, *Clin. Dermatol.*, 2016, **34**, 563-570.

5 G. J. Clydesdale, G. W. Dandie and H. K. Muller, *Immunol. Cell Biol.*, 2001, **79**, 547.

6 S. Chen, A. Z. Weitemier, X. Zeng, L. He, X. Wang, Y. Tao, A. J. Y. Huang, Y. Hashimotodani, M. Kano, H. Iwasaki, L. K. Parajuli, S. Okabe, D. B. L. Teh, A. H. All, I. Tsutsui-Kimura, K. F. Tanaka, X. Liu and T. J. McHugh, *Science*, 2018, **359**, 679-684.

7 E. Hemmer, P. Acosta-Mora, J. Mendez-Ramos and S. Fischer, *J. Mater. Chem. B*, 2017, **5**, 4365-4392.

8 H. J. Cho, M. Chung and M. S. Shim, *J. Ind. Eng. Chem.*, 2015, **31**, 15-25.

9 D. Wang, B. Liu, Z. Quan, C. Li, Z. Hou, B. Xing and J. Lin, *J. Mater. Chem. B*, 2017, **5**, 2209-2230.

10 B. Zhou, B. Shi, D. Jin and X. Liu, *Nat. Nanotechnol.*, 2015, **10**, 924-936.

11 M. Haase and H. Schäfer, *Angew. Chem. Int. Edit.*, 2011, **50**, 5808-5829.

12 C. Duan, L. Liang, L. Li, R. Zhang and Z. P. Xu, *J. Mater. Chem. B*, 2018, **6**, 192-209.

13 S. Wu and H.-J. Butt, *Adv. Mater.*, 2016, **28**, 1208-1226.

14 S. Wang, A. Bi, W. Zeng and Z. Cheng, *J. Mater. Chem. B*, 2016, **4**, 5331-5348.

15 G. Chen, H. Qiu, P. N. Prasad and X. Chen, *Chem. Rev.*, 2014, **114**, 5161-5214.

16 B. Yan, J.-C. Boyer, N. R. Branda and Y. Zhao, *J. Am. Chem. Soc.*, 2011, **133**, 19714-19717.

17 M. L. Viger, M. Grossman, N. Fomina and A. Almutairi, *Adv. Mater.*, 2013, **25**, 3733-3738.

18 Y. Yuan, Y. Min, Q. Hu, B. Xing and B. Liu, *Nanoscale*, 2014, **6**, 11259-11272.

19 Q. Xing, N. Li, Y. Jiao, D. Chen, J. Xu, Q. Xu and J. Lu, *RSC Adv.*, 2015, **5**, 5269-5276.

20 G. Jalani, R. Naccache, D. H. Rosenzweig, L. Haglund, F. Vetrone and M. Cerruti, *J. Am. Chem. Soc.*, 2016, **138**, 1078-1083.

21 H. Zhao, W. Hu, H. Ma, R. Jiang, Y. Tang, Y. Ji, X. Lu, B. Hou, W. Deng, W. Huang and Q. Fan, *Adv. Funct. Mater.*, 2017, **27**, 1702592.

22 Y. Zhang, K. Ren, X. Zhang, Z. Chao, Y. Yang, D. Ye, Z. Dai, Y. Liu and H. Ju, *Biomaterials*, 2018, **163**, 55-66.

23 T. Zhao, P. Wang, Q. Li, A. A. Al-Khalaf, W. N. Hozzein, F. Zhang, X. Li and D. Zhao, *Angew. Chem. Int. Edit.*, 2018, **57**, 2611-2615.

24 J. Wang, B. Wu, S. Li and Y. He, *J. Polym. Sci., Part A: Polym. Chem.*, 2017, **55**, 2450-2457.

25 S. Chen, Y. Gao, Z. Cao, B. Wu, L. Wang, H. Wang, Z. Dang and G. Wang, *Macromolecules.*, 2016, **49**, 7490-7496.

26 K. Yan, M. Chen, S. Zhou and L. Wu, *RSC Adv.*, 2016, **6**, 85293-85302.

27 G. Liu, N. Liu, L. Zhou, Y. Su and C.-M. Dong, *Polym. Chem.*, 2015, **6**, 4030-4039.

28 R. Cheng, M. Tian, S. Sun, C. Liu, Y. Wang, Z. Liu, Z. Liu and J. Jiang, *Langmuir.*, 2015, **31**, 7758-7763.

29 G. Liu, L. Zhou, Y. Su and C.-M. Dong, *Chem. Commun.*, 2014, **50**, 12538-12541.

30 G. Chen, R. Jaskula-Sztul, C. R. Esquibel, I. Lou, Q. Zheng, A. Dammalapati, A. Harrison, K. W. Eliceiri, W. Tang, H. Chen and S. Gong, *Adv. Funct. Mater.*, 2017, **27**, 1604671.

31 J. O. Zoppe, N. C. Ataman, P. Mocny, J. Wang, J. Moraes and H.-A. Klok, *Chem. Rev.*, 2017, **117**, 1105-1318.

32 S. Wilhelm, M. Kaiser, C. Wurth, J. Heiland, C. Carrillo-Carrion, V. Muhr, O. S. Wolfbeis, W. J. Parak, U. Resch-Genger and T. Hirsch, *Nanoscale*, 2015, **7**, 1403-1410.

33 F. Shi and Y. Zhao, *J. Mater. Chem. C*, 2014, **2**, 2198-2203.

34 T. Suteewong, H. Sai, M. Bradbury, L. A. Estroff, S. M. Gruner and U. Wiesner, *Chem. Mater.*, 2012, **24**, 3895-3905.

35 G. Louis Chakkalakal, M. Alexandre, C. Abetz, A. Boschetti-de-Fierro and V. Abetz, *Macromol. Chem. Phys.*, 2012, **213**, 513-528.

36 H. T. T. Duong, Y. Chen, S. A. Tawfik, S. Wen, M. Parviz, O. Shimoni and D. Jin, *RSC Adv.*, 2018, **8**, 4842-4849.

37 T. Ma, Y. Ma, S. Liu, L. Zhang, T. Yang, H.-R. Yang, W. Lv, Q. Yu, W. Xu, Q. Zhao and W. Huang, *J. Mater. Chem. C*, 2015, **3**, 6616-6620.

38 Z. Jia, W. Yuan, H. Zhao, H. Hu and G. L. Baker, *RSC Adv.*, 2014, **4**, 41087-41098.

39 A. A. Brown, O. Azzaroni and W. T. S. Huck, *Langmuir.*, 2009, **25**, 1744-1749.

40 F. Liu, X. He, Z. Lei, L. Liu, J. Zhang, H. You, H. Zhang and Z. Wang, *Adv. Healthc. Mater.*, 2015, **4**, 559-568.

41 J. Cui, T.-H. Nguyen, M. Ceolín, R. d. Berger, O. Azzaroni and A. n. del Campo, *Macromolecules.*, 2012, **45**, 3213-3220.

42 S. Kumar, Y. L. Dory, M. Lepage and Y. Zhao, *Macromolecules.*, 2011, **44**, 7385-7393.

43 S. Louguet, B. Rousseau, R. Epherre, N. Guidolin, G. Goglio, S. Mornet, E. Duguet, S. Lecommandoux and C. Schatz, *Polym. Chem.*, 2012, **3**, 1408-1417.

44 Q. Ding, Q. Zhan, X. Zhou, T. Zhang and D. Xing, *Small*, 2016, **12**, 5944-5953.

45 Y. Chen, K. Ai, J. Liu, G. Sun, Q. Yin and L. Lu, *Biomaterials*, 2015, **60**, 111-120.

46 S. Wu, X. Huang and X. Du, *Angew. Chem. Int. Edit.*, 2013, **52**, 5580-5584.

47 D. Kim, E. S. Lee, K. T. Oh, Z. G. Gao and Y. H. Bae, *Small*, 2008, **4**, 2043-2050.

1.3.6 Supporting Information

1.3.6.1 Synthetic route

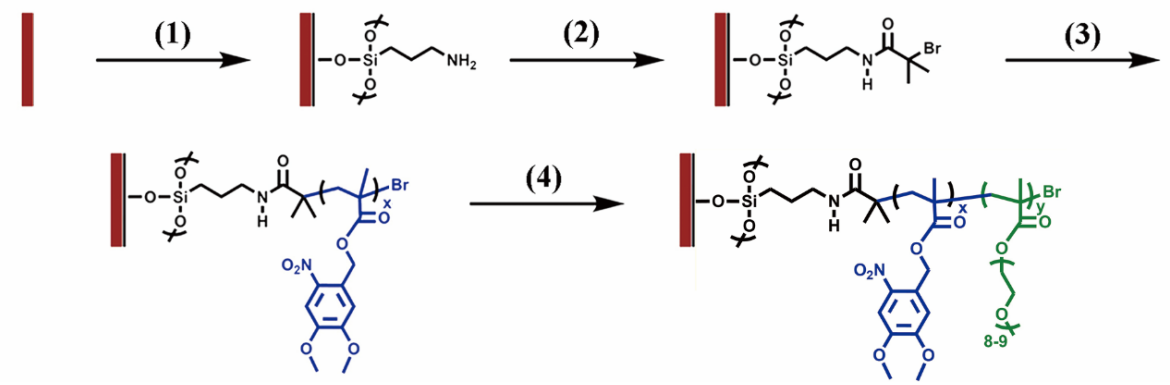

Figure S1 Surface modification of UCNP through a bottom-up strategy: (1) silica layer coating, (2) immobilization of ATRP initiators, (3) growth of hydrophobic block that is a UV-responsive polymer (PNB), and (4) growth of hydrophilic block (POEG). The UCNP and thin silica layers are depicted as red and black rods, respectively.

1.3.6.2 TEM images

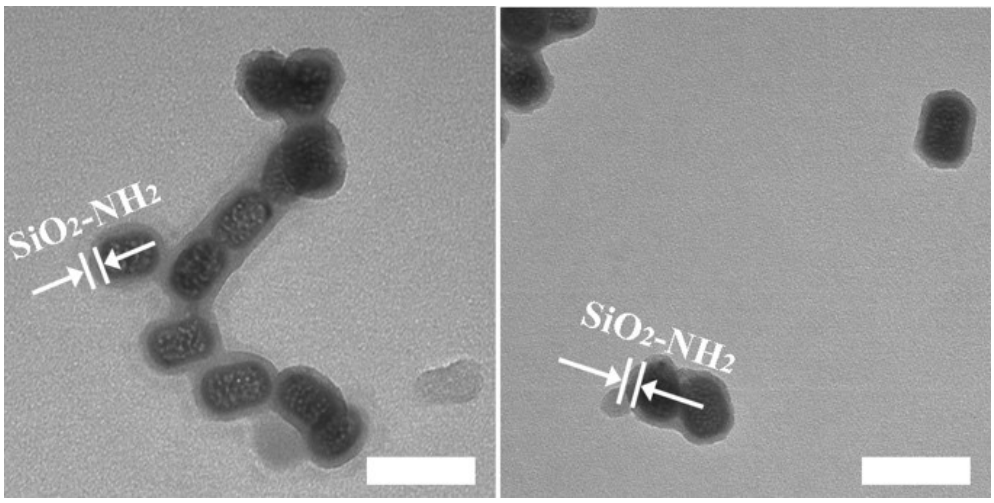

Figure S2. TEM images for UCNP-NH_2. Scale bar is 60 nm.

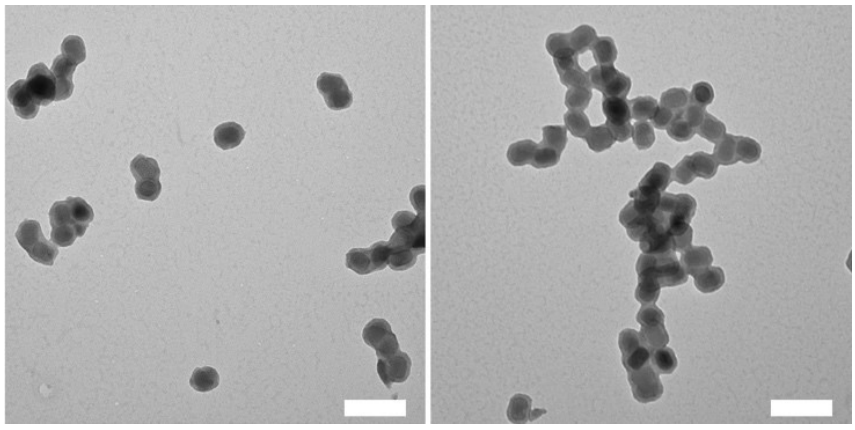

Figure S3. TEM image of UCNP-Br. Scale bar is100 nm.

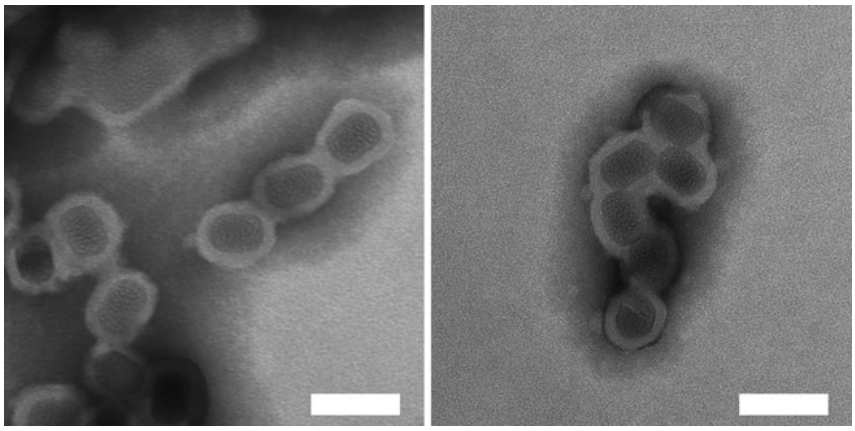

Figure S4. TEM images of UCNP@PNB. Scale bar is 60 nm.

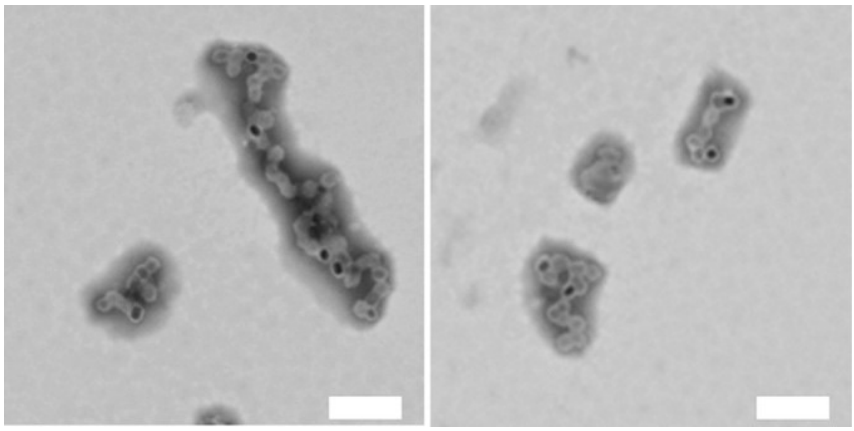

Figure S5. TEM images of UCNP@PNB-b-POEG. Scale bar is 200 nm.

1.3.6.3 TGA analysis

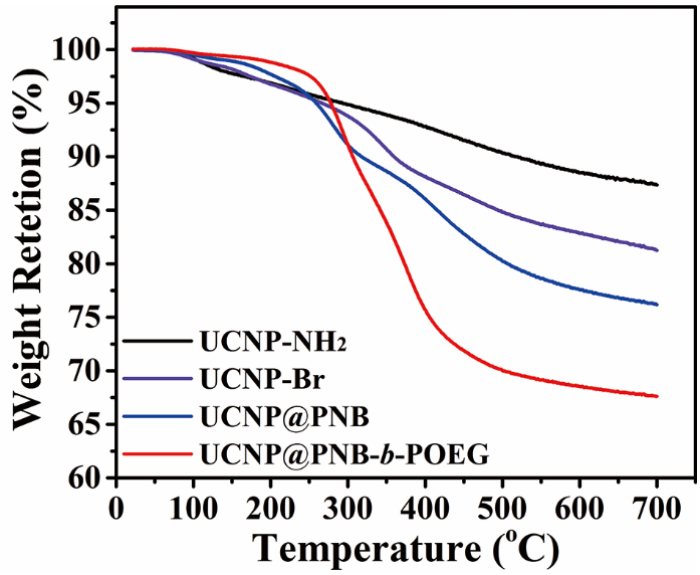

Figure S6. TGA analysis of UCNP-NH_2, UCNP-Br, UCNP@PNB and UCNP@PNB-*b*-POEG.

1.3.6.4 SEC

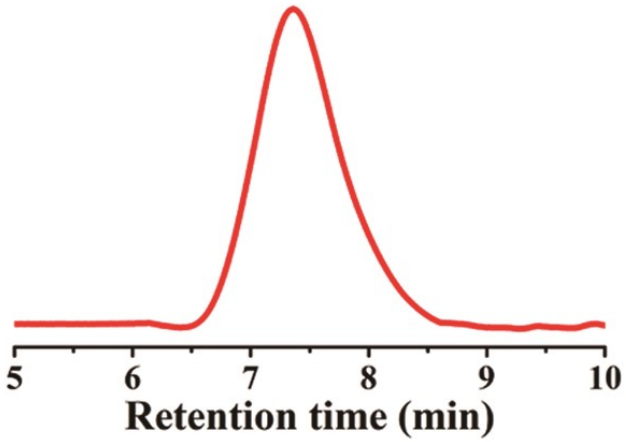

Figure S7. SEC curve of PNB-*b*-POEG cleaved by HF etching of UCNP-*b*-POEG.

1.3.6.5 Calculations

Table S1. Basic information of nanoparticles.

Mass of NPs at room temperature: **1. assuming the residual mass of all NPs is 10 mg at 700 °C.** **2. equation to calculate the mass of NPs at room temperature: mass = (10 mg) / (the wt.% of NPs at 700 °C).**		
mass of UCNP-NH_2 at room temperature (mg)	= 10/0.874	= 11.44
mass of UCNP-Br at room temperature (mg)	= 10/0.813	= 12.30
mass of UCNP@PNB-*b*-POEG at room temperature (mg)	= 10/0.676	= 14.79
Mole weight of organic species in NPs (MWO, g/mol)		
MWO in UCNP-NH_2 (g/mol)	$-(CH_2)_3-NH_2$	= 58
MWO in UCNP-Br (g/mol)	$-(CH_2)_3-NH-C=O-C(CH_3)_2-Br$	= 207
MWO in UCNP@PNB-*b*-POEG	–PNB-*b*-POEG	= 1.09×10^4
UCNP and UCNP-Br: **1. the shape of the UCNP is approximated to be a cylinder and the density of $NaYF_4$:Yb,Tm@$NaYF_4$ is taken to be the same as for $NaYF_4$.** **2. the shape of the UCNP-Br is approximated to be a cylinder and the thickness of silica-Br layer is 6 nm.** **3. assuming the density of silica is 2.1 g/m^3 [a] and the density of silica-Br is taken to be the same as for silica.**		
density of UCNP (g/cm^3) [b]		= 4.31

length of UCNP (nm)		= 34.7
width of UCNP (nm)		= 22.1
volume of one UCNP (nm^3) using $v = \pi r^2 h$	$= 3.14 \times (22.1/2)^2 \times 34.7$	$= 1.33 \times 10^4$
mass of one UCNP (mg)	$= 4.31 \times 10^{-18} \times 1.33 \times 10^4$	$= 5.73 \times 10^{-14}$
surface area of one UCNP (nm^2) using $s = 2\pi r^2 + 2\pi rh$	$= 2 \times 3.14 \times (22.1/2)^2 + 2 \times 3.14 \times (22.1/2) \times 34.7$	$= 3.20 \times 10^3$
length of UCNP-Br (nm)		= 47
width of UCNP-Br (nm)		= 34
volume of one UCNP-Br (nm^3) using $v = \pi r^2 h$	$= 3.14 \times (34/2)^2 \times 47$	$= 4.26 \times 10^4$
surface area of one UCNP-Br (nm^2) using $s = 2\pi r^2 + 2\pi rh$	$= 2 \times 3.14 \times (34/2)^2 + 2 \times 3.14 \times (34/2) \times 47$	$= 6.8 \times 10^3$
volume of silica-Br (nm^3)	$= 4.26 \times 10^4 - 1.33 \times 10^4$	$= 2.93 \times 10^4$
density of UCNP-Br (g/cm^3)	$= (4.31 \times 1.33 \times 10^4 + 2.1 \times 2.93 \times 10^4) / (4.26 \times 10^4)$	= 2.79
mass of one UCNP-Br (mg)	$= 2.79 \times 10^{-18} \times 4.26 \times 10^4$	$= 1.19 \times 10^{-13}$
Number of NPs (10 mg NPs at 700 °C)	$= (10) / (1.19 \times 10^{-13})$	$= 8.41 \times 10^{13}$
Mole of NPs (10 mg NPs at 700 °C)	$= (8.41 \times 10^{13}) / (6.02 \times 10^{23})$	$= 1.40 \times 10^{-10}$

[a] This value was obtained from *J. Eng. Thermophys-Rus.,* **2016***, 25,* 174.

[b] This value was obtained from *Nat. Commun.*, **2015**, *6*, 6938.

Table S2. Useful information from TGA analysis.

Mass loss at different temperature regions	UCNP-NH_2 (mg)	UCNP-Br (mg)	UCNP@PNB-*b*-POEG (mg)
T<80 °C	0.039	0.052	0.014
80 °C<T<150 °C	0.0217	0.175	0.081
250 °C<T<450 °C	0.492	1.11	3.80
Mass of organic species (mg)	= 0.492	= (1.11 - 0.492) = 0.618	= (3.80 - 1.11) = 2.69
Mole of organic species (mmol) [a]	$= 8.5 \times 10^{-3}$	$= 4.2 \times 10^{-3}$	$= 2.5 \times 10^{-4}$
Number of organic species (N) [b]	$= 5.12 \times 10^{18}$	$= 2.47 \times 10^{18}$	$= 1.51 \times 10^{17}$

[a] Mole of organic species = (mass of organic species) / (MWO), MWO is from **Table S1**.

[b] $N = N_A \times$ mole of organic species, N_A is Avogadro constant.

Based on the values from **Table S1** and **S2**, the grafting densities of initiator and polymer can be obtained by the equation below:

Grafting density = (number of organic species) / (surface area of one UCNP-Br × number of NPs)

Therefore, the initiator and polymer grafting densities are approximately 4.4 (or 0.34 mmol/g) and 0.26 chains/nm^2, respectively.

In addition, the initiation efficiency of initiators can be calculated by the following equation:

Initiation efficiency = (grafting density of polymer) / (grafting density of initiator)

Hence, the initiation efficiency is around 6%.

1.3.6.6 Upconversion emission spectra

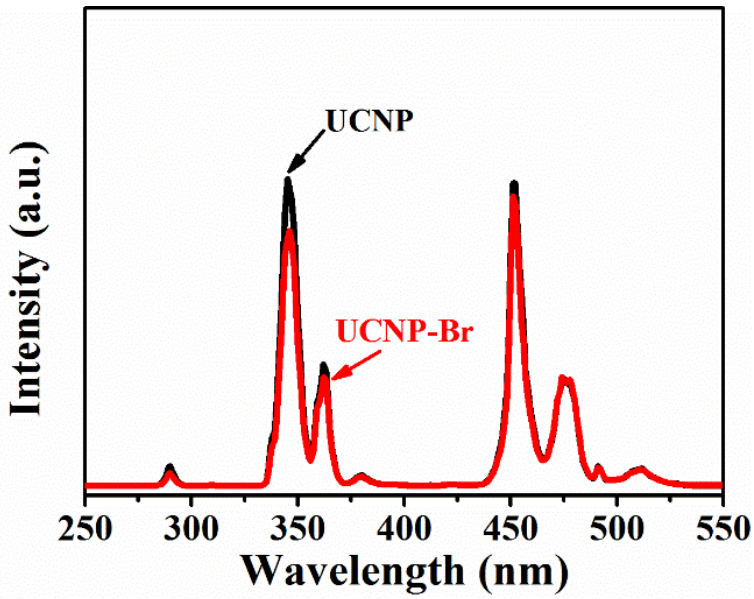

Figure S8. The emission spectra of the neat UCNP (black) in hexane and UCNP-Br (red) in DMF.

1.4 Summary of the Project

In this work, we put forward a bottom-up strategy to prepare a NIR light-controllable drug release nanoplatform with a high degree of monodispersity based on the growth of UV-responsive polymer brushes on the surface of core-shell UCNP ($NaYF_4$:18%Yb/0.5%Tm@$NaYF_4$). First, thin silica (SiO_2) layer (~6 nm) was utilized to incorporate ATRP initiators through covalent bonding and no considerable influence on upconversion luminescence (UCL) emissions of UCNP was found. Next, the initiator-anchored nanoparticles were grafted with UV-sensitive poly(4,5-dimethoxy-2-nitrobenzyl methacrylate) (PNB) for loading hydrophobic payloads and poly(methoxy poly(ethylene glycol) monomethacrylate$_{500}$) (POEG) for stabilizing the system in H_2O by surface-initiated atom transfer radical polymerization (SI-ATRP), respectively. The core-shell-shell (UCNP@SiO_2@Polymers) structured nanoparticles with an average diameter of 120 nm (dry state) were confirmed by TEM measurements while the DLS results indicated the hydrodynamic diameter was ~130 nm (PDI<0.1) in water. The photolysis study revealed that the UV photons emitted by single UCNP within one micelle were enough to trigger the cleavage of photolabile groups in PNB. Finally, drug release study demonstrated that release of doxorubicin could be initiated or terminated by switching on or off a continuous-wave (CW) 980 nm laser. In all, for the first time, we propose a bottom-up approach to preparing a nanoplatform for NIR light-controllable drug release by using UCNP-assisted photolysis reactions of grafted polymer brushes. Our strategy represents a generalized method to obtain UCNP/polymer nanocomposites and may enrich types of polymers (well-developed ATRP technique) in these hybrid materials.

CHAPTER 2 NANOCOMPLEXES OF UV-SENSITIVE POLYELECTROLYTE AND UPCONVERSION NANOPARTICLES FOR NEAR-INFRARED LIGHT-TRIGGERED PAYLOAD RELEASE

2.1 About the Project

In the past two decades, a large number of polymer or polymer/inorganic hybrid nanovectors that respond to an external stimulus, like pH, voltage, temperature and light, have been developed for stimuli-triggered drug delivery. As discussed in the previous chapter, among the many systems, light-responsive nanovectors have attracted broad interest, because light-controlled drug delivery has the appealing spatiotemporal control. Although a significant amount of light-sensitive nanovectors have been reported in the past decade, for the reasons given in Introduction and Chapter 1, only those responding to near-infrared (NIR) light have a significant potential for biomedical applications. Therefore, in this chapter, we continued our effort in designing and preparing new UCNP/polymer nanovectors that can be disrupted by NIR light. While keeping UCNP at the center of the nanovector structure for NIR excitation, the approach employed here is different from the growth of amphiphilic diblock copolymer from UCNP surface as described in the previous chapter. Here the nanovector is built by complexation of a UV-sensitive polyelectrolyte and surface-charged UCNP through electrostatic interactions. Our assumption is that during the electrostatic-driven assembly between UCNP and polyelectrolyte, charged drug molecules can be encapsulated into the nanovector. When NIR light is applied, if UCNP-emitted UV light can induce a photoreaction that causes a charge reversal to the structure of the polyelectrolyte, which may dissolve the polymer layer and result in the release of drug molecules into aqueous solution. Conceptually, even just a tiny fraction of positive charges of polyelectrolyte is replaced by negative charges, the equilibrium can be destabilized and the disruption can lead to drug release. As will be shown further on, experimental results support the nanovector design principle.

2.2 Contributions

This work was published in *ACS Applied Materials & Interfaces*, **2018**, 10, 20790 by Jun Xiang, Feijie Ge, Bing Yu, Qiang Yan, Feng Shi and Yue Zhao. This research work was conducted in the Université de Sherbrooke under the supervision of Prof. Zhao. I designed and performed the experiments described in this study. I collected all the experimental data and analyzed them with my collaborators. Moreover, I drew all the figures in this work and got some useful advice from my collaborators. Feijie Ge helped me with some characterizations, especially the thermogravimetric analysis of resulted nanocomplexes. Bing Yu assisted me with the synthesis of photoresponsive polyelectrolyte and also gave me a lot of useful suggestions. Qiang Yan participated in the design of the UV-labile polyelectrolyte structure and helped the characterizations of the nanocomplexes, particularly TEM observation (sample preparation including the negative staining with phosphotungstic acid) and DLS analysis. Feng Shi synthesized two types of upconversion nanoparticles and gave me valuable suggestions during the characterization of nanoparticles. I have written the full manuscript and submitted it to Prof. Zhao for final revision.

2.3 Paper Published in ACS Applied Materials & Interfaces 2018, 10, 20790.

Nanocomplexes of Photolabile Polyelectrolyte and Upconversion Nanoparticles for Near-Infrared Light-Triggered Payload Release

Jun Xiang[†], Feijie Ge[†], Bing Yu[†], Qiang Yan[§], Feng Shi[*,‡], and Yue Zhao[*,†]

[†]Département de Chimie, Université de Sherbrooke, Sherbrooke, Québec J1K 2R1, Canada.

[‡]School of Materials Science and Engineering, Shaanxi Normal University, Xi'an 710119, China.

[§]State Key Laboratory of Molecular Engineering of Polymers, Department of Macromolecular Science, Fudan University, Shanghai 200433, China.

2.3.1 Abstract

A new approach to encapsulating charged cargo molecules into a nanovector and subsequently using near-infrared (NIR) light to trigger the release is demonstrated. NIR light-responsive nanovector was prepared through electrostatic interaction-driven complexation between negatively charged silica-coated upconversion nanoparticles (UCNP@silica, 87 nm hydrodynamic diameter, polydispersity index ~0.05) and a positively charged UV-labile polyelectrolyte bearing pendants of poly(ethylene glycol) and *o*-nitrobenzyl side groups; while charged fluorescein (FLU) was loaded through a co-complexation process. By controlling the amount of polyelectrolyte, UCNP@silica can be covered by the polymer while remaining dispersed in aqueous solution. Under 980 nm laser excitation, UV light emitted by UCNP is absorbed by photolytic side groups within polyelectrolyte, which results in cleavage of *o*-nitrobenzyl groups and formation of carboxylic acid groups. Such NIR light-induced partial reversal of positive charge to negative charge on the polyelectrolyte layer disrupts the equilibrium among UCNP@silica, polyelectrolyte and FLU and, consequently, leads to release of FLU molecules.

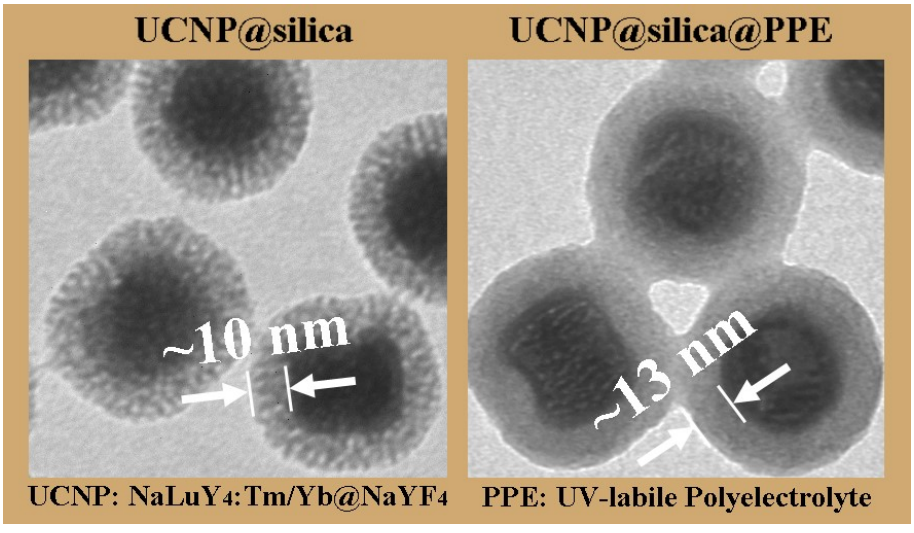

2.3.2 Introduction

In contrast to traditional chemotherapy in which antitumor drugs diffuse nonspecifically, polymer nanovectors are capable of delivering drugs to targeted sites owing to the enhanced permeability and retention (EPR) effect or the conjunction of active ligands.[1-3] To maintain plasma drug concentrations within a therapeutic window, the drug-encapsulated nanovectors are required to liberate molecules in a controllable manner, thereby avoiding multiple-dosage usually required to maintain prolonged therapeutic activity, reducing toxicity in healthy cells and resulting in enhanced patient's compliance. Given this consideration, lots of polymer or polymer/inorganic hybrid nanovectors that respond to an external stimulus, like pH,[4-6] voltage,[7-8] temperature,[9-10] and light,[11-13] have been developed for stimuli-triggered drug delivery. Among them, light-responsive nanovectors have attracted broad interest, because light-controlled drug delivery has the appealing spatiotemporal control.[14-16] Although a significant amount of light-responsive nanovectors, especially those with UV light sensitivity, have been reported in the past decade, only those responsive to near-infrared (NIR) light have significant potential for biomedical applications.[17-20] In the past few years, a widely applied approach to preparing NIR-sensitive nanovectors is the combination of upconversion nanoparticles (UCNP) and UV-sensitive polymers.[21-28] The underlying principle is that UV photons emitted by UCNP from inside the nanovector under NIR light excitation are absorbed by the UV-sensitive polymer to bring about the photochemical reaction, which leads to the nanovectors' disruption and simultaneous payload release.

Hitherto diverse methodologies have been put forward to organize UCNP and UV-sensitive polymers in constructing hybrid nanovectors for NIR light-triggered drug delivery. Of them, amphiphilic polymer assembly is the most frequently utilized method, in which hydrophobic UCNP and drugs are entrapped into the hydrophobic core of micelles, while the hydrophilic corona stabilizes them in water.[21, 25, 29-31] However, this method has certain limitations: the co-assembly of UCNP and polymer lacks control in that two or more UCNP can be encapsulated inside the same micelle, resulting in heterogeneity and a high UCNP

content; and it is restricted to loading non-water soluble drugs. Although other methods are proposed to construct UCNP/polymer nanovectors, like the surface coating of UCNP or the introduction of photocaged drug into polymers, they all involve multistep chemical modifications which make the preparation of nanovectors complicated and demanding.[23-24, 32-33] Therefore, despite the numerous progresses, it is still challenging and necessary to develop robust and straightforward methodologies for preparing UCNP-loaded polymer assemblies with well-controlled architectures.

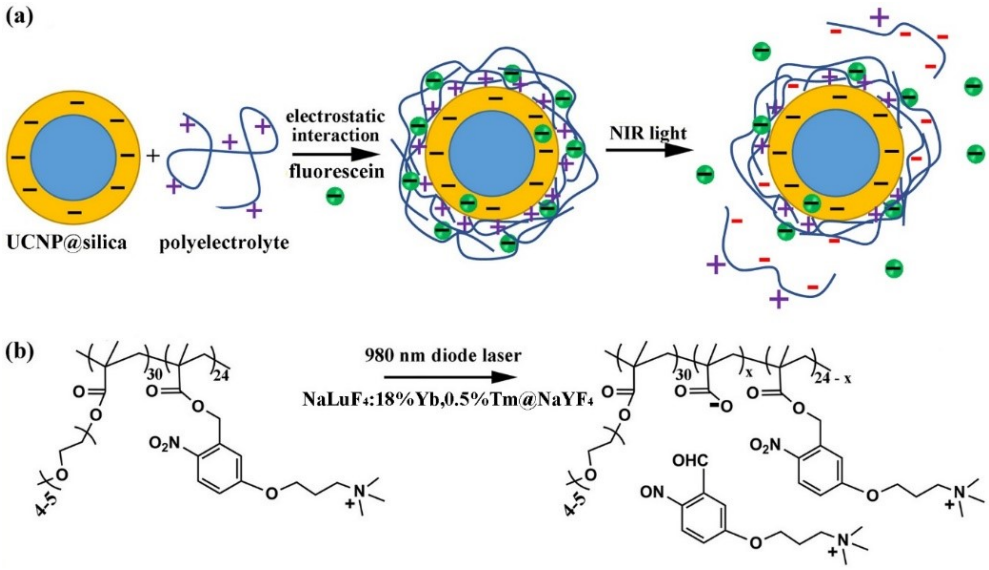

Figure 1. (a) Schematic illustration of near-infrared (NIR) light-triggered polymer layer disruption and drug release from the nanovector of UCNP@silica@polyelectrolyte self-assembled through electrostatic interactions. (b) Polymer chemical structure, used UCNP ($NaLuF_4$:18%Yb,0.5%Tm@$NaYF_4$) and the NIR light-triggered photocleavage reaction of the photolabile polyelectrolyte.

Here we report a new strategy to build the hybrid nanovector based on the complexation of a UV-sensitive polyelectrolyte and surface-charged UCNP through electrostatic interactions. Our method first endows UCNP with water-dispersity by introducing electric charges on their surface. The presence of electrostatic repulsion force hence reduces the propensity for the nanoparticles to aggregate. Then the oppositely charged polyelectrolyte is added into

the solution to complex with UCNP. Since the amount of polymer can be easily tuned by changing the concentration of polymer or volume of polymer solution, the preparation of UCNP/polymer nanovectors has a high degree of flexibility. Moreover, this design allows for the encapsulation of water-soluble drugs during the nanovector preparation process through electrostatic interactions, which facilitates the encapsulation step.

The design of our NIR-responsive nanovector is depicted in Figure 1a. UCNP is coated with mesoporous silica with negatively charged surface, referred to as UCNP@silica hereafter. The nanoparticles are complexed with a positively charged photolabile polyelectrolyte (PPE) in the presence of a negatively charged drug. Our assumption is that during PPE deposition on the UCNP@silica surface, drug molecules can be co-assembled with polymer chains and loaded in the polyelectrolyte layer, or even in the mesoporous silica that is a known drug carrier system[34-35]. After equilibrium of the electrostatic interactions involved in the assembly, when NIR light is applied, if UCNP-emitted UV light can induce a photochemical reaction that turns the positive charges on the polymer chains into negative charges, an increased electrostatic repulsion force between UCNP@silica and PPE should dissolve the polymer layer and result in release of drug molecules into aqueous solution. Conceptually, even just a very small fraction of positive charges of PPE are replaced by negative charges, the electrostatic equilibrium can still be destabilized and the disruption can lead to drug release. Notably, payload release by regulating surface charges of UCNP/polymer has been recently reported in the literature, in which the amphiphilic polymer assembly was employed.[26] The differences in the present work are the use of electrostatic interaction-driven assembly and the negatively charged surface of the fluorescein-loaded nanovectors. It's worthy of noting that the negatively charged nanovector may lead to longer circulation half-lives in the biomedical applications.[36]

To validate this new nanovector for NIR light-triggered drug delivery, the designed UV-sensitive polyelectrolyte has the chemical structure shown in Figure 1b. It is a methacrylate random copolymer bearing hydrophilic pendants of poly(ethylene glycol) and photolytic side groups with positive charges. After photocleavage of the *o*-nitrobenzyl

(ONB) groups, carboxylic acid is formed; as the cleaved nitroso compound diffuses away into the solution, the polyelectrolyte contains negative charges, which can lead to the destabilization of the electrostatic equilibrium in nanovector and release of the loaded drug. In this study, fluorescein (FLU) was used as a model drug for encapsulation and release upon NIR light irradiation. As will be shown further on, experimental results support the nanovector design principle. Here, it should be mentioned that using a photolabile charge on an ONB ester to change the electrostatic assembly of polymers is a well-established approach and has been applied to a variety of materials systems such as DNA-polymer complexes,[37] silica colloids,[38] and layer-by-layer assembled films.[39]

2.3.3 Experimental Sections

2.3.3.1 Materials. All chemicals were of analytical grade and used without further purification except where noted. Rare earth chloride hexahydrate ($LuCl_3 \cdot 6H_2O$ 99.99%, $YbCl_3 \cdot 6H_2O$ 99.99%, $TmCl_3 \cdot 6H_2O$ 99.99%, $ErCl_3 \cdot 6H_2O$ 99.99%, and $YCl_3 \cdot 6H_2O$ 99.99%) were obtained from Shandong Yutai Chemical Reagent Co., Ltd. Ammonium fluoride (NH_4F, 98%), sodium hydroxide (NaOH, 98%), anhydrous ethanol (EtOH), and methanol (MeOH) were supplied by Sinopharm Chemical Reagent Co., Ltd. Other chemical reagents were purchased from Sigma-Aldrich and Fisher Scientific.

2.3.3.2 Synthesis of Photolabile Polyelectrolyte. The synthetic route for the photolabile polyelectrolyte is shown in Scheme S1. Details for each reaction step are given below.

Synthesis of 5-hydroxy-2-nitrobenzyl alcohol (2). A round-bottom flask was charged with 1.93 g 5-hydroxy-2-nitrobenzaldehyde (**1**) and 30 mL methanol. After cooling by an ice-water bath, 0.95 g sodium borohydride ($NaBH_4$) was slowly added under argon gas protection. When the reaction was completed (revealed by thin-layer chromatography), the reaction mixture was quenched with dilute HCl to pH 4, following by extraction with ethyl acetate three times. The combined organic layers were washed with brine (5 wt.%), dried over anhydrous $MgSO_4$, filtered, and then concentrated on a rotary evaporator. ^1H and ^{13}C NMR spectra of **2** are shown in Figure S1 and S2, respectively.

Synthesis of (5-(3-(dimethylamino) propoxy)-2-nitrophenyl) methanol (3). A 250 mL one-neck round-bottom flask was charged with 2.0 g **2**, 2.02 g 3-dimethylamino-1-propyl chloride hydrochloride, 1.10 g NaOH, 65 mL toluene, and 13 mL EtOH. This solution was heated to 80 ºC and stirred for 60 h. After cooling to room temperature, solvents were removed by a rotary evaporator and diluted with 150 mL sodium carbonate (Na_2CO_3, 5 wt.%). Then this solution was extracted with diethyl ether (DEE) twice. The organic phase was combined and washed with Na_2CO_3 solution three times, dried over $MgSO_4$, filtered, and concentrated using a rotary evaporator. Finally, a light brown solid was obtained as the product and used in the following experiment without further purification. ^1H and ^{13}C NMR spectra of **3** are presented in Figure S3 and S4, respectively.

Synthesis of 5-(3-(dimethylamino)propoxy)-2-nitrobenzyl methacrylate (4). A 20 mL vial was charged with 0.71 g **3**, 0.22 mL triethylamine (TEA), and 12 mL dry CH_2Cl_2 (DCM). After cooling with an ice-water bath, 0.33 mL methacryloyl chloride was dropwise added under the protection of argon gas. The reaction mixture was then stirred at room temperature for another 20 h. Then the whole solution was diluted with DCM and washed with 5 wt.% Na_2CO_3 solution and 15 wt.% brine, dried over anhydrous $MgSO_4$, filtered, and then concentrated on a rotary evaporator. Finally, compound **4** was stored in a refrigerator before use. ^1H and ^{13}C NMR spectra of **4** are shown in Figure S5 and S6, respectively.

Synthesis of photolabile polyelectrolyte (PPE). Firstly, poly(ethylene glycol) methyl ether methacrylate (OEGMA, M_n = 300 g/mol) was purified by passing through a column filled with basic alumina. To a round-bottom flask (5 mL) was charged with 204 mg **4** (0.63 mmol), 221 mg OEGMA (0.74 mmol), 4.1 mg 2,2′-azobis(2-methylpropionitrile) **(**AIBN) and 1 mL DMF. This solution was purged with argon gas for 10 min and then stirred at 70 °C for 20 h. The reaction was stopped with liquid nitrogen and precipitated into a mixture of hexane and DEE (1:1 v/v) for three times. The resulting precipitate was collected by centrifugation. 0.18 g gel-like polymer (**5**) with dark-brown color was obtained. The ONB units account for ~44% in number in **5** (Figure S7a). Moreover, the GPC result

shows that its molecular weight is 16,800 (M_n) with PDI 1.60 after removing low-molecule-weight compounds by dialyzing (MWCO 3,500). Afterward, 0.1 g **5** was dissolved in 30 mL of dried DCM in a one-neck flask. Iodomethane (MeI, 0.1 g) was slowly added to this solution. The resulting mixture was stirred at room temperature for one day in the dark, and then DCM and excess CH_3I were removed by a rotary evaporator and vacuum. Finally, PPE was obtained by dialysis against deionized water (3,500 MWCO dialysis tubing from Spectra/Por) and recovered after freeze-drying. The degree of quaternization was found to be ~93% (Figure S7b).

2.3.3.3 Synthesis of Silica-coated Upconversion Nanoparticles. Two kinds of upconversion nanoparticles were synthesized, namely, $NaLuF_4$:18%Yb,0.5%Tm@$NaYF_4$ (denoted as UCNP) and $NaYF_4$:18%Yb,2%Er@$NaYF_4$. Unless otherwise stated, UCNP was used in all experiments in this study. Er-UCNP, which basically emits no UV light under 980 nm laser excitation, was only used for control experiments (synthetic details in Supporting Information). They were synthesized by following the same experimental procedures but with the differences in types and contents of the added rare earth ions. To avoid redundant description, only detailed synthesis steps leading to silica coated $NaLuF_4$:18%Yb,0.5%Tm@$NaYF_4$ (UCNP@silica) are described below. While the details on the synthesis of Er-UCNP are given in Supporting Information, the synthesis of Er-UCNP@silica used the same conditions as detailed below for UCNP@silica.

Synthesis of β-$NaLuF_4$:18%Yb,0.5%Tm Nanoparticles. β-$NaLuF_4$:18%Yb,0.5%Tm nanoparticles were synthesized by the solvothermal method reported in the literature.[40] $LuCl_3 \cdot 6H_2O$ (0.815 mmol), $YbCl_3 \cdot 6H_2O$ (0.18 mmol), $TmCl_3 \cdot 6H_2O$ (0.005 mmol) were mixed with 6 mL oleic acid (OA) and 15 mL 1-octadecene (ODE) in a 100 mL three-neck round flask. The mixture was heated to 160 °C for 60 min to form a homogeneous solution under argon gas protection. When the solution was cooled down to room temperature, 10 mL methanol solution containing NH_4F (4 mmol) and NaOH (2.5 mmol) was added drop by drop into the solution, forming a milky mixture. The mixture was stirred rigorously under argon gas protection for 60 min, then slowly heated to 60 °C to evaporate excess

methanol for another 60 min. Moreover, it was degassed for 20 min at 120 °C. After that, the mixture was heated to 300 °C with a heating rate of 15 °C/min and then maintained at the temperature for 60 min under argon gas protection. After the reaction, the solution was cooled down to room temperature and the product was precipitated by the addition of an excess amount of EtOH, and collected by centrifugation at 9000 rpm for 10 min. The precipitate was washed with an EtOH/hexane mixture (3:1 v/v) three times, and the NPs were finally dispersed in cyclohexane as the core for further use.

Synthesis of β-NaLuF$_4$:18%Yb,0.5%Tm@NaYF$_4$ Nanoparticles (UCNP). $YCl_3 \cdot 6H_2O$ (0.5 mmol) was mixed with 6 mL OA and 15 mL ODE in a 100 mL three-neck round flask and heated to 160 °C for 60 min to form a homogeneous solution under argon gas protection. Then the mixture was cooled down under 40 °C and the β-NaLuF$_4$:18%Yb,0.5%Tm core was added. The mixture was immediately degassed at 80 °C for 20 min to evaporate the extra cyclohexane. Then, it was cooled down to room temperature. The next experimental steps were the same as for the synthesis of β-NaLuF$_4$:18%Yb,0.5%Tm core. The final product was dispersed in cyclohexane. The obtained NaLuF$_4$:18%Yb,0.5%Tm@NaYF$_4$ nanoparticles have an average dimension of 48 (*L*) × 38 (*W*) nm (Figure S8).

Synthesis of UCNP@silica. Typically, 100 mg UCNP in chloroform ($CHCl_3$) was added to an aqueous solution (80 mL) containing 0.2 g cetyltrimethylammonium bromide (CTAB). This solution was stirred at 60 °C to remove $CHCl_3$ until a transparent solution was obtained. After sonicating for 1 h, it was heated up to 70 °C and its pH was adjusted to around 9 with NaOH solution. Then an anhydrous EtOH (0.4 mL) solution of tetraethyl orthosilicate (TEOS, 0.32 mL) was added to the above solution. After 0.5 h, the mixture of (3-aminopropyl) triethoxysilane (APTES, 10 μL) and EtOH (200 μL) was slowly added. Then the reaction was kept at 70 °C for another 5 h. Finally, UCNP@silica-NH_2 with CTAB were isolated by centrifugation with EtOH. This washing procedure was repeated for four times and dried by a freezing vacuum. The amine groups in UCNP@silica-NH_2 with CTAB were converted into carboxylic acid groups via the reaction with succinic anhydride

to endow them with negatively charged surface. Typically, 0.38 g nanoparticles were added to a DMSO solution (15 mL) containing succinic anhydride (90 mg) and TEA (130 uL). This solution was maintained at 40 ^{o}C for 48 h and purified by centrifugation with EtOH for four times. The ion exchange method was employed to remove CTAB.[41] UCNP@silica-COOH with CTAB was redispersed into EtOH (60 mL) solution with NH_4NO_3 (0.33 g) and refluxed at 80 ^{o}C overnight. The final product (UCNP@silica) was kept in EtOH for further use. FTIR spectra revealed that the successful removal of CTAB (Figure S9).

2.3.3.4 Preparation of UCNP@silica@PPE. Complexes of UCNP@silica and PPE were formed in M.Q. H_2O. An aqueous solution of PPE (~0.01 mg/mL) was dropwise added (speed: 0.5 mL/min) into UCNP@silica (1 mg/mL, 10 mL) under vigorously stirring (1000 rpm). The resulting solution was stirred for 10 min for equilibrium after each addition of 56 μg PPE. The molar ratio of PPE chains to UCNP@silica is determined by the total amount of PPE added into the solution for complexation. As an example, the molar ratio of 56 μg PPE to 10 mg UCNP@silica is 45:1 based on the analysis shown in Table S1. Afterwards, 1 mL of the resulting UCNP@silica@PPE solution was taken out for further analysis or experiment.

2.3.3.5 Preparation of Fluorescein Loaded UCNP@silica@PEE complex (FLU-UCNP@silica@PPE. The conditions for preparing FLU-UCNP@silica@PPE (USP-X) samples are shown in **Table 1**. UCNP@silica and FLU were first dispersed into EtOH (15 mL) to form a transparent solution with yellow color. Next, EtOH was slowly removed by a rotatory evaporator at 30 ^{o}C. Water (2 mL) was added to the dried product, and the whole solution was sonicated in an ice-water bath for one hour (70 W/40 kHz). After addition of PPE solution for complexation and FLU co-assembly, free FLU was removed by centrifugation with a large amount of Tris buffer solution (10 mM, pH 7.4). The absorbance at 490 nm of supernatants was used as quality control (≤0.05 for 1 cm light path length). The FLU-UCNP@silica@PPE samples were redispersed into Tris buffer solution (5 mg/mL) for further use.

Table 1. Preparation conditions for samples of FLU-UCNP@silica@PPE nanocomplexes

Acronym of FLU-UCNP@silica @PPE sample	10 mg UCNP@silica (nmol) [a]	PPE (μg) [b]	PPE : UCNP@silica [c]	FLU : UCNP@silica [d]
USP-1	6.24×10^{-2}	168	135:1	1:1
USP-2	6.24×10^{-2}	168	135:1	2.2:1
USP-3	6.24×10^{-2}	168	135:1	4.5:1
USP-4	6.24×10^{-2}	0	0	4.5:1
USP-5	6.24×10^{-2}	21	17:1	4.5:1
USP-6	6.24×10^{-2}	42	34:1	4.5:1
USP-7	6.24×10^{-2}	84	67:1	4.5:1

[a] Value from the analysis in **Table S1**.

[b] Value from mass = concentration × volume of PPE added.

[c] Molar ratio of PPE chains to UCNP@silica.

[d] Feed mass ratio before the addition of PPE.

2.3.3.6 Photolysis Studies of UCNP@silica@PPE under 980 nm Excitation. The aqueous solution of UCNP@silica@PPE nanovector (5 mg/mL, 0.5 mL) was placed in a dialysis cup (MWCO 3,500, Slide-A-Lyzer™ MINI Dialysis Devices) and placed on top of a quartz cuvette filled with aqueous solution. A continuous-wave (CW) 980 nm NIR laser was applied vertically from the top to the solution for a number of consecutive cycles of 5 min irradiation-on followed by 5 min irradiation-off. Photocleaved, low-molar-mass molecules in the UCNP@silica@PPE solution can diffuse through a membrane into the bottom solution in the cuvette. The absorption spectra of the bottom solution were recorded every 20 min during the test.

2.3.3.7 Release of FLU under 980 nm Excitation. To investigate NIR light-triggered release of FLU loaded in UCNP@silica@PPE, the aqueous solution of FLU-UCNP@silica@PPE (5 mg/mL, 0.4 mL) was placed in the dialysis cup and subjected to 980 nm NIR light irradiation under the same conditions as described above. Likewise, FLU molecules released from the nanovector in the solution in the dialysis cup can diffuse into the bottom solution in the cuvette. The absorption spectra of the bottom solution were recorded every 10 min during the measurement. For the control test, the whole device was kept in the dark and the absorption spectra were collected at the same time points.

2.3.3.8 Characterizations. ^{1}H NMR spectra were recorded on a Bruker Advance III HD 300 MHz spectrometer using deuterated solvents at 25 °C. The residual solvent peak was used as an internal standard. Gel permeation chromatography (GPC) measurements were carried out at 45 °C on a Tosoh EcoSEC GPC system, equipped with three TSK-GEL Super AWM-H columns (6 × 150 mm). DMSO containing 1.25 mg/mL of LiBr was used as the eluent (flow rate: 0.3 mL/min) and poly(methyl methacrylate) (PMMA) was used for calibration. UV light irradiation experiments were performed using an OmniCure@Series 1000 UV lamp. The power density of the UV light was calibrated by an Oriel Radiant Power Meter (MODEL 70260; SER. NO. 76376) coupled with an Ophir's Laser Measurement Photodiode (PD300-UV; P/N 1Z02413). FT-IR spectra were recorded on a Bomen FTIR spectrometer (ABB MB104PH) using the diffuse reflection technique. Spectra were obtained in the region of 4000-600 cm^{-1} at a resolution of 4 cm^{-1}. Thermogravimetric analysis (TGA) was performed with a SETARAM thermogravimetric analyzer (SETSYS, TG-DTA 1600) at a heating rate of 10 °C/min from room temperature to 700 °C under an argon atmosphere. The UV-vis absorption spectra were acquired on a Varian 50 Bio UV-vis spectrophotometer. TEM measurements were carried out using a Hitachi H-7500 microscope at an acceleration voltage of 80 kV. TEM specimens were prepared by dropping dilute solutions of samples (~10 μL) onto carbon-coated copper grids while allowing the solvent to evaporate completely and then stained with phosphotungstic acid. The sizes of the nanoparticles (hydrodynamic diameter: D_H) and their zeta potentials were measured on a Malvern Zetasizer Nano ZS ZEN3600 system with a helium-neon laser

(wavelength, λ = 633 nm), using a scattering angle of 173°. To monitor the zeta potential of UCNP@silica@PPE after NIR irradiation, 10 μL of nanocomplexes (1 mg/mL) in a 1.5 mL Eppendorf tube was irradiated by the 980 nm laser for consecutive cycles of 1 min irradiation-on followed by 1 min irradiation-off; it was then diluted for the zeta potential measurements. UCL spectra were recorded with a double-monochromator Fluorolog 2 instrument from Spex. A power-adjustable 980 nm laser diode (MDL-H-980 nm-4W, Changchun New Industries Optoelectronics Tech. Co., Ltd.) was employed as the upconversion pump source.

2.3.4 Results and Discussion

2.3.4.1 Characterization of UCNP@silica@PPE

To confirm the formation of UCNP@silica@PEE nanocomplexes, TEM and DLS measurements were carried out, and the results are shown in Figure 2. As can be seen, UCNP@silica has a *core-shell* structure and the silica layer has an average thickness of 10 nm (Figure 2a). The size histogram obtained from a statistical analysis (Figure S10) indicates that the diameter of UCNP@silica is around 67 nm. After complexation of UCNP@silica with PPE (molar ratio of PPE to UCNP@silica is 135:1), TEM images reveal that the silica layer becomes blurred (Figure 2b) and the size histogram shows that the size of UCNP@silica@PPE is increased to around 74 nm (Figures S11 and S12), which indicates the covering of the UCNP@silica surface by the polyelectrolyte chains and thus confirms the successful preparation of the UCNP@silica@PPE nanocomplexes. On the other hand, DLS results show that UCNP@silica nanoparticles in aqueous solution have an average hydrodynamic diameter (D_H) of 87 nm with a high degree of uniformity (PDI 0.05) (Figure 2c), and that the dispersion is stable at room temperature (Figure S13). The inset photo in Figure 2c shows the transparent aqueous solution of UCNP@silica. The as-synthesized UCNP@silica possessing extremely low PDI and high stability in water is the key to prepare the well-controlled architecture of UCNP-loaded polymer assemblies in this work. By contrast, after complexation with PPE, the DLS results indicate D_H ~112 nm

for UCNP@silica@PPE with relatively low PDI 0.17 (Figure 2d). The increase in size after complexation is also reflected by the increased light scattering of the UCNP@silica@PPE solution, while the nanocomplex particles remain well dispersed in solution (Figure 2d). Moreover, the covering of UCNP@silica by PPE chains was indicated by thermogravimetric analysis (Figure S14, **Tables** S2 and S3). All these data confirm the successful preparation of the UCNP@silica@PPE nanocomplexes.

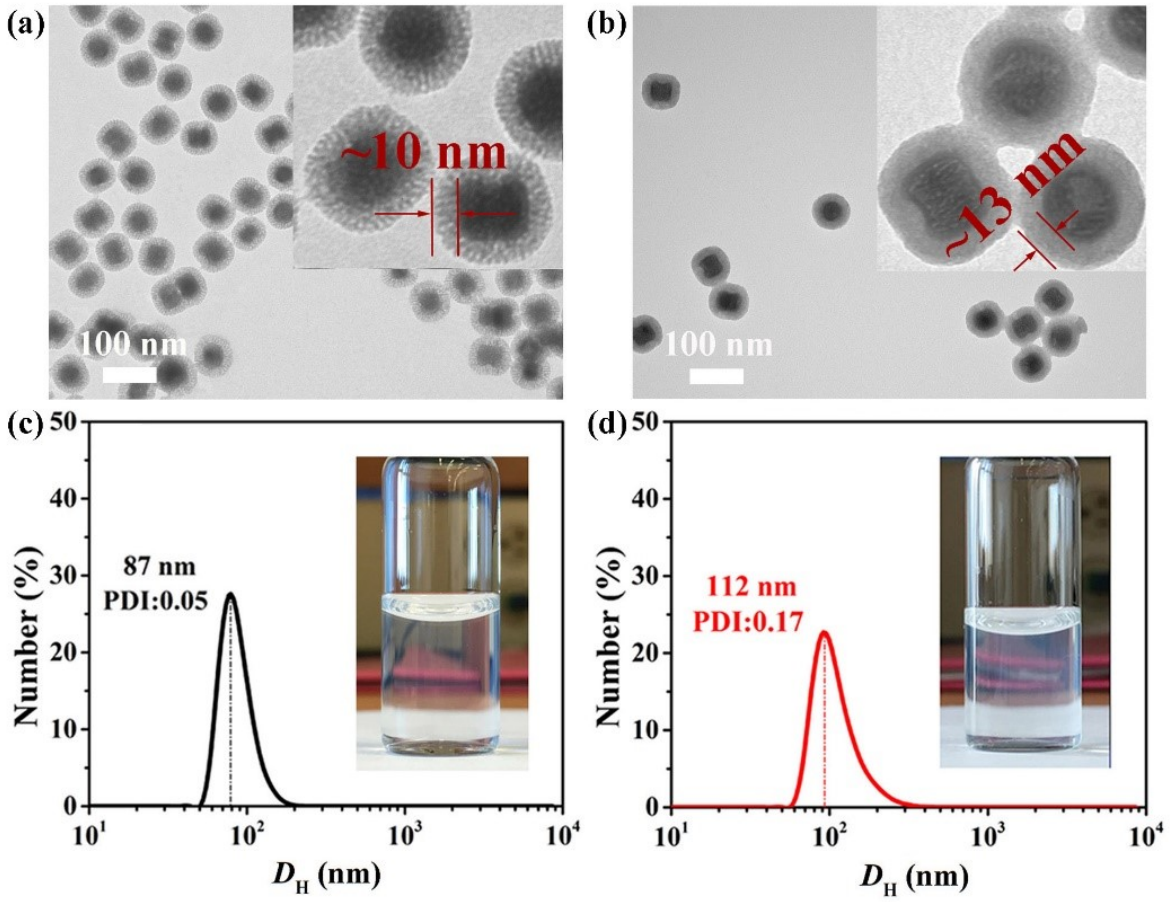

Figure 2. TEM images and the size distributions as revealed by DLS for UCNP@silica (a and c) and UCNP@silica@PPE (b and d). The inset photos show the corresponding aqueous solution of UCNP@silica (in c) and UCNP@silica@PPE (in d).

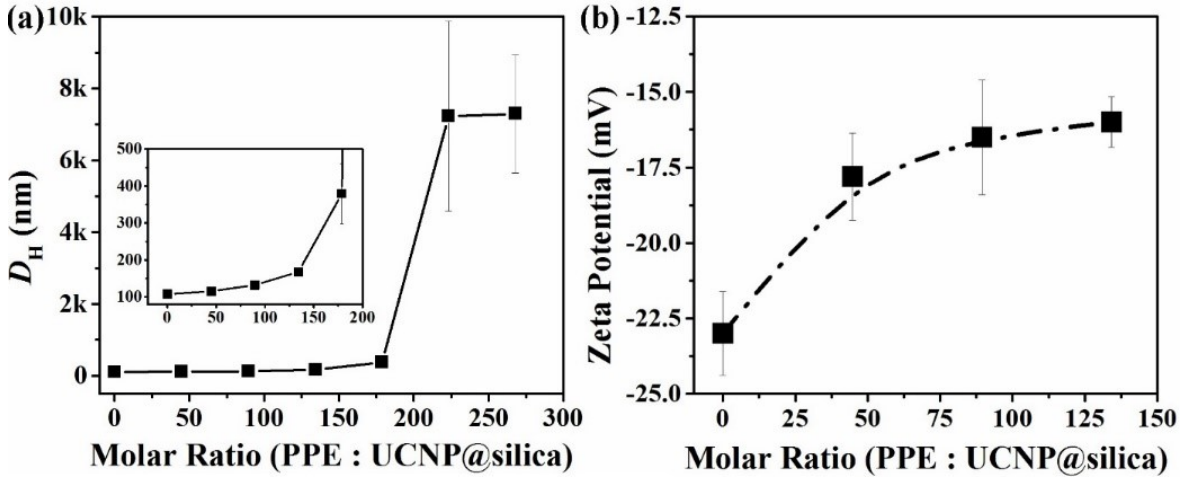

Figure 3. (a) D_H *vs.* molar ratio of PPE chains to UCNP@silica obtained from DLS measurements in H_2O. The inset is an enlarged plot over the region of interest. (b) The effect of molar ratio of PPE chains to UCNP@silica on the zeta potential of the resulting UCNP@silica@PPE after complexation (pH 6.6).

It was found that the molar ratio of PPE chains to UCNP@silica affects the stability of the resulting nanocomplexes. To avoid aggregation, the molar ratio should be kept below 135:1 to control the size below 200 nm (Figure 3a). The change in zeta potential of UCNP@silica over the molar ratio of PPE chains to UCNP@silica was monitored during the preparation process (Figure 3b). UCNP@silica had an average zeta potential of -23 mV (1 mg/mL) before the formation of complexes owing to the deprotonation of carboxylic acids (pKa ~4.5)[42] at pH 6.6. Upon complexation with positively charged PPE chains, the negative zeta potential of the nanoparticles decreased. Since the pH of the complex solution remained unchanged, the variation of zeta potential arises from the adsorption of PPE on the surface of UCNP@silica. The decrease in the negative surface potential is more prominent with increasing the amount of PPE, reaching a magnitude of ~21% when molar ratio reaches 45:1 and ~28% when molar ratio achieves 90:1. Upon further increment of molar ratio, the decrease of the negative charge became more slowly. With molar ratio at 135:1, the complex solution showed a zeta potential of -16 mV that, for this nanocomplex system, appears to be sufficient to keep the nanoparticles well dispersed in aqueous solution. At this

point, the complexes still have negatively charged surface, which suggests that the cationic units in PPE are not enough to offset the large number of negative charges in UCNP@silica. Moreover, despite the seemingly small amount of PPE with respect to UCNP@silica, the actual anchoring density is significant due to the large density difference between the two constituents. For example, for the USP-3 sample (PPE/UCNP@silica 135:1), the estimated density of positively charged ONB units in the polyelectrolyte layer is 0.21 per nm^2 (**Table S1**).

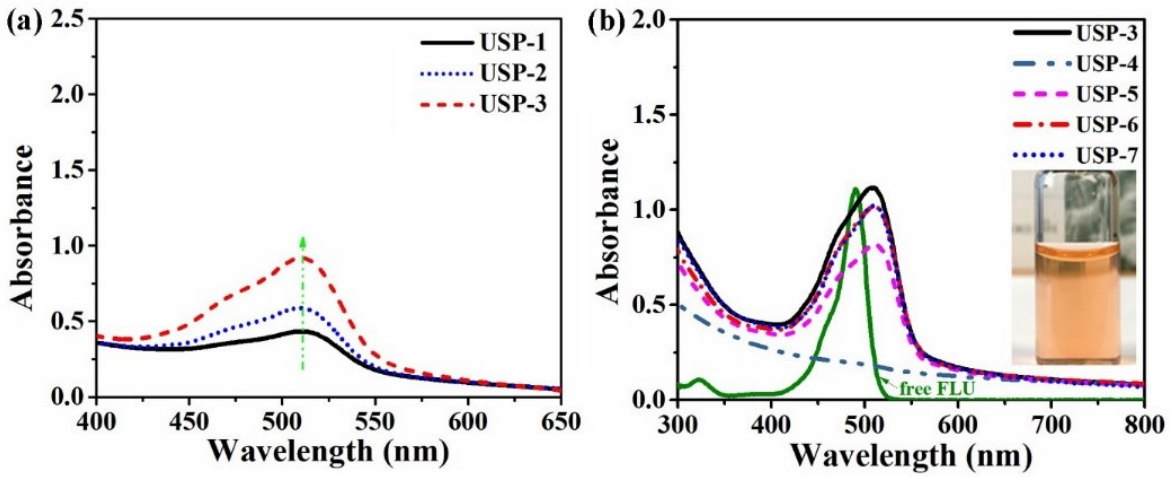

Figure 4. (a) UV-vis absorption spectra of USP-1, USP-2 and USP-3. The three USP samples have the same molar ratio of PPE chains to UCNP@silica (135:1) but differ in the mass ratio of FLU to UCNP@silica used for the preparation of FLU-loaded UCNP@silica@PPE nanocomplexes (1:1 for USP-1, 2.2:1 for USP-2, and 4.5:1 for USP-3) (**Table 1**). (b) UV-vis absorption spectra of FLU-UCNP@silica@PPE (0.4 mg/mL, from USP-3 to USP-7) and free FLU. The samples of USP-4, USP-5, USP-6 and USP-7 have the same mass ratio of FLU to UCNP@silica used for the loading as USP-3 (4.5:1) but different molar ratios of PPE to UCNP@silica (0 for USP-4, 17:1 for USP-5, 34:1 for USP-6, and 67:1 for USP-7) (**Table 1**). The inset picture shows an aqueous solution of USP-3 (0.4 mg/mL).

Fluorescein (FLU) was utilized as a model drug to check the loading capacity of the nanovector. First, UCNP@silica was mixed with FLU and then PPE was added using the

same procedure as with the preparation of FLU-free complexes. Eventually, unloaded FLU molecules were removed by centrifugation. Different FLU-loaded samples were prepared by adjusting the weight ratio of FLU to UCNP@silica while keeping the molar ratio of PPE chains to UCNP@silica constant (135:1) (USP-1 – USP-3 in **Table 1**). As can be seen in Figure 4a, the absorption peak centered at 510 nm corresponding to entrapped FLU molecules increases with increasing the feed mass ratio of FLU to UCNP@silica. Based on the spectra, the estimated amount of FLU encapsulated by 1 g UCNP@silica@PPE is 7 mg for USP-3. This value may look very small due to the large difference in density. However, the estimated number of FLU loaded by per UCNP@silica particle is 3,380 (0.24 per nm^2) (**Table S1**). In our further experiments, the feed mass ratio of 4.5:1 (FLU to UCNP@silica) was used to investigate the effect of the amount of PPE on the loading of FLU (USP-4 – USP-7 in **Table 1**). As shown in Figure 4b, there is basically no absorption at 510 nm without PPE (USP-4). However, an increase in absorbance at 510 nm is observable when the molar ratio of PPE chains to UCNP@silica reaches 17, but this peak varies little when it is over 34, which may suggest that the electrostatic interactions among UCNP@silica, FLU, and PPE reach an equilibrium. A photo of the USP-3 solution is also given (Figure 4b). The payload-encapsulated nanovector appears a dark-orange color, which is consistent with the observations reported in the literature.[43] It can be noticed that the absorption spectrum of FLU-UCNP@silica@PPE exhibits a red-shift from 490 to 510 nm, which may be attributed to the specific interactions involving FLU molecules (e.g., π-π stacking and electrostatic interactions) and the varying microenvironment.[43-45]

2.3.4.2 Photolysis Study of UCNP@silica@PPE

The photolysis of PPE under UV light (365 nm) irradiation was first investigated as a control. The absorption spectral changes of the polyelectrolyte over UV irradiation time are visible (Figure S15). Before irradiation, the PPE has a strong absorption peak at 312 nm due to the absorption of the photolabile ONB groups. After 20 min of UV illumination, a decrease in the absorbance at 312 nm (~43%) and a new peak at ~350 nm corresponding to

the cleaved *o*-nitrobenzaldehyde are observable, indicating the occurrence of the photocleavage reactions induced by 365 nm light.

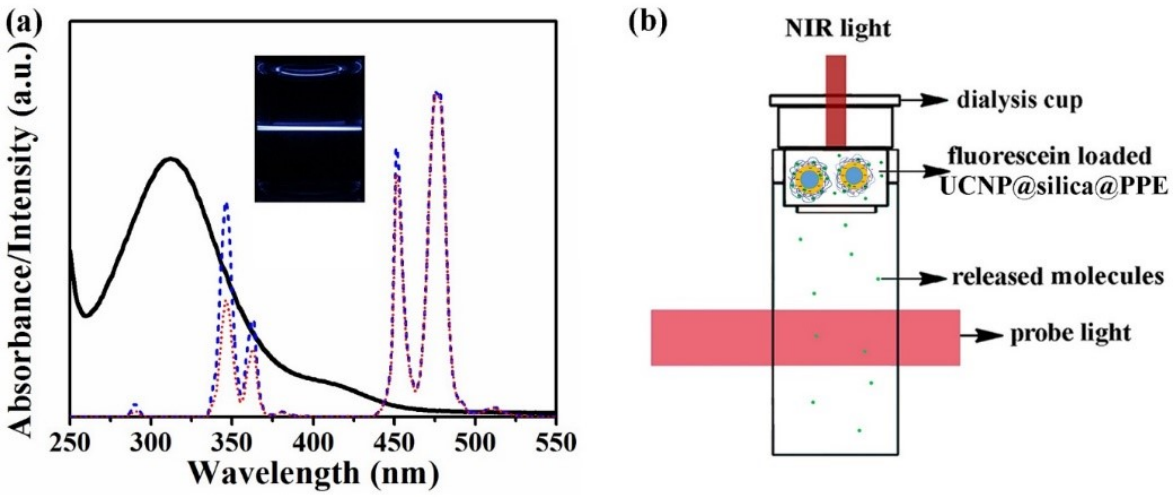

Figure 5. (a) The absorption spectrum (black continuous line) of a mixture of UCNP@silica and PPE as well as its UCL spectrum (red dotted line) under 980 nm laser irradiation. The emitted UV light (325-375 nm) by UCNP in the mixture displays a decrease in intensity as compared to the UCL spectrum of neat UCNP (blue dashed line). The inset photograph shows the mixture emitting visible light where the 980 nm laser beam passes through the solution. (b) The setup used to detect released molecules diffusing through a dialysis membrane into aqueous solution underneath (Tris buffer, 10 mM, pH 7.4) upon NIR light irradiation (~29 W/cm^{-2}, 980 nm).

To verify whether the presence of PPE affects the photoluminescence property of UCNP, a mixture of PPE (2 mL, 0.1 mg/mL) and UCNP@silica (0.2 mg) was prepared. Figure 5a shows a photograph of this mixture upon exposure to a continuous-wave 980 nm diode laser. The emitted visible light can be readily observed where the laser beam passes through the solution. Moreover, the absorption and upconversion luminescence (UCL) spectra of the mixture, as well as the absorption spectrum of UCNP@silica, are also shown in Figure 5a. The UCL spectrum of UCNP in the UV region overlaps well with the broad absorption band of PPE and only decreased intensities in the upconverted UV emissions can be noticed

(peaks between 325 and 375 nm), indicating the absorption of the upconverted UV light by the ONB groups in PPE. The UV light absorption appears to be partial, likely due to the small amount of PPE used in the mixture. The photo-induced payload release triggered by 980 nm NIR light was investigated using the setup depicted in Figure 5b. A mini dialysis cup with an aqueous solution of nanocomplexes was put on the top of a quartz cell filled with aqueous solution. The FLU together with cleaved molecules resulting from photolysis reactions can diffuse through the dialysis membrane on the bottom of the cup into the solution below. Hence, the released molecules or chromophores with specific absorption bands can be detected by means of a UV-vis spectrophotometer.

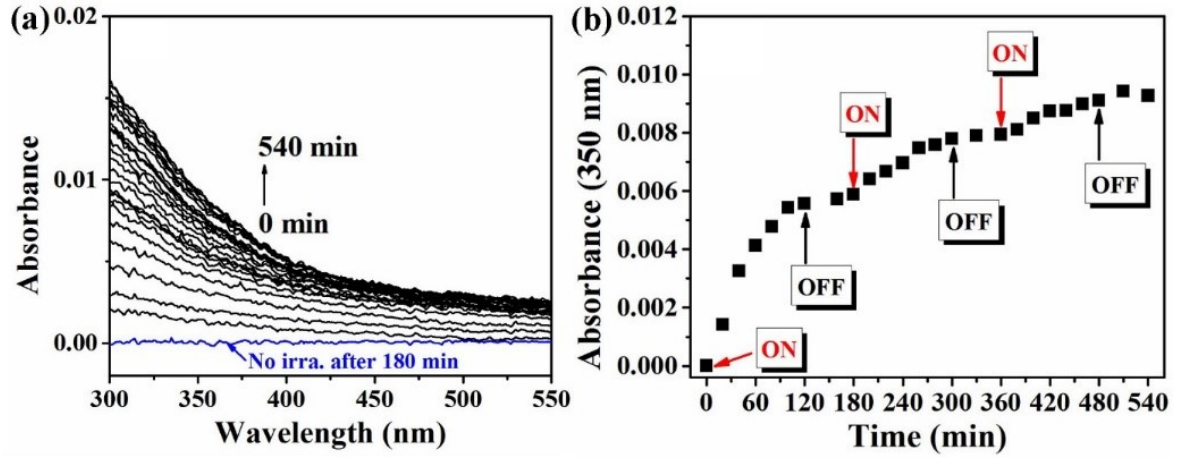

Figure 6. (a) Absorption spectral change over time for the cleaved molecules from UCNP@silica@PPE (5 mg/mL, 0.5 mL) triggered by a CW 980 nm laser (~29 W/cm^{-2}) using the setup in Figure 5b. (b) Plot of absorbance at 350 nm *vs.* time. "ON" labels indicate the beginning of the NIR light irradiation experiment in the following two hours, while "OFF" labels mean the switching off the NIR light laser in the following one hour.

Utilizing this setup, the photolysis of UCNP@silica@PPE without loading FLU under 980 nm excitation was first investigated. The details for the NIR irradiation experiment are already given in Experimental Section. The solution in the dialysis cup was irradiated by a NIR laser from the top for a number of cycles, each of which contains 5 min irradiation-on followed by 5 min irradiation-off. The absorption spectra of the bottom solution were

recorded once every 20 min during the irradiation test. As shown in Figure 6a, the absorbance in the 300-550 nm region was zero over 180 min when the UCNP@silica@PPE solution was kept in the dark (without NIR light irradiation). By contrast, an increase in absorption, especially at wavelengths below 400 nm, can be seen upon only 20 min of 980 nm irradiation. In addition, this absorption band increases with increasing the irradiation time. This result clearly indicates the occurrence of photocleavage of ONB groups in PPE chains complexed with UCNP@silica nanoparticles. To observe the release profile of the cleaved chromophores, a plot of absorbance at 350 nm as a function of time is presented in Figure 6b. The result shows that the release of cleaved nitrobenzaldehyde species can be modulated by turning on or turning off the 980 nm NIR laser.

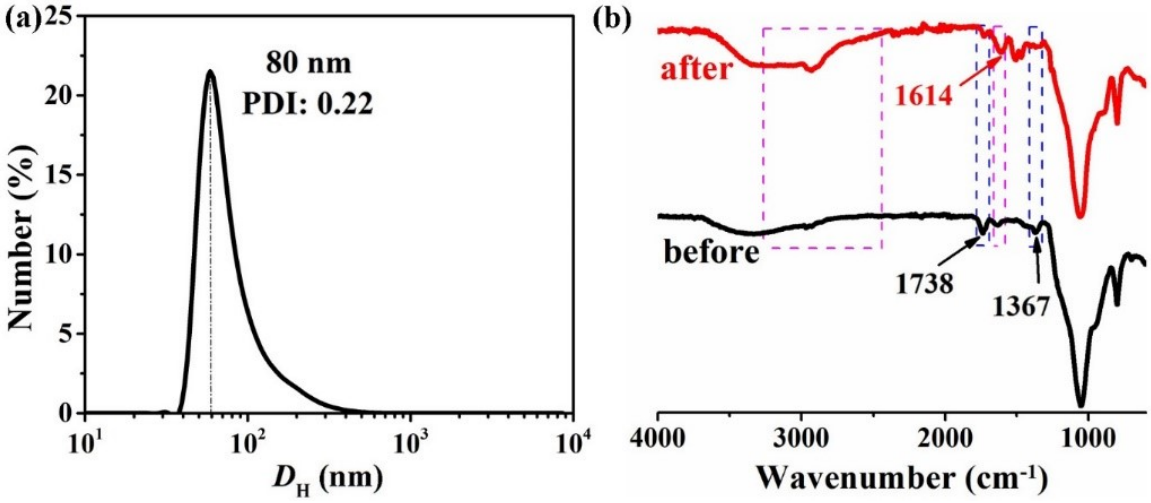

Figure 7. (a) D_H of UCNP@silica@PPE after three hours of NIR irradiation. (b) FT-IR spectra of UCNP@silica@PPE before (black) and after (red) 980 nm illumination for three hours.

After a total of three hours of NIR light irradiation, the variation of nanoparticle size and functional groups of UCNP@silica@PPE were analyzed by DLS and IR spectroscopy. The residual solution in the dialysis cup was dialyzed against a large amount of water to remove remained small molecular weight compounds before the measurements. As shown in Figure 7a, the resulting sample has a D_H around 80 nm with a relatively low PDI (0.22). The

decrease in size after the NIR light irradiation implies partial dissociation of the nanocomplexes. More information was obtained from the FT-IR spectral analysis. As shown in Figure 7b, a decrease of the characteristic bands at 1367 cm^{-1} (symmetric vibration of the nitro group) and 1738 cm^{-1} (ester carbonyl stretching of the methacrylate) was observed, suggesting removal of photolabile ONB groups from PPE after 980 nm irradiation. On the contrary, the vibrational bands at 2500-3300 cm^{-1} (stretching of O–H in carboxylic acid) and 1614 cm^{-1} (asymmetric stretching of $–COO^-$)[46] are enhanced, which indicates the presence of carboxylate anions after the UCNP-assisted photoreactions. Furthermore, the negative zeta potential of UCNP@silica@PPE was found to be increased over 980 nm irradiation, which is also consistent with the formation of carboxylate anions on PPE (Figure S16). All these results confirm the disruption of the UCNP@silica@PPE nanocomplex due to the ONB photocleavage triggered by UV light emitted from UCNP under NIR light excitation.

2.3.4.3 NIR Light-triggered Fluorescein Release from FLU-UCNP@silica@PPE

The NIR light-induced release of fluorescein from FLU-UCNP@silica@PPE aqueous solution was then investigated using the same setup. The absorption spectra of the bottom solution over time for USP-6 (**Table 1**) were recorded with the nanocomplex solution in the dialysis cup subjected to 980 nm light irradiation, in an on/off manner. The results are shown in Figure 8. In this case, the FLU molecules diffusing through the membrane can be detected from the absorption peak at 490 nm (Figure 8a). Notably, this absorption band shifts from 510 to 490 nm, indicating the “free” state of the released FLU molecules. The plot in Figure 8b shows that the release of FLU can also be tuned by NIR light, although a slight amount of FLU can escape from the nanovector without NIR light irradiation, as revealed by the control test. At the end of the measurement, the data show that the released amount of guest molecules upon 980nm light irradiation is about seven times higher than that observed in the control test without irradiation.

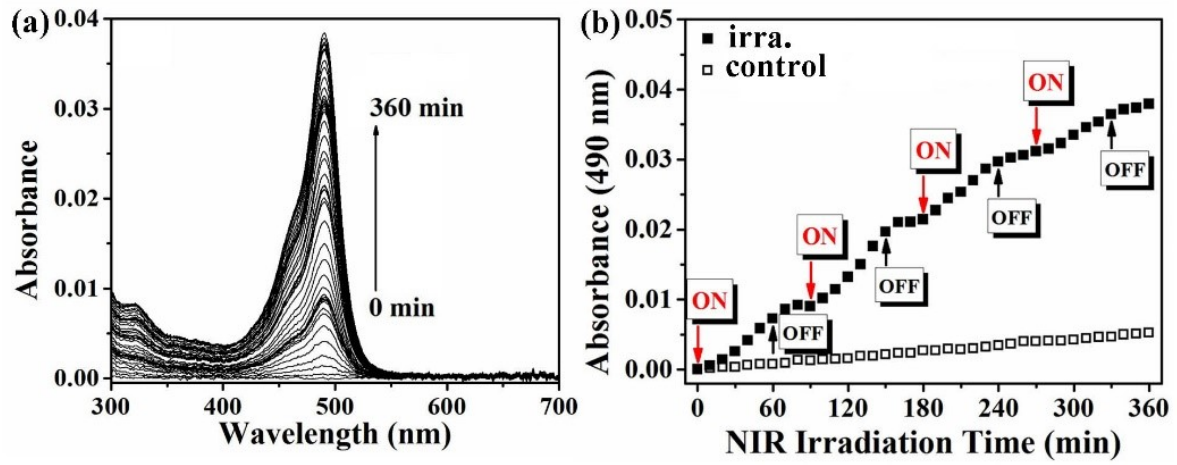

Figure 8. (a) Absorption spectral changes over time from the bottom solution of USP-6 (0.4 mL in dialysis cup; molar ratio of PPE chains to UCNP@silica is 34:1). (b) Plot of absorbance at 490 nm *vs.* time, "ON" labels indicate the beginning of the NIR light irradiation experiment in the following one hour, while "OFF" labels mean the switching off the NIR light laser in the following thirty minutes. The control test is for the solution without NIR light irradiation.

The effect of molar ratio of PPE chains to UCNP@silica on the NIR light-induced cargo release was then studied using the same experimental procedure. The results obtained for USP-3, USP-6, and USP-7 (see **Table 1**) are summarized in Figure 9, plotting the absorbance at 490nm *vs.* time. It is noted that (1) the accumulation time of NIR irradiation was two hours for all samples, (2) the accumulation period of switching off NIR laser was four hours for all samples, and (3) the ON/OFF labels for USP-3 and USP-7 are the same but different from that of USP-6. As pointed out above, all three samples almost encapsulated the same amount of FLU at the same concentration (Figure 4b). Therefore, the only difference in the three samples is the molar ratio of PPE chains to UCNP@silica for the complexation. For all nanovectors, their control tests show only few FLU released from the nanocomplex without NIR light irradiation. The release becomes much greater upon NIR irradiation. These results indicate that all nanovectors can efficiently prevent leakage of guest molecules and that the NIR light illumination can initiate the liberation of FLU. It

can also be noticed that based on the detected absorption, the amount of released FLU molecules for USP-6 and USP-7 samples are the same within the total of 360 min, but that of USP-3 only reaches ~82% of release in comparison. Overall, the effect of the amount of PPE on UCNP@silica surface appears to be quite small. Another notable finding is the difference in their UV-vis spectra in the 300-420 nm region after 360 min (Figure S17). An increase in absorption was observed for UCNP@silica@PPE with increasing PPE amount. This result indicates that more ONB groups on PPE are cleaved with more PPE chains on UCNP@silica surface under the same experimental conditions, which should be no surprise.

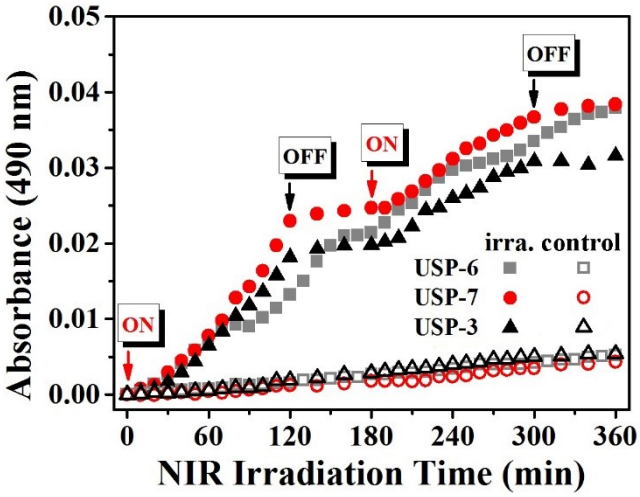

Figure 9. Plots of absorbance *vs.* time for three FLU-UCNP@silica@PPE samples differing only in the amount of polyelectrolyte (**Table 1**). For USP-3 (molar ratio of PPE chains to UCNP@silica is 135:1) and USP-7 (the ratio is 67:1), "ON" labels indicate the beginning of the NIR light irradiation experiment in the following two hours, while "OFF" labels mean the switching off the NIR light laser in the following one hour. For USP-6, the "ON" and "OFF" are the same as in Figure 8b. For all control tests (open symbols), the same solutions were not subjected to NIR irradiation.

Finally, a control experiment was designed and carried out in order to make sure that the described mechanism is truly what leads to the observed NIR light-triggered payload

release. Even with the intermittent 980 nm laser exposure (5 min) used in this study, the solution temperature may increase due to strong water absorption at this wavelength (up to 80 ^{o}C for the test solution in the dialysis cup owing to the small volume). As mentioned above, Er-UCNP differs from Tm-doped UCNP in that under 980 nm NIR excitation, the UCL emission in the UV region (below 400 nm) is negligible. Using the same preparation conditions as with UCNP, we were able to synthesize similarly monodispersed Er-UCNP (Figure S18), Er-UCNP@silica (Figure S19) and Er-UCNP@silica@PPE nanocomplex (Figure S20, **Table S4**). Their UCL spectral measurements under 980 nm laser excitation confirmed basically the absence of UV emission from Er-UCNP (Figure S21). Also using the same conditions as described above, fluorescein was efficiently loaded through co-assembly (Figure S22), the resulting FLU-Er-UCNP@silica@PPE was subjected to the same 980 nm laser on/off cycles as in Figure 8b, and the release of FLU molecules was monitored. The rationale of the control is as follows. The two FLU-loaded nanovectors are the same except the no-UV-emission of Er-UCNP; since no UV light-induced cleavage of ONB groups can occur with FLU-Er-UCNP@silica@PPE under 980 nm laser exposure, any enhanced release with respect to the solution without NIR irradiation should be caused by solution heating effect on the nanovector. The results presented in Figure S23 show that under the intermittent 980 nm laser exposure, the release of FLU increases as compared to the release without NIR irradiation, implying an effect of solution heating on the FLU release. However, the release level of FLU-Er-UCNP@silica@PPE under 980 nm laser exposure remains substantially below that of FLU-UCNP@silica@PPE. This result thus confirms without ambiguity that the primary contributing mechanism for the NIR-triggered payload release is the charge reversal on the polyelectrolyte chains as a result of ONB groups cleavage caused by the UV light emitted from UCNP under 980 nm laser exposure.

The whole of the above results allow us to conclude that the release of FLU is attributed to the envisioned mechanism as depicted in Figure 1a. For the encapsulation of negatively charged FLU molecules, there is an electrostatic equilibrium among UCNP, FLU, and PPE, which makes drug molecules trapped in the PPE layer on the nanoparticle surface. For this reason, the diffusion of FLU molecules from the samples in the control tests without NIR

irradiation is very small and does not exhibit a burst release under the used conditions. Once the 980 nm laser is switched on, upconverted UV light is absorbed by the polyelectrolyte, inducing the charge sign reversal from positive to negative due to cleaved ONB units from PPE. This breaks the electrostatic equilibrium and thereby leads to repelled FLU molecules from the nanocomplex. By contrast, when the NIR light is turned off, no more changes in surface charge can be caused by the removal of photolabile groups, and thus a new electrostatic equilibrium is established and halts the release process of FLU molecules. Since the release of FLU depends on the charge reversal of the nanocomplexes, the larger amount of PPE complexed with UCNP@silica, the more prolonged NIR irradiation time is required to produce the charge reversal to repel FLU. This may explain why the amount of FLU released from USP-3 is smaller than the other two samples after 360 min.

2.3.5 Conclusions

We have reported a novel method to prepare NIR-sensitive nanovectors based on UCNP/UV-sensitive polymers by utilizing electrostatic interactions. The UV-labile polyelectrolyte bearing hydrophilic poly(ethylene glycol) pendants and photolabile ONB side groups with positive charges can be utilized to form nanocomplexes with negatively charged silica-coated UCNP (UCNP@silica) in water. The amount of PPE added to the solution for complexation with UCNP@silica has a significant effect on the stability of the resulting complex nanoparticles. The UCNP@silica@PPE was investigated as a new NIR light-responsive nanovector for controlled drug delivery. The negatively charged model compound fluorescein could be loaded into the nanovector through a co-complexation process. The fluorescein-loaded UCNP@silica@PPE samples exhibit controllable release behavior under 980 nm excitation, which was attributed to the modulation of electrostatic interactions by the upconverted UV light through the photocleavage reaction. Our approach offers an easy way to prepare NIR light-responsive nanovectors, and the method is general and can be extended to other designs. For instance, to encapsulate a positively charged drug for NIR light-triggered release, it can be co-complexed and co-assembled with a negatively

charged UV-labile polyelectrolyte in an aqueous solution of UCNP with positively charged surface.c

ASSOCIATED CONTENT

Supporting Information

The Supporting Information is available free of charge on the ACS Publications website at DOI: 10.1021/acsami.8b05063. More information including characterization results of NMR, TEM, FTIR, DLS, TGA and UV-vis spectroscopy for both Tm and Er-doped UCNP-based systems.

AUTHOR INFORMATION

Corresponding Author

* E-mail: shifeng@snnu.edu.cn (F.S.)

* E-mail: yue.zhao@usherbrooke.ca (Y.Z.)

Notes

The authors declare no competing financial interest.

ACKNOWLEDGMENTS

This work was supported by the Natural Sciences and Engineering Research Council of Canada (NSERC), le Fonds de recherche du Quebec: Nature et technologies (FRQNT), the National Key Research and Development Program of China (2017YFC0107400 and 2017YFC0107401), and the National Natural Science Foundation of China (21674022 and 51703034). J. Xiang, F. Ge, and B. Yu thank FRQNT and China Scholarship Council (CSC) for awarding them a scholarship. Y. Zhao is a member of the FRQNT-funded Centre Québécois sur les matériaux fonctionnels (CQMF).

REFERENCES

(1) Bertrand, N.; Wu, J.; Xu, X.; Kamaly, N.; Farokhzad, O. C. Cancer Nanotechnology: the Impact of Passive and Active Targeting in the Era of Modern Cancer Biology. *Adv. Drug Deliver. Rev.* **2014**, *66*, 2-25.

(2) Chow, E. K.-H.; Ho, D. Cancer Nanomedicine: From Drug Delivery to Imaging. *Sci. Transl. Med.* **2013**, *5*, 216rv214-216rv214.

(3) Davis, M. E.; Chen, Z.; Shin, D. M. Nanoparticle Therapeutics: an Emerging Treatment Modality for Cancer. *Nat. Rev. Drug Discov.* **2008**, *7*, 771.

(4) Chen, Y.; Han, H.; Tong, H.; Chen, T.; Wang, H.; Ji, J.; Jin, Q. Zwitterionic Phosphorylcholine–TPE Conjugate for pH-Responsive Drug Delivery and AIE Active Imaging. *ACS Appl. Mater. Inter.* **2016**, *8*, 21185-21192.

(5) Koren, E.; Apte, A.; Jani, A.; Torchilin, V. P. Multifunctional PEGylated 2C5-Immunoliposomes containing pH-Sensitive Bonds and TAT Peptide for Enhanced Tumor Cell Internalization and Cytotoxicity. *J. Control. Release* **2012**, *160*, 264-273.

(6) Lee, Y.; Fukushima, S.; Bae, Y.; Hiki, S.; Ishii, T.; Kataoka, K. A Protein Nanocarrier from Charge-Conversion Polymer in Response to Endosomal pH. *J. Am. Chem. Soc.* **2007**, *129*, 5362-5363.

(7) Ge, J.; Neofytou, E.; Cahill, T. J.; Beygui, R. E.; Zare, R. N. Drug Release from Electric-Field-Responsive Nanoparticles. *ACS Nano* **2012**, *6*, 227-233.

(8) Yan, Q.; Yuan, J.; Cai, Z.; Xin, Y.; Kang, Y.; Yin, Y. Voltage-Responsive Vesicles Based on Orthogonal Assembly of Two Homopolymers. *J. Am. Chem. Soc.* **2010**, *132*, 9268-9270.

(9) Liu, X.; Appelhans, D.; Wei, Q.; Voit, B. Photo-Cross-Linked Dual-Responsive Hollow Capsules Mimicking Cell Membrane for Controllable Cargo Post-Encapsulation and Release. *Adv. Sci.* **2017**, *4*, 1600308.

(10) Li, W.; Huang, L.; Ying, X.; Jian, Y.; Hong, Y.; Hu, F.; Du, Y. Antitumor Drug Delivery Modulated by A Polymeric Micelle with an Upper Critical Solution Temperature. *Angew. Chem. Int. Edit.* **2015**, *54*, 3126-3131.

(11) Hu, X.; Feeney, M. J.; McIntosh, E.; Mullahoo, J.; Jia, F.; Xu, Q.; Thomas, S. W. Triggered Release of Encapsulated Cargo from Photoresponsive Polyelectrolyte Nanocomplexes. *ACS Appl. Mater. Inter.* **2016**, *8*, 23517-23522.

(12) Song, J.; Fang, Z.; Wang, C.; Zhou, J.; Duan, B.; Pu, L.; Duan, H. Photolabile Plasmonic Vesicles Assembled from Amphiphilic Gold Nanoparticles for Remote-Controlled Traceable Drug Delivery. *Nanoscale* **2013**, *5*, 5816-5824.

(13) He, J.; Wei, Z.; Wang, L.; Tomova, Z.; Babu, T.; Wang, C.; Han, X.; Fourkas, J. T.; Nie, Z. Hydrodynamically Driven Self-Assembly of Giant Vesicles of Metal Nanoparticles for Remote-Controlled Release. *Angew. Chem. Int. Edit.* **2013**, *52*, 2463-2468.

(14) Olejniczak, J.; Carling, C.-J.; Almutairi, A. Photocontrolled Release using One-photon Absorption of Visible or NIR light. *J. Control. Release* **2015**, *219*, 18-30.

(15) Gohy, J.-F.; Zhao, Y. Photo-responsive Block Copolymer Micelles: Design and Behavior. *Chem. Soc. Rev.* **2013**, *42*, 7117-7129.

(16) Mura, S.; Nicolas, J.; Couvreur, P. Stimuli-Responsive Nanocarriers for Drug Delivery. *Nat. Mater.* **2013**, *12*, 991-1003.

(17) Chen, S.; Weitemier, A. Z.; Zeng, X.; He, L.; Wang, X.; Tao, Y.; Huang, A. J. Y.; Hashimotodani, Y.; Kano, M.; Iwasaki, H.; Parajuli, L. K.; Okabe, S.; Teh, D. B. L.; All, A. H.; Tsutsui-Kimura, I.; Tanaka, K. F.; Liu, X.; McHugh, T. J. Near-Infrared Deep Brain Stimulation via Upconversion Nanoparticle-Mediated Optogenetics. *Science* **2018**, *359*, 679-684.

(18) Wu, S.; Butt, H.-J. Near-Infrared-Sensitive Materials Based on Upconverting Nanoparticles. *Adv. Mater.* **2016**, *28*, 1208-1226.

(19) Cho, H. J.; Chung, M.; Shim, M. S. Engineered Photo-Responsive Materials for Near-Infrared-Triggered Drug Delivery. *J. Ind. Eng. Chem.* **2015**, *31*, 15-25.

(20) Smith, A. M.; Mancini, M. C.; Nie, S. Second Window for In Vivo Imaging. *Nat. Nanotechnol.* **2009**, *4*, 710.

(21) Yan, B.; Boyer, J.-C.; Branda, N. R.; Zhao, Y. Near-Infrared Light-Triggered Dissociation of Block Copolymer Micelles Using Upconverting Nanoparticles. *J. Am. Chem. Soc.* **2011**, *133*, 19714-19717.

(22) Viger, M. L.; Grossman, M.; Fomina, N.; Almutairi, A. Low Power Upconverted Near-IR Light for Efficient Polymeric Nanoparticle Degradation and Cargo Release. *Adv. Mater.* **2013**, *25*, 3733-3738.

(23) Yuan, Y.; Min, Y.; Hu, Q.; Xing, B.; Liu, B. NIR Photoregulated Chemo- and Photodynamic Cancer Therapy based on Conjugated Polyelectrolyte-Drug Conjugate Encapsulated Upconversion Nanoparticles. *Nanoscale* **2014**, *6*, 11259-11272.

(24) Jalani, G.; Naccache, R.; Rosenzweig, D. H.; Haglund, L.; Vetrone, F.; Cerruti, M. Photocleavable Hydrogel-Coated Upconverting Nanoparticles: A Multifunctional Theranostic Platform for NIR Imaging and On-Demand Macromolecular Delivery. *J. Am. Chem. Soc.* **2016**, *138*, 1078-1083.

(25) Chen, S.; Gao, Y.; Cao, Z.; Wu, B.; Wang, L.; Wang, H.; Dang, Z.; Wang, G. Nanocomposites of Spiropyran-Functionalized Polymers and Upconversion Nanoparticles for Controlled Release Stimulated by Near-Infrared Light and pH. *Macromolecules.* **2016**, *49*, 7490-7496.

(26) Zhao, H.; Hu, W.; Ma, H.; Jiang, R.; Tang, Y.; Ji, Y.; Lu, X.; Hou, B.; Deng, W.; Huang, W.; Fan, Q. Photo-Induced Charge-Variable Conjugated Polyelectrolyte Brushes Encapsulating Upconversion Nanoparticles for Promoted siRNA Release and Collaborative Photodynamic Therapy under NIR Light Irradiation. *Adv. Funct. Mater.* **2017**, *27*, 1702592.

(27) Zhang, Y.; Ren, K.; Zhang, X.; Chao, Z.; Yang, Y.; Ye, D.; Dai, Z.; Liu, Y.; Ju, H. Photo-Tearable Tape Close-Wrapped Upconversion Nanocapsules for Near-Infrared Modulated Efficient SiRNA Delivery and Therapy. *Biomaterials* **2018**, *163*, 55-66.

(28) Zhao, T.; Wang, P.; Li, Q.; Al-Khalaf, A. A.; Hozzein, W. N.; Zhang, F.; Li, X.; Zhao, D. Near-Infrared Triggered Decomposition of Nanocapsules with High Tumor Accumulation and Stimuli Responsive Fast Elimination. *Angew. Chem. Int. Edit.* **2018**, *57*, 2611-2615.

(29) Liu, G.; Liu, N.; Zhou, L.; Su, Y.; Dong, C.-M. NIR-Responsive Polypeptide Copolymer Upconversion Composite Nanoparticles for Triggered Drug Release and Enhanced Cytotoxicity. *Polym. Chem.* **2015**, *6*, 4030-4039.

(30) Cheng, R.; Tian, M.; Sun, S.; Liu, C.; Wang, Y.; Liu, Z.; Liu, Z.; Jiang, J. Light-Triggered Disruption of PAG-Based Amphiphilic Random Copolymer Micelles. *Langmuir.* **2015**, *31*, 7758-7763.

(31) Wang, J.; Wu, B.; Li, S.; He, Y. NIR Light and Enzyme Dual Stimuli-Responsive Amphiphilic Diblock Copolymer Assemblies. *J. Polym. Sci., Part A: Polym. Chem.* **2017**, *55*, 2450-2457.

(32) Xing, Q.; Li, N.; Jiao, Y.; Chen, D.; Xu, J.; Xu, Q.; Lu, J. Near-infrared Light-Controlled Drug Release and Cancer Therapy with Polymer-Caged Upconversion Nanoparticles. *RSC Adv.* **2015**, *5*, 5269-5276.

(33) Chen, G.; Jaskula-Sztul, R.; Esquibel, C. R.; Lou, I.; Zheng, Q.; Dammalapati, A.; Harrison, A.; Eliceiri, K. W.; Tang, W.; Chen, H.; Gong, S. Neuroendocrine Tumor-Targeted Upconversion Nanoparticle-Based Micelles for Simultaneous NIR-Controlled Combination Chemotherapy and Photodynamic Therapy, and Fluorescence Imaging. *Adv. Funct. Mater.* **2017**, *27*, 1604671.

(34) Zhao, L.; Ge, X.; Zhao, H.; Shi, L.; Capobianco, J. A.; Jin, D.; Sun, L. Double-Sensitive Drug Release System Based on MnO_2 Assembled Upconversion Nanoconstruct for Double-Model Guided Chemotherapy. *ACS Appl. Nano Mater.* **2018**, *1*, 1648-1656.

(35) Li, Z.; Barnes, J. C.; Bosoy, A.; Stoddart, J. F.; Zink, J. I. Mesoporous Silica Nanoparticles in Biomedical Applications. *Chem. Soc. Rev.* **2012**, *41*, 2590-2605.

(36) Blanco, E.; Shen, H.; Ferrari, M. Principles of Nanoparticle Design for Overcoming Biological Barriers to Drug Delivery. *Nat. Biotechnol.* **2015**, *33*, 941.

(37) Green, M. D.; Foster, A. A.; Greco, C. T.; Roy, R.; Lehr, R. M.; Epps, T. H., III; Sullivan, M. O. Catch and Release: Photocleavable Cationic Diblock Copolymers as a Potential Platform for Nucleic Acid Delivery. *Polym Chem* **2014**, *5*, 5535-5541.

(38) Plunkett, K. N.; Mohraz, A.; Haasch, R. T.; Lewis, J. A.; Moore, J. S. Light-Regulated Electrostatic Interactions in Colloidal Suspensions. *J. Am. Chem. Soc.* **2005**, *127*, 14574-14575.

(39) Koylu, D.; Thapa, M.; Gumbley, P.; Thomas, S. W. Photochemical Disruption of Polyelectrolyte Multilayers. *Adv. Mater.* **2012**, *24*, 1451-1454.

(40) Shi, F.; Wang, J.; Zhai, X.; Zhao, D.; Qin, W. Facile Synthesis of β-$NaLuF_4$: Yb/Tm Hexagonal Nanoplates with Intense Ultraviolet Upconversion Luminescence. *CrystEngComm* **2011**, *13*, 3782-3787.

(41) Lang, N.; Tuel, A. A Fast and Efficient Ion-Exchange Procedure To Remove Surfactant Molecules from MCM-41 Materials. *Chem. Mater.* **2004**, *16*, 1961-1966.

(42) Perni, S.; Martini-Gilching, K.; Prokopovich, P. Controlling Release Kinetics of Gentamicin from Silica Nano-Carriers. *Colloid Surf. A-Physicochem. Eng. Asp.* **2018**, *541*, 212-221.

(43) Scarpa, E.; Bailey, J. L.; Janeczek, A. A.; Stumpf, P. S.; Johnston, A. H.; Oreffo, R. O. C.; Woo, Y. L.; Cheong, Y. C.; Evans, N. D.; Newman, T. A. Quantification of Intracellular Payload Release from Polymersome Nanoparticles. *Sci. Rep.* **2016**, *6*, 29460.

(44) Yu, B.; Jiang, X.; Qin, N.; Yin, J. Thiol-ene Photocrosslinked Hybrid Vesicles from Co-assembly of POSS and Poly(ether amine) (PEA). *Chem. Commun.* **2011**, *47*, 12110-12112.

(45) Wang, R.; Yu, B.; Jiang, X.; Yin, J. Understanding the Host–Guest Interaction Between Responsive Core-Crosslinked Hybrid Nanoparticles of Hyperbranched Poly(ether amine) and Dyes: The Selective Adsorption and Smart Separation of Dyes in Water. *Adv. Funct. Mater.* **2012**, *22*, 2606-2616.

(46) Huang, H.; Zeng, X.; Li, W.; Wang, H.; Wang, Q.; Yang, Y. Reinforced Conducting Hydrogels Prepared from the In Situ Polymerization of Aniline in an Aqueous Solution of Sodium Alginate. *J. Mater. Chem. A* **2014**, *2*, 16516-16522.

2.3.6 Supporting Information

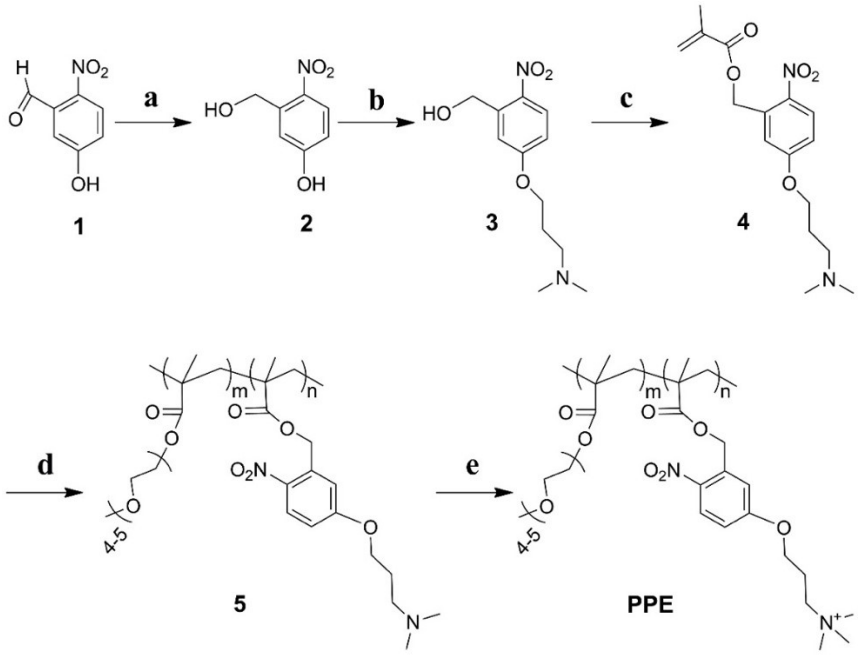

Scheme S1. The synthetic route for the UV-labile polyelectrolyte PPE.

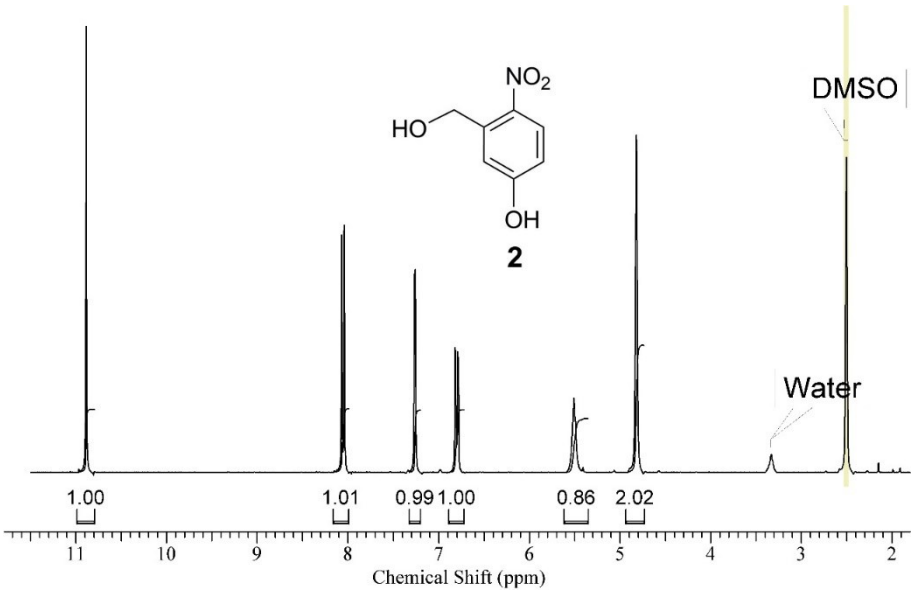

Figure S1. ^{1}H NMR spectrum of 5-hydroxy-2-nitrobenzyl alcohol (**2**).

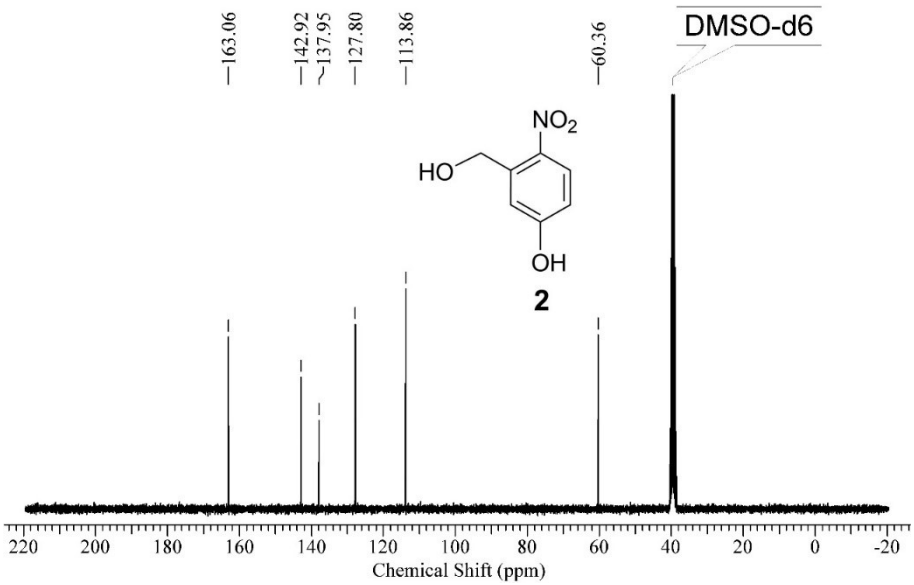

Figure S2. ^{13}C NMR spectrum of 5-hydroxy-2-nitrobenzyl alcohol (**2**).

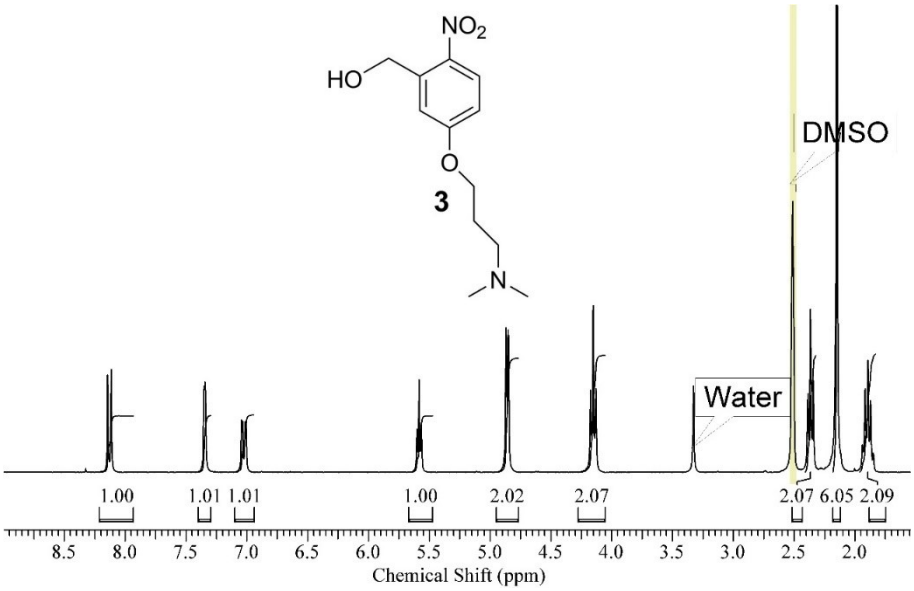

Figure S3. ^{1}H NMR spectrum of (5-(3-(dimethylamino) propoxy)-2-nitrophenyl) methanol (**3**).

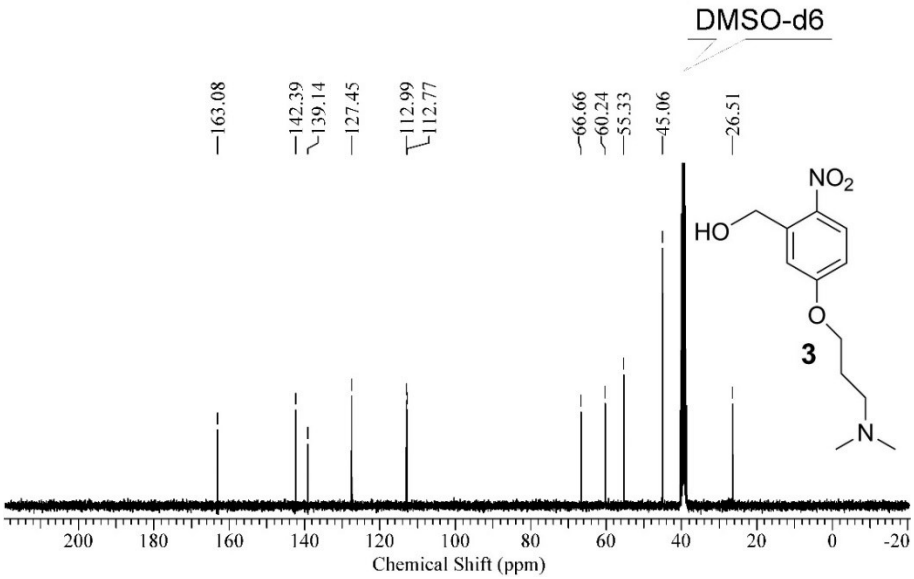

Figure S4. ^{13}C NMR spectrum of (5-(3-(dimethylamino) propoxy)-2-nitrophenyl) methanol (**3**).

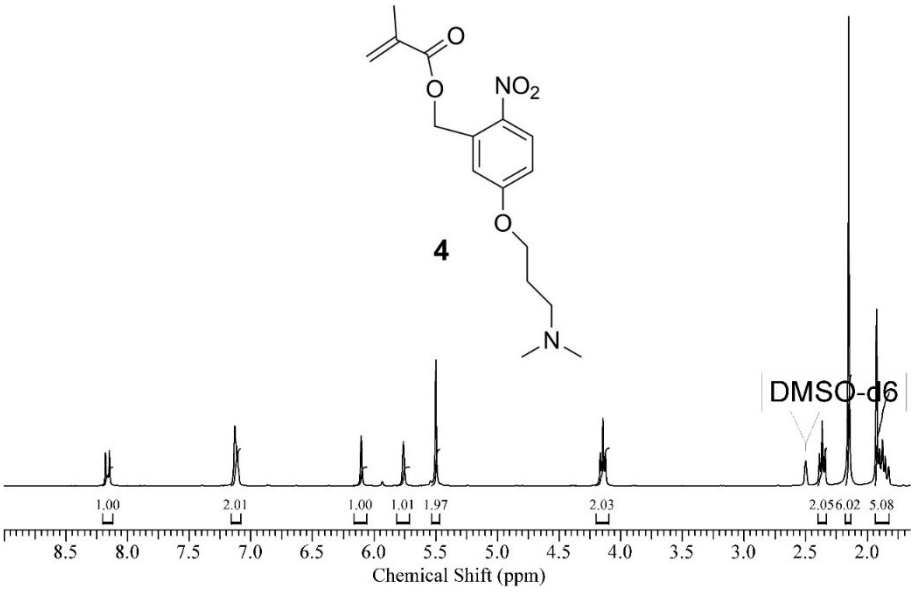

Figure S5. ^{1}H NMR spectrum of 5-(3-(dimethylamino)propoxy)-2-nitrobenzyl methacrylate (**4**).

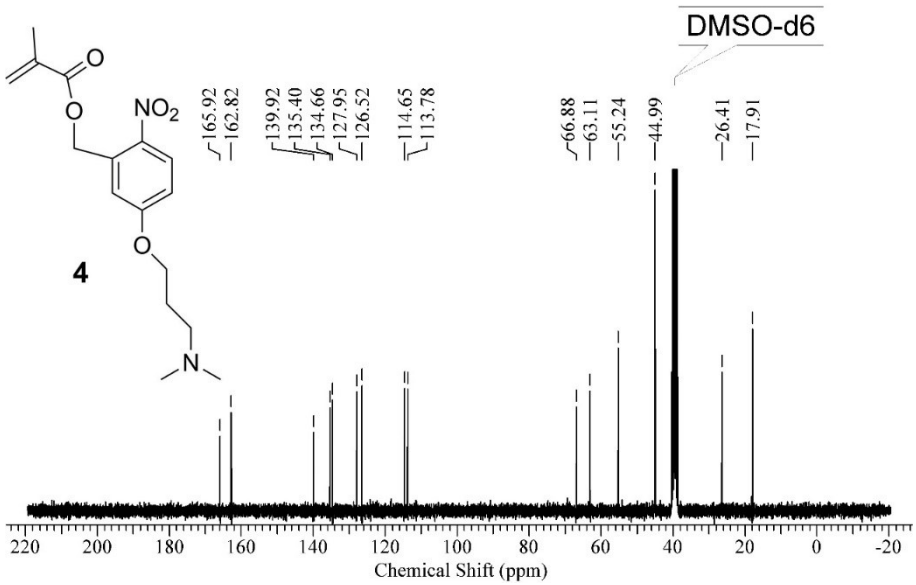

Figure S6. ^{13}C NMR spectra of 5-(3-(dimethylamino)propoxy)-2-nitrobenzyl methacrylate (**4**).

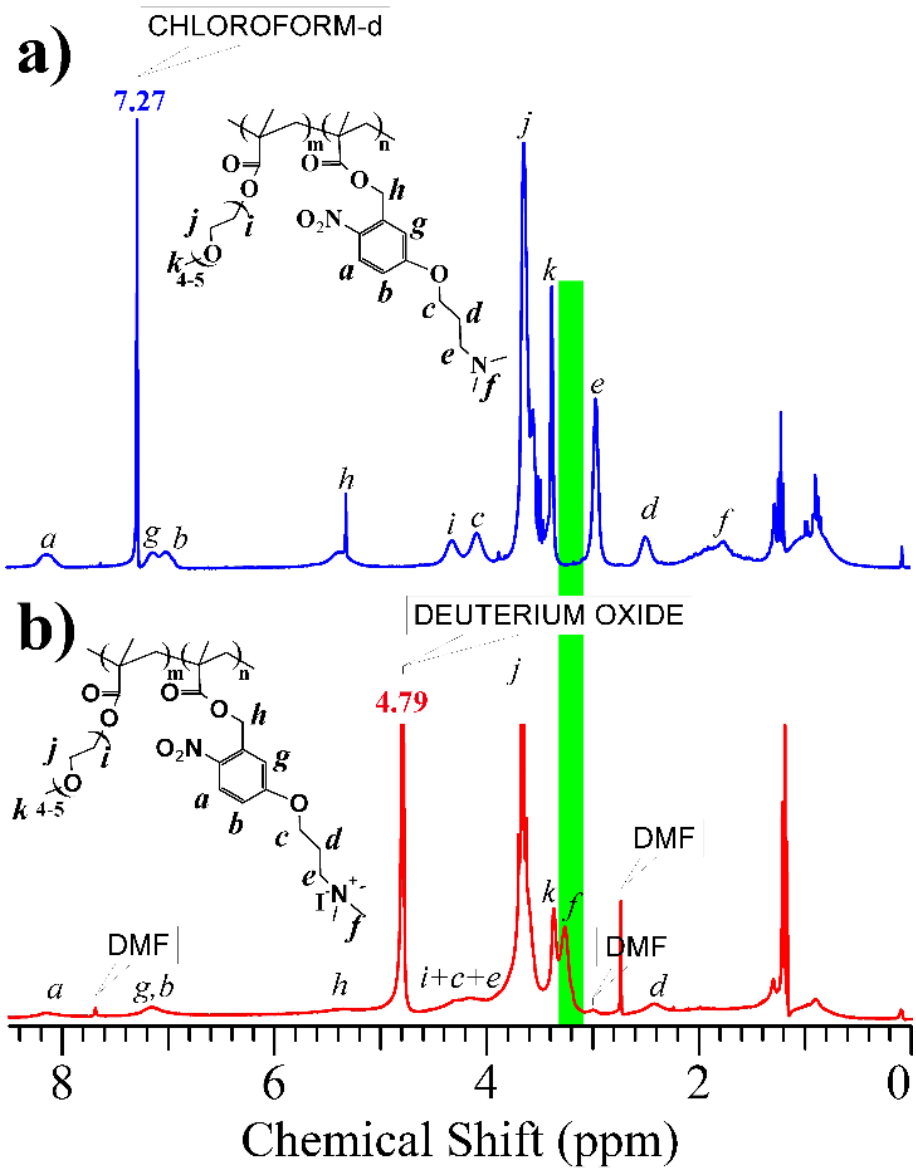

Figure S7. ^{1}H NMR spectra and main peak labeling for: (a) **5** and (b) PPE. The ratio of integrated areas of methyl hydrogen (C***H***$_3$-O, 3.37 ppm) and ethyl hydrogen (Ph-C***H***$_2$-O, 5.34 ppm) peaks in Fig. S7a indicates that the NB units account for ~44% in number. The ratio of integrated areas of nitro aromatic hydrogen peak (NO_2-Ph-***H***, 8.16 ppm) and overlapped peaks of methyl hydrogen (N-C***H***$_3$, 3.27 ppm) and methyl hydrogen (C***H***$_3$-O, 3.37 ppm) in Fig. S7b indicates that the degree of quaternization is ~93%.

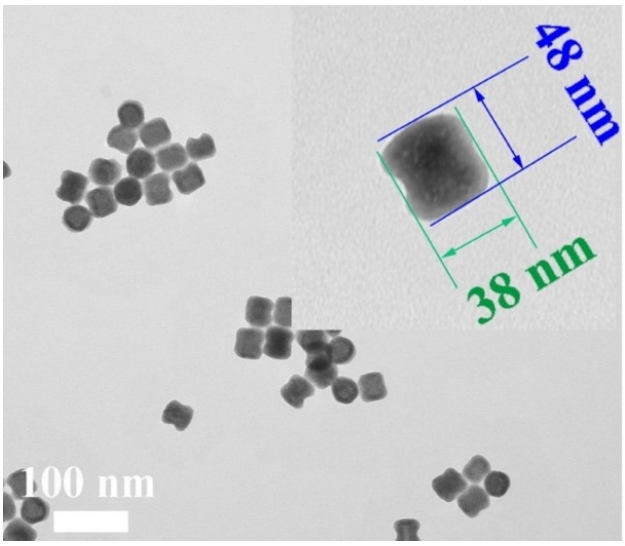

Figure S8. TEM image for UCNP ($NaLuF_4$:18%Yb,0.5%Tm@$NaYF_4$).

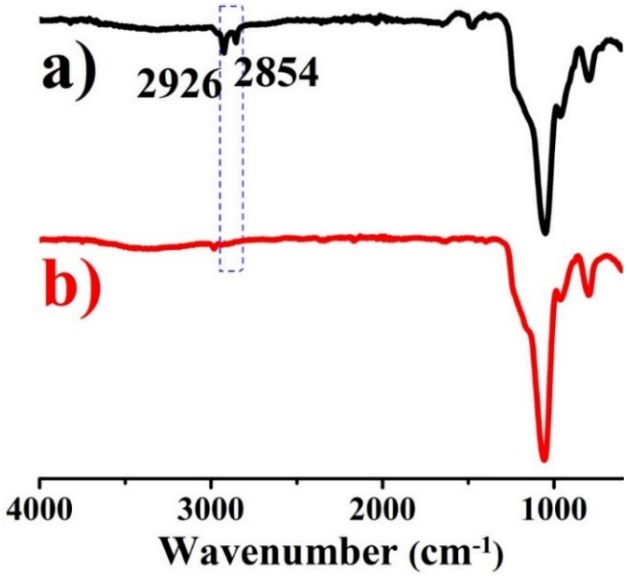

Figure S9. FTIR spectra of UCNP@silica before (a) and after (b) the removal of CTAB. In comparison with the FTIR spectrum of nanoparticles with CTAB, the disappearance of the characteristic bands at approximately 2926 and 2854 cm^{-1} assigned to the asymmetric (ν_{as}) and symmetric (ν_s) stretching of C—H in CTAB molecules after washing indicates the successful elimination of surfactant.

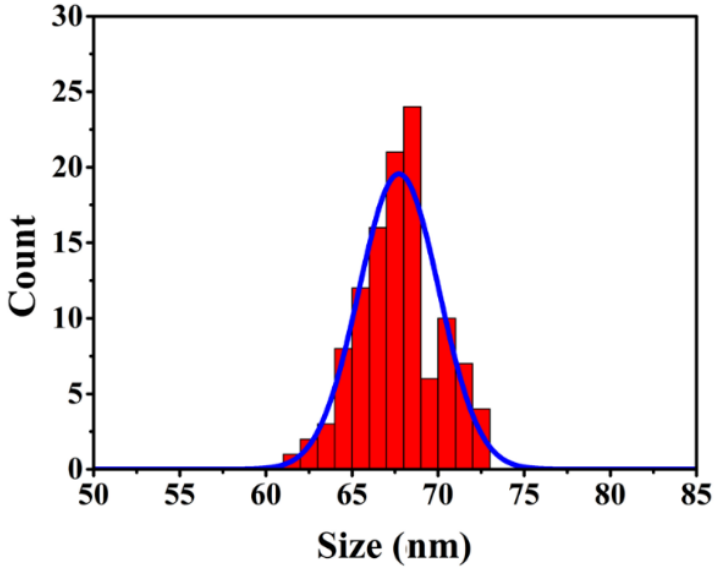

Figure S10. Size histogram for UCNP@silica from TEM observations (N>100).

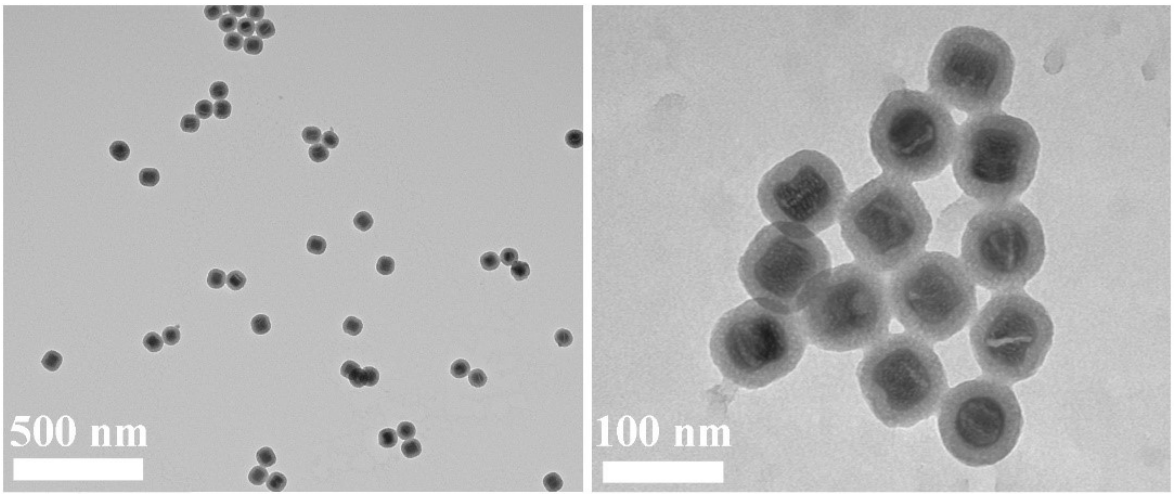

Figure S11. TEM images for UCNP@silica@PPE (molar ratio of PPE chains to UCNP@silica is 135:1).

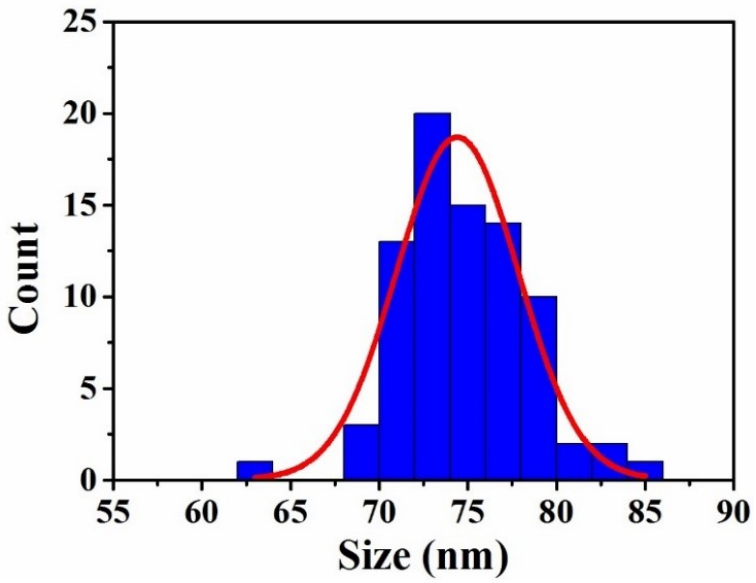

Figure S12. Size histogram for UCNP@silica@PPE from TEM observations (N>80).

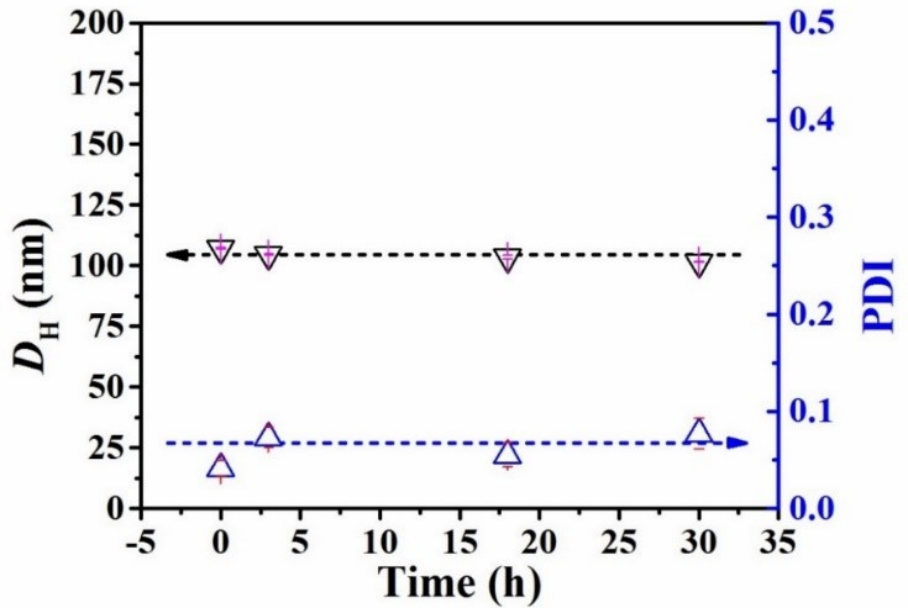

Figure S13. Hydrodynamic diameter (D_H) and polydispersity index (PDI) of UCNP@silica in H_2O (~1.1 mg/mL).

Analysis of FLU-UCNP@silica@PPE

Here we take USP-3 as an example to calculate the anchoring densities of positively charged ONB units and FLU in one single particle. At the end of **Table S1**, we obtained that the amount of FLU that could be loaded by 1 mol UCNP@silica@PPE was around 3,380 mol. In addition, the anchoring densities of FLU and positively charged ONB units are in the same order of magnitude (~0.2 per nm^2).

Table S1. Analysis of the USP-3 sample.

USP-3		
UCNP@silica (mg)	= 10	
PPE (μg)	= 168	
loaded fluorescein (mg)	= 0.07	
PPE		
***M*n before quaternization with MeI (g/mol)**	$= 1.68 \times 10^4$	
***M*n after quaternization (degree is 93%) with MeI (g/mol)**	$= 1.68 \times 10^4 + 24 \times 0.93 \times 142$	$= 2.00 \times 10^4$
moles of 168 μg PPE	$= (1.68 \times 10^{-4}) / 2.00 \times 10^4$	$= 8.40 \times 10^{-9}$
moles of positive charges	$= 8.40 \times 10^{-9} \times 24 \times 0.93$	$= 1.87 \times 10^{-7}$
UCNP and UCNP@silica: **1. the shape of the UCNP is approximated to be a cylinder and the density of $NaLuF_4$: Yb/Tm@$NaYF_4$ is taken to be the same as for $NaYF_4$.** **2. the shape of the UCNP@silica (diameter = 67.4 nm) is approximated to be a sphere.** **3. assuming the density of silica is 0.34 g/m^3. [a]**		
density of UCNP (g/cm^3) [b]	= 4.21	
length of UCNP (nm)	= 48	

width of UCNP (nm)	= 38	
radius of one UCNP@silica on average (cm)	= 3.37×10^{-6}	
volume of one UCNP@silica (cm^3) using $v = 4/3\pi r^3$	= $4/3 \times 3.14 \times (3.37 \times 10^{-6})^3$	= 1.60×10^{-16}
surface area of one UCNP@silica (cm^2) using $s = 4\pi r^2$ (assuming its solid surface without pores)	= $4 \times 3.14 \times (3.37 \times 10^{-6})^2$	= 1.43×10^{-10}
volume of one UCNP on average (cm^3) using $v = \pi r^2 h$	= $3.14 \times (19 \times 10^{-7})^2 \times 48 \times 10^{-7}$	= 5.44×10^{-17}
volume of silica per particle (cm^3)	= 1.60×10^{-16} - 5.44×10^{-17}	= 1.06×10^{-16}
density of UCNP@silica (g/cm^3)	= $(4.21 \times 5.44 \times 10^{-17} + 0.34 \times 1.06 \times 10^{-16}) / (1.60 \times 10^{-16})$	= 1.66
mass of one UCNP@silica (g)	= $1.66 \times 1.60 \times 10^{-16}$	= 2.66×10^{-16}
moles of 10 mg UCNP@silica	= $(10 \times 10^{-3}) / (2.66 \times 10^{-16} \times 6.02 \times 10^{23})$	= 6.24×10^{-11}
molar ratio of PPE chains to UCNP@silica	= $(8.4 \times 10^{-9}) / (6.24 \times 10^{-11})$	= 135
FLU		
molecule weight of FLU (g/mol)	= 332	
moles of 70 µg FLU	= $70 \times 10^{-6} / 332$	= 2.11×10^{-7}
loading of FLU per particle	= $(2.11 \times 10^{-7}) / (6.24 \times 10^{-11})$	= 3.38×10^3
anchoring density of positive charged ONB per nm^2	= $(1.87 \times 10^{-7}) / (6.24 \times 10^{-11} \times 1.43 \times 10^{-10} \times 10^{14})$	= 0.21
anchoring density of FLU per	= $(2.11 \times 10^{-7}) / (6.24 \times 10^{-11} \times$	= 0.24

nm^2	$1.43 \times 10^{-10} \times 10^{14}$)

[a] This value was obtained from *Chem. Eur. J.* **2011**, 17, 9893-9896.

[b] This value was obtained from *Chem. Mater.*, **2015**, 27 (13), 4899-4910.

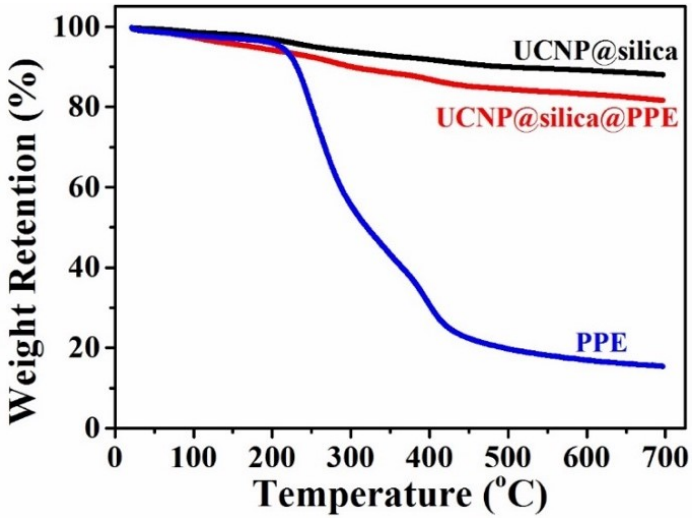

Figure S14. TGA analysis of UCNP@silica, PPE, and UCNP@silica@PPE (molar ratio of PPE chains to UCNP@silica is 122:1, which is obtained from the feed ratio used for preparing this nanocomplex).

Table S2. Mass of UCNP@silica and UCNP@silica@PPE at room temperature.

1. assuming the residual mass of both is 10 mg at 700 °C. 2. equation to calculate the mass at room temperature: mass = (10 mg) / (the wt.% of NPs at 700 °C).		
mass of UCNP@silica at room temperature (mg)	= 10/0.882	= 11.34
mass of UCNP@silica@PPE at room temperature (mg)	= 10/0.819	= 12.21

Table S3. Analysis of the UCNP@silica@PPE nanocomplex in Figure S14.

Mass loss	UCNP@silica (mg)	UCNP@silica@PPE (mg)
200 ºC<T<450 ºC	= 0.696	= 1.100
mass of organic species (mg)	= 0.696	= (1.100 - 0.696) = 0.404

Based on the values in **Table S2** and **Table S3**, there are 404 μg of PPE complexed with 12.21 mg of UCNP@silica, namely, 342 μg of PPE complexed with 10 mg of UCNP@silica, which indicates the molar ratio of PPE chains to UCNP@silica is 274:1. Although in the same order of magnitude, the molar ratio of PPE chains to UCNP@silica from the TGA analysis (274:1) is about twice that obtained from the feed ratio (122:1) used for preparing the nanocomplex, which may be attributed to the assumption used in the TGA data analysis that no dehydration of silica takes place in the 200-450 ºC region during the measurement.

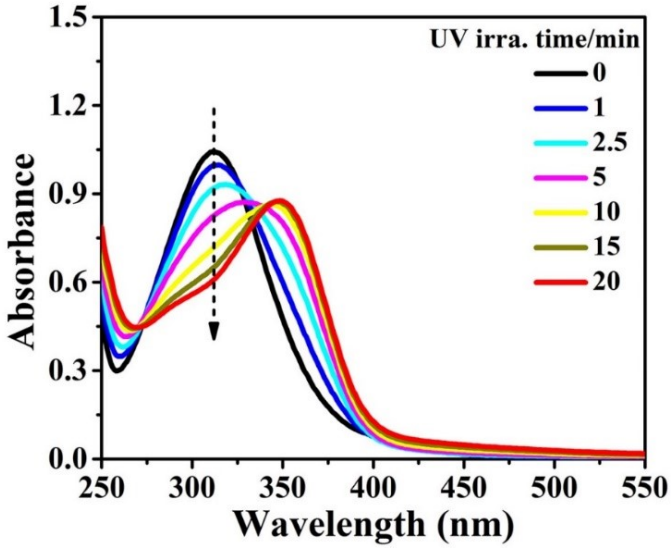

Figure S15. The absorption spectral change of PPE (0.1 mg/mL in H_2O) over 365 nm exposure time (80 mW/cm^2).

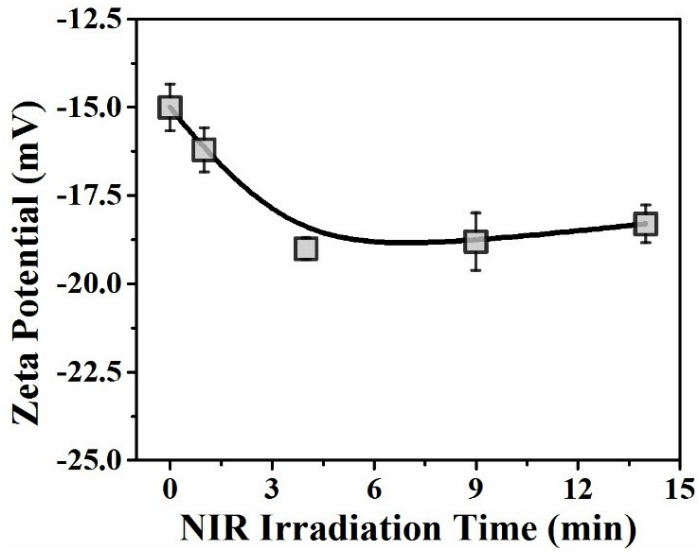

Figure S16. Zeta potential of the UCNP@silica@PPE nanocomplex (molar ratio of PPE chains to UCNP@silica is 135:1) changes over NIR irradiation time. Due to the small beam of the 980 nm laser, it's hard to monitor the zeta potential for the solution in the dialysis cup during the illumination. Instead, 10 μL of the nanocomplex solution (1 mg/mL) in an Eppendorf tube was irradiated by the 980 nm laser and then diluted for the measurements.

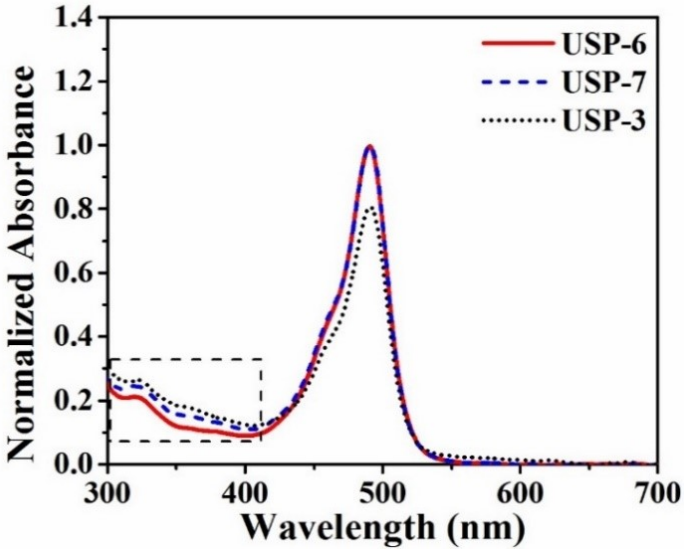

Figure S17. Normalized UV-vis spectra of bottom solutions for three FLU-UCNP@silica@PPE samples after 360 min.

Synthesis of β-$NaYF_4$:18%Yb,2%Er@$NaYF_4$ Nanoparticles (Er-UCNP).

Oleic acid-capped β-$NaYF_4$:18%Yb,2%Er were synthesized via a solvothermal route adapted from the literature (CrystEngComm, 2011, 13, 3782). Briefly, 1 mmol of $RECl_3 \cdot 6H_2O$ (RE = 80 mol% Y, 18 mol% Yb, and 2 mol% Er) was dissolved in a mixture of ODE (15 mL) and OA (6 mL). The solution was heated to 160 °C for 30 min under argon protection to form the lanthanide oleate complexes. The temperature was then cooled to room temperature with a gentle flow of argon gas through the reaction flask. During this time, a solution of NH_4F (4 mmol) and NaOH (2.5 mmol) dissolved in methanol (10 mL) was added to the flask, and the resulting mixture was stirred for 60 min. The temperature was then increased to 60 °C for evaporating methanol from the reaction mixture; in succession, the solution was heated to 300 °C in an argon atmosphere for 60 min and then cooled to room temperature naturally. The resulting solid products were precipitated by addition of ethanol and collected by centrifugation at 9000 rpm for 10 min. The precipitate was washed with an EtOH/hexane mixture (3:1 v/v) three times, and the NPs were finally dispersed in cyclohexane as the core for further use.

$YCl_3 \cdot 6H_2O$ (0.5 mmol) was mixed with 6 mL OA and 15 mL ODE in a 100 mL three-neck round flask and heated to 160 °C for 60 min to form a homogeneous solution under argon gas protection. Then the mixture was cooled down under 40 °C and the β-$NaYF_4$:18%Yb,2%Er core was added. The mixture was immediately degassed at 80 °C for 20 min to evaporate the extra cyclohexane. Then, it was cooled down to room temperature. The next experimental steps were the same as for the synthesis of β-$NaYF_4$:18%Yb,2%Er core. The final product was dispersed in cyclohexane for further use.

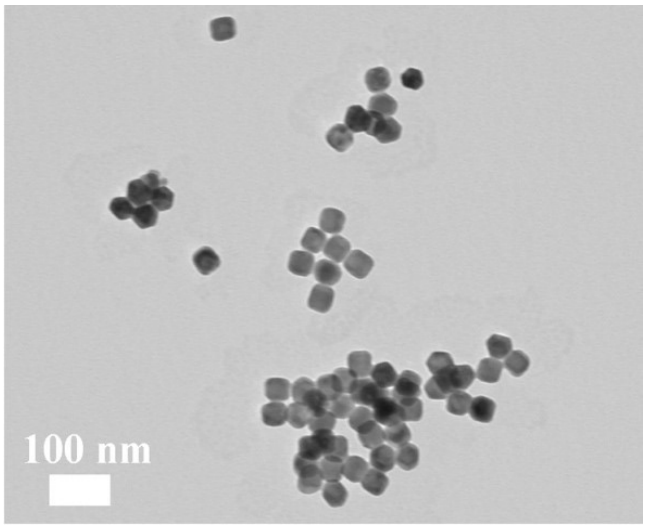

Figure S18. TEM image for Er-UCNP ($NaYF_4$:18%Yb,2%Er@$NaYF_4$). Er-UCNP have an average dimension of 46 (*L*) × 42 (*W*) nm.

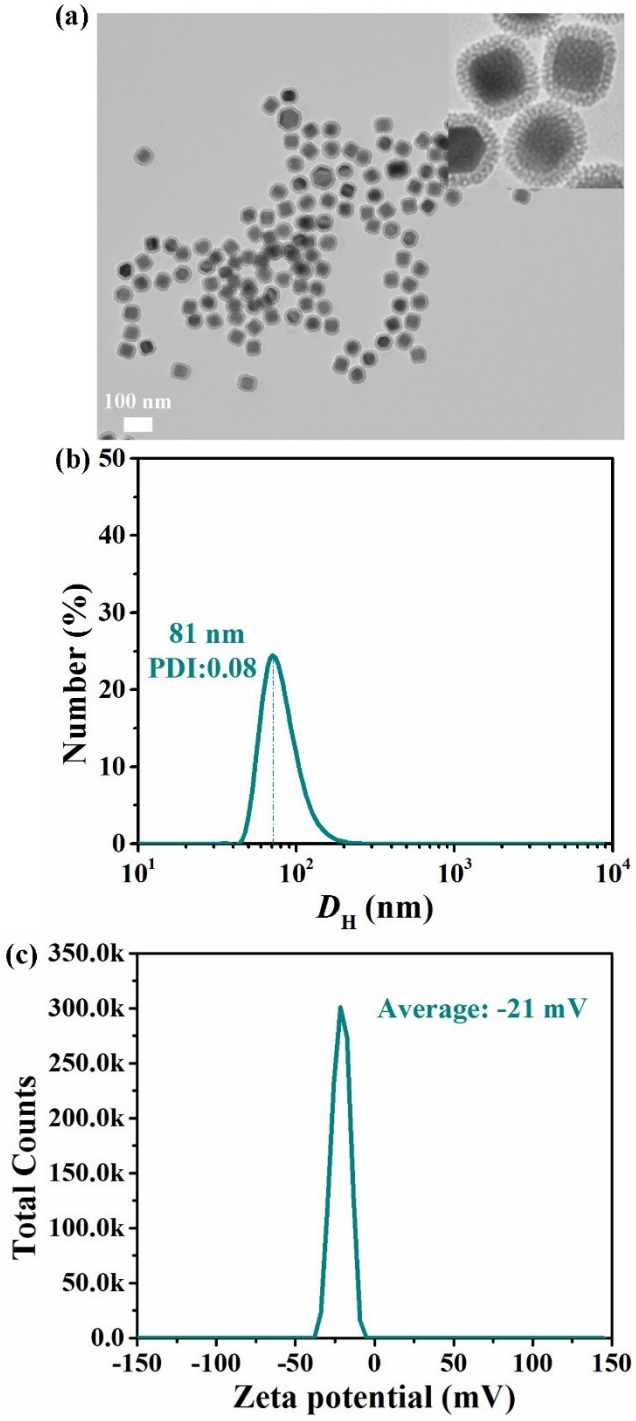

Figure S19. (a) TEM image, (b) size distribution from DLS measurement and (c) zeta potential for Er-UCNP@silica (1 mg/mL in H_2O, pH 6.6). The average thickness of silica layer is 9 nm.

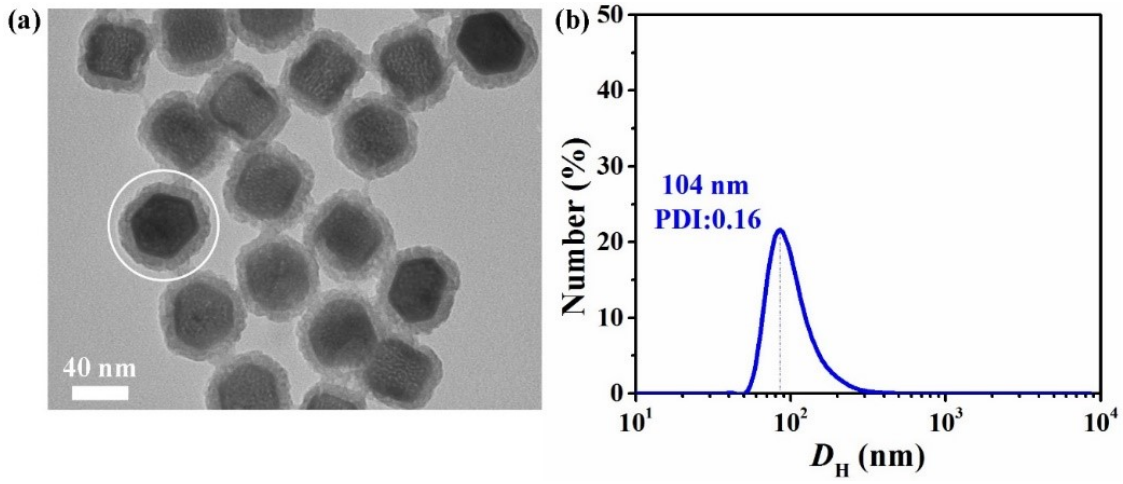

Figure S20. (a) TEM image and (b) size distribution from DLS measurement (1 mg/mL, H_2O) for Er-UCNP@silica@PPE (molar ratio of PPE chains to UCNP@silica is 124:1).

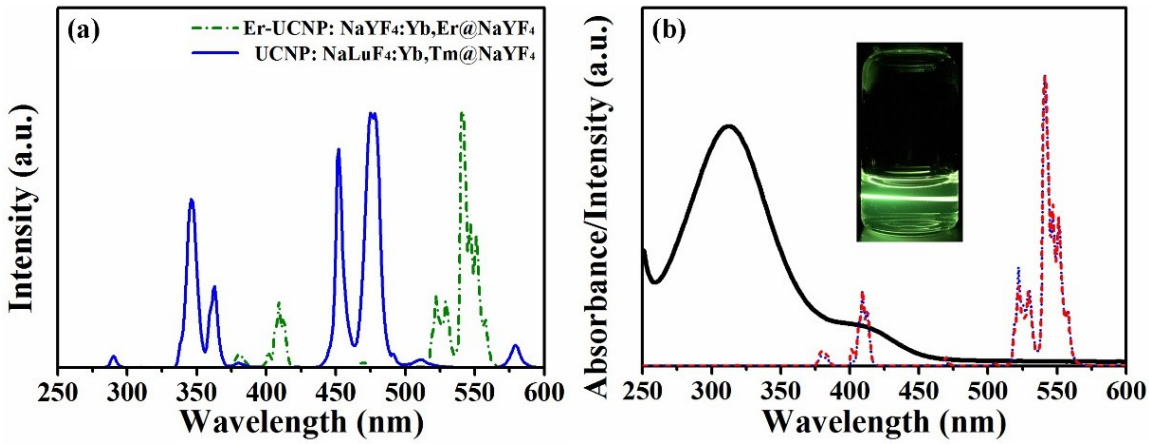

Figure S21. (a) UCL spectra of Er-UCNP and UCNP. (b) The absorption (continuous line) and UCL spectrum (dotted line) of the mixture of Er-UCNP@silica and PPE. Also shown is the UCL spectrum of neat Er-UCNP in hexane. Note: the composition of the mixture is PPE (2 mL, 0.1 mg/mL) and Er-UCNP@silica (0.2 mg). The inset photograph shows that the aqueous solution of Er-UCNP@silica (1 mg/mL) emits visible light (mainly green light) where the 980 nm laser beam passes through the solution.

Table S4. Analysis of the molar ratio of PPE chains to Er-UCNP@silica in nanocomplexes of Er-UCNP@silica@PPE.

Feed Ratio for Preparation of Er-UCNP@silica@PPE		
Er-UCNP@silica (mg)	= 10	
PPE (μg)	= 142	
moles of 142 μg PPE	= $(1.42 \times 10^{-4}) / 2.00 \times 10^{4}$	= 7.10×10^{-9}
Information of Er-UCNP and Er-UCNP@silica: **1. the shape of the Er-UCNP is approximated to be a cylinder and the density of is taken to be the same as for $NaYF_4$.** **2. the shape of the Er-UCNP@silica (diameter = 62 nm) is approximated to be a sphere.** **3. assuming the density of silica is 0.34 g/m^3. [a]**		
density of Er-UCNP (g/cm^3) [b]		= 4.21
length of Er-UCNP (nm)		= 46
width of Er-UCNP (nm)		= 42
radius of one Er-UCNP@silica on average (cm)		= 3.10×10^{-6}
volume of one Er-UCNP@silica (cm^3) using $v = 4/3\pi r^3$	= $4/3 \times 3.14 \times (3.10 \times 10^{-6})^3$	= 1.25×10^{-16}
surface area of one Er-UCNP@silica (cm^2) using $s = 4\pi r^2$ (assuming its solid surface without pores)	= $4 \times 3.14 \times (3.10 \times 10^{-6})^2$	= 1.21×10^{-10}
volume of one Er-UCNP on average (cm^3) using $v = \pi r^2 h$	= $3.14 \times (21 \times 10^{-7})^2 \times 46 \times 10^{-7}$	= 6.37×10^{-17}
volume of silica per particle (cm^3)	= $1.25 \times 10^{-16} - 6.37 \times 10^{-17}$	= 6.13×10^{-17}

density of Er-UCNP@silica (g/cm^3)	$= (4.21 \times 6.37 \times 10^{-17} + 0.34 \times 6.37 \times 10^{-17}) / (1.25 \times 10^{-16})$	$= 2.32$
mass of one UCNP@silica (g)	$= 2.32 \times 1.25 \times 10^{-16}$	$= 2.90 \times 10^{-16}$
moles of 10 mg UCNP@silica	$= (10 \times 10^{-3}) / (2.90 \times 10^{-16} \times 6.02 \times 10^{23})$	$= 5.73 \times 10^{-11}$
molar ratio of PPE chains to Er-UCNP@silica	$= (7.1 \times 10^{-9}) / (5.73 \times 10^{-11})$	$= 124$

[a] This value was obtained from *Chem. Eur. J.* **2011**, 17, 9893-9896.

[b] This value was obtained from *Chem. Mater.*, **2015**, 27 (13), 4899-4910.

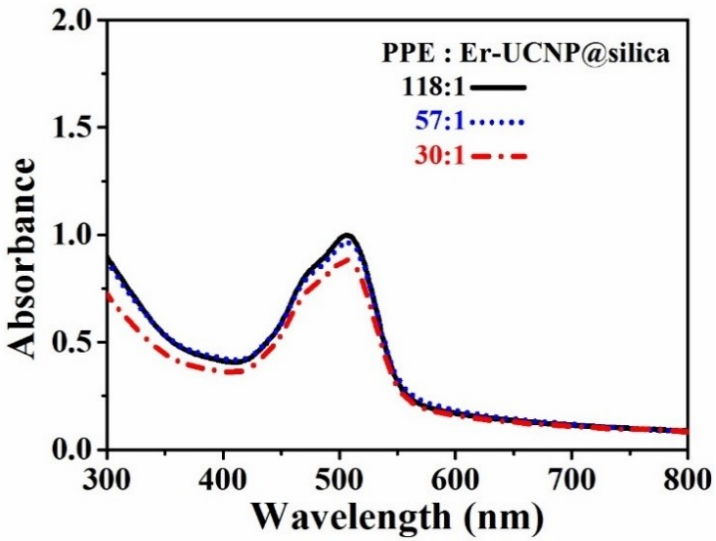

Figure S22 UV-vis absorption spectra of FLU loaded Er-UCNP@silica@PPE as a function of molar ratio of PPE chains to Er-UCNP@silica while keeping the mass ratio of FLU to Er-UCNP@silica at 4.5:1.

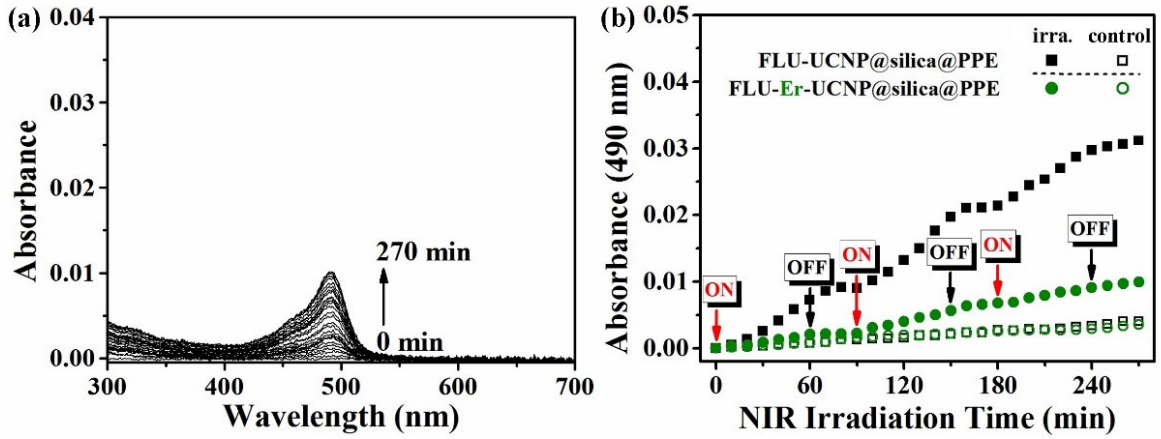

Figure S23. (a) Absorption spectral changes over time from the bottom solution of FLU-Er-UCNP@silica@PPE. (b) Plot of absorbance at 490 nm *vs.* time, "ON" labels indicate the beginning of 980 nm laser exposure in the following one hour, while "OFF" labels mean the switching off the NIR laser in the following thirty minutes. The control test is for the solution without NIR light irradiation. For comparison, the data obtained with FLU-UCNP@silica@PPE (USP-6) in Figure 8b are also shown.

2.4 Summary of the Project

In this work, we develop a simple and robust approach to fabricating NIR light-triggered drug release nanovectors by utilizing electrostatic interaction-driven assembly between a UV-sensitive polyelectrolyte and UCNP ($NaLuF_4$:18%Yb/0.5%Tm@$NaYF_4$) in water. A UV-sensitive copolymer was synthesized via a free radical copolymerization of 5-(3-(dimethylamino) propoxy)-2-nitrobenzyl methacrylate and poly(ethylene glycol) methyl ether methacrylate. Then the positively charged polyelectrolyte was obtained through a quaternization reaction by utilizing this copolymer to react with iodomethane. As for the negatively charged UCNP, they were synthesized by coating a 10 nm-thick silica layer on their surface (UCNP@silica). Due to the repulsion forces, UCNP@silica exhibited a highly stable dispersion in water. During the preparation process of nanovectors, the solution of PPE was dropwise added into an aqueous solution of UCNP@silica, where the PPE added amount should be kept below a critical value to stabilize the resulted nanocomplexes in water. We also found that the model drug molecules, fluorescein (FLU), could be encapsulated into the nanocomplexes during the assembly process. By utilizing a mini dialysis device, the release of cleaved by-products from the designed nanocomplexes as well as FLU loaded ones can be precisely controlled by turning on or off a 980 nm diode laser. The release of FLU was ascribed to the modulation of electrostatic equilibrium in the resulted nanocomplexes by the photolysis reactions triggered by the upconversion emissions in the UV region. Our method offers several distinct features (1) disruption of electrostatic equilibrium will the release of drug molecules, (2) completing the encapsulation of drug and surface functionalization of UCNP in one single step, which allows us to realize the preparation of NIR light-triggered release nanovectors in a simple and robust way.

CHAPTER 3 SPATIAL ORGANIZATION AND OPTICAL PROPERTIES OF LAYER-BY-LAYER ASSEMBLED UPCONVERSION AND GOLD NANOPARTICLES IN THIN FILMS

3.1 About the Project

In the previous two chapters, we have demonstrated two types of NIR light-responsive nanovectors for controlled drug delivery. Both are based on the use of UCNP combined with UV-labile polymers. Although the preparation approaches are different, they are nanoparticles for use in aqueous solution and function on the same mechanism, that is, using 980 nm NIR laser for excitation of UCNP covered by the polymer and obtaining the nanovector disruption through photolysis of the polymer upon absorption of UCNP-emitted UV light. In the present chapter, we present a research work that is somewhat different, which deals with NIR-responsive UCNP/polymer hybrid materials in the form of thin film. The reasons for us to conduct this work are multi-fold. First, the fabrication of upconversion luminescence (UCL) thin films has raised considerable interest in recent years due to their extensive applications, such as multilayer optical storage disks, photoluminescence screens for optically written displays and photovoltaic cells. It is our belief that NIR-responsive thin films can also be exploited for drug delivery application. On the other hand, gold nanoparticles (AuNP) have also been extensively used to combine with polymers to make optically active hybrid materials through the surface plasmon resonance (SPR). The integration of UCNP with AuNP has been a hot research topic, which shows enormous potential applications in bioimaging, sensing and detection. Especially, researches of modulating the interactions between UCNP and AuNP to precisely control the electronic and optical properties of the resulting materials have witnessed a rapid increase. In the present study, we also aim to rationally design the structure of the resulting multilayer films containing these two types of nanoparticles by changing the deposition sequence. Knowledge on the organization control and interactions of UCNP and AuNP within polymers can help to establish the basis for exploring the applications of these two

types of nanoparticles of great importance in polymer materials. Finally, NIR-responsive polymer thin films can also be used for drug delivery. The present study will also provide a knowledge base for our future works on NIR light-triggered drug delivery using thin films as patches. As will be shown further on in this chapter, the results demonstrate that LbL is an effective way to incorporate either UCNP or AuNP, or both, into polymer thin films, and that the deposition order of UCNP/polyelectrolyte and AuNP/polyelectrolyte bilayers affect the optical properties and upconversion photoluminescence property of as-made thin films.

3.2 Contributions

This work was published in *Journal of Materials Chemistry C*, **2016**, 4, 9343 by Jun Xiang, Xia Tong, Feng Shi, Paul-Ludovic Karsenti and Yue Zhao. This research work was conducted in the Université de Sherbrooke under the supervision of Prof. Zhao. I designed and performed the experiments described in this study. I collected all the experimental data and analyzed them with my collaborators. Moreover, I drew all the figures in this work and got a lot of useful suggestions from my collaborators. Xia Tong helped me with some characterizations and gave me valuable suggestions on the preparation of samples. Feng Shi assisted me with the synthesis of upconversion nanoparticles and characterizations. Paul-Ludovic Karsenti helped me a lot in the upconversion luminescence spectra experiments as well as the calibration of the beam size of 980 nm light laser. I have written the full manuscript and submitted it to Prof. Zhao for final revision.

3.3 Paper Published in Journal of Materials Chemistry C 2016, 4, 9343.

Spatial Organization and Optical Properties of Layer-by-Layer Assembled Upconversion and Gold Nanoparticles in Thin Films

Jun Xiang, Xia Tong, Feng Shi, Paul-Ludovic Karsenti and Yue Zhao*

[†]Département de Chimie, Université de Sherbrooke, Sherbrooke, Québec J1K 2R1, Canada.
Email: yue.zhao@usherbrooke.ca.

3.3.1 Abstract

Multilayers of $NaYF_4$:Yb,Tm@$NaYF_4$ upconversion nanoparticles (UCNP), up to 10 UCNP/polyelectrolyte bilayers, were prepared using the layer-by-layer (LBL) method. The assembled thin film of UCNP was found to display good stability of upconversion luminescence (UCL) upon 980 nm near-infrared (NIR) excitation. Moreover, LBL assembled films comprising four UCNP/polyelectrolyte bilayers and four gold nanoparticles (AuNP)/polyelectrolyte bilayers were prepared while adjusting their deposition order to give rise to three different spatial organizations of the two types of nanoparticles. The UV-vis-NIR extinction spectra and UCL emission spectra revealed that the spatial organization determined by the sequence of deposition influences the interaction between UCNP and AuNP and thus their optical properties. The alternating deposition of UCNP and AuNP layers appears to be the best way to preserve their "individual" properties, as a result of reducing both the agglomeration of AuNP and the scattering of the 980 nm excitation light that results in an apparent quenching effect on the UCL of UCNP. By contrast, with the same numbers of UCNP and AuNP layers, successive deposition of UCNP followed by successive addition of AuNP results in more agglomeration of AuNP leading to a broad surface plasmon resonance (SPR) band in the NIR region and also a significant quenching of the UCL intensity of UCNP. This study demonstrates an easy and effective way to prepare NIR-responsive and plasmonic hybrid thin films with the possibility to tune their optical properties through spatially controlled organization of the nanoparticles.

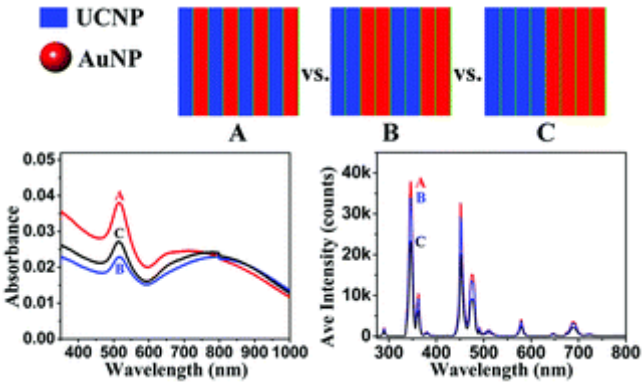

3.3.2 Introduction

Fabrication of lanthanide-doped upconversion luminescence (UCL) thin films has raised much interest due to the potential applications including multilayer optical storage disks, photoluminescence screens for optically written displays and photovoltaic cells.[1-6] Increasingly, UCL films are produced by directly using upconversion nanoparticles (UCNP) or nanocrystals with high visible light emission upon near infrared (NIR) excitation, which avoids heat treatment in the postdeposition step and makes the luminescence properties more predictable.[7-11] Recently, a single UCNP layer-based system was reported to exhibit excellent performance for cell adhesion/detachment and fingerprint identification.[12-14] An ability to construct well-organized multilayer UCNP films may open the door to novel optical materials. Among the thin film fabrication techniques, layer-by-layer (LBL) deposition is particularly useful and has long been established as a simple, robust and versatile method.[15-19] Thus far, only few works used LBL to prepare UCNP multilayer.[20,21] The purpose of the present study is twofold. On one hand, the use of LBL to assemble multilayers of UCNP was investigated. As shown in Fig.1 (a), this can be obtained by sequentially dipping quartz/poly(diallyldimethylammonium chloride) (quartz/PDDA) into poly(acrylic acid)-capped UCNP (UCNP-PAA) and poly(allylamine hydrochloride) (PAH) solution at room temperature. On the other hand, controlling frequency conversion of UCNP continues to be the subject of extensive studies for a wide range of applications, such as detection, bioimaging, and therapy.[22-25] Of the many approaches, studies about tuning the interaction between UCNP (Yb/Er or Yb/Tm doped into $NaYF_4$ matrix) and gold nanoparticles (AuNP) to fine-tune the electronic and optical properties of the resulting materials has witnessed a rapid increase.[26-32] Being motivated by this, we also investigated the possibility of spatially organizing both UCNP and AuNP into a thin film by means of LBL assembly. As schematically illustrated in Fig. 1 (b), for the same total numbers of UCNP and AuNP layers, there are different ways of depositing the two types of nanoparticles in a film by changing the deposition order. The resulting optical properties were characterized and analyzed. As shown below, the results of our study show that

altering the order of UCNP or AuNP layer deposition affects significantly the upconversion emission of UCNP as well as the SPR of AuNP, as a result of different interactions between the two nanoparticle constituents. These findings point out that using the LBL assembly is an easy way to modulate the interaction between UCNP and AuNP and thus to construct thin films of varying optical properties.

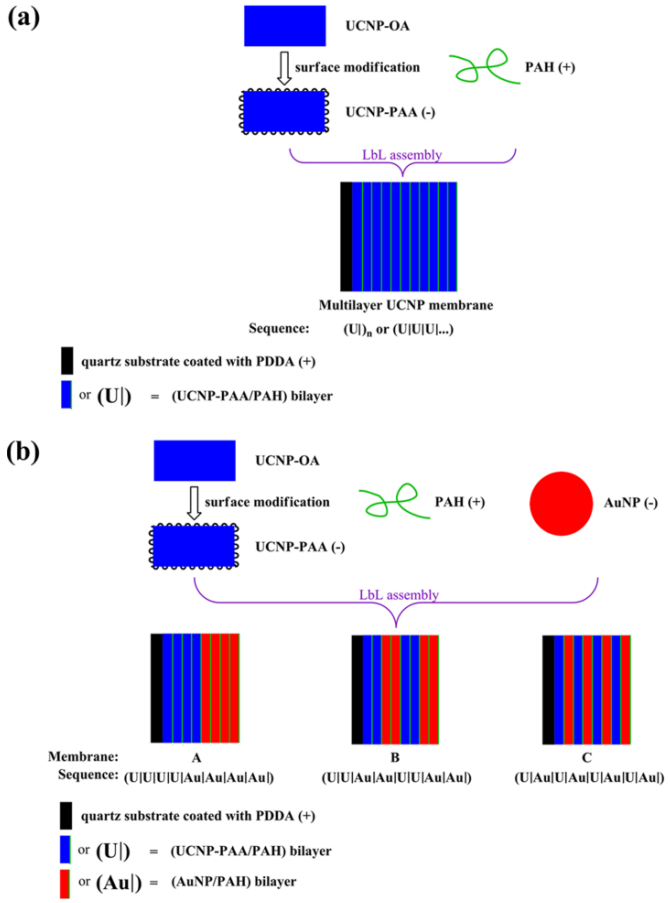

Figure 1. Schematic illustration of using the LBL assembly method to fabricate multilayer nanocomposite film on quartz/PDDA substrate: (a) multilayer film of UCNP ($NaYF_4$:Yb,Tm@$NaYF_4$); and (b) multilayer film comprising UCNP and AuNP spatially organized in different ways. *Note*: the deposition is on both sides of the substrate but only one side is shown in the sketch; n is the number of bilayers (nanoparticles with polyelectrolyte form one bilayer); from left to right corresponds to the 1st bilayer on the substrate to the nth bilayer.

3.3.3 Experimental

Materials

All chemicals were of analytical grade and used as received. Lanthanide chlorides ($YCl_3 \cdot 6H_2O$, $YbCl_3 \cdot 6H_2O$, $TmCl_3 \cdot 6H_2O$, 99.999%) were purchased from Shandong Yutai Chemical Reagent Company, China. Oleic acid (OA, 90%) and 1-octadecene (ODE, 90%) were obtained from Alfa Aesar. Hydrogen peroxide (H_2O_2, 30%) and sulphuric acid (H_2SO_4, 95–98%) were obtained from Fisher Chemical and Anachemia, respectively. Poly(acrylic acid) (PAA, *M*w *ca*. 1.8 kDa), poly(allylamine hydrochloride) (PAH, *M*w *ca*. 58 kDa), poly(diallyldimethylammonium chloride) solution (PDDA, *M*w *ca*. 200–350 kDa, 20 wt%), ammonium citrate (97%), tris(hydroxymethyl)aminomethane hydrochloride (Tris HCl, 99%), tris(hydroxymethyl)aminomethane (Tris base, 99.8%), nitrosyl tetrafluoroborate ($NOBF_4$, 95%), and gold(III) chloride trihydrate ($HAuCl_4 \cdot 3H_2O$, 99.9%) were purchased from Sigma-Aldrich. Ultrapure water (resistivity higher than 17 MΩ cm^{-1}) from a Milli-Q water system was used in all experiments.

Synthesis of $NaYF_4$:Yb,Tm@$NaYF_4$

$NaYF_4$:Yb,Tm parent *core* nanoparticles were prepared according to a reported method.[33] Typically, 1 mmol $RECl_3 \cdot 6H_2O$ (RE = 81.5 mol% Y^{3+}, 18 mol% Yb^{3+}, 0.5 mol% Tm^{3+}) was dissolved in a mixture of ODE (15 mL) and OA (6 mL). The solution was heated to 160 °C for 1 h under argon protection to form lanthanide-oleate coordination complexes. The solution was then cooled to room temperature. Afterwards, a solution of NH_4F (4 mmol) and NaOH (2.5 mmol) dissolved in methanol (MeOH, 10 mL) was added to the flask and the resulting mixture was stirred for 30 min. The temperature was then increased to 50 °C for evaporating methanol from the reaction mixture; in succession, the solution was heated to 300 °C in an argon atmosphere for 1 h and then cooled to room temperature. The nanoparticles were precipitated by addition of ethanol (EtOH), collected by centrifugation, washed with EtOH several times, and finally re-dispersed in hexane for further experiments.

The $NaYF_4$ shell was grown by following a similar procedure to that described above, except that the $NaYF_4$:Yb,Tm *core* nanoparticles were added to the solution before the injection of the NH_4F and NaOH solution. Typically, $YCl_3 \cdot 6H_2O$ (0.8 mmol) was added to a 100 mL flask containing ODE (15 mL) and OA (6 mL) and heated to 160 °C under argon gas flow with constant stirring for 1 h to form a transparent solution. It was then cooled to 80 °C. Afterwards, 1 mmol $NaYF_4$:Yb,Tm in hexane (6 mL) was added to the above solution and stirred for 30 min. After the removal of hexane, 10 mL of MeOH solution containing NH_4F (3.2 mmol) and NaOH (2 mmol) was added and stirred at 50 °C for another 30 min. Then the solution was heated to 300 °C under argon gas flow with stirring for 1 h and then cooled to room temperature. The obtained *core-shell* UCNP were collected with the same procedure as described in the preparation of the $NaYF_4$:Yb,Tm.

Synthesis of UCNP-PAA Nanoparticles

We employed a modified ligand-exchange strategy as reported by Wilhelm *et al*.[34] and Dong *et al*.[35]. In detail, $NOBF_4$ (0.48 mmol) was added into 45 mL of DMF/CH_2Cl_2 (1:25 by volume) with a *ca*. 120 mL glass tube. Another 0.5 mL of DMF was added to the above solution for enhancing the solubility of $NOBF_4$ during this step. Then, 15 mL of UCNP (12.85 mg mL^{-1}) dispersed in hexane were added at once. The resulting mixture was shaken vigorously and the precipitation of UCNP was observed within 5 min. To purify the $NOBF_4$ modified UCNP, they were collected *via* centrifugation (10 krpm, 10 min) twice from the original solution and then washed by the mixture of DMF/chloroform (2:15 by volume) twice again. The nanoparticles were redispersed in DMF (8 mL) used as stock for further ligand-exchange reactions.

To form UCNP-PAA, 7 mL of the stock dispersion of UCNP-BF_4 in DMF and 84.2 mg of PAA were dissolved in 1 mL of ultrapure water under vigorous stirring (1.5 krpm). The turbid mixture was further stirred for 3 h for completing the ligand exchange reaction. Afterwards, the dispersion was centrifuged for 15 min at 15 krpm. The transparent pellet

was gently washed by water. This step was repeated twice. Finally, the pellet was redispersed in 12 mL ultrapure water (6.07 mg mL^{-1}) for use in experiments.

Synthesis of Triammonium Citrate-Capped Gold Nanoparticles

The triammonium citrate-capped gold nanoparticles (AuNP) were prepared by using triammonium citrate as the reducing agent, which was similar to the procedure in the literature.[36] An aqueous solution of $HAuCl_4 \cdot 3H_2O$ (300 mL, 0.25 mM) was heated up to boiling point with vigorous stirring (900 rpm), then the aqueous solution of triammonium citrate (1 mL, 243 mM) was introduced rapidly using a syringe. The solution was boiled for additional 30 min in an oil bath. Afterwards, the solution was cooled down to room temperature slowly. The final red solution of AuNP was kept at room temperature.

Preparation of (UCNP-PAA/PAH) Bilayers on Quartz Substrate

A substrate of quartz was immersed in a piranha solution (1 : 3 mixture of 30% H_2O_2 and 98% H_2SO_4) at 75 °C for 45 min. (***Caution: piranha solution reacts violently with organic materials and should be handled carefully)*.** Then, the freshly prepared, negatively charged quartz substrate was immersed in a cationic polyelectrolyte solution of 1.02 mg mL^{-1} PDDA at pH = 8.2 (20 mM Tris buffer solution) for 35 min to obtain a positive charged surface. Successively, the PDDA-modified substrate was first immersed into the UCNP-PAA solution for 17 min followed by rinsing in three ultrapure water baths (250 mL for each) for 3, 2, and 1 min, respectively. Then, the substrate was immersed into a PAH solution at pH 7.8 (1 mg mL^{-1} in 20 mM Tris buffer solution) for 18 min, followed also by rinsing in three ultrapure water baths for 3, 2, and 1 min. The drying step (blowing N_2 gas for 10 min) was carried out between deposition of each bilayer. For simplicity, the optimized protocol for one UCNP bilayer was that adsorption of UCNP-PAA, washing, adsorption of PAH, washing, and drying. Multilayer coatings of $(UCNP\text{-}PAA/PAH)_n$ (n refers to the number of bilayers) can be fabricated by repeating these steps in a cyclic fashion.

Preparation of (AuNP/PAH) Bilayers on Quartz Substrate

As designed, LBL assembly of (AuNP/PAH) coatings was conducted in a similar way to that of the (UCNP-PAA/PAH) coating by using the original AuNP solution as the dipping solution when the (AuNP/PAH) layers were required. Firstly, the negatively charged AuNP due to the stabilizing layer of triammonium citrate at pH 6.0 in ultrapure water were confirmed by the zeta-potential analysis (Table S1). The PAH polyelectrolyte, like in the (UCNP-PAA/PAH) coating layer, was chosen again as a LBL partner polymer for the (AuNP/PAH) bilayer. In details, after quartz substrate coated with 1, 2 or 4 UCNP bilayers, the washed and dried substrate was then immersed into the AuNP solution (80 mL) for 17 min. Before the subsequent dipping into the PAH solution, the plate was rinsed with ultrapure water thoroughly and dried with N_2 gas to ensure the reproducibility of the LBL multilayer film. For simplicity, the optimized protocol for one (AuNP/PAH) bilayer consisted in adsorption of AuNP, washing, drying, washing, adsorption of PAH, washing, and drying. Then a given designed spatial organization of the bilayers of (UCNP-PAA/PAH) and (AuNP/PAH) can easily be achieved using the procedures described above.

Characterization

TEM observations were carried out using a Hitachi H-7500 microscope at an acceleration voltage of 80 kV. TEM specimens were prepared by dropping dilute solution of products (~10 μL) onto carbon-coated copper grids while allowing the solvent to evaporate completely. Extinction spectra were recorded on an Agilent Cary 6000i UV-vis-NIR spectroscopy. Quartz slides coated with functional bilayers were placed perpendicular to the beam and their extinction spectra were taken in the same area of the sample. FT-IR spectra were obtained on a Bomen FTIR spectrometer (ABB MB104PH) using the diffuse reflection technique. Samples were milled with potassium bromide (KBr) to form a fine powder for testing. The UCL spectra of thin films containing UCNP built on a quartz plate before and after each bilayer deposition (UCNP-PAA or AuNP/PAH) were recorded with a double-monochromator Fluorolog instrument from Horiba (used parameters: front angle

detection; 0.25 s integration time; 1.0 nm for both side entrance slit and side exit slit). A power-adjustable 980 nm laser diode (MDL-H-980 nm-4W, Changchun New Industries Optoelectronics Tech. Co., Ltd.) was employed as the upconversion pump source. The real power of the laser beam was measured using a power-meter (model 1918-R, Newport) and the beam diameter was measured by a knife-edge method. Surface zeta-potential of the nanoparticles was measured using a Malvern Zetasizer Nano ZS ZEN3600 system with a helium-neon laser (λ = 633 nm). All measurements were carried out with disposable folded capillary cells (DTS1060) at a scattering angle of 173^{o} and data were analyzed by the Malvern software. The surface of LBL assembled multilayer films with nanoparticles was examined using a Hitachi S-4700 field-emission-gun scanning electron microscope (SEM) operating at 1.0 KV. For SEM observation, a fine platinum coating layer (a few nm) was deposited on sample surface by using a K550 sputter coater for 1 or 2 min. Atomic force microscopy (AFM) observation was performed using a Veeco Dimension Icon equipped with a Nanoscope V controller. Silicon cantilevers with a resonance frequency of 320 kHz and a force constant of 42 N m^{-1} were utilized.

3.3.4 Results and Discussion

3.3.4.1 Multilayers of UCNP

Oleic-acid capped *core-shell* $NaYF_4$:Yb,Tm@$NaYF_4$ upconversion nanoparticles (UCNP-OA; length: 38.7 ± 2.2 nm; width: 21.3 ± 2.2 nm) were prepared using a solvothermal method (Fig.2 (a)).[33] These as-synthesized nanoparticles functionalized with OA ligands have a hydrophobic character. To be able to carry out the LBL assembly in aqueous solution, the UCNP have to be dispersible in water. Hence two surface-modification steps were employed to convert the hydrophobic UCNP-OA into water-dispersible UCNP-PAA (Fig. S1 and S2). The negatively charged UCNP-PAA was confirmed by zeta potential test (Table S1). To form the UCNP/polyelectrolyte bilayer, positively charged PAH at pH 8.2 (pKa = 9.7[37]) in 20 mM tris buffer solution was chosen as its polyelectrolyte partner. By alternately dipping a positive charged quartz/PDDA into

UCNP-PAA and PAH buffer solutions, and then repeating the same procedure for n times, a multilayer film of (**U**|)$_n$ (**U** represents one UCNP-PAA layer and | stands for PAH layer) could be prepared.

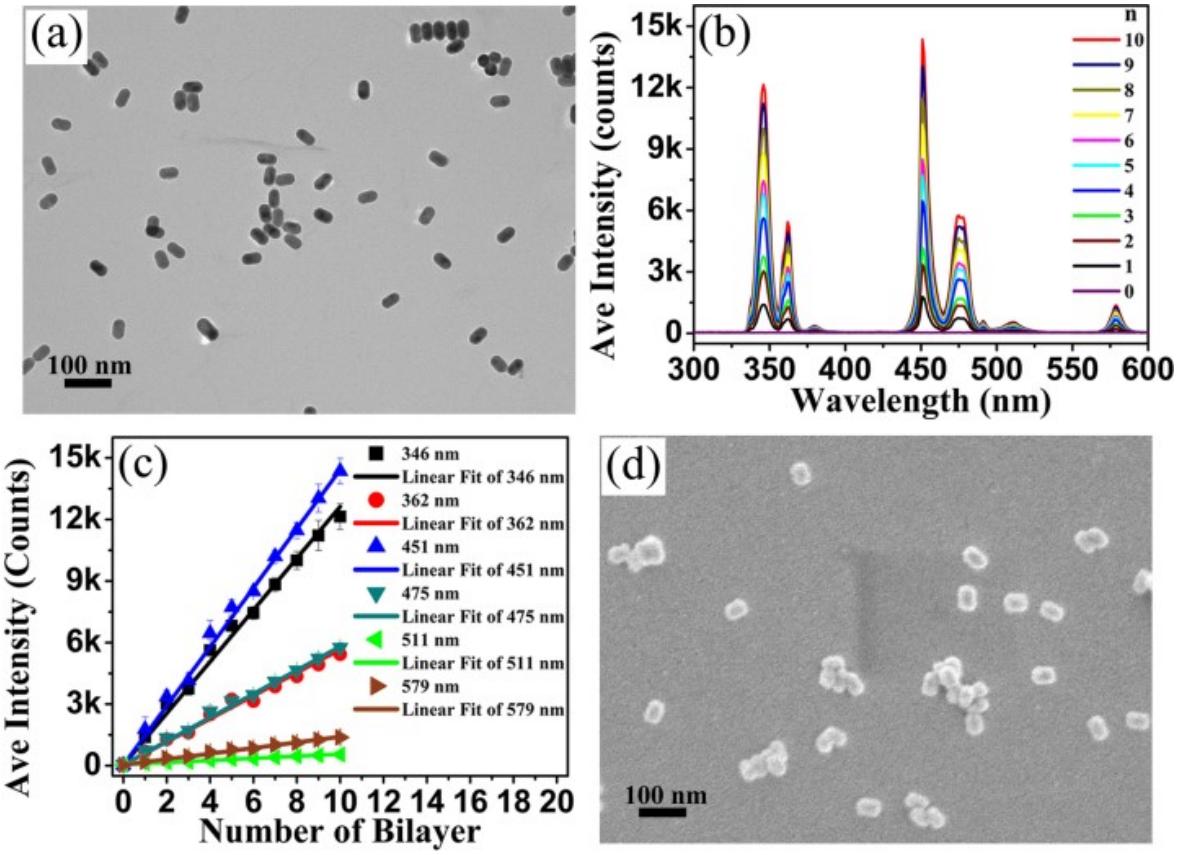

Figure 2. (a) TEM image of $NaYF_4$:Yb,Tm@$NaYF_4$. (b) Upconversion luminescence spectra of (UCNP-PAA/PAH)$_n$ (n is the number of bilayers, n = 0-10) formed on quartz/PDDA substrate upon 980 nm excitation at 2.55 kW cm^{-2}. (c) Plots of intensity of the major emission peaks in (b) vs. number of bilayers. (d) SEM image of (UCNP-PAA/PAH)$_{11}$.

To confirm the LBL assembly, the multilayer UCNP films were subjected to UCL spectral analysis, because no absorption around 980 nm could be observed for the (**U**|)$_n$ films even with n = 11 (Fig. S3). The UCL data were collected after each deposition and with the film dried by N_2 gas. As can be seen from the emission spectra in Fig. 2 (b), all the major emission peaks upon 980 nm NIR excitation remain the same as those of UCNP dispersed

in hexane[38] or chloroform[39]. Moreover, the emission intensity increases continuously by a certain amount after each deposition of a new bilayer. In Fig. 2 (c), the emission intensity for a given peak is plotted as a function of the number of bilayers, showing a linear increase for all major emission peaks (linear regression data in Table S2). This result indicates that a similar amount of UCNP is deposited after each dipping/rinsing step, which is characteristic of a successful LBL assembly. It is worth to note that the maximum and minimum slopes are seen from the 451 nm and 511 nm emission peaks, respectively. A higher slope is better suited for quantitative analysis of the LBL assembly of UCNP. Fig. 2 (d) shows the SEM image of the $(\mathbf{U}|)_{11}$ film. It is clear that under the used conditions, each dip-coating cycle deposits a certain number of UCNP that cannot cover the entire surface of the film. The average number density of UCNP was found to be about 37 μm^{-2} calculated from various SEM images. By scratching part of the film, AFM image revealed a rough surface with an average thickness of 75 nm.

Furthermore, the aging effect on the UCL of the UCNP multilayers was investigated. After storage at room temperature for 16 h, a dried $(\mathbf{U}|)_{10}$ film showed a reduction of 5% for the average emission intensity (Fig. S4). The intensity of peaks increased again after depositing another bilayer from the aged $(\mathbf{U}|)_{10}$ film, yielding $(\mathbf{U}|)_{11}$. Subsequently, the effect of aging on the photoluminescence was further monitored using the $(\mathbf{U}|)_{11}$ film. It was found that the UCL intensity only declined by 10% after 11 days (Fig. S5). This observed aging effect is weak as compared to the single UCNP layer sandwiched by LBL assembled polyelectrolyte layers, whose photoluminescence declined to 68% of the initial intensity after one week.[40] This finding suggests that the multilayers of UCNP have a long-term UCL stability upon storage at room temperature.

3.3.4.2 Multilayers of Spatially Organized UCNP and AuNP

As mentioned above, the main purpose of the present study is to investigate the possibility of using the LBL assembly method to construct thin films containing both UCNP and AuNP with spatially controlled organization. To this end, triammonium citrate-capped

AuNP with SPR peak centered at 528 nm (Figs. 3 (a) and (b)) were synthesized. The average diameter of AuNP from TEM analysis was *ca.* 58.1 nm and the surface zeta potential was -41.5 mV at pH 6.0 (Table S1). Hence multilayer films of $(\mathbf{Au}|)_n$ (**Au** stands for a AuNP layer; | represents one PAH layer), could easily be fabricated in a similar way to obtaining UCNP-PAA/PAH.

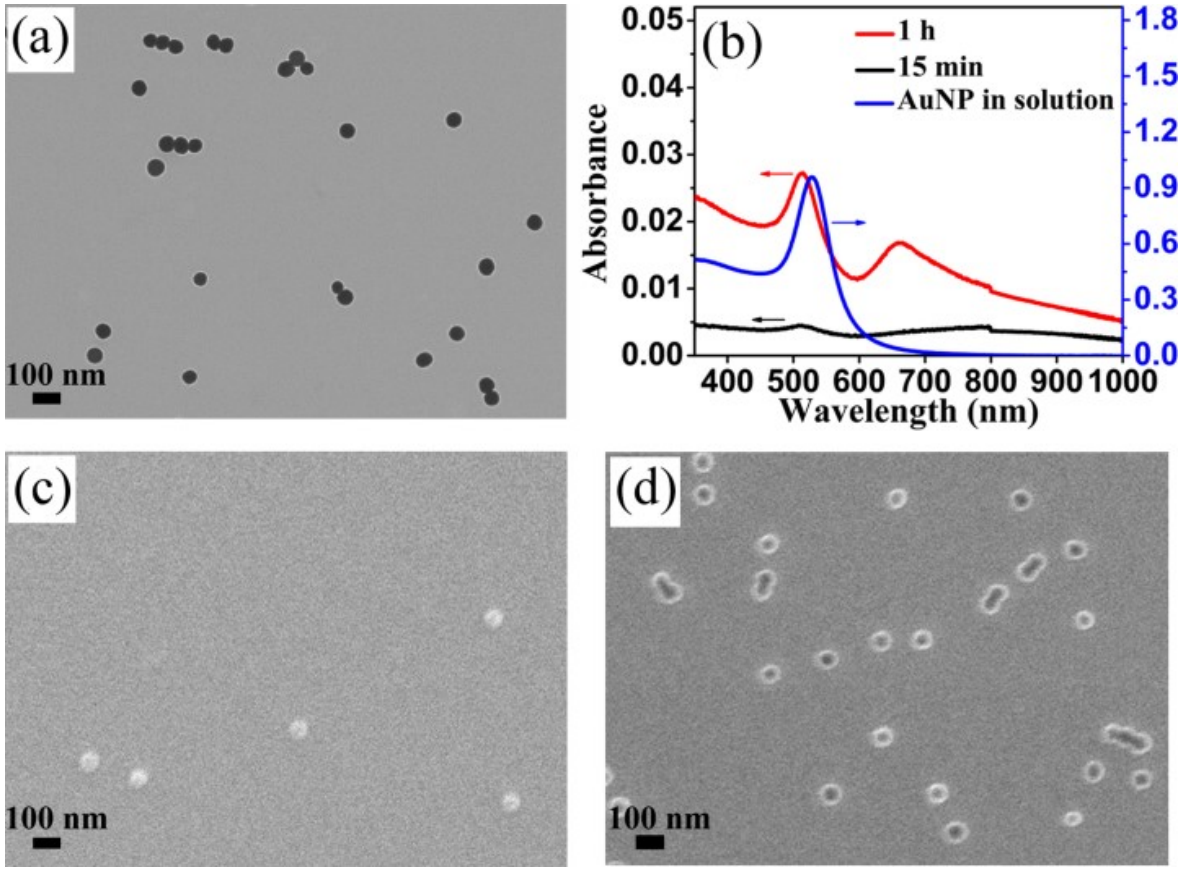

Figure 3. (a) TEM image of AuNP. (b) Extinction spectra of single AuNP/PAH $((\mathbf{Au}|)_1)$ bilayer built up with different dip-coating time and AuNP solution. (c, d) SEM images of one $(AuNP/PAH)_1$ bilayer at different dip-coating times: (c) 15 min; (d) 1 h.

Using the LBL method for building $(\mathbf{Au}|)_n$, it was found that the number density of AuNP deposited on the quartz substrate became greater with increasing the dip-coating time (Figs. 3 (c) and (d)), which is consistent with a previous report.[41] More specifically, the average number density of the island-like distributed AuNP was 1.3 μm^{-2} for 15 min dip-coating

and 6.7 μm^{-2} for 1 h dip-coating, respectively. This change was also reflected on the recorded UV-vis-NIR spectrum. At first, the SPR at 528 nm in water showed a blue-shift to 513 nm after deposition (Fig. 3 (b)) as a result of changing local refractive index.[42] Furthermore, a new SPR peak appeared at 659 nm for long time dip-coating, which was attributed to the interparticle interactions between neighboring AuNP (parallel to the substrate) in the same layer.[43,44] The aggregation of AuNP with a dip-coating time of 1 h was observable on the SEM image (Fig 3(d)). Unless otherwise stated, a dip-coating time of 15 min was chosen for each AuNP bilayer (**Au**|) to keep the interaction among AuNP at a low level within the same layer.

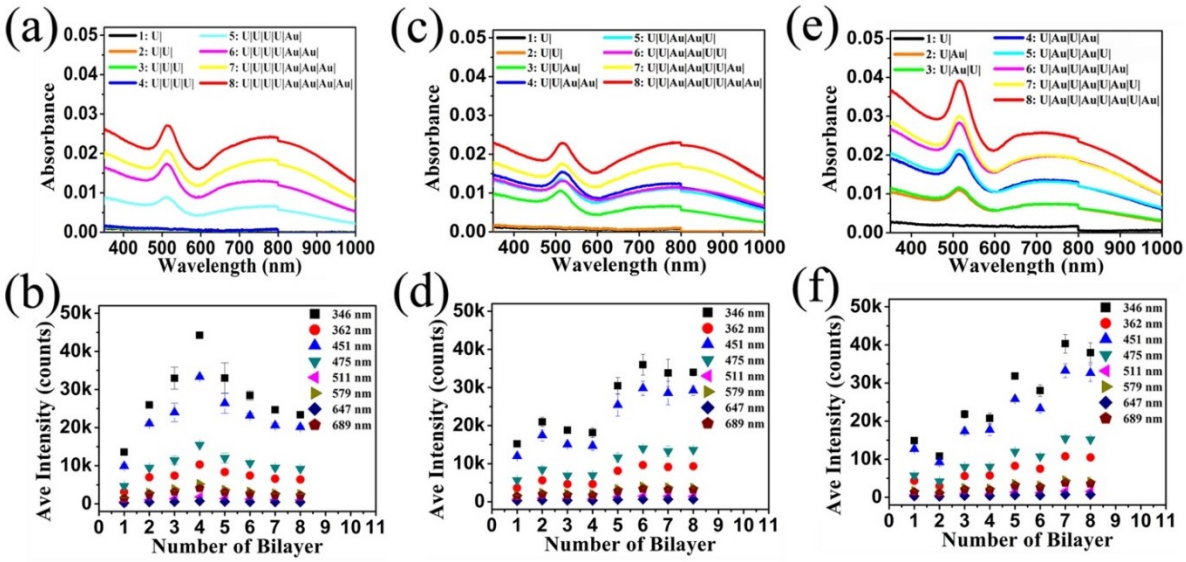

Figure 4. Extinction spectra (a, c, e) and emission spectra (980 nm excitation, CW laser at 11.77 kW cm^{-2}) (b, d, f) for LBL assembled films comprising UCNP-PAA/PAH (**U**|) and AuNP/PAH (**Au**|) bilayers built up with different deposition sequences giving rise to different spatial organizations of the two types of nanoparticles: (**U**|**U**|**U**|**U**|**Au**|**Au**|**Au**|**Au**|) (a and b); (**U**|**U**|**Au**|**Au**|**U**|**U**|**Au**|**Au**|) (e and f); and (**U**|**Au**|**U**|**Au**|**U**|**Au**|**U**|**Au**|) (e and f).

To fabricate thin films comprised of (**U**|) and (**Au**|) bilayers by the LBL assembly, the order of each bilayer deposition determines the spatial organization of the two types of nanoparticles and hence their optical properties. To demonstrate this, we chose the three

deposition sequences in Fig. 1 (b) to construct three 8-bilayer thin films (A, B, and C) containing four (**U**|) bilayers and four (**Au**|) bilayers but organized in different ways. In Fig. 4, we tracked the UV-vis-NIR spectra and UCL intensity at various emission peaks of the three films during the formation process. Several observations can be made. First, for all three films, the SPR peaks are observable after deposition of the first AuNP bilayer and their intensities increase with increasing the number of AuNP bilayers. As seen from the example of film C (Fig. S6), the apparent absorbance of the 513 nm SPR peak increases linearly with the number of AuNP bilayers. Moreover, the presence of UCNP has little effect on the extinction spectrum of AuNP. This is particularly noticeable with films B and C, where the SPR spectrum shows no change every time following the deposit of a UCNP bilayer on top of an AuNP bilayer. On the other hand, in all cases, right after deposition of the first AuNP bilayer, the spectrum not only shows one distinct SPR peak at *ca.* 513 nm, but also a weak and broad band appearing between 600 and 1000 nm. This observation suggests that most of the AuNP in the 1st bilayer were well dispersed but part of the nanoparticles already aggregate.

However, on a closer inspection, difference exits between the three films. For film A (Fig. 4 (a)), as the number of (**Au**|) increased, the 513 nm band remained the same; but the other one moved toward longer wavelength and became much stronger around 780 nm. The situation basically is similar for film B (Fig. 4 (c)). The broad band peaked at 780 nm is likely originated from both intra-layer and inter-layer aggregation of AuNP with varying axial ratios. In contrast to films A and B, the 513 nm band in sample C is the dominant SPR band and the red-shift broad band appears relatively weak and peaked at appeared at 720 nm. The film C was built with alternating deposition of UCNP and AuNP bilayers, while the films A and B involved successive deposition of AuNP bilayers. The results in Figure 4 imply that the UCNP bilayer between two AuNP bilayers exert an effect of blocking or reducing the inter-layer interaction of AuNP.

Regarding the UCL of UCNP in the LBL films, the spatial organization of the two types of nanoparticles also imposes strong effect. The photoluminescence properties of the three

films were monitored by recording the emission spectra upon 980 nm excitation as a function of number of bilayers; the average intensities of main emission peaks are also reported in Figure 4. In all cases, the UCL intensities were reduced to some extent after each (**Au**|) deposition. For film A (Fig. 4 (b)), the UCL intensities increased continuously upon successive deposition of four UCNP bilayers, before decreasing significantly with the successive addition of four AuNP bilayers. The drop is about 40% between the (**U**|)$_4$ film and the (**U**|)$_4$(**Au**|)$_4$ film. The same effect of AuNP was translated into the trends noticed for the two other LBL assembly sequences. For film B (Fig. 4 (d)), since two (**Au**|) layers were deposited after each two (**U**|) layers, the UCL peak intensities could not rise continuously; instead they followed a step-like change. However, the "quenching" effect of AuNP appeared less prominent as compared to the film A. In the case of alternating deposition leading to film C (Fig. 4 (f)), the intensities of some peaks decreased a little after (**Au**|) bilayer deposition but the others showed basically no changes. It seems that the "quenching" effect was minimized when a single AuNP layer was inserted into two (**U**|) layers. There may be two reasons for the reduced UCL peak intensity upon AuNP bilayer deposition. On one hand, as revealed by the absorption (extinction) spectra, AuNP undergo aggregation, shifting the SPR peaks into near-infrared region. This could increase the scattering of the 980 nm excitation light by the film, which has an effect of reducing the effective excitation and thus causing an apparent quenching of the UCL emissions.[32] The observed difference between films A and C seem to support this mechanism. The aggregation of AuNP is the most important in film A with four AuNP bilayers together, which causes more scattering of the excitation light. By contrast, the aggregation of AuNP is the least in film C with single AuNP bilayer sandwiched between two UCNP bilayers, which may account for the limited quenching effect. On the other hand, it cannot be ruled out that part of the UCL photons emitted from UCNP, especially in the visible region, were absorbed by AuNP in the LBL films. The multilayer films of UCNP and AuNP have also rough surfaces; their average thickness as measured by AFM was about 85 nm.

Although the above data analysis supports the assumption that different UCNP and AuNP deposition sequences gave rise to varying spatial organization of the two types of

nanoparticles, we do not have direct evidence at this point of time due to the lack of cryo-TEM or SEM facilities required for cross-section imaging. Nevertheless, the SEM images in Figure 5 provide indirect evidence. For film A with four layers of UCNP followed by four layers of AuNP, only larger particles of AuNP can be observed on surface (Fig.5 (a)). By contrast, for film B, with two UCNP layers separated by two AuNP layers, a few smaller UCNP start to appear (Fig. 5(b)). In the case of film C with alternately deposited UCNP and AuNP layers, it is visible that a number of UCNP are mixed with AuNP. As stated earlier, under the used conditions, only part of the surface was covered by either UCNP or AuNP after each deposition. This means that the nanoparticles in two or more neighboring layers will interdigitate. In other words, there would be an extensive interface between two close layers of UCNP and AuNP. However, despite such a diffuse layering, the spatial organization or distribution of the two types of nanoparticles is clearly influenced by their deposition sequences. For film A, the two layers of AuNP on top are likely to be separated from the two layers of UCNP at bottom, while in the middle layers UCNP and AuNP are interdigitated. Although in film C the two kinds of nanoparticles are mostly mixed, film B likely presents an intermediate state with periodically changing density of either UCNP or AuNP along the film thickness direction.

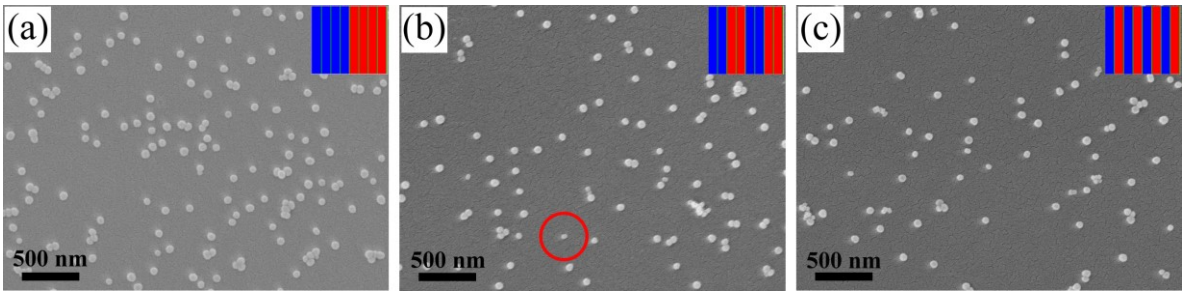

Figure 5. SEM images of three thin films: (a) (**U**|**U**|**U**|**U**|**Au**|**Au**|**Au**|**Au**|); (b) (**U**|**U**|**Au**|**Au**|**U**|**U**|**Au**|**Au**|); and (c) (**U**|**Au**|**U**|**Au**|**U**|**Au**|**U**|**Au**|). Red ring in (b) indicates one UCNP.

3.3.5 Conclusions

We have used the LBL method to assemble multilayers of either UCNP alone or UCNP and AuNP combined with different spatially organized arrangements. On one hand, the UCNP multilayers were found to exhibit good long-term luminescence stability. On the other hand, the multilayers of UCNP and AuNP display SPR and UCL properties that are dependent on the specific sequence used to deposit the two types of nanoparticles, which determines their spatial organization and interactions. The results revealed that alternating diposition of UCNP and AuNP is the best way to preserve their distinct optical properties owing to the minimized aggregation of AuNP in two layers separated by one UCNP layer. By contrast, successive deposition of UCNP followed by successive addition of AuNP layers results in more agglomeration of AuNP, which gives rise to an intense broad SPR band in the NIR region as well as the most significant quenching effect on the UCL peak intensities of UCNP, likely due to a decrease in the effective 980 nm excitation intensity resulting from scattering by aggregated AuNP. This study has thus paved a facile and effective way to organizing UCNP and AuNP into thin films in a spatially controlled fashion, which offers new possibilities for preparing NIR-responsive and plasmonic materials. For instance, the interest in polymer hybrid materials is growing fast, while both UCNP and AuNP are often used as nanofillers and their placement or organization in polymers is an important issue. It can be foreseen that the demonstrated LBL method may find useful applications in designing and developing polymer hybrid materials such as stimuli-responsive systems.

Acknowledgements

This work was financially supported by the Natural Sciences and Engineering Research Council of Canada (NSERC) and le Fonds de recherche du Quebec: Nature et technologies (FRQNT). J. X. acknowledges the Merit Scholarship for Foreign Students awarded by the Ministère de I'Éducation, du Loisir et du Sport du Québec and the China Scholarship Council. Y.Z. is a member of the FRQNT-funded Center for Self-Assembled Chemical Structures (CSACS) and Centre québécoissur les matériauxfonctionnels (CQMF).

Notes and references

1 C. Zhang, H.-P. Zhou, L.-Y. Liao, W. Feng, W. Sun, Z.-X. Li, C.-H. Xu, C.-J. Fang, L.-D. Sun, Y.-W. Zhang and C.-H. Yan, *Adv. Mater.*, 2010, **22**, 633-637.

2. H. P. Ho, W.-W. Wong and S.-Y. Wu, *Opt. Eng.*, 2003, **42**, 2349-2353.

3. Z. M. Yang, Z. M. Feng and Z. H. Jiang, *J. Phys. D: Appl. Phys.*, 2005, **38**, 1629-1632.

4. L. Zhang, Q. Tian, W. Xu, X. Kuang, J. Hu, M. Zhu, J. Liu and Z. Chen, *J. Mater. Chem.*, 2012, **22**, 18156-18163.

5. A. Shalav, B. S. Richards, T. Trupke, K. W. Krämer and H. U. Güdel, *Appl. Phys. Lett.*, 2005, **86**, 013505.

6. M.-K. Tsang, G. Bai and J. Hao, *Chem. Soc. Rev.*, 2015, **44**, 1585-1607.

7. A. R. Hong, J. Kim, S. Y. Kim, S.-I. Kim, K. Lee and H. S. Jang, *Opt. Lett.*, 2015, **40**, 4959-4962.

8. L. Yan, Y.-N. Chang, W. Yin, X. Liu, D. Xiao, G. Xing, L. Zhao, Z. Gu and Y. Zhao, *Phys. Chem. Chem. Phys.*, 2014, **16**, 1576-1582.

9. L. Xie, Y. Qin and H.-Y. Chen, *Anal. Chem.*, 2012, **84**, 1969-1974.

10. B. Tyler, M. Jeevan, P. S. May, K. Jon, C. William, A. Krishnamraju, V. Swathi and N. L. QuocAnh, *Nanotechnology*, 2012, **23**, 185305.

11. C. Lin, M. T. Berry, R. Anderson, S. Smith and P. S. May, *Chem. Mater.*, 2009, **21**, 3406-3413.

12. W. Li, Z. Chen, L. Zhou, Z. Li, J. Ren and X. Qu, *J. Am. Chem. Soc.*, 2015, **137**, 8199-8205.

13. W. Li, J. Wang, J. Ren and X. Qu, *J. Am. Chem. Soc.*, 2014, **136**, 2248-2251.

14. X. Chen, W. Xu, L. Zhang, X. Bai, S. Cui, D. Zhou, Z. Yin, H. Song and D.-H. Kim, *Adv. Funct. Mater.*, 2015, **25**, 5462-5471.

15. X. Hu, E. McIntosh, M. G. Simon, C. Staii and S. W. Thomas, *Adv. Mater.*, 2016, **28**, 715-721.

16. X. Zhang, H. Chen and H. Zhang, *Chem. Commun.*, 2007, 1395-1405.

17. J. F. Quinn, A. P. R. Johnston, G. K. Such, A. N. Zelikin and F. Caruso, *Chem. Soc. Rev.*, 2007, **36**, 707-718.

18. P. Bertrand, A. Jonas, A. Laschewsky and R. Legras, *Macromol. Rapid. Comm.*, 2000, **21**, 319-348.

19. G. Decher, *Science*, 1997, **277**, 1232-1237.

20. C. Bao, B. Ma, J. Liu, Z. Wu, H. Zhang, Y.-J. Jiang and J. Sun, *Langmuir*, 2016, **32**, 3393-3399.

21. D. Lu, S. K. Cho, S. Ahn, L. Brun, C. J. Summers and W. Park, *ACS Nano*, 2014, **8**, 7780-7792.

22. R. Wei, Z. Wei, L. Sun, J. Z. Zhang, J. Liu, X. Ge and L. Shi, *ACS Appl. Mater. Interfaces*, 2016, **8**, 400-410.

23. Y. Huang, F. Rosei and F. Vetrone, *Nanoscale*, 2015, **7**, 5178-5185.

24. X. Ge, L. Sun, B. Ma, D. Jin, L. Dong, L. Shi, N. Li, H. Chen and W. Huang, *Nanoscale*, 2015, **7**, 13877-13887.

25. F. Wang, D. Banerjee, Y. Liu, X. Chen and X. Liu, *Analyst.*, 2010, **135**, 1839-1854.

26. L.-L. Li and Y. Lu, *J. Am. Chem. Soc.*, 2015, **137**, 5272-5275.

27. W. Park, D. Lu and S. Ahn, *Chem. Soc. Rev.*, 2015, **44**, 2940-2962.

28. A. Priyam, N. M. Idris and Y. Zhang, *J. Mater. Chem.*, 2012, **22**, 960-965.

29. L. Cheng, K. Yang, Y. Li, X. Zeng, M. Shao, S.-T. Lee and Z. Liu, *Biomaterials.*, 2012, **33**, 2215-2222.

30. Z. Li, L. Wang, Z. Wang, X. Liu and Y. Xiong, *J. Phys. Chem. C,* 2011, **115**, 3291-3296.

31. L. P. Qian, L. H. Zhou, H.-P. Too and G.-M. Chow, *J. Nanopart. Res.*, 2011, **13**, 499-510.

32. H. Zhang, Y. Li, I. A. Ivanov, Y. Qu, Y. Huang and X. Duan, *Angew. Chem., Int. Ed.*, 2010, **49**, 2865-2868.

33. F. Shi and Y. Zhao, *J. Mater. Chem. C*, 2014, **2**, 2198-2203.

34. S. Wilhelm, M. Kaiser, C. Wurth, J. Heiland, C. Carrillo-Carrion, V. Muhr, O. S. Wolfbeis, W. J. Parak, U. Resch-Genger and T. Hirsch, *Nanoscale*, 2015, **7**, 1403-1410.

35. A. Dong, X. Ye, J. Chen, Y. Kang, T. Gordon, J. M. Kikkawa and C. B. Murray, *J. Am. Chem. Soc.*, 2011, **133**, 998-1006.

36. H. Kawasaki, T. Sugitani, T. Watanabe, T. Yonezawa, H. Moriwaki and R. Arakawa, *Anal. Chem.*, 2008, **80**, 7524-7533.

37. C. P. Silva and H. M. Carapuça, *Electrochim Acta*, 2006, **52**, 1182-1190.

38. H. Qiu, C. Yang, W. Shao, J. Damasco, X. Wang, H. Ågren, P. N. Prasad and G. Chen, *Nanomaterials*, 2014, **4**, 55-68.

39. B. Yan, J.-C. Boyer, N. R. Branda and Y. Zhao, *J. Am. Chem. Soc.*, 2011, **133**, 19714-19717.

40. Y. Bao, Q. A. N. Luu, C. Lin, J. M. Schloss, P. S. May and C. Jiang, *J. Mater. Chem.*, 2010, **20**, 8356-8361.

41. H. Kawasaki, T. Sugitani, T. Watanabe, T. Yonezawa, H. Moriwaki and R. Arakawa, *Anal. Chem.*, 2008, **80**, 7524-7533.

42. C. Louis and O. Pluchery, *Gold nanoparticles for physics, chemistry and biology*, World Scientific, 2012.

43. C. Jiang, S. Markutsya and V. V. Tsukruk, *Langmuir*, 2004, **20**, 882-890.

44. C. Lu, H. Möhwald and A. Fery, *J. Phys. Chem. C*, 2007, **111**, 10082-10087.

3.3.6 Supporting Information

Table S1. Size and Zeta Potential of Nanoparticles

Sample	Physical size [nm][a]	Zeta potential [mV][b]
UCNP-PAA[c]	—	-33.2
AuNP[d]	58.1	-41.5

[a]The values are obtained from TEM statistics over 100 particles. [b]Measured by a Malvern Zetasizer Nano ZS ZEN3600 system. Results are given in number mean. [c]pH 6.0 in ultrapure H_2O. [d]pH 8.0 in 20 mM Tris buffer solution.

Table S2. Linear Regression ($y = a + b \cdot x$) of the Plots of Luminescence Intensity (y) vs. Number of Bilayer (x) for Different Emission Peaks.

Wavelength [nm]	Intercept		Slope		R-square
	a	Std. Error	b	Std. Error	
451	35.74739	9.8602	1438.887722	19.08683	0.99873
346	34.12757	4.3579	1259.55466	23.15576	0.99786
475	45.46109	7.19823	576.35443	8.15784	0.99893
362	42.39889	4.57817	561.50592	8.94388	0.99355
579	41.28572	3.74999	136.94878	2.25938	0.99783
511	47.33908	4.56176	52.29483	1.51735	0.99540

1. TEM

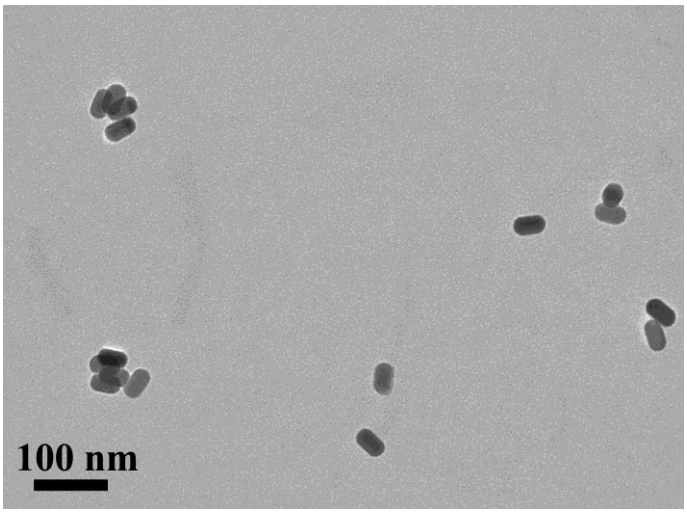

Figure S1. TEM image of UCNP functionalized with poly(acrylic acid) (PAA).

2. FTIR

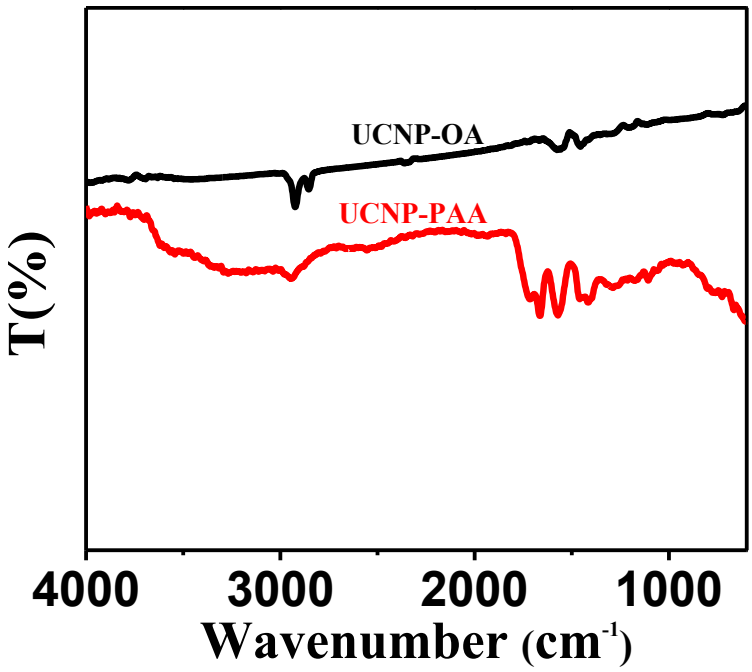

Figure S2. FT-IR spectra of UCNP-OA (oleic acid) and UCNP-PAA.

3. UV-vis-NIR

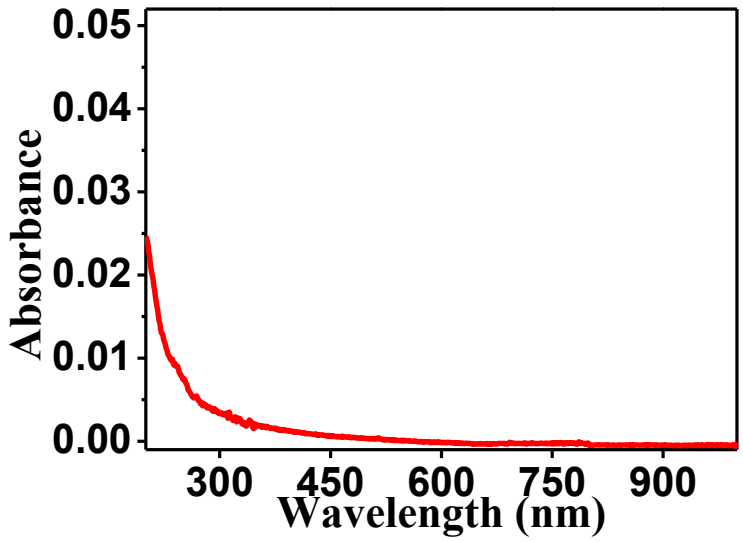

Figure S3. UV-vis-NIR extinction spectrum of $(UCNP\text{-}PAA/PAH)_{11}$.

4. Upconversion Luminescence

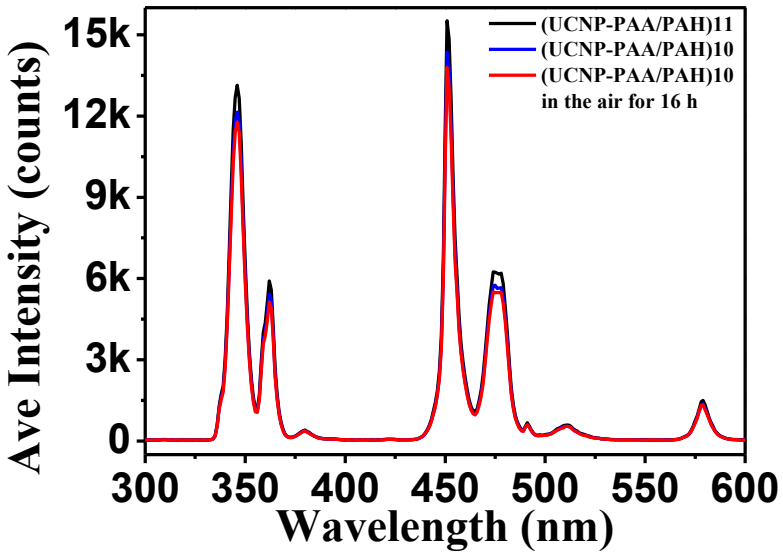

Figure S4. UCL emission spectra of $(UCNP\text{-}PAA/PAH)_{10 \text{ or } 11}$ LBL films (λ_{ex}=980 nm, 2.55 kW cm^{-2}): $(UCNP\text{-}PAA/PAH)_{10}$ (blue); $(UCNP\text{-}PAA/PAH)_{10}$ kept in the air for 16 h (red); $(UCNP\text{-}PAA/PAH)_{11}$ (black).

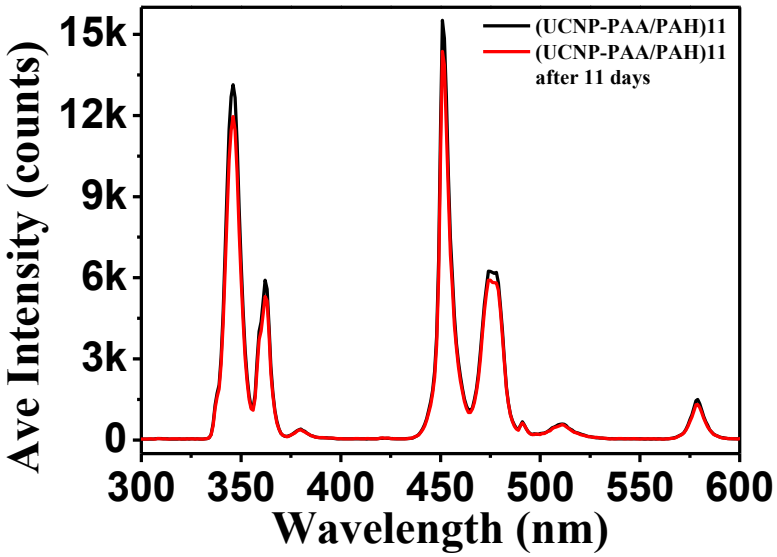

Figure S5. UCL emission spectra of $(UCNP\text{-}PAA/PAH)_{11}$ film (λ_{ex}=980 nm, 2.55 kW cm^{-2}): 0 h (black); after keeping in the air for 11 d (red).

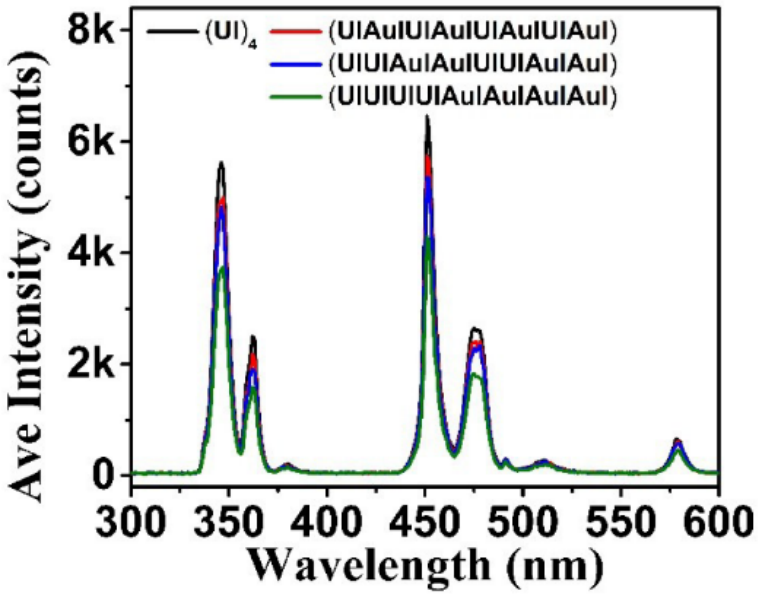

Figure S6. UCL emission spectra for a 4-bilayer UCNP and three UCNP/AuNP multilayers containing the same number of UCNP bilayers and prepared using different LBL deposition sequences. The spectra were recorded under the same 980 nm excitation intensity of 2.55 kW/cm^2.

5. LBL Assembly of AuNP Bilayers

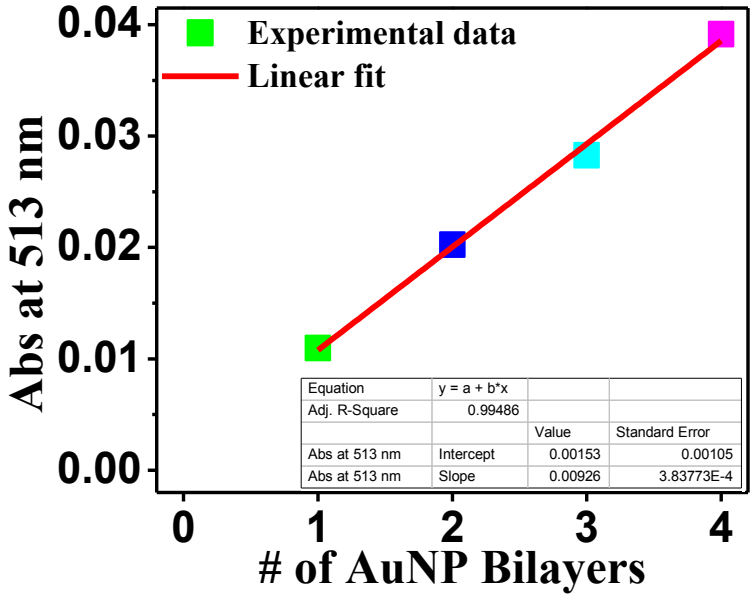

Figure S7. Linear fit of the plot of absorbance at 513 nm vs. number of AuNP bilayers.

6. NIR Laser Power Density Calibration

The real power and the beam diameter (*d*) are two key parameters used to calculate the real excitation power density. At first, the real irradiation power at the LbL site was accurately measured and the data were summarized in Table S3. Then, the beam diameter was measured by a Knife-edge method. Briefly, the razor blade was mounted on a wide metal sheet on the motorized stage, and moved in a direction (z-axis) perpendicular to the propagation direction of the 980 nm light. Each power was recorded while varying the z-axis position over a range from 3.00 mm to 5.00 mm (in steps of 0.05 mm). Measured power profile of Gaussian beam can be fitted with an error function, where we got a standard deviation of 0.06373, see Figure S6. To get the FWHM, it has to multiply by $2\sqrt{2ln2}$. So the valid beam diameter was ~150 μm and an irradiation area of 0.01767 mm^2 ($S_{laser\ beam} = (\frac{d}{2})^2\pi$) was used to calculate the average exciting power density.

Table S 3. The Relationship between the Output Power of 980 nm Laser and its Real Power when the Light Beam Reached Sample

Output power/mW	1000	2000	3500
Real power/mW	450.5	1113.3	2080.0
Power density/Kw cm^{-2}	2.55	6.30	11.77

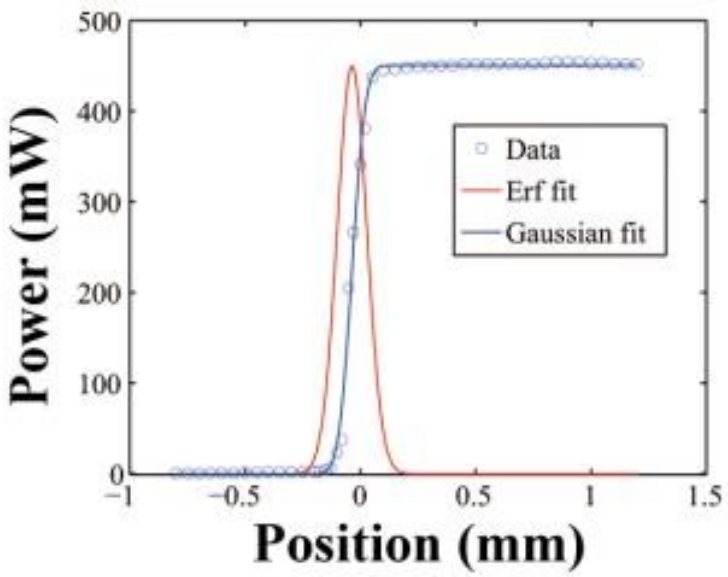

Figure S8. The power distribution of 980 nm laser across the calibrated beam. The plot was fitted by Gauss curve (red line).

References

1. G. Ok, S.-W. Choi, K. Park and H. Chun, *Sensors*, 2013, 13, 71-85.

3.4 Summary of the Project

The methodology developed here allows us to obtain UCNP alone or AuNP and UCNP contained thin films. First, the layer-by-layer assembled films with only UCNP were found to exhibit good long-term upconversion luminescent stability (at least 11 days). Second, three eight-bilayer thin films comprising four UCNP/polyelectrolyte bilayers and four AuNP/polyelectrolyte bilayers were prepared by changing the deposition order of bilayers. The successful growth of these thin films was verified by atomic force microscopy, scanning electron microscopy, UV-vis absorption, and upconversion luminescence (UCL) spectra. Particularly, we found that surface plasmon resonance (SPR) peaks and the UCL intensities of these thin films were greatly influenced by their deposition orders used to prepare films. Interestingly, the alternating deposition sequence of one UCNP/polyelectrolyte bilayer followed by another one bilayer of AuNP/polyelectrolyte could keep the interactions of AuNP at a low level, which was indicated by the broad SPR peak in the 600-1000 nm region. Moreover, this deposition order was beneficial for the preservation of upconversion emissions of UCNP from the resulted film. Despite the not fully separated bilayers (two or more neighboring layers interdigitated indeed), the SEM observations revealed that the spatial organization or distribution of the two types of nanoparticles was clearly influenced by their deposition sequences. In all, this study demonstrates an easy and efficient way to prepare NIR-responsive and plasmonic hybrid thin films with the possibility to tune their optical properties through the spatially controlled organization of the nanoparticles.

CHAPTER 4. GENERAL DISCUSSION AND PERSPECTIVE

4.1 General Discussion

In the whole body of this thesis, we described three systems comprising UCNP and polymers, from nanovectors to thin films. Two main contributions have been made to the field of UCNP/polymers hybrid materials. Our first contribution is the demonstration of novel strategies for the preparation of nanovectors for NIR light-controllable drug release through integrating UCNP into photoresponsive polymers. Although significant efforts have been devoted to achieving the NIR light-triggered release based on these two materials, like the conjugation of photocaged drug molecules into the nanovector structure through covalent bonding or the combination of photoresponsive polymers with UCNP through self-assembly, those systems have two shortcomings. On the one hand, the introduction of photocaged molecules into nanovectors involves multistep chemical modifications, making the fabrication of nanovectors tedious and demanding. And the functionalization of drug molecules must not affect their therapeutic effect. On the other hand, encapsulation via amphiphilic polymer self-assembly has been considered as a simple method to build the NIR light-sensitive nanovectors, which simultaneously accomplishes coating of UCNP and loading of guest molecules. However, a uniform distribution of UCNP and obtaining nearly monodisperse nanovectors (PDI<0.1 from DLS) are hard to achieve, which may hamper the prospects for practical applications. In the case of loading UCNP in polymer micelles, there is lack of control on the number of nanoparticles in each micelle (often with uneven numbers), whether or not a single UCNP inside a nanovector is enough for NIR light-induced disruption and payload release remains an unanswered question.

To address the above important issues, in Chapter 1, we proposed a “bottom-up” strategy to synthesize an UV-responsive amphiphilic diblock copolymer on the surface of UCNP and, in a sense, to allow the micelle formation to occur through self-assembly in aqueous solution around a single UCNP. This way, monodisperse nanovectors with well-controlled

structure can be prepared. Our results show that under NIR light irradiation, the diblock copolymer micelle surrounding a single UCNP can be disrupted by absorbing the UV light emitted from UCNP, which leads to the release of an antitumor drug loaded in the micelle. At first, we employ a silica-assisted coating strategy to introduce ATRP initiators via covalent binding, which can preserve the photoluminescence property of UCNP. For the light-sensitivity, a UV-cleavable *o*-nitrobenzyl (ONB) monomer is synthesized for the growth of inner light-responsive polymer block on UCNP surface. This UV-responsive hydrophobic polymer layer is used for the micelle core region and to load hydrophobic guest molecules. Then the outer block is hydrophilic POEG that ensures high water-dispersity of the nanovector. With this controlled structure, upon NIR light irradiation, the photolysis reaction of ONB groups on the inner photoresponsive block can be activated by the UV upconversion luminescence of UCNP, which generates carboxylic acid groups and makes the diblock copolymer increasingly hydrophilic. This NIR light-induced shift of hydrophobic-hydrophilic balance results in increased solubility of the diblock copolymer layer in aqueous solution and thus leads to the release of entrapped drug molecules. To the best of our knowledge, our work is the first demonstration of this approach to constructing NIR light-controlled UCNP/polymer nanovectors. Owing to well-established polymerization techniques, one can easily fabricate novel nanovectors or hybrid materials with our proposed strategy. In the perspective section, we will give more details about this potential. In addition, our approach is also beneficial for exploring nanovectors with complicated structures. An example is the preparation of core-movable drug release systems (the so-called yolk-shell nanoparticles), which have high drug loading capacity and can release two types (hydrophobic and hydrophilic) of guest molecules from one nanovector. In this system, core-shell-shell structured nanovectors are prepared by using our method first. Taking UCNP@silica@Polymer as an example, the silica layer can be etched to create a space (or void) for hydrophilic payloads. In the meanwhile, polymer layer should remain the whole structure integrity (physical or chemical cross-linking) and encapsulate hydrophobic molecules. Again, these payloads will be released by using the upconversion emissions of UCNP to induce the photoreactions of the polymer layers.

In Chapter 2, we demonstrated a simple and robust method to assemble a nanovector using the electrostatic interactions between UCNP and a photolabile polyelectrolyte (PPE). Moreover, the release of the anionic model drug, fluorescein, can be switched on or off by turning on or off the NIR light. Conventionally, amphiphilic polymer self-assembly for the fabrication of UCNP-based nanovectors is carried out by dropwise adding their organic solution (miscible with water) into an aqueous solution, which allows the assembly of UCNP, polymers, and payloads. This step is followed by removal of the organic solvent. Owing to the hydrophobic interactions, however, the quick change in microenvironment results in entrapping two or more UCNP in one micelle. In other words, the loading of UCNP proceeds in an uncontrolled way. In our study, we put forward a titration method, in which an aqueous solution of PPE with positive charges is added directly to an aqueous solution of negatively charged UCNP. The designed polymer is readily prepared by free radical copolymerization of UV-sensitive *o*-nitrobenzyl monomer and methoxy PEG methacrylate monomer and then quaternized. An excellent water-dispersity of mesoporous silica coated UCNP is ensured before the addition of PPE solution, and the amount of polyelectrolyte influences the stability of the obtained complexes. Our results also found that the encapsulation of guest molecules and the coating of UCNP can be accomplished in one step. Furthermore, we investigated how the amount of PPE relative to UCNP could affect the payload encapsulation and release. Under NIR excitation, again, the cleavage of *o*-nitrobenzyl groups results in the partial charge reversal of PPE and then release of fluorescein as a result. This new strategy for fast construction of NIR light-sensitive nanovectors is an interesting step forward towards in designing novel nanovectors.

The second main contribution of the thesis is the research work presented in Chapter 3. In previous works from our group, gold nanoparticles (AuNPs) and UCNP are two types of nanofillers often used. Among other things, smart materials utilizing the photothermal effect of AuNPs may find applications in the fields of actuators (161), shape memory (162) and self-healing materials (163). If UCNP and AuNPs can be integrated into the same polymer matrix, novel hybrid stimuli-responsive polymer materials can be envisaged. However, to achieve this goal, fundamental questions like “how to organize UCNP and

AuNPs into a polymer film?" and "can their spatial organization affect their optical properties (upconversion photoluminescence of UCNP and surface plasmon resonance of AuNPs)?" should be addressed. Hence this work is devoted to answering the above questions. For the first time, we utilized the layer-by-layer (LBL) technique to build thin films composed of UCNP and AuNPs with the same numbers of nanoparticle/polyelectrolyte bilayers. We successfully prepared thin films with three different deposition sequences with the two types of inorganic nanoparticles. By tracking the UV-vis-NIR extinction spectra and UCL spectra under NIR light excitation, we found that the spatial organization determined by the sequence of deposition influences the interactions between UCNP and AuNPs and thus their optical properties. The alternating deposition of UCNP and AuNPs bilayers allows one to better preserve their "individual" properties as a result of reducing both the agglomeration of AuNPs and the scattering of the 980 nm excitation light that accounts for a quenching effect on the UCL of UCNP. By contrast, successive deposition of UCNP bilayers followed by AuNPs bilayers results in more agglomeration of AuNPs leading to a broad surface plasmon resonance (SPR) band in the NIR region and the most significant quenching of the UCL intensity of UCNP. Our study demonstrates an easy and efficient way to prepare NIR-responsive and plasmonic hybrid thin films with the possibility to tune their optical properties through the spatially controlled organization of the nanoparticles.

In all, we successfully developed three methods to prepare hybrid materials comprised of UCNP and polymer materials. We show that through the use of a bottom-up strategy (self-assembly of the covalently bonded diblock copolymer), electrostatic interactions and LbL assembly, novel nanovectors for NIR light-triggered drug release with low polydispersity as well as thin films containing spatially organized UCNP can be easily prepared. These methods offer new possibilities for combining polymers and UCNP to construct NIR light-responsive hybrid materials.

4.2 Future Studies

We have demonstrated three powerful strategies to obtain UCNP/polymers hybrid systems and shown their potential applications in the drug release field. To conclude the thesis, we discuss an example of future development.

Thermoresponsive polymeric materials are one kind of smart materials that exhibit a drastic and discontinuous change of their physical properties with temperature. Among them, poly(N-isopropylacrylamide) (PNIPAM) is a well-studied thermoresponsive polymer for several decades with a lower critical solution temperature (LCST) at ~32 ^{o}C. When an aqueous solution of PNIPAM is heated above or cooled below LCST, it undergoes a coil-to-globule or globule-to-coil transition during this process, respectively. Similarly, thermoresponsive polymers with an upper critical solution temperature (UCST) will experience a phase transition from a shrunken dehydrated state to a swollen hydrated state upon heating. Over the past few years, the non-ionic UCST based polymers of poly(acrylamide-*co*-acrylonitrile) (P(AAm-*co*-AN)), as an emerging type of UCST polymers, have received broad interest around the world due to the ease of tunable UCST, commercially available and low-priced monomers. Based on these two types of thermoresponsive polymers, our group and others have carried out studies in exploring their uses in various areas, like drug delivery, bioseparation and tissue engineering. In the light of the accomplished research work in this thesis, it will be interesting to expand their applications in drug delivery using UCNP through the strategies developed in this thesis.

As mentioned in the introduction part, we know that the release profile of drug from nanovectors strongly depends on the local microenvironment, when the temperature change is utilized as a stimulation source. Once the temperature is given, the release profile will be determined and thus lacks real-time controllability. To surmount this, one solution is to synthesize a series of thermoresponsive polymer nanovectors with different drug release rates by adjusting parameters (chemical compositions, molecular weights, porosity, etc.). However, this approach makes the preparation process tedious and complicated. On the

contrary, another solution is to endow thermoresponsive polymers with the property of photo-tunable LCST or UCST. In a previously published paper, the LCST behaviors of PNIAM can be easily tuned by the introduction of photocleavable ONB monomers by UV light irradiation. It is reported that only 6% of hydrophobic ONB monomers can shift the LCST of PNIPAM from 33 ºC to ~7 ºC (164). Interestingly, its LCST increases to ~55 ºC after the photolysis reaction by UV irradiation because of the generation of carboxylic acid groups. These results offer the possibility of applying upconverted UV emissions to induce the phase transitions by cleaving only a few number of chromophores (amplifying effect), which may be used to initiate the drug release. Preparation of NIR light-responsive nanovectors based on these polymers and UCNP has not been explored.

Why is the integration of UCNP with light-modulated LCST or UCST polymers for drug release interesting? There are many reasons, including but not limited to (1) amplifying effect (a few photochromic groups could make a large difference, e.g., from hydrophobic to hydrophilic), (2) NIR light excitation (deep penetration length and minimal photodamage to bio-tissues) and (3) combination of chemotherapy and bioimaging (upconversion visible lights). Of them, the amplification effect is significant for designing drug release systems with UCNP and photoresponsive polymers. Although diverse classes of nanovectors based on UCNP and photoresponsive polymers are designed, the low quantum yield of UCNP, especially for those processes requiring multi-photons absorption (e.g., 4- or 5- NIR photons for UV light), limits the translation of UCNP from the laboratory to practical applications. To overcome this problem, one solution is to obtain UCNP with strong UV upconversion emissions by enhancing their quantum yield through host lattice manipulation, energy transfer modulation, surface plasmon coupling and photonic crystal engineering (165, 166). In addition, ongoing efforts focus on the rational design of nanovectors by choosing suitable photoresponsive materials or making full use of upconversion emissions with less NIR photon absorption required (2- or 3- NIR photons) to induce photoreactions (167, 168). However, no attention has been paid to the number of chromophores in the design.

Figure 20 shows the drug release nanovector worthy of being studied. At first, we need to synthesize photoresponsive polymers with LCST or UCST (random or diblock copolymer) below or above body temperature (37 ^{o}C), respectively, to maintain the polymer chains in a dehydrated state for drug loading. After introducing UCNP, the UV upconversion emissions can initiate photoreactions for tuning the LCST above or UCST below the body temperature respectively, leading to a hydrophobic-to-hydrophilic balance shift. Using this concept, three systems can be designed. Figure 20b shows UCNP core grafted with a photo-tunable LCST or UCST polymer as the inner layer and a hydrophilic layer as the outmost layer by utilizing the approach described in Chapter 1. To realize the encapsulation and release of hydrophobic and hydrophilic payloads, as depicted in Figure 20c, a vesicle nanovector can be prepared by the self-assembly of the amphiphilic UCNP/polymer nanoparticles in Figure 20b. Owing to the large space within the vesicle, water-soluble biomolecules, like DNA and siRNA, can be entrapped inside. Moreover, the membrane enclosing the vesicle is composed of the hydrophobic area, which can be used to load hydrophobic guest antitumor molecules (e.g., doxorubicin). Last but not the least, implantable membrane systems for drug release is accessible by a spin coating method using the mixture of designed polymers and UCNP as depicted in Figure 20d.

We conducted some preliminary experiments and the results are promising as shown in Figure 21. Here, a photo-controllable LCST of PNIPAM is taken as an example to make our ideas clear. Figure 21 shows the chemical structure of the polymer and the photolysis reaction of it upon exposure to light. According to the designed principle discussed above, the LCST of the UV-sensitive polymer should below the 37 ^{o}C without light irradiation, which is good for holding hydrophobic drugs in nanovector at body temperature. Upon UV or NIR excitation, the photocleavage reaction of polymer will cause the hydrophobicity-hydrophilic shift, which gradually raises its LCST to or above 37 ^{o}C and results in drug release. Figure 21b and c demonstrate the changes of LCST-related cloud point of ONB modified PNIPAM (poly(NIPAM-*co*-2.8-ONB) and poly(NIPAM-*co*-4.9-ONB)) under UV irradiation. As can be seen in these two figures, only 2.8% and 4.9% of ONB monomers can shift the cloud points of PNIPAM to 20 ^{o}C and 8 ^{o}C,

respectively. After UV irradiation, their cloud points are above 37 ºC, which meets the requirements and can be considered as a candidate for our designs. Afterward, UCNP was successfully functionalized with poly(NIPAM-*co*-2.8-ONB) (UCNP@LCST-1) by using the strategy proposed in our first work. As revealed in Figure 21d, the UCNP@LCST-1 exhibits a cloud point at ~19 ºC, which implies the encapsulation of hydrophobic payload can be completed over 19 ºC. Moreover, under UV irradiation, the resulted UCNP@LCST-2 possessed a cloud point ~42 ºC. The dramatic difference of cloud points proved the regulation of the polymer's hydrophilicity by UV photons, which is helpful for drug release.

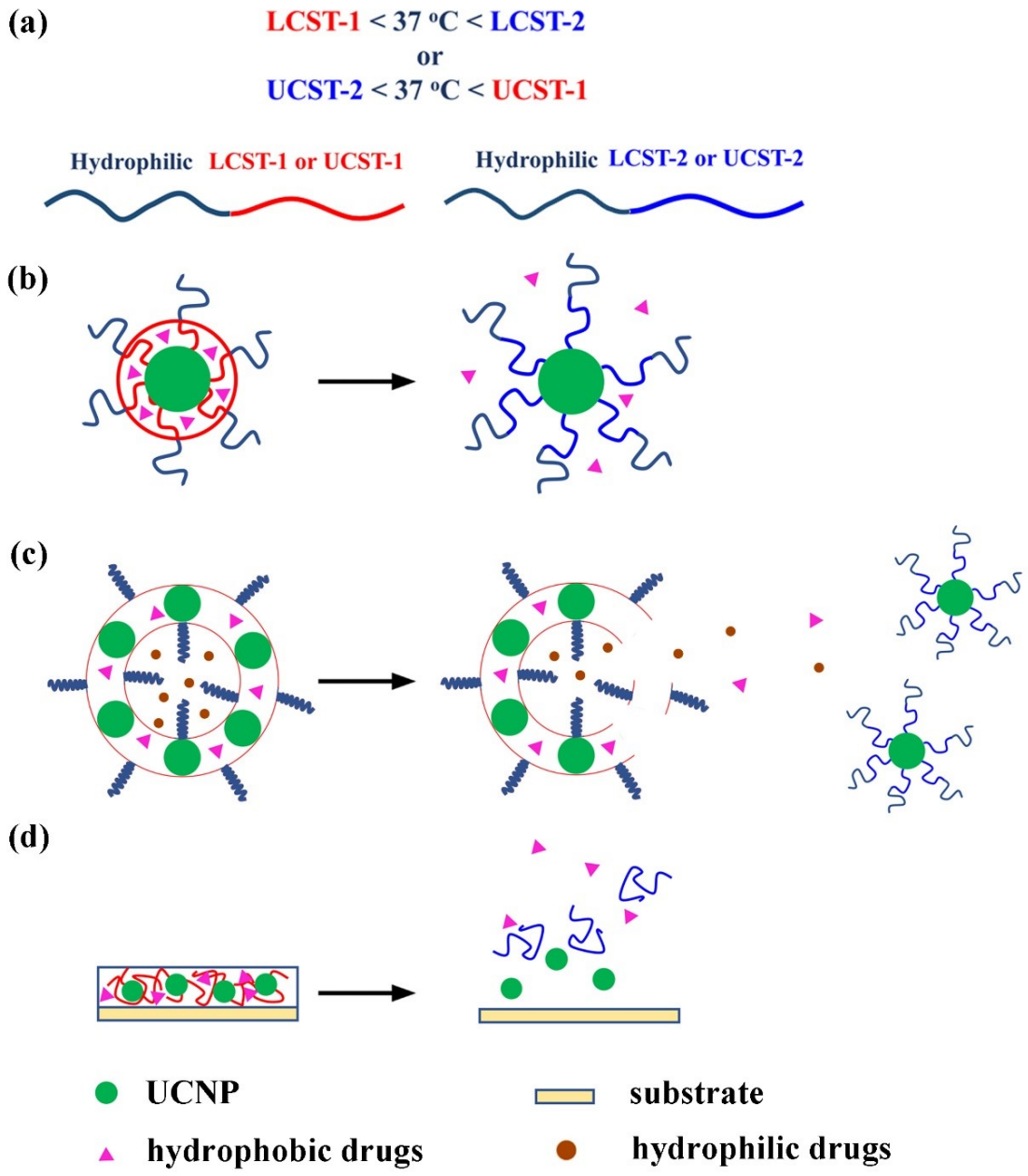

Figure 20. Schematic illustration of drug release systems based on UCNP and photoresponsive polymers with photo-tunable LCST or UCST. (a) The basic design principle is the synthesis of photoresponsive polymers (random or diblock copolymers) with temperature sensitivity. Release of drugs from several types of systems: (b) polymer micelles, (c) vesicles and (d) thin films.

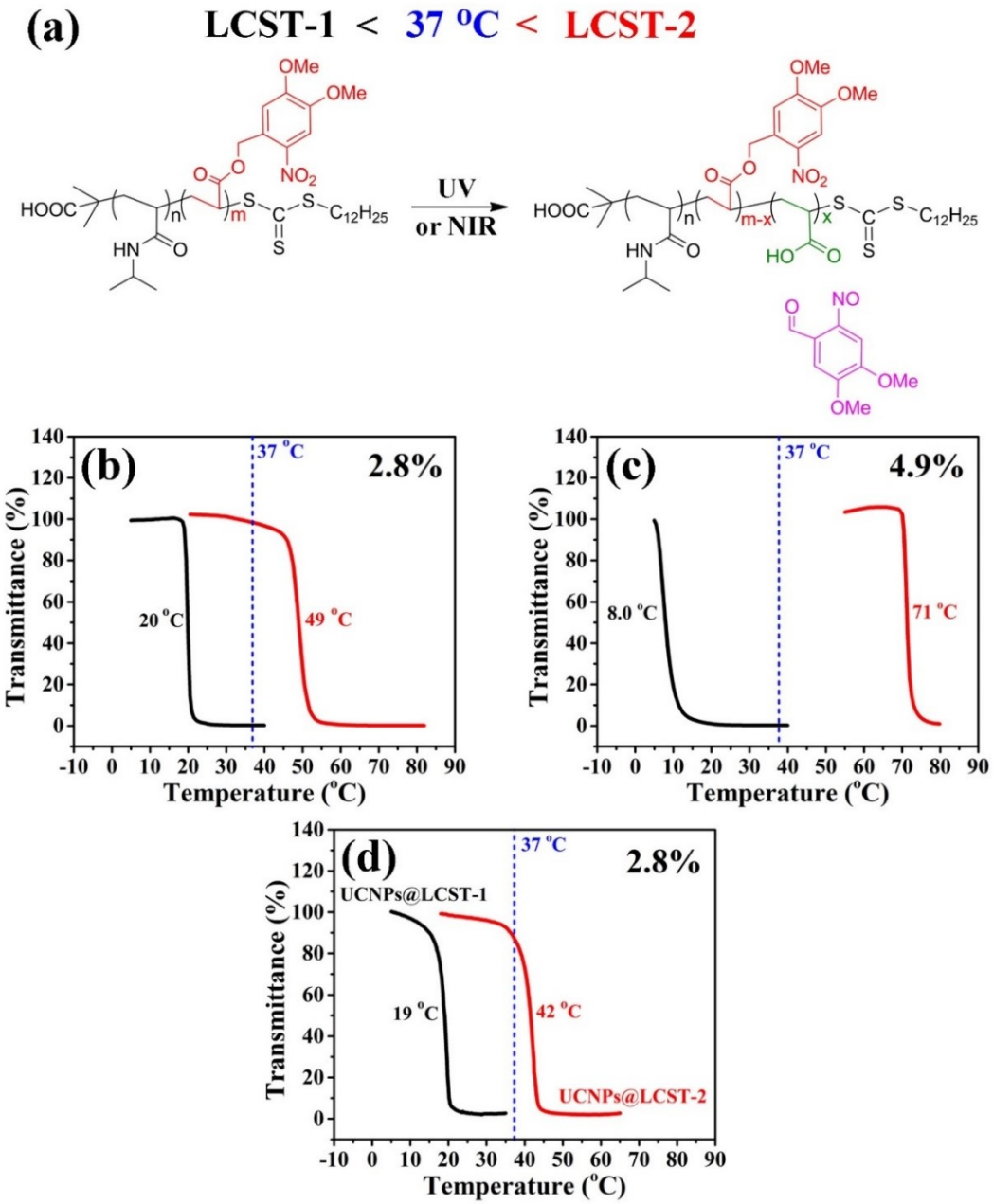

Figure 21. (a) UV or NIR light-triggered photolysis reaction of poly(NIPAM-*co*-ONB), resulting in the shift of LCST from below 37 ºC to above 37 ºC. Plots of solution transmittance *vs.* temperature for poly(NIPAM-*co*-ONB) (b and c) and poly(NIPAM-*co*-ONB) grafted UCNP. (d) (5 mg/mL) before (black) and after (red) UV irradiation in PBS saline solution (10 mM, pH 7.4).

CONCLUSIONS

In this thesis, we developed three methods to design UCNP/polymer hybrid materials with well-controlled architectures. The first two methods described in Chapter 1 and Chapter 2 allow one to obtain NIR-sensitive nanovectors (<200 nm) with a high degree of monodispersity by combining UCNP and UV-sensitive polymer. The underlying mechanism of releasing drug molecules from them is the same, which is to use NIR light to excite UCNP, and the UV light emitted by UCNP from inside the nanovector is then absorbed by the UV-sensitive polymer to carry out the photocleavage reaction, leading to nanovector disruption and concurrent drug release. Although both of them are capable of releasing drug molecules upon 980 nm irradiation, each meticulously designed nanovector has its own distinct features.

By employing the method in Chapter 1, one UCNP can be loaded into single polymer micelle, resulted in a high degree of monodispersity and a high utilization ratio of UCNP. Specifically, a thin silica layer was coated on UCNP to introduce ATRP initiators and connect UV-sensitive polymers with UCNP. Due to the covalent bonding, the designed nanovector can keep its structural integrity at high dilution. Moreover, hydrophobic drug molecules can be encapsulated into the nanoplatform during the process of diblock copolymer self-assembly on UCNP. Upon 980 nm irradiation, the surface UV-cleavable polymer undergoes a hydrophobic-hydrophilic balance shift due to the occurrence of photocleavage reactions, which leads to the drug release. In comparison with this method, we utilize the electrostatic-driven assembly to prepare another type of NIR-sensitive nanovectors in Chapter 2. In that work, UCNP are also modified with a silica layer, but the purpose is to endow UCNP with a charged surface, which benefits for the formation of nanocomplexes with the designed UV-sensitive polyelectrolyte later. Another distinct feature of this approach is the surface functionalization of UCNP and encapsulation of charged drug molecules can be completed in one single step where the solution of polyelectrolyte is dropwise added into an aqueous solution of UCNP alone or the mixture of UCNP and drug molecules. By design, when 980 nm light is applied to the nanocomplex,

the disruption of electrostatic equilibrium among UCNP, polyelectrolyte and drug caused by the photocleavage reaction (charge reversal occurs on the structure of polyelectrolyte) will lead to the drug release.

As for the method proposed in Chapter 3, the UCNP/polymer hybrid materials are presented in the form of thin films instead of nanoscale platforms. Despite the lack of data to demonstrate the application of the NIR-responsive polymer thin films, we believe they can also be used in the drug delivery field because the LbL films devised for this purpose have been known in the literature. By incorporating UCNP and gold nanoparticles (AuNP) into the same film, we can imagine that a thin film with dual-wavelength excitation for initiating drug release, that is, 980 nm is responsible for triggering drug release and 530 nm (equal to or close to SPR peak of AuNP) is good for drug diffusion due to the well-known photothermal effect of AuNP. Our contribution in this work is that the deposition sequence of UCNP/polyelectrolyte and plasmonic nanoparticles/polyelectrolyte bilayers has a great influence on the upconversion luminescence intensities and the SPR peak of the resulted hybrid thin films. In terms of the preservation of individual optical properties in the same film, the alternating organization of UCNP/polyelectrolyte and AuNP/polyelectrolyte bilayers is the best way.

In conclusion, we have made significant contributions to the research area of UCNP/polymer hybrid materials by developing new approaches to organizing these two fantastic building blocks together for obtaining well-controlled architectures. All approaches to making drug delivery nanosystems or plasmonic/luminescent systems also represent powerful tools to design advanced functional materials in related fields. Of course, we admit that further basic researches for a fundamental understanding of their behaviors *in vivo* are needed. Although there is a long way to send them into the clinics being the real products, it is our belief that these methods will be powerful weapons to clean some obstacles on the way.

BIBLIOGRAPHY

(1) Cheng, Z.; Lin, J. *Macromol. Rapid. Comm.* **2015**, *36*, 790-827.

(2) Zhou, B.; Shi, B.; Jin, D.; Liu, X. *Nat. Nanotechnol.* **2015**, *10*, 924-936.

(3) Wang, F.; Banerjee, D.; Liu, Y.; Chen, X.; Liu, X. *Analyst.* **2010**, *135*, 1839-1854.

(4) Gargas, D. J.; Chan, E. M.; Ostrowski, A. D.; Aloni, S.; Altoe, M. V. P.; Barnard, E. S.; Sanii, B.; Urban, J. J.; Milliron, D. J.; Cohen, B. E.; Schuck, P. J. *Nat. Nanotechnol.* **2014**, *9*, 300-305.

(5) Cheng, L.; Wang, C.; Liu, Z. *Nanoscale* **2013**, *5*, 23-37.

(6) Zhang, C.; Sun, L.; Zhang, Y.; Yan, C. *J. Rare Earth.* **2010**, *28*, 807-819.

(7) Roh, J.; Yu, H.; Jang, J. *ACS Appl. Mater. Inter.* **2016**, *8*, 19847-19852.

(8) Naccache, R.; Vetrone, F.; Capobianco, J. A. *ChemSusChem* **2013**, *6*, 1308-1311.

(9) Chen, C. K.; Chen, H. M.; Chen, C.-J.; Liu, R.-S. *Chem. Commun.* **2013**, *49*, 7917-7919.

(10) Wang, J.; Wei, T.; Li, X.; Zhang, B.; Wang, J.; Huang, C.; Yuan, Q. *Angew. Chem. Int. Edit.* **2014**, *53*, 1616-1620.

(11) Lu, Y.; Zhao, J.; Zhang, R.; Liu, Y.; Liu, D.; Goldys, E. M.; Yang, X.; Xi, P.; Sunna, A.; Lu, J.; Shi, Y.; Leif, R. C.; Huo, Y.; Shen, J.; Piper, J. A.; Robinson, J. P.; Jin, D. *Nat. Photonics* **2013**, *8*, 32-36.

(12) Won Jin, K.; Marcin, N.; Paras, N. P. *Nanotechnology* **2009**, *20*, 185301.

(13) Yang, Y.; Shao, Q.; Deng, R.; Wang, C.; Teng, X.; Cheng, K.; Cheng, Z.; Huang, L.; Liu, Z.; Liu, X.; Xing, B. *Angew. Chem. Int. Edit.* **2012**, *51*, 3125-3129.

(14) Yu, X.-F.; Chen, L.-D.; Li, M.; Xie, M.-Y.; Zhou, L.; Li, Y.; Wang, Q.-Q. *Adv. Mater.* **2008**, *20*, 4118-4123.

(15) He, M.; Pang, X.; Liu, X.; Jiang, B.; He, Y.; Snaith, H.; Lin, Z. *Angew. Chem. Int. Edit.* **2016**, *55*, 4280-4284.

(16) Hu, J.; Chen, Y.; Li, Y.; Zhou, Z.; Cheng, Y. *Biomaterials* **2017**, *112*, 133-140.

(17) Mase, J. D.; Razgoniaev, A. O.; Tschirhart, M. K.; Ostrowski, A. D. *Photochem. Photobiol. Sci.* **2015**, *14*, 775-785.

(18) Cheng, T.; Ortiz, R. F.; Vedantham, K.; Naccache, R.; Vetrone, F.; Marks, R. S.; Steele, T. W. J. *Biomacromolecules* **2015**, *16*, 364-373.

(19) Jalani, G.; Naccache, R.; Rosenzweig, D. H.; Lerouge, S.; Haglund, L.; Vetrone, F.; Cerruti, M. *Nanoscale* **2015**, *7*, 11255-11262.

(20) Lee, J.; Bisso, P. W.; Srinivas, R. L.; Kim, J. J.; Swiston, A. J.; Doyle, P. S. *Nat. Mater.* **2014**, *13*, 524.

(21) Ma, X.; Ni, X. *J. Nanopart. Res.* **2013**, *15*, 1547.

(22) Capobianco, J. A.; Vetrone, F.; D'Alesio, T.; Tessari, G.; Speghini, A.; Bettinelli, M. *Phys. Chem. Chem. Phys.* **2000**, *2*, 3203-3207.

(23) Wang, F.; Wang, J.; Liu, X. *Angew. Chem. Int. Edit.* **2010**, *49*, 7456-7460.

(24) Li, C.; Quan, Z.; Yang, J.; Yang, P.; Lin, J. *Inorg. Chem.* **2007**, *46*, 6329-6337.

(25) Dong, H.; Sun, L.-D.; Yan, C.-H. *Nanoscale* **2013**, *5*, 5703-5714.

(26) Shi, F.; Wang, J.; Zhai, X.; Zhao, D.; Qin, W. *CrystEngComm* **2011**, *13*, 3782-3787.

(27) Shi, F.; Wang, J.; Zhang, D.; Qin, G.; Qin, W. *J. Mater. Chem.* **2011**, *21*, 13413-13421.

(28) Yan, C.; Zhao, H.; Perepichka, D. F.; Rosei, F. *Small* **2016**, *12*, 3888-3907.

(29) Ostrowski, A. D.; Chan, E. M.; Gargas, D. J.; Katz, E. M.; Han, G.; Schuck, P. J.; Milliron, D. J.; Cohen, B. E. *ACS Nano* **2012**, *6*, 2686-2692.

(30) Zhao, J.; Wei, Z.; Feng, X.; Miao, M.; Sun, L.; Cao, S.; Shi, L.; Fang, J. *ACS Appl. Mater. Inter.* **2014**, *6*, 14945-14951.

(31) Boyer, J.; Johnson, N.; Van Veggel, F. *Chem. Mater.* **2009**, *21*, 2010-2012.

(32) Chen, C.; Li, C.; Shi, Z. *Adv. Sci.* **2016**, *3*, 1600029.

(33) Yang, Y. *Microchim. Acta* **2014**, *181*, 263-294.

(34) Wang, M.; Abbineni, G.; Clevenger, A.; Mao, C.; Xu, S. *Nanomed-Nanotechnol.* **2011**, *7*, 710-729.

(35) Park, B. J.; Hong, A. R.; Park, S.; Kyung, K.-U.; Lee, K.; Seong Jang, H. *Sci. Rep.* **2017**, *7*, 45659.

(36) Watanabe, S.; Asanuma, T.; Sasahara, T.; Hyodo, H.; Matsumoto, M.; Soga, K. *Adv. Funct. Mater.* **2015**, *25*, 4390-4396.

(37) Na, H.; Jeong, J. S.; Chang, H. J.; Kim, H. Y.; Woo, K.; Lim, K.; Mkhoyan, K. A.; Jang, H. S. *Nanoscale* **2014**, *6*, 7461-7468.

(38) Bagheri, A.; Arandiyan, H.; Boyer, C.; Lim, M. *Adv. Sci.* **2016**, *3*, 1500437.

(39) Liu, Z.; Dong, K.; Liu, J.; Han, X.; Ren, J.; Qu, X. *Small* **2014**, *10*, 2429-2438.

(40) Alexis, F.; Pridgen, E.; Molnar, L. K.; Farokhzad, O. C. *Mol. Pharmaceut.* **2008**, *5*, 505-515.

(41) Drummond, D. C.; Zignani, M.; Leroux, J.-C. *Prog. Lipid. Res.* **2000**, *39*, 409-460.

(42) Wang, M.; Mi, C.-C.; Liu, J.-L.; Wu, X.-L.; Zhang, Y.-X.; Hou, W.; Li, F.; Xu, S.-K. *J. Alloy. Compd.* **2009**, *485*, L24-L27.

(43) Naccache, R.; Vetrone, F.; Mahalingam, V.; Cuccia, L. A.; Capobianco, J. A. *Chem. Mater.* **2009**, *21*, 717-723.

(44) Johnson, N. J.; Oakden, W.; Stanisz, G. J.; Scott Prosser, R.; van Veggel, F. C. *Chem. Mater.* **2011**, *23*, 3714-3722.

(45) Wang, Z.-L.; Hao, J.; Chan, H. L. W.; Law, G.-L.; Wong, W.-T.; Wong, K.-L.; Murphy, M. B.; Su, T.; Zhang, Z. H.; Zeng, S. Q. *Nanoscale* **2011**, *3*, 2175-2181.

(46) Xia, L.; Kong, X.; Liu, X.; Tu, L.; Zhang, Y.; Chang, Y.; Liu, K.; Shen, D.; Zhao, H.; Zhang, H. *Biomaterials* **2014**, *35*, 4146-4156.

(47) Wang, L.; Liu, J.; Dai, Y.; Yang, Q.; Zhang, Y.; Yang, P.; Cheng, Z.; Lian, H.; Li, C.; Hou, Z.; Ma, P. a.; Lin, J. *Langmuir.* **2014**, *30*, 13042-13051.

(48) Wang, C.; Cheng, L.; Liu, Y.; Wang, X.; Ma, X.; Deng, Z.; Li, Y.; Liu, Z. *Adv. Funct. Mater.* **2013**, *23*, 3077-3086.

(49) Cheng, L.; Yang, K.; Li, Y.; Chen, J.; Wang, C.; Shao, M.; Lee, S.-T.; Liu, Z. *Angew. Chem. Int. Edit.* **2011**, *50*, 7385-7390.

(50) Zhang, H.; Li, Y.; Ivanov, I. A.; Qu, Y.; Huang, Y.; Duan, X. *Angew. Chem. Int. Edit.* **2010**, *49*, 2865-2868.

(51) Liras, M.; González-Béjar, M.; Peinado, E.; Francés-Soriano, L.; Pérez-Prieto, J.; Quijada-Garrido, I.; García, O. *Chem. Mater.* **2014**, *26*, 4014-4022.

(52) Johnson, N. J. J.; Oakden, W.; Stanisz, G. J.; Scott Prosser, R.; van Veggel, F. C. J. M. *Chem. Mater.* **2011**, *23*, 3714-3722.

(53) Dong, A.; Ye, X.; Chen, J.; Kang, Y.; Gordon, T.; Kikkawa, J. M.; Murray, C. B. *J. Am. Chem. Soc.* **2011**, *133*, 998-1006.

(54) Li, L.; Hao, P.; Wei, P.; Fu, L.; Ai, X.; Zhang, J.; Zhou, J. *Biomaterials* **2017**, *136*, 43-55.

(55) Shi, Y.; Shi, B.; Dass, A. V. E.; Lu, Y.; Sayyadi, N.; Kautto, L.; Willows, R. D.; Chung, R.; Piper, J.; Nevalainen, H.; Walsh, B.; Jin, D.; Packer, N. H. *Sci. Rep.* **2016**, *6*, 37533.

(56) Zhang, W.; Peng, B.; Tian, F.; Qin, W.; Qian, X. *Anal. Chem.* **2014**, *86*, 482-489.

(57) Wilhelm, S.; Kaiser, M.; Wurth, C.; Heiland, J.; Carrillo-Carrion, C.; Muhr, V.; Wolfbeis, O. S.; Parak, W. J.; Resch-Genger, U.; Hirsch, T. *Nanoscale* **2015**, *7*, 1403-1410.

(58) Boyer, J.-C.; Vetrone, F.; Cuccia, L. A.; Capobianco, J. A. *J. Am. Chem. Soc.* **2006**, *128*, 7444-7445.

(59) Liu, J.; Wu, R.; Li, N.; Zhang, X.; Zhan, Q.; He, S. *Biomed. Opt. Express* **2015**, *6*, 1857-1866.

(60) Wang, X.; Liu, K.; Yang, G.; Cheng, L.; He, L.; Liu, Y.; Li, Y.; Guo, L.; Liu, Z. *Nanoscale* **2014**, *6*, 9198-9205.

(61) He, L.; Feng, L.; Cheng, L.; Liu, Y.; Li, Z.; Peng, R.; Li, Y.; Guo, L.; Liu, Z. *ACS Appl. Mater. Inter.* **2013**, *5*, 10381-10388.

(62) Wang, L.; Yan, R.; Huo, Z.; Wang, L.; Zeng, J.; Bao, J.; Wang, X.; Peng, Q.; Li, Y. *Angew. Chem. Int. Edit.* **2005**, *44*, 6054-6057.

(63) Wang, D.; Rogach, A. L.; Caruso, F. *Nano Lett.* **2002**, *2*, 857-861.

(64) Decher, G. *Science* **1997**, *277*, 1232-1237.

(65) Zhao, N.; Wu, B.; Hu, X.; Xing, D. *Biomaterials* **2017**, *141*, 40-49.

(66) Zhang, X.; Ai, F.; Sun, T.; Wang, F.; Zhu, G. *Inorg. Chem.* **2016**, *55*, 3872-3880.

(67) Wei, R.; Wei, Z.; Sun, L.; Zhang, J. Z.; Liu, J.; Ge, X.; Shi, L. *ACS Appl. Mater. Inter.* **2016**, *8*, 400-410.

(68) Pierri, A. E.; Huang, P.-J.; Garcia, J. V.; Stanfill, J. G.; Chui, M.; Wu, G.; Zheng, N.; Ford, P. C. *Chem. Commun.* **2015**, *51*, 2072-2075.

(69) Pospisilova, M.; Mrazek, J.; Matuska, V.; Kettou, S.; Dusikova, M.; Svozil, V.; Nesporova, K.; Huerta-Angeles, G.; Vagnerova, H.; Velebny, V. *J. Nanopart. Res.* **2015**, *17*, 383.

(70) Wu, T.; Kaur, S.; Branda, N. R. *Org. Biomol. Chem.* **2015**, *13*, 2317-2322.

(71) Wang, C.; Cheng, L.; Liu, Z. *Biomaterials* **2011**, *32*, 1110-1120.

(72) Wu, S.; Han, G.; Milliron, D. J.; Aloni, S.; Altoe, V.; Talapin, D. V.; Cohen, B. E.; Schuck, P. J. *Proc. Natl. Acad. Sci. U. S. A.* **2009**, *106*, 10917-10921.

(73) Cheng, R.; Tian, M.; Sun, S.; Liu, C.; Wang, Y.; Liu, Z.; Liu, Z.; Jiang, J. *Langmuir.* **2015**, *31*, 7758-7763.

(74) Plohl, O.; Kralj, S.; Majaron, B.; Frohlich, E.; Ponikvar-Svet, M.; Makovec, D.; Lisjak, D. *Dalton T.* **2017**, *46*, 6975-6984.

(75) Liu, J.-N.; Bu, W.-B.; Shi, J.-L. *Accounts. Chem. Res.* **2015**, *48*, 1797-1805.

(76) Argyo, C.; Weiss, V.; Bräuchle, C.; Bein, T. *Chem. Mater.* **2014**, *26*, 435-451.

(77) Lee, J. E.; Lee, N.; Kim, T.; Kim, J.; Hyeon, T. *Accounts. Chem. Res.* **2011**, *44*, 893-902.

(78) M. Rosenholm, J.; Sahlgren, C.; Linden, M. *Curr. Drug Targets* **2011**, *12*, 1166-1186.

(79) Inglefield, D. L.; Merritt, T. R.; Magill, B. A.; Long, T. E.; Khodaparast, G. A. *J. Mater. Chem. C* **2015**, *3*, 5556-5565.

(80) Yang, Y.; Velmurugan, B.; Liu, X.; Xing, B. *Small* **2013**, *9*, 2937-2944.

(81) Chen, F.; Zhang, S.; Bu, W.; Chen, Y.; Xiao, Q.; Liu, J.; Xing, H.; Zhou, L.; Peng, W.; Shi, J. *Chem.-Eur. J.* **2012**, *18*, 7082-7090.

(82) Zhao, Z.; Han, Y.; Lin, C.; Hu, D.; Wang, F.; Chen, X.; Chen, Z.; Zheng, N. *Chem Asian J.* **2012**, *7*, 830-837.

(83) Qian, H. S.; Guo, H. C.; Ho, P. C.-L.; Mahendran, R.; Zhang, Y. *Small* **2009**, *5*, 2285-2290.

(84) Tian, B.; Liu, S.; Lu, W.; Jin, L.; Li, Q.; Shi, Y.; Li, C.; Wang, Z.; Du, Y. *Sci. Rep.* **2016**, *6*, 21335.

(85) Chen, C.; Kang, N.; Xu, T.; Wang, D.; Ren, L.; Guo, X. *Nanoscale* **2015**, *7*, 5249-5261.

(86) Zhang, X.; Yang, P.; Dai, Y.; Ma, P. a.; Li, X.; Cheng, Z.; Hou, Z.; Kang, X.; Li, C.; Lin, J. *Adv. Funct. Mater.* **2013**, *23*, 4067-4078.

(87) Chen, D.; Lei, L.; Yang, A.; Wang, Z.; Wang, Y. *Chem. Commun.* **2012**, *48*, 5898-5900.

(88) Li, Z.; Zhang, Y.; Jiang, S. *Adv. Mater.* **2008**, *20*, 4765-4769.

(89) Soukka, T.; Rantanen, T.; Kuningas, K. *Ann. Ny. Acad. Sci.* **2008**, *1130*, 188-200.

(90) Lee, H.; Dellatore, S. M.; Miller, W. M.; Messersmith, P. B. *Science* **2007**, *318*, 426-430.

(91) Cho, J. H.; Vasagar, V.; Shanmuganathan, K.; Jones, A. R.; Nazarenko, S.; Ellison, C. J. *Chem. Mater.* **2015**, *27*, 6784-6790.

(92) Zhou, J.; Duan, B.; Fang, Z.; Song, J.; Wang, C.; Messersmith, P. B.; Duan, H. *Adv. Mater.* **2014**, *26*, 701-705.

(93) Liu, N.; Wu, H.; McDowell, M. T.; Yao, Y.; Wang, C.; Cui, Y. *Nano Lett.* **2012**, *12*, 3315-3321.

(94) Ryou, M.-H.; Lee, Y. M.; Park, J.-K.; Choi, J. W. *Adv. Mater.* **2011**, *23*, 3066-3070.

(95) Liu, X.; Cao, J.; Li, H.; Li, J.; Jin, Q.; Ren, K.; Ji, J. *ACS Nano* **2013**, *7*, 9384-9395.

(96) Nurunnabi, M.; Khatun, Z.; Nafiujjaman, M.; Lee, D.-g.; Lee, Y.-k. *ACS Appl. Mater. Inter.* **2013**, *5*, 8246-8253.

(97) Hong, S.; Kim, K. Y.; Wook, H. J.; Park, S. Y.; Lee, K. D.; Lee, D. Y.; Lee, H. *Nanomedicine* **2011**, *6*, 793-801.

(98) Batul, R.; Tamanna, T.; Khaliq, A.; Yu, A. *Biomater. Sci.* **2017**, *5*, 1204-1229.

(99) Liu, F.; He, X.; Lei, Z.; Liu, L.; Zhang, J.; You, H.; Zhang, H.; Wang, Z. *Adv. Healthc. Mater.* **2015**, *4*, 559-568.

(100) Liu, B.; Li, C.; Xing, B.; Yang, P.; Lin, J. *J. Mater. Chem. B* **2016**, *4*, 4884-4894.

(101) Wang, D.; Chen, C.; Ke, X.; Kang, N.; Shen, Y.; Liu, Y.; Zhou, X.; Wang, H.; Chen, C.; Ren, L. *ACS Appl. Mater. Inter.* **2015**, *7*, 3030-3040.

(102) Plohl, O.; Kraft, M.; Kovač, J.; Belec, B.; Ponikvar-Svet, M.; Würth, C.; Lisjak, D.; Resch-Genger, U. *Langmuir.* **2017**, *33*, 553-560.

(103) Hayat, K. *Therapeutic Window and Therapeutic Index*; MEDIMOON, **2014**, http://medimoon.com/2014/12/therapeutic-window-and-therapeutic-index/.

(104) *Goodman & Gilman's the pharmacological basis of therapeutics, 12e*; Brunton, L. L.; McGraw-Hill Education, **2011**, 1808 pages.

(105) Davis, M. E.; Chen, Z.; Shin, D. M. *Nat. Rev. Drug Discov.* **2008**, *7*, 771.

(106) Yang, G.; Liu, J.; Wu, Y.; Feng, L.; Liu, Z. *Coordin. Chem. Rev.* **2016**, *320-321*, 100-117.

(107) Cevik, O.; Gidon, D.; Kizilel, S. *Acta Biomater.* **2015**, *11*, 151-161.

(108) Khaletskaya, K.; Reboul, J.; Meilikhov, M.; Nakahama, M.; Diring, S.; Tsujimoto, M.; Isoda, S.; Kim, F.; Kamei, K.-i.; Fischer, R. A.; Kitagawa, S.; Furukawa, S. *J. Am. Chem. Soc.* **2013**, *135*, 10998-11005.

(109) Yang, X.; Liu, X.; Liu, Z.; Pu, F.; Ren, J.; Qu, X. *Adv. Mater.* **2012**, *24*, 2890-2895.

(110) Yang, Y.; Mu, J.; Xing, B. *WIRes. Nanomed. Nanobio.* **2017**, *9*, e1408.

(111) Olejniczak, J.; Carling, C.-J.; Almutairi, A. *J. Control. Release* **2015**, *219*, 18-30.

(112) Shell, T. A.; Lawrence, D. S. *Accounts. Chem. Res.* **2015**, *48*, 2866-2874.

(113) Gohy, J.-F.; Zhao, Y. *Chem. Soc. Rev.* **2013**, *42*, 7117-7129.

(114) Lim, D. J.; Park, H. *J Biomater Sci Polym Ed* **2017**, 1-13.

(115) Jayakumar, M. K. G.; Idris, N. M.; Zhang, Y. *Proc. Natl. Acad. Sci. U. S. A.* **2012**, *109*, 8483-8488.

(116) Weissleder, R. *Nat. Biotechnol.* **2001**, *19*, 316.

(117) Clydesdale, G. J.; Dandie, G. W.; Muller, H. K. *Immunol. Cell Biol.* **2001**, *79*, 547.

(118) Wu, S.; Blinco, J. P.; Barner-Kowollik, C. *Chem.-Eur. J.* **2017**, *23*, 8325-8332.

(119) Cho, H. J.; Chung, M.; Shim, M. S. *J. Ind. Eng. Chem.* **2015**, *31*, 15-25.

(120) Bort, G.; Gallavardin, T.; Ogden, D.; Dalko, P. I. *Angew. Chem. Int. Edit.* **2013**, *52*, 4526-4537.

(121) Goodwin, A. P.; Mynar, J. L.; Ma, Y.; Fleming, G. R.; Fréchet, J. M. J. *J. Am. Chem. Soc.* **2005**, *127*, 9952-9953.

(122) Hao, W.; Liu, D.; Wang, Y.; Han, X.; Xu, S.; Liu, H. *Colloids Surf. A Physicochem. Eng. Asp.* **2018**, *537*, 446-451.

(123) Liu, R.; Chen, H.; Li, Z.; Shi, F.; Liu, X. *Polym. Chem.* **2016**, *7*, 2457-2463.

(124) Wu, S.; Butt, H.-J. *Adv. Mater.* **2016**, *28*, 1208-1226.

(125) Lederhose, P.; Chen, Z.; Müller, R.; Blinco, J. P.; Wu, S.; Barner-Kowollik, C. *Angew. Chem. Int. Edit.* **2016**, *55*, 12195-12199.

(126) Li, W.; Wang, J.; Ren, J.; Qu, X. *J. Am. Chem. Soc.* **2014**, *136*, 2248-2251.

(127) Chen, Z.; He, S.; Butt, H.-J.; Wu, S. *Adv. Mater.* **2015**, *27*, 2203-2206.

(128) Yang, Y.; Liu, F.; Liu, X.; Xing, B. *Nanoscale* **2013**, *5*, 231-238.

(129) Liu, G.; Zhou, L.; Su, Y.; Dong, C.-M. *Chem. Commun.* **2014**, *50*, 12538-12541.

(130) Yan, B.; Boyer, J.-C.; Habault, D.; Branda, N. R.; Zhao, Y. *J. Am. Chem. Soc.* **2012**, *134*, 16558-16561.

(131) Klán, P.; Šolomek, T.; Bochet, C. G.; Blanc, A.; Givens, R.; Rubina, M.; Popik, V.; Kostikov, A.; Wirz, J. *Chem. Rev.* **2013**, *113*, 119-191.

(132) Zhao, H.; Sterner, E. S.; Coughlin, E. B.; Theato, P. *Macromolecules.* **2012**, *45*, 1723-1736.

(133) Ma, M.; Gao, N.; Sun, Y.; Ren, J.; Qu, X. *Small* **2017**, *13*, 1701817.

(134) Li, J.; Lee, W. Y.-W.; Wu, T.; Xu, J.; Zhang, K.; Hong Wong, D. S.; Li, R.; Li, G.; Bian, L. *Biomaterials* **2016**, *110*, 1-10.

(135) Alonso-Cristobal, P.; Oton-Fernandez, O.; Mendez-Gonzalez, D.; Díaz, J. F.; Lopez-Cabarcos, E.; Barasoain, I.; Rubio-Retama, J. *ACS Appl. Mater. Inter.* **2015**, *7*, 14992-14999.

(136) Wang, S.; Yang, W.; Cui, J.; Li, X.; Dou, Y.; Su, L.; Chang, J.; Wang, H.; Li, X.; Zhang, B. *Biomater. Sci.* **2016**, *4*, 338-345.

(137) Yuan, Y.; Min, Y.; Hu, Q.; Xing, B.; Liu, B. *Nanoscale* **2014**, *6*, 11259-11272.

(138) Yan, B.; Boyer, J.-C.; Branda, N. R.; Zhao, Y. *J. Am. Chem. Soc.* **2011**, *133*, 19714-19717.

(139) Chen, S.; Gao, Y.; Cao, Z.; Wu, B.; Wang, L.; Wang, H.; Dang, Z.; Wang, G. *Macromolecules.* **2016**, *49*, 7490-7496.

(140) Wang, J.; Wu, B.; Li, S.; He, Y. *J. Polym. Sci., Part A: Polym. Chem.* **2017**, *55*, 2450-2457.

(141) Zhang, R.; Yao, R.; Ding, B.; Shen, Y.; Shui, S.; Wang, L.; Li, Y.; Yang, X.; Tao, W. *Adv. Mater. Sci. Eng.* **2014**, *2014*, 1-9.

(142) Liu, G.; Liu, N.; Zhou, L.; Su, Y.; Dong, C.-M. *Polym. Chem.* **2015**, *6*, 4030-4039.

(143) Viger, M. L.; Grossman, M.; Fomina, N.; Almutairi, A. *Adv. Mater.* **2013**, *25*, 3733-3738.

(144) Zhao, H.; Hu, W.; Ma, H.; Jiang, R.; Tang, Y.; Ji, Y.; Lu, X.; Hou, B.; Deng, W.; Huang, W.; Fan, Q. *Adv. Funct. Mater.* **2017**, *27*, 1702592.

(145) Jalani, G.; Naccache, R.; Rosenzweig, D. H.; Haglund, L.; Vetrone, F.; Cerruti, M. *J. Am. Chem. Soc.* **2016**, *138*, 1078-1083.

(146) Xing, Q.; Li, N.; Jiao, Y.; Chen, D.; Xu, J.; Xu, Q.; Lu, J. *RSC Adv.* **2015**, *5*, 5269-5276.

(147) Chen, G.; Jaskula-Sztul, R.; Esquibel, C. R.; Lou, I.; Zheng, Q.; Dammalapati, A.; Harrison, A.; Eliceiri, K. W.; Tang, W.; Chen, H.; Gong, S. *Adv. Funct. Mater.* **2017**, *27*, 1604671.

(148) Ho, H. P.; Wong, W.-W.; Wu, S.-Y. *Opt. Eng.* **2003**, *42*, 2349-2353.

(149) Zhongmin, Y.; Zhouming, F.; Zhonghong, J. *J. Phys. D: Appl. Phys.* **2005**, *38*, 1629-1632.

(150) Shalav, A.; Richards, B. S.; Trupke, T.; Krämer, K. W.; Güdel, H. U. *Appl. Phys. Lett.* **2005**, *86*, 013505.

(151) Lin, C.; Berry, M. T.; Anderson, R.; Smith, S.; May, P. S. *Chem. Mater.* **2009**, *21*, 3406-3413.

(152) Richardson, J. J.; Cui, J.; Björnmalm, M.; Braunger, J. A.; Ejima, H.; Caruso, F. *Chem. Rev.* **2016**, *116*, 14828-14867.

(153) Zhao, Y.; Bertrand, J.; Tong, X.; Zhao, Y. *Langmuir.* **2009**, *25*, 13151-13157.

(154) Quinn, A.; Such, G. K.; Quinn, J. F.; Caruso, F. *Adv. Funct. Mater.* **2008**, *18*, 17-26.

(155) Bo, Q.; Tong, X.; Zhao, Y.; Zhao, Y. *Macromolecules.* **2008**, *41*, 3562-3570.

(156) Zhang, X.; Chen, H.; Zhang, H. *Chem. Commun.* **2007**, 1395-1405.

(157) Chen, J.; Huang, S.-W.; Lin, W.-H.; Zhuo, R.-X. *Small* **2007**, *3*, 636-643.

(158) Bao, C.; Ma, B.; Liu, J.; Wu, Z.; Zhang, H.; Jiang, Y.-J.; Sun, J. *Langmuir.* **2016**, *32*, 3393-3399.

(159) Bao, Y.; Luu, Q. A. N.; Lin, C.; Schloss, J. M.; May, P. S.; Jiang, C. *J. Mater. Chem.* **2010**, *20*, 8356-8361.

(160) Borges, J.; Mano, J. F. *Chem. Rev.* **2014**, *114*, 8883-8942.

(161) Ge, F.; Lu, X.; Xiang, J.; Tong, X.; Zhao, Y. *Angew. Chem. Int. Edit.* **2017**, *56*, 6126-6130.

(162) Zhang, H.; Zhao, Y. *ACS Appl. Mater. Inter.* **2013**, *5*, 13069-13075.

(163) Zhang, H.; Fortin, D.; Xia, H.; Zhao, Y. *Macromol. Rapid. Comm.* **2013**, *34*, 1742-1746.

(164) Ionov, L.; Diez, S. *J. Am. Chem. Soc.* **2009**, *131*, 13315-13319.

(165) Han, S.; Deng, R.; Xie, X.; Liu, X. *Angew. Chem. Int. Edit.* **2014**, *53*, 11702-11715.

(166) Huang, P.; Zheng, W.; Zhou, S.; Tu, D.; Chen, Z.; Zhu, H.; Li, R.; Ma, E.; Huang, M.; Chen, X. *Angew. Chem. Int. Edit.* **2014**, *53*, 1252-1257.

(167) Chen, Z.; Sun, W.; Butt, H.-J.; Wu, S. *Chem. -Eur. J.* **2015**, *21*, 9165-9170.

(168) He, S.; Krippes, K.; Ritz, S.; Chen, Z.; Best, A.; Butt, H.-J.; Mailander, V.; Wu, S. *Chem. Commun.* **2015**, *51*, 431-434.